Ifremer
Direction de la Technologie Marine et des Systèmes d'Information
Cellule Océano-Météo
Marc Prevosto, Sylvie Van Iseghem, Benjamin Moreau

Shell Global Solutions U.S.
George Z. Forristall

January 2001

Shell Global Solutions U.S.

WACSIS
Wave Crest Sensor Intercomparison Study

- *Common Data Base*
- *Analyses*
- *Crest Height Models*

WACSIS
- Common Data Base
- Analyses
- Crest Height Models

Marc Prevosto*
George Z. Forristall**
Sylvie Van Iseghem*
Benjamin Moreau*

*** Ifremer - Centre de Brest**
**** Shell Global Solutions U.S.**

This report is dedicated to Benjamin Moreau, a young student engineer who worked hard with us on the simulations and analyses of the WACSIS data during summer 1999. He died suddenly in October 2000.

CHAPTER 1

Introduction

Despite its great theoretical and practical importance, the statistical distribution of crest heights has remained poorly known. The uncertainties are due to difficulties both with the theory, where nonlinear effects must be accurately modeled, and with measurements, where different sensors appear to give different results. In response to this uncertainty, the Wave Crest Sensor Intercomparison Study (WACSIS) was formed as a Joint Industry Project in order to provide data for comparing the response of wave sensors and for comparing theories of crest height distributions with the measurements.

The key to the WACSIS experiment was to place all of the popular sensors on the same platform located where they were likely to experience large waves in one season. The location of the measurements was in shallow water because the nonlinearities that produce extreme wave crests are stronger in shallow water. Measurements in shallow water thus give better tests of both instruments and theories.

The project was set up on the Meetpost Noordwijk (MPN) measurement platform. The platform is a piled steel jacket structure in 18 meters deep water, located 9 kilometers off the Dutch coast near the coastal resort of Noordwijk, whence it got its name. The platform is one of the stations of the North Sea Monitoring Network ('Meetnet Noordzee', MNZ), that gathers on-line hydrological and meteorological information from the North Sea. A complete description of the project is given by van Unen et al. (1998)[28].

WACSIS was very successful in collecting a nearly complete data set from all of the instruments during the winter of 1997-98. The second phase of the WACSIS project focused on the interpretation of the wave data. Many aspects of wave statistics have been studied, but the main emphasis has been on crest height distributions, and recommendations for crest heights to be used in air gap calculations.

This report will describe, first the different steps which have been followed to construct a common data base from the raw data collected at the Meetpost Noordwijk measurement platform, secondly various analyses of the data base in term of crest height-period joint distributions, intercomparison of the crest measurements by the sensors and comparisons with numerical second order irregular wave models. Finally, new models of crest distribution will be proposed and compared with other state of the art models.

WACSIS Common Data Base. During the 1997/1998 storm season, December to May, measurements were collected from a set of wave sensors at the Dutch Meetpost Noordwijk measurement platform. The wave sensors used on or close to the platform were a Baylor wave staff, a THORN wave height sensor, a MAREX SO5 wave radar, a SAAB radar, a Vlissingen step gauge, a directional Waverider buoy and a S4ADW current meter and pressure sensor. All the raw data collected onboard have been qualified and processed to furnish a reference data base for the project

Height-Period Joint Distributions. Parametric and non parametric models for the joint crest height-period and crest height-wavelength distributions have been compared with the wave measurements. They are of both theoretical and practical interest since the distribution of wave steepness in particular can be derived from it.

Sensor measurements comparison. One of the main objectives of the WACSIS project was the intercomparison of different sensors used to measure the crest heights. In this project, we have focused our studies on the ability of a sensor to give the correct statistics of the crest heights. Some analyses has been made to understand the discrepancies between the sensors.

Simulation methods - Effect of simulation parameters. In order to compare crest statistics given by second order models of wave kinematics with the measurements and to fit parameterized models of crest heights, we have used simulation methods for the elevation of the free surface. The formulas are based on the irregular wave version of the second order Stokes expansion. The effects of the parameters of the simulation have been studied in order to use wave simulators that are as accurate as possible in our following work.

2nd order simulations - Comparison with measurements. Then, the results of the simulations have been exploited to compare the statistics of the crest heights with those obtained from the measurements. The aim was to try to answer the question: do the simulations validate the results obtained by one or more sensors?

Models of distribution - Comparison with simulations. In the case of a positive answer to the previous question, it seems very logical to validate and fit models of crest height distribution on extensive data bases obtained from the simulators, corresponding to a great variety of sea state situations and water depths. The positive answer would also validate the use of the second order 3D irregular wave model in the simulators for crest height studies.

Simplified Hs-dependent models. As, very often, the climatology on a site is only available for Hs, it is relevant to analyse if the complex parametric models, necessary to take into account main of the sea state characteristics influencing the crest height statistics, could be reduced to models depending from Hs alone. We have tried to answer this issue and so to propose to the engineer a complete range of accurate models for calculating crest height design values.

CHAPTER 2

WACSIS Common Data Base

Marc Prevosto

During the 1997/1998 storm season, December to May, measurements were collected from a set of wave sensors at the Dutch Meetpost Noordwijk measurement platform (figure 2.1). The wave sensors deployed on or close to the platform were: a Baylor wave staff, a THORN wave height sensor (an upgrade of the EMI laser), a MAREX SO5 wave radar, a SAAB radar, a Vlissingen step gauge and Marine 300 step gauge, a directional Waverider buoy, a SMART 800 GPS buoy, a WAVEC directional buoy and a S4ADW current meter and pressure sensor.

The platform was located approximately 10 kilometers from the Dutch coast, in a mean water depth of 18 meters.

FIGURE 2.1 : Meetpost Noordwijk platform location

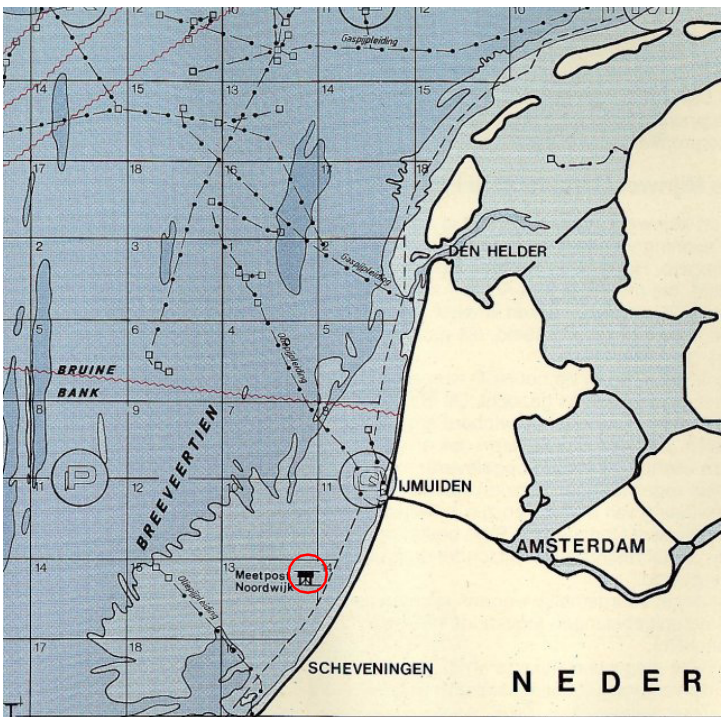

Additional fully operational sensors of the Dutch North Sea Monitoring Network resulting in hydrological and meteorological data sets complemented the measurements.

Data base description

For the construction of the WACSIS Common Data Base, only seven of these sensors were used (the abbreviated form of each, used in the sequel of the processing and analyses is given in parentheses): The Baylor wave staff (BAYLORWS), the THORN wave height sensor (EMILASER), the MAREX SO5 wave radar (MAREXSGN), the SAAB radar (SAABRNIV), the Vlissingen step gauge (VLISSING), the directional Waverider buoy (WAVERGHR) and the S4ADW current meter and pressure sensor (S4PRVELO).

The wind speed and direction, coming from the Dutch North Sea Monitoring Network were added.

Sensor configurations

Sensor locations. Each sensor was located at a different point on the structure, and as we will see in the studies of comparison between sensors, some differences are partly explained by this fact. Their positions relative to the EMILASER are given in table 2.1 where z is the altitude relative to a mean water level, the N.A.P.(*). Each sensor is positioned horizontally relatively to the structure in figure 2.2. The platform is 7 degrees westward from the North:

(*) The Amsterdam Ordonance Datum: N.A.P. (Normaal Amsterdams Peil) is the altitude reference level for most European countries and historically derives from a gauge-mark on the Haarlemmer Lock corresponding with the average flood-level of the IJ Inlet, measured between 1 September 1683 and 1 September 1684. The present level differs from the actual maritime situation by a few centimetres. The statutory zero point for measuring altitude is located beneath the pavement in front of the Royal Palace on the Dam. By means of a spectacular spirit-level operation a geodetically true copy of the Amsterdam Ordnance Datum was transferred to an exhibition in the exhibition chamber below the Town Hall mall. The bronze button set into a concrete pillar, which provides the calibration point for levelling in Europe, is at eye-level.

TABLE 2.1 : Sensors positions

Sensor	x (m)	y (m)	z (m)
EMILASER	0	0	15.18
MAREXSGN	-0.78	-0.06	14.95
BAYLORWS	-1.1	-1.75	11.50
S4PRVELO	-2.1	-1.75	-11.5
SAABRNIV	18.23	2.82	15.03
VLISSING	10.86	21.39	8.33
WAVERGHR	~ 30	~ 200	water level

Time periods and amount of data

The measurement campaign took place during six months. During all this time the different instruments furnished a very high rate of available data, apart from the S4. The gaps in the S4 data were caused by a broken communication cable at the end of December and by a bug in the Interocean (supplier of the instrument) software which did not permit the storage of more than 10 continuous days of valid data. The periods of functioning are given in figure 2.3.

In table 2.2, the number of 20 min. time series for each sensors shows again the very high density of the data base. These figures have to be compared to 11561, the total number of 20 min. time series between the beginning and the end of the measurement campaign

FIGURE 2.2 : **Sensors layout**

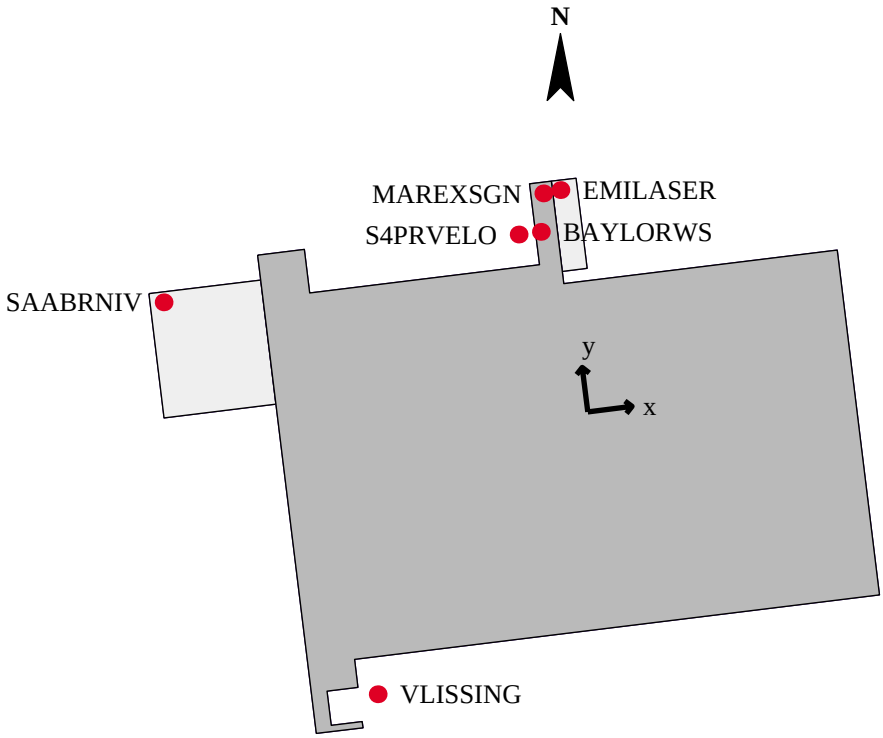

FIGURE 2.3 : **Periods of functioning**

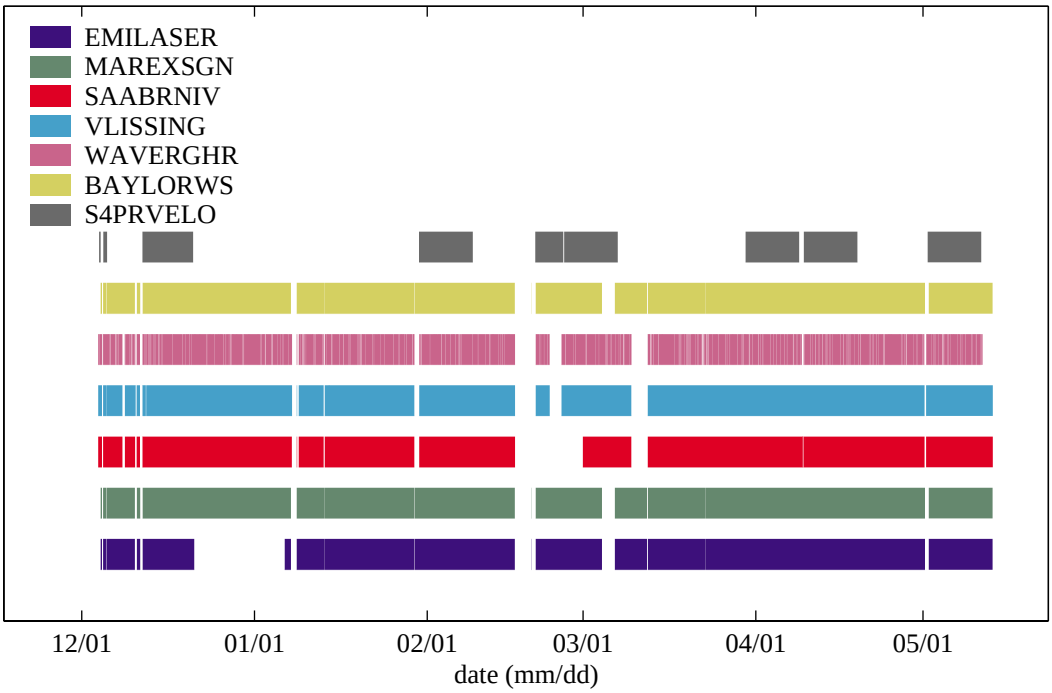

TABLE 2.2 : **Number of 20 min. time series - Raw data base**

EMILASER	MAREXSGN	SAABRNIV	VLISSING	WAVERGHR	BAYLORWS	S4PRVELO
9711	10880	10192	10666	10457	10880	4569

Generation of the raw WACSIS data base

The generation of the raw WACSIS data base was the first step in building the WACSIS common data base. The different steps are summarized in appendix 2.1.

Raw data

The raw data were furnished by OCN on CD-ROMs. For each instruments (apart from the S4) the raw measurement data are organised on a monthly basis, each of the six months corresponding to a large binary file (up to 312Mb for VLISSING without compressing).

All entries are 32 bit integer values ('INTEGER*4' in the FORTRAN programming language, 'long int' in the 'C' programming language).

Wave height sensors have a DATE, TIME and WAVE_HEIGHT which can be formatted as: '(I8.8,1X,I6.6,1X,I5)' (FORTRAN format string) or "%8.8ld %6.6ld %5ld" ('C' format string).

The WAVE_HEIGHT is given in cm apart for BAYLORWS where it is furnished in mV. A transformation into physical wave heights [cm] has been applied using an equation calculated from a physical calibration in the field by OCN:

Wave_Height = 1722.200 - 0.787 * Milli_Volts

The Directional Waverider records include DATE, TIME, VERTICAL, NORTH_SOUTH, EAST_WEST (latter three are displacements in [cm]) which can be formatted as: '(I8.8,1X,I6.6,1X,I5,1X,I5,1X,I5)' (FORTRAN format string) or "%8.8ld %6.6ld %5ld %5ld %5ld" ('C' format string).

For all these sensors the TIME is given in rounded seconds.

S4 data. The S4 data files have the internal binary format of the instrument. The duration corresponding to each file depends on the dates of intervention by OCN on the sensor acquisition system. All the files have been transformed in ASCII format by the software furnished by INTEROCEAN.

Split raw data

In a first step, all the files have been split in 20 min. long time series, each beginning on the exact hour, exact hour plus 20 min., and exact hour plus 40 min. This procedure has encountered some problems which has obliged us to attentively develop a robust software to process the data. Each time a time gap or erroneous data was detected the time series was thrown away.

Problems encountered during the processing. In the raw files the **time stamp** has a ONE SECOND resolution, and this time stamp can jump back and forth due to the time synchronisation in the network and some computations done 'on the fly' in the data acquisition programs. Hereafter is an example of the time values (in second) given in a file of EMILASER (sampled at 4 Hz, (11148, 11148, 11148, 11148, 11149, 11149, 11149, **11149, 11150, 11149**, 11149, 11149, 11150, 11150, 11150, 11150, 11151, 11151, 11151, 11151, 11151). Sometimes errors exist also in the DATE, for example from (file 199803.bin, 11353096th point) where the DATE is given YYYYMMDD (19980323, 19980323, 19980323, 19980323, 19980323, **19980323, 19980323, 19980322, 19980322**, 19980322, 19980322, 19980322, 19980322). So it was not possible to blindly use the clock DATE and TIME and the time series were constructed using a validated starting time for the time series and in using the sampling frequency to calculate the number of points necessary to reach 20 min.

This gave for the different sensors values given in table 2.3. Unfortunately for some sensors the **sampling frequency** was not exactly the value given and could fluctuate. This was strongly the case for the Saab radar, for which if we look at the estimated values of the sampling frequency on blocks of 300000 points (~ 16 hours) (table 2.4), it is clear that the sampling frequency not equals 5.12 and slightly fluctuates. It is clear that this difference gives for SAABRNIV an average shift at the end of 20 min. of 0.9s. So, at the end of each 20 min. time series, the starting date plus 20 min. was compared to the time clock given in the file. If the difference was higher than 1 sec., the starting point of the next 20mn time series was chosen to be in agreement with the clock. This procedure induced for SAABRNIV a possible maximum shift of 0.9s at the beginning of a time series and a maximum of 1.8s at the end, with the wave events in the generated time series occurring before the actual events.

TABLE 2.3 : Number of points in the 20 min. time series

	EMILASER	MAREXSGN	SAABRNIV	VLISSING	WAVERGHR	BAYLORWS	S4PRVELO
Sampling frequency (Hz)	4	4	5.12	10	1.28	4	2
Number of points	4800	4800	6144	12000	1536	4800	2400

TABLE 2.4 : Estimated sampling frequencies, December raw file

Block	1	3	4	5	6	8
Value	5.1163	5.1164	5.1162	5.1165	5.1162	5.1164

The **starting times of the S4** files were also sometimes given incorrect values. The year, day, hour, minute, or second could be wrong. Thanks to the measurements of the tide by all the sensors, the date has been corrected using a correlation procedure between the S4 mean level measurement and that of the other sensors. A precise correction of the minutes and seconds was made in a second step by correlation of the wave measurements with the Baylor wave staff. Of course this procedure does not insure exact clock time, but it does permit good comparison of wave height measurements between the S4 and the other sensors. Another problem was that a bug in the Interocean software necessary to decode the S4 binary files did not permit the processing of more than 10 continuous days of valid data, limiting the amount of data available with the S4.

The complete processing of the raw data has furnished a large base of 20 min. time series distributed as indicated in table 2.2.

Generation of the common WACSIS data base

To limit the amount of data investigated during the project, a limited number of time series have been selected on which detrend, re-sampling and directional analyses procedures have been applied.

Selection of the dates for the common WACSIS data base

Video analysis. The first selection procedure was applied by OCEANOR to a data base of sea state parameters to select the dates that would be used to analyse the video records as follows:

- extract the highest 750 Hs (Hs>2.3 m) -> 200 hours of data
- select all records with Hs higher than 3.1 m -> 70 hours
- select 30 hours of the highest index weighted in decreasing order by "Daylight criteria", representative wave direction, number of operating sensors and high steepness (Daylight is 0800-1700) -> 30 hours
- select 50 hours among the above 100 hours, first only retaining daylight hours with video data and then weighting for high Hs and bright daylight hours (1000-1500).

The second procedure applied by Shell was to:

- select the 50 hours of the video analysis from OCEANOR selection
- complete taking all hours with Hs>4m -> 16 hours
- complete with Hs>3m and wave periods, directions and steepness not well represented in the data already selected

Directions close to 320 deg.	-> 5 hours
Hours with Tp>10 sec or Tp<8 sec	-> 7 hours
Hours with Tm<6	-> 2 hours
Hours with steepness > 0.07	-> 9 hours
Highest remaining Hs	-> 11 hours

Finally these 100 hours with wave steepness between 0.04 and 0.07 were complemented by 20 hours with wave steepness between 0 and 0.04.

The number of 20 min. time series available for each sensor from these 120 selected hours is given in table 2.5.

TABLE 2.5 : Number of 20 min. time series

		EMILASER	MAREXSGN	SAABRNIV	VLISSING	WAVERGHR	BAYLORWS	S4PRVELO
Video	**(150x 20 min.)**	111	129	126	149	123	129	90
High Hs	**(150x 20 min.)**	62	140	147	150	122	140	30
Low steepness	**(60x 20 min.)**	59	59	60	60	48	59	35
Total	**(360x 20 min.)**	232	328	333	359	293	328	155

MWL, H_s, T_{02}, C_{max}, 5 minutes synthetic parameters

At the same time split raw files of 5 minutes duration were generated. For each of these files, sea state parameters were calculated for each sensor and so for each sensor a contemporaneous vector time series sampled at 5 minutes resulted.

The 4 (6 for the S4) parameters are:

- Mean Water Level (cm), (MWL)
- Significant Wave Height (cm), (H_s)
- Mean Period (s), (time version of T02)
- Maximum Crest Height (cm), (Cmax)
- Mean value of the north-south velocity (cm/s), (VN) (for the S4)
- Mean value of the east-west velocity (cm/s), (VE) (for the S4)

For the S4, MWL, Hs, T02, and Cmax have been calculated directly from the pressure measurements, so MWL corresponds to the immersion of the sensor.

Two time values are added to these parameters:

- Hour (h), (number of hours since 01/01/1900)
- Minute (min.)

These files are ASCII files (param.dat). When the data was not available the value has been replaced by NaN. There are 6 (8 for the S4) columns:

- Hour Minute MWL H_s T_{02} C_{max} (V_N V_E)

The two first columns (time information) are exactly identical for all the sensors.

Tide, surge, offset detrend

At the location of the measurement campaign the tide and storm surge effects on the mean water level are important and comparable to the wave heights (see figure 2.8). So before processing and analysing the wave elevation it is necessary to subtract from the measurements the part due to the tide and storm surge.

This has been done by first locally smoothing the 5 min. mean water level (see above) using cubic splines. The local smoothing used the previous, current and next 20 min. period corresponding to the 20 min. time series being processed. Then the smoothed mean water level was subtracted from the measured sea surface elevation. When compared to a simple linear detrend, the difference is not so important apart the moment of the passage from flood to ebb tide and ebb to flood tide.

Oversampling-Undersampling

To have at our disposal measurements of the wave elevation by the different sensors but with a common sampling frequency, the common WACSIS data base with the original sampling frequencies has been re-sampled at 4Hz, 2Hz and 1Hz. When the original sampling frequency was lower than the new one we applied a over-sampling procedure, when the original sampling frequency was higher than the new one we applied a under-sampling procedure. Of course no processing was applied in the case of equality of the two sampling frequencies.

Under-sampling. In a classical way, the under-sampling is realized by Fourier transforming (using FFT) the time series, applying a anti-aliasing filter with a cut-off frequency at the Nyquist frequency corresponding to the new sampling frequency and finally deciminating by eliminating in the frequency decomposition the components with frequencies higher than this cut-off frequency. An inverse Fourier transform furnished the under-sampled time series.

Over-sampling. The over-sampling is realized by Fourier transforming (using FFT) the time series, adding components up to the mid new sampling frequency with zero amplitude and applying an inverse Fourier transform to furnish the over-sampled time series.

In both under- and over-sampling frequency the previous and next 20 min. period (when available) were pasted to the corresponding 20 min. time series in process to eliminate the boundary (leakage) effects. An example of the under-sampling to 1 Hz at the beginning of a time series is given in figure 2.4 for VLISSING, an example of the over-sampling to 4 Hz at the beginning of a time series is given in figure 2.5 for WAVERGHR.

FIGURE 2.4 : Example of under-sampling, 28 February 1998 at 02:00

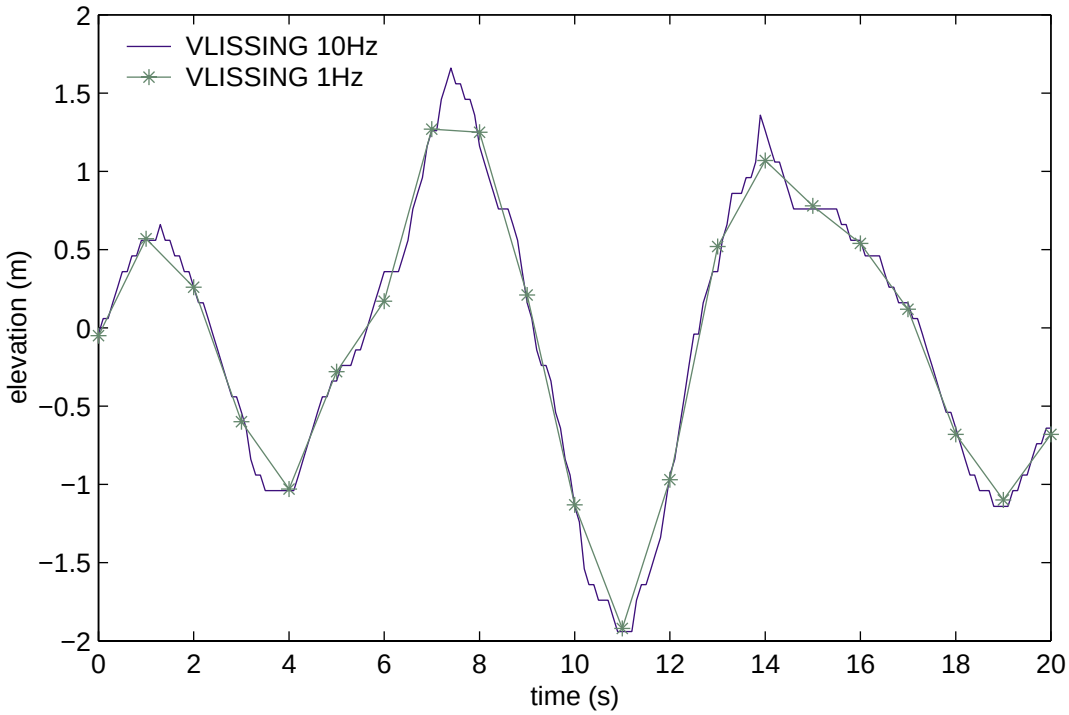

FIGURE 2.5 : Example of over-sampling, 28 February 1998 at 02:00

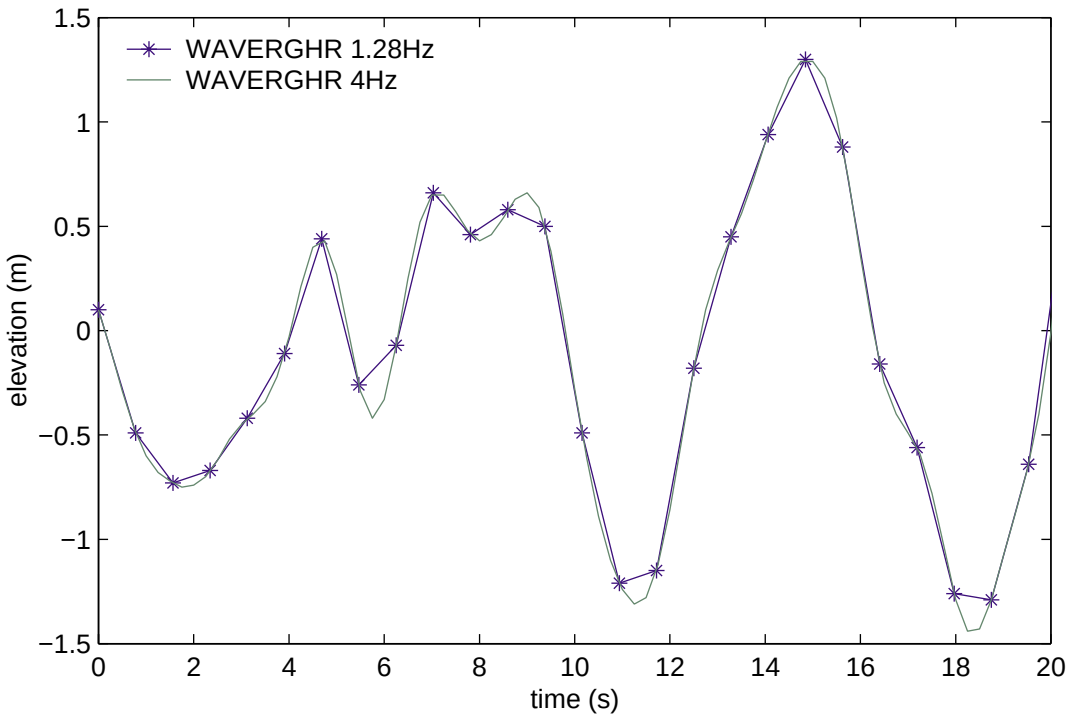

Intersection of sensors data base

As could be seen in table 2.5, the number of available time series corresponding to high Hs is poor for e.g. EMILASER. So to not degrade the sensor intercomparison different intersections of the data bases have been used. These data bases are named in this report by the first letters of the sensors considered. For example MSVB means intersection of MAREXSGN, SAABRNIV, VLISSING and BAYLORWS data bases (S4PRVELO has not been considered in the intercomparisons).

Waverider directional information

Directional information has been computed by SHELL starting from the Directional Waverider time series of the common data base, with the original sampling frequency (1.28Hz). The directional spectrum can be expressed as

$$S(f,\theta) = S(f)H(f,\theta) \qquad \textbf{(EQ 2.1)}$$

where S(f) is the power spectrum and $H(f,\theta)$ is the spreading function. The spreading function can be expanded as the Fourier series

$$H(f,\theta) = \frac{1}{\pi}\left\{\frac{1}{2} + \sum_{n=1}^{\infty}[a_n(f)\cos(n\theta) + b_n(f)\sin(n\theta)]\right\} \qquad \textbf{(EQ 2.2)}$$

The Directional Waverider uses accelerometers to measure the x, y and z displacements of the buoy. Assuming that the buoy follows the motion of the wave surface and that linear wave theory applies, coefficients a_1, b_1, a_2, and b_2 can be found from this information. The cospectra of the displacement time series are calculated using fast Fourier transforms and then the relationships between cospectra and the series expansion of the spreading function are inverted to find the coefficients.

The mean wave direction as a function of frequency is

$$\theta_1(f) = \arctan[b_1(f)/a_1(f)] \qquad \textbf{(EQ 2.3)}$$

The rms wave spreading σ can be defined as

$$\sigma(f) = \{2[1-m_1(f)]\}^{\frac{1}{2}} \qquad \textbf{(EQ 2.4)}$$

where m_1 is the first moment of the spreading function defined as

$$m_1(f) = [a_1^2(f) + b_1^2(f)]^{\frac{1}{2}} \qquad \textbf{(EQ 2.5)}$$

The second order trigonometric moments of the spreading function give only a coarse representation of the spectrum with non-physical negative values. It is thus customary to use the moments to estimate the parameters of some smooth model for the directional spreading function. The most common of these is the cosine 2s form given by

$$H(f,\theta) = A(s)\cos\left(\frac{\theta-\theta_1(f)}{2}\right)^{2s(f)} \qquad \textbf{(EQ 2.6)}$$

The exponent s(f) can be calculated either using the first moments by solving

$$[a_1^2(f) + b_1^2(f)]^{\frac{1}{2}} = \frac{s_1(f)}{s_1(f) + 1} \qquad \textbf{(EQ 2.7)}$$

or from the second moments by solving

$$[a_2^2(f) + b_2^2(f)]^{\frac{1}{2}} = \frac{s_2(f)[s_2(f) - 1]}{[s_2(f) + 1][s_2(f) + 2]} \qquad \textbf{(EQ 2.8)}$$

The calculations were made on one hour blocks of data. The direction convention is that 0 radians means waves from the north and $\pi/2$ radians means waves from the east.

All of these parameters are stored in files on the WACSIS web site as described at the end of this chapter.

Figure 2.6 shows an example of the parameters of the directional spectrum calculated for 00Z on 5 January 1998. The three panels of the figure show, from the bottom, the power spectrum, the mean wave direction as a function of frequency, and the rms wave spreading as a function of frequency. The mean direction and spreading are given in radians.

The characteristics of this example spectrum are quite normal for a wind generated sea. The power spectrum has a strong peak at about 0.1 Hz. The mean direction is roughly constant with frequency, showing waves from the west. The rms spreading reaches a minimum of about 0.4 radians at the frequency of the peak of the spectrum. The spreading increases slowly with increasing frequency and more rapidly with decreasing frequency, where there is very little energy. All of these features are commonly observed in the directional spectra of wind seas.

Climatology

In using the Hs calculated each 5 min. for all the sensors and taking each time the median value of the available data, the Hs probability law has been estimated. It appears that a Weibull law (EQ 2.9) fits the samples well. The result of the fitting is given in figure 2.7.

$$P(H_s > h) = \exp\left(-\left(\frac{c}{\alpha}\right)^{\beta}\right) \qquad \textbf{(EQ 2.9)}$$

with $\alpha = 1.265$, $\beta = 1.494$.

Water depth

In looking at the measurements of the mean water level by the different sensors we observe some differences (see figure 2.8). These differences are probably due to electronic offset fluctuations. To obtain a reference water depth evolution we have chosen to use the mean water level calculated from the mean values each 5 minutes of the Saab radar and the Vlissingen Step Gauge which give very close values. Moreover, both of these sensors are calibrated and monitored by the Rijkswaterstaat (Dutch Institute) in the scope of their National Water Level Measuring Program. The mean value of the water depth all over the measurement campaign has

FIGURE 2.6 : Parameters of the directional spectrum at 00Z on 5 Jan 1998

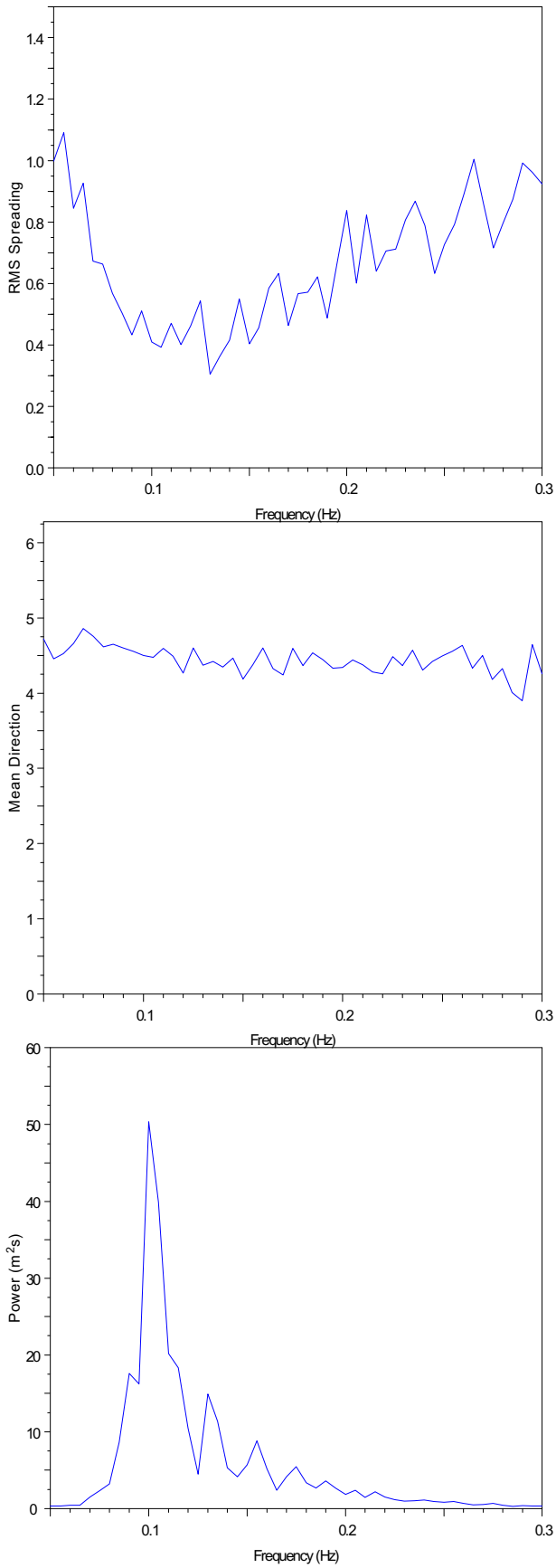

FIGURE 2.7 : Fitting of an Hs law

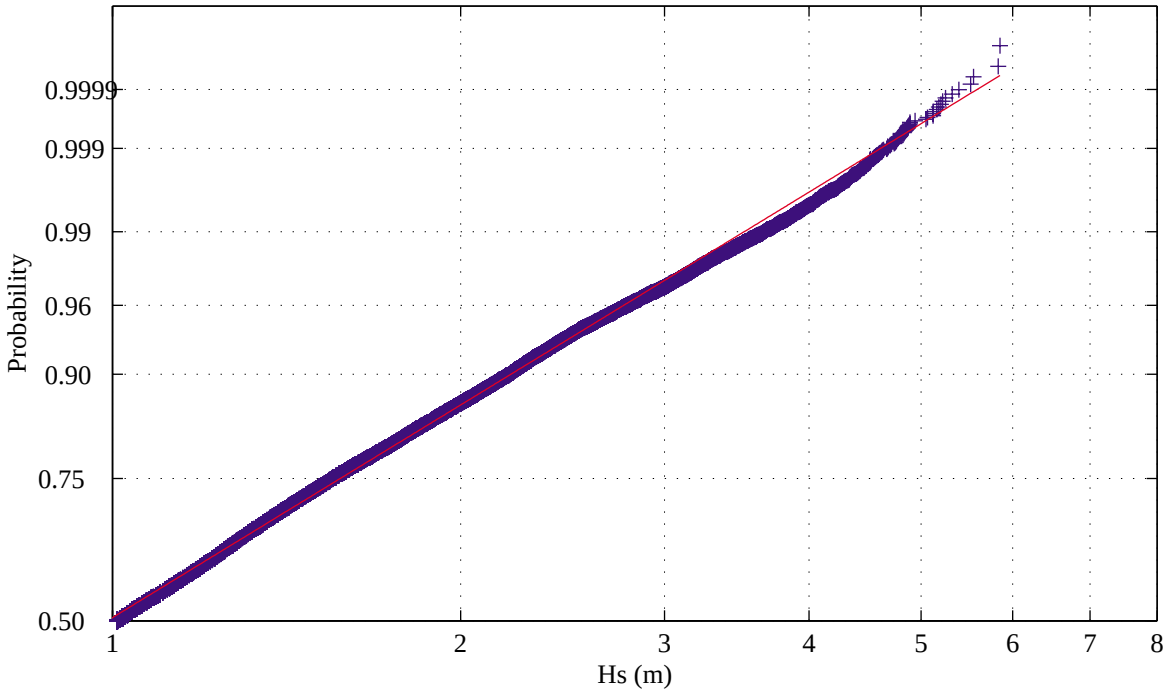

been fixed to 18 meters. An equivalent file of the sea state parameters file has been generated. The parameters are:

- Water Depth (cm), (WaD)

Two time values are added to this parameter:

- Hour (h), (number of hours since 01/01/1900)
- Minute (min.)

The file is an ASCII file (water_depth.dat). When the data was not available the value has been replaced by NaN. There are 3 columns:

- Hour Minute WaD

The two first columns (time information) are exactly identical with the sea-state parameters files.

As a curiosity, in figure 2.9 we could observe the effect of the water depth on the mean period of the waves. This effect is probably due to effect of tidal currents.

FIGURE 2.8 : Mean water level

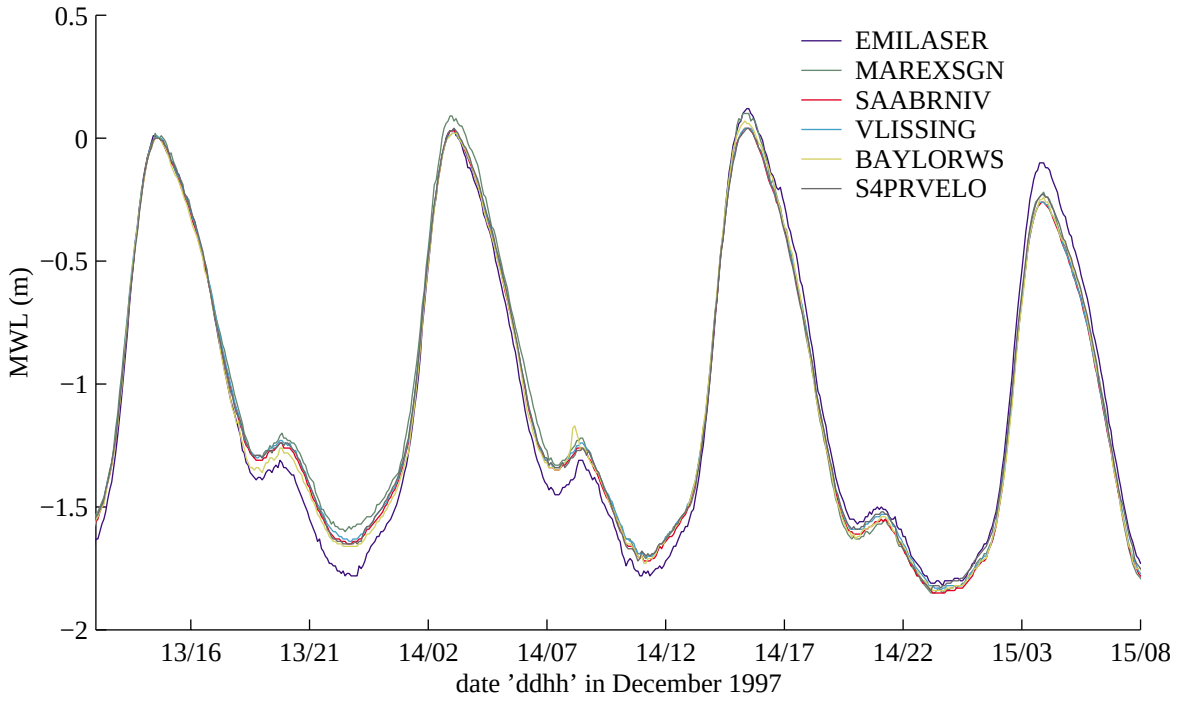

FIGURE 2.9 : Tidal effect

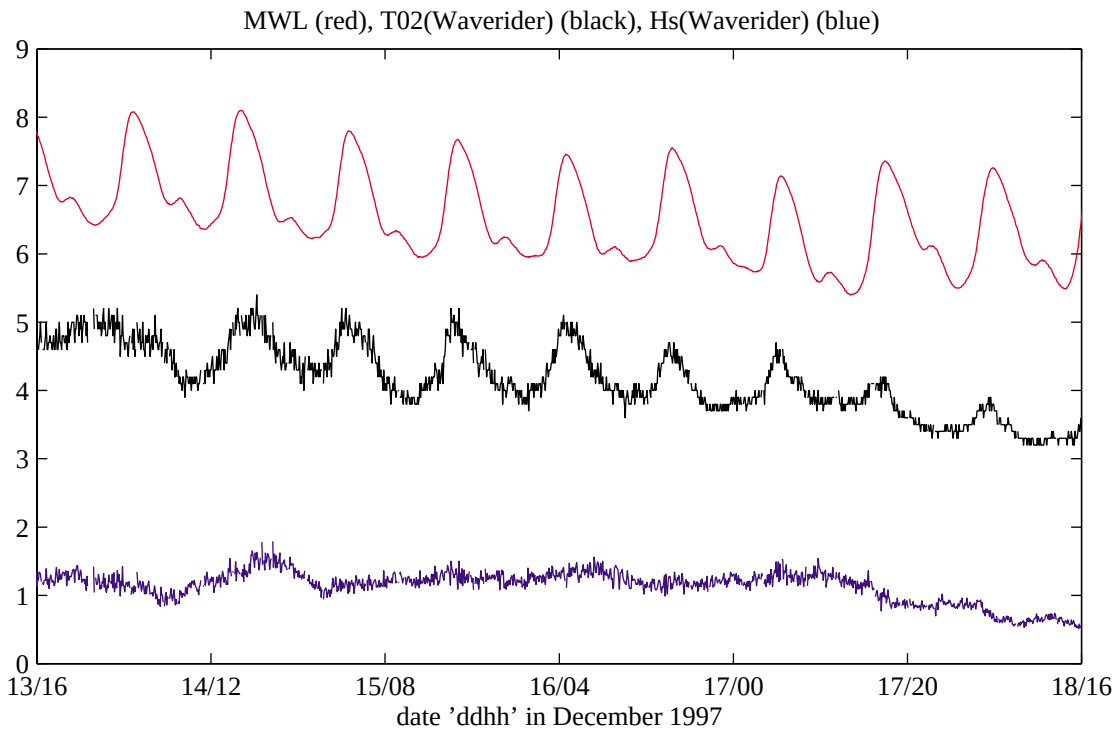

WACSIS Web site

To exchange information and data within the group of the WACSIS project, a Web site (http://www.ifremer.fr/ditigo/com/wacsis/) has been maintained on the Ifremer Web site. Some information about its content is given hereafter.

Contents

WACSIS Phase 1.

- Scope of work
- Reports

  WACSIS - Wave Crest Sensor Intercomparison Study at the Meetpost Noordwijk Measurement Platform
- Images

  Meetpost Noordwijk Measurement Platform
- Presentations

  Oceans'98 - Nice - September 1998 - Robert F. van Unen (OCN)

WACSIS Phase 2.

Scope of work

- Wacsis data base

  Wacsis common data base (see below for details)

  Wave Directional information (see below for details)

  Water depth (see below for details)

  Meteorological parameters (see below for details)
- Reports

  Second Order Models and Maximum Crest Heights - Harald E. Krogstad (NTNU)
- Presentations

  JIP Week - Houston - March 1999 - Marc Prevosto (Ifremer)

  JIP Week - Venice - October 1999 - Marc Prevosto (Ifremer)

  JIP Week - Houston - April 2000 - Harald E. Krogstad (NTNU)

  JIP Week - Paris - September 2000 - Harald E. Krogstad (NTNU)

  JIP Week - Paris - September 2000 - Harald E. Krogstad (NTNU)

  JIP Week - Paris - September 2000 - Harald E. Krogstad (NTNU)

  JIP Week - Paris - September 2000 - Marc Prevosto (Ifremer)
- Publications

  Wave Crest Distributions: Observations and Second Order Theory - George Z. Forristall (Shell E&P Technology)

WACSIS common data base

The selected data base of wave sensors measurements is gathered in a Common Data Base. It contents the data corresponding to:

- Vlissingen Step Gauge
- SAAB Radar Level Meter
- MAREX SO/5 Radar Level Meter

- Thorn EMI Laser
- BAYLOR Wave Staff
- Directional Waverider Buoy
- S4 Pressure and Particle Velocities sensor

It gives access to compressed files which contain the data files (see *Data files organization*, *Data files format*), a sea-state parameter file (see *Sea-state parameter file*) and a log file (see *Log file*).

Data files organization. The data files are organized in 4 directories:

- FSAMP0, corresponds to original data (without re-sampling)
- FSAMP4, re-sampling 4Hz
- FSAMP2, re-sampling 2Hz
- FSAMP1, re-sampling 1Hz

each of these directories are organized in a subdirectory **V** which contains all the files selected for the comparisons with the videos, a subdirectory **C** which contains all the files selected to complement the data base with time series with low steepness, and a main directory containing all the other selected time series.

The name of the files indicates the starting time of the time series in the format «yymmddhhmm».

Data files format. The files are ASCII files. The data are integers which gives in cm a value (or 3 values for the directional sensors) at each sampling time. The duration of the series is 20mn. The sampling frequencies are:

- FSAMP0:

  Vlissingen Step Gauge, 10Hz (12000 pts)
  SAAB Radar Level Meter, 5.12Hz (6144 pts)
  MAREX SO/5 Radar Level Meter, 4Hz (4800 pts)
  Thorn EMI Laser, 4Hz (4800 pts)
  BAYLOR Wave Staff, 4Hz (4800 pts)
  Directional Waverider Buoy, 1.28Hz (1536 pts) (VERTICAL disp. (positive up), NORTH_SOUTH disp., EAST_WEST disp.)
  S4 Pressure and Particle Velocities sensor, 2Hz (2400 pts) (NORTH_SOUTH velo.(cm/s), EAST_WEST velo.(cm/s), PRESSURE (cm)
- FSAMP4: For all sensors, 4Hz (4800 pts)
- FSAMP2: For all sensors, 2Hz (2400 pts)
- FSAMP1: For all sensors, 1Hz (1200 pts)

Sea-state parameter file. Sea-state parameters have been computed each 5mn from the original raw time series, the 4 parameters are:

- Mean Water Level (cm), (MWL)
- Significant Wave Height (cm), (H_s)
- Mean Period (s), (time version of T02)
- Maximum Crest Height (cm), (Cmax)
- Mean value of the north-south velocity (cm/s), (VN) (for the S4)
- Mean value of the east-west velocity (cm/s), (VE) (for the S4)

For the S4, MWL, Hs, T02, Cmax have been calculated directly on the pressure measurements, so MWL corresponds to the immersion of the sensor.

Two time values are added to these parameters:

- Hour (h), (number of hours since 01/01/1900)
- Minute (min.)

The files are ASCII files (param.dat). When the data was not available the value has been replaced by NaN. There are 6 (8 for the S4) columns:

- Hour Minute MWL H_s T_{02} C_{max} (V_N V_E)

The two first columns (time information) are exactly identical for all the sensors.

Log file. During the operation of extraction of time series from selected dates two problems occurred:

- For some sensors the data were not available (sensor out of order or acquisition problems), this is indicated in the log files by the date followed by a line of star symbols.
- During the operation of over-(under-)sampling the previous and following time series were used to eliminate leakage problems. If one of these files was missing (for the same reasons as previously) this is indicated in the log file by a line of date(s) beginning with the date of the current time series and the dates of the previous or (and) following time series which are unavailable or missing.

Directional Information

Directional information has been computed by SHELL starting from the Directional Waverider time series of the common data base, with the original sampling frequency (1.28Hz).

Data files organization. The files are organized in a subdirectory **V** which contains all the files selected for the comparisons with the videos, a subdirectory **C** which contains all the files selected to complement the data base with time series with low steepness, and a main directory containing all the other selected time series.

The spectral information has been computed on 1 hour, so the name of the files indicates the starting time of the time series in the format «yymmddhh».

Data files format. The files are ASCII files. There are 6 columns of data in each file. They are:

- Center frequency of spectral band (Hz)
- Power spectrum (m^2.sec)
- a1, first pair of Fourier coefficients
- b1, “
- a2, second pair of Fourier coefficients
- b2, ”
- Mean direction from which the waves travel (radians)
- Sigma, the rms wave spreading (radians)
- S1 - the exponent in a $\cos^{2s}$ spreading function, from first moments
- S2 - the exponent in a $\cos^{2s}$ spreading function, from second moments

Water depth

The water depth has been calculated from the mean values each 5 minutes of the Saab radar and the Vlissingen Step Gauge which give very close values. The mean value of the water depth all over the measurement campaign has been fixed to 18 meters. The parameters are:

- Water Depth (cm), (WaD)

Two time values are added to this parameter:

- Hour (h), (number of hours since 01/01/1900)
- Minute (min.)

The file is an ASCII file (water_depth.dat). When the data was not available the value has been replaced by NaN. There are 3 columns:

- Hour Minute WaD

The two first columns (time information) are exactly identical with the sea-state and meteorological parameters files.

Meteorological parameters

Meteorological parameters files have been generated from data measured each 10mn.The parameters are:

- Wind Speed (m/s), (WC10)
- Wind gust (m/s), (WG3)
- Air Pressure (daPa), (PQFF)
- Wind Direction (^{o}), (WD10)
- Air Temperature (^{o}C), (T10)
- Relative Humidity (%), (U10)

Two time values are added to these parameters:

- Hour (h), (number of hours since 01/01/1900)
- Minute (min.)

The file is an ASCII file (meteo.dat). When the data was not available the value has been replaced by NaN. There are 8 columns:

- Hour Minute WC10 WG3 PQFF WD10 T10 U10

The two first columns (time information) are exactly identical with the sea-state and water depth parameters files.

Appendix 2.1: WACSIS Common Database

WACSIS Common Database

EMI Laser, SAAB Radar, VLISSINGENBAAK Step Gauge,

Marex Radar, Directional WAVERIDER, Baylor Wave Staff, S4

- **6 months of continuous measurements**
  - **-> 6 binary files** **(Raw measurements)**
- **Raw measurements**
  - **-> 10,000 binary files (20mn)** **(Raw time series)**
  - **-> 1 ASCII file of sea-state parameters** **(SSSP time series)**
    - **MWL,H_s,T_{02},C_{max} calculated on 5 minutes**
- **Raw time series + SSSP time series (MWL)**
  - **Re-sampling (4Hz, 2Hz, 1Hz) and detrend (tide+surge+offset)**
  - **-> 100 hours = 300 ASCII files** **(HHS time series)**
    - **High Hs Selected time series**
  - **-> 20 hours = 60 ASCII files** **(LSS time series)**
    - **Low Steepness (<.04) Selected time series**

WACSIS Common Database = SSSP + HHS + LSS time series

CHAPTER 3

Height-Period Joint Distributions

S. Van Iseghem

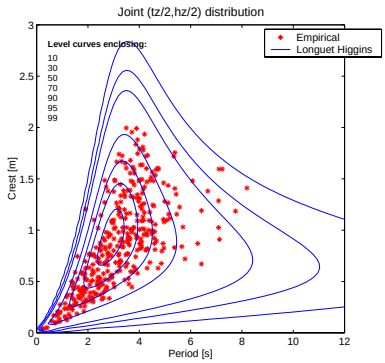

We will analyse in this chapter, the joint wave height - wave period and the joint wave height - wavelength distributions. They are of both theoretical and practical interest since the distribution of wave steepness in particular can be derived from it.

Can those joint distributions be accurately estimated for a given sea state from which some information is known? If so, what information is needed?

Some models have been established. Since they are based on different wave definitions, the first part of this chapter is devoted to the definitions of those wave parameters. The description of their corresponding modelling is presented in the second part.

The accuracy of those models will be tested on two sea states 40 minutes long. For each sea state, estimated distributions will be compared to the corresponding empirical ones.

Most of results have been obtained by using the Matlab Toolbox Wave Analysis for Fatigue and Oceanography WAFO which has been developed in Lund University [2] [23].

The computing time has been tested on a computer ALPHA 400Mhz, 1Giga Memory.

Definitions

Wave height and period

Wave height and period can be defined in different ways. The two currently popular definitions are used in this report.

The first one is the down-crossing definition (see figure 3.1). The down-crossing height h_z is the maximum vertical distance between adjacent down crossings at the reference level. Note that in this report the reference level corresponds to the most often crossed level. The period t_z is the time between adjacent down crossings.

The second definition is the crest-to-crest wave (see figure 3.1). The wave height h_c is the vertical distance from a local maximum to the following local minimum. The wave period t_c is the time from this maximum to the following local maximum.

The third definition we use is crest height and period. The height h_{Ac} is the maximum vertical distance between the up-crossing and the following down-crossing. The period t_{Ac} is the time between this up-crossing and the following down crossing.

In order to make those joint densities comparable, we will analyse

- (1) $(h_z/2, t_z/2)$
- (2) $(h_c/2, t_c/2)$
- (3) (h_{Ac}, t_{Ac})

It is sometimes assumed that the distribution of (1) and (2) are comparable but this is only true for very narrow band spectra.

FIGURE 3.1 : Definition of empirical wave height and period

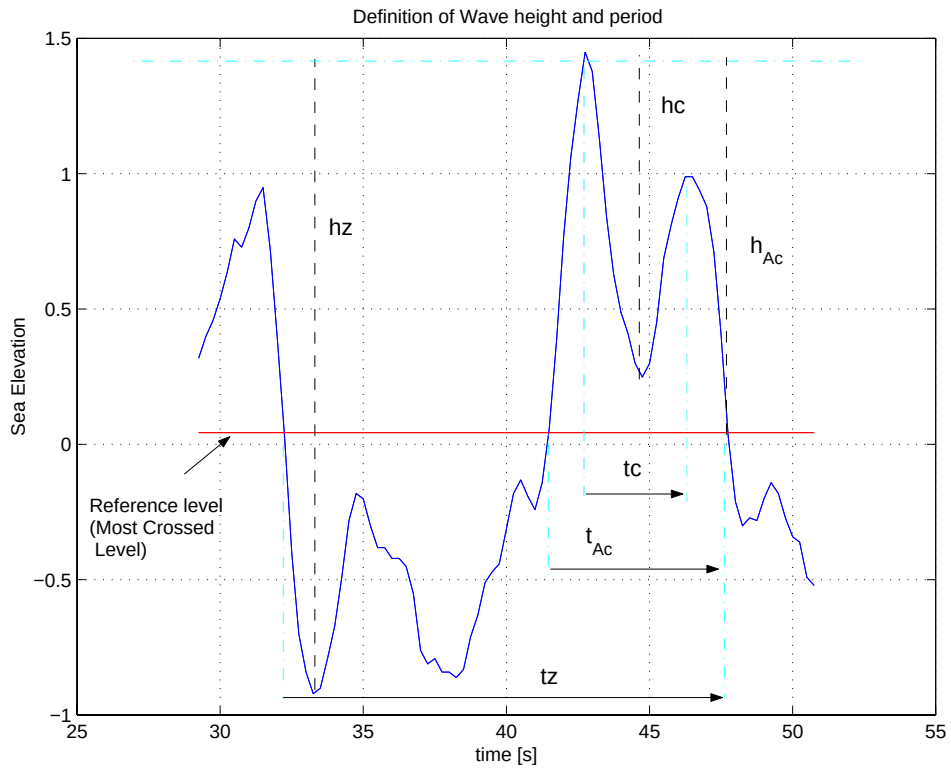

Estimation of wave height and period density

The three theoretical estimates we have studied described by Cavanié (1976) [3], Longuet-Higgins (1983) [14] and Lindgren and Rychlik (1982) [13], which will be called the Lund model in this study.

Model by Longuet-Higgins

Longuet-Higgins [14] derives his distribution by considering the joint distribution of the envelope amplitude and the time derivative of the envelope phase. The model

is based on the narrow band approximation and the estimated density can then be compared to the (1) ($h_z/2,t_z/2$) empirical distribution.

The spectral width parameter is defined as:

$$\nu = \sqrt{\frac{m_0 m_1}{m_1^2} - 1} \qquad \text{(EQ 3.1)}$$

and the model is given by:

$$f^{LH}_{T_c, A_c}(t, a) = C_{LH}\left(\frac{a}{t}\right)^2 \exp\left(-\frac{a^2}{8}(1 + \nu^{-2}(1 - t^{-1})^2)\right) \qquad \text{(EQ 3.2)}$$

with

$$C_{LH} = \frac{1}{8}(2\pi)^{-0.5}\nu^{-1}(1 - (1 + \nu^2)^{-0.5})^{-1} \qquad \text{(EQ 3.3)}$$

Model by Cavanié *et al.*

Cavanié [3] proposes an explicit formula depending on ν and the bandwidth parameter

$$\varepsilon = \sqrt{1 - \frac{m_2^2}{m_0 m_4}} \qquad \text{(EQ 3.4)}$$

Here any positive local maximum is considered as a crest of a wave, and then the second derivative (curvature) of the local maximum defines the wave period by means of a cosine function with the same height and curvature.

For a narrow band process, ε is near 0, the Cavanié distribution is given by:

$$f^{CA}_{T_c, A_c}(t, a) = C_{CA}\left(\frac{a^2}{t^5}\right)\exp\left(-\frac{a^2}{8\varepsilon^2 t^4}\left(\left(t^2 - \frac{1-\varepsilon^2}{1+\nu^2}\right)^2 + \beta^2\frac{1-\varepsilon^2}{1+\nu^2}\right)\right) \qquad \text{(EQ 3.5)}$$

with

$$C_{CA} = \frac{1}{4}(1 - \varepsilon^2)(2\pi)^{-0.5}\varepsilon^{-1}\alpha_2^{-1}(1 + \nu^2)^{-2} \qquad \text{(EQ 3.6)}$$

and (EQ 3.7)

$$\alpha_2 = \frac{1}{2}(1 + (1 - \varepsilon^2)^{0.5})$$

$$\beta = \frac{\varepsilon^2}{1 - \varepsilon^2} \qquad \text{(EQ 3.8)}$$

This model corresponds to the (2) ($h_c/2,t_c/2$) empirical distribution.

Lindgren and Rychlik model

G. Lindgren and I. Rychlik have developed a theory for evaluating the joint distribution of height and period for Gaussian waves given the covariance function of the process [18] [23].

The joint distribution that we will estimate with the model is the joint (3) (h_{Ac},t_{Ac}) distribution.

As it is known that the measured data often exhibit asymmetry between crests and troughs, the data are analysed by using the transformed Gaussian model for which it is assumed that

$$W(t) = G(X(t)) \quad \text{(EQ 3.9)}$$

where $X(t)$ is a Gaussian process with some spectrum $S(\omega)$ and G is some invertible non-random function.

The transformed Gaussian models are particularly convenient for the computations of the distributions of the wave characteristics.

There are many ways of choosing the transformation G. Here we will follow the non parametric approach proposed in Rychlik *et al.* (1997) [22]. We also could have used some of the parametric functions proposed in the literature (see Winterstein [29] or Ochi *et al.* [17]).

Data description

Results presented in this report are relative to the Baylor wave staff sensor. Joint wave height period distributions have been analysed for two sea states 40 minutes long.

The choice of sea states has been made with respect mainly on the basis of Hs and ν: For two sea states with Hs big enough, the first one has been chosen with a broad banded spectrum and the other with a narrower one (as narrow as we could find in the Wacsis data base).

The spectrum used is the non smoothed periodogram (S1) with cut-off frequency 4 rad/s, see figures 3.2 and 3.3. The sensitivity of the model to the exact shape of the spectrum has been tested by using the smoothed periodogram (S2) (smoothed by using a Parzen window function on the estimated autocovariance function) or the JONSWAP spectrum (S3) defined by parameters Hs, T_{02} and γ. γ is approximated with the following equations:

$$\gamma = \exp\left(3.484\left(1 - 0.1975 D \frac{T_p^4}{H_{m_0}^2}\right)\right) \quad \text{(EQ 3.10)}$$

with

$$D = 0.036 - 0.0056 \frac{T_p}{\sqrt{H_{m_0}}} \quad \text{(EQ 3.11)}$$

The two sea states are described in the tables 3.1 and 3.2.

TABLE 3.1 : Sea State 1 Characteristics: Date 98/03/01/12:00

Nb Waves (h_z,t_z)	Nb Waves (h_c,t_c)	Nb Waves (h_{Ac},t_{Ac})	Hs (m)	$T_{02\ (s)}$	ν	ε
374	**604**	**374**	**2.95**	**6.8**	**0.47**	**0.71**

TABLE 3.2 : Sea State 2 Characteristics: Date 98/01/05/08:00

Nb Waves (h_z,t_z)	Nb Waves (h_c,t_c)	Nb Waves (h_{Ac},t_{Ac})	Hs (m)	$T_{02\ (s)}$	ν	ε
394	648	394	3.5	6.0	0.35	0.63

FIGURE 3.2 : Spectrum for sea state 1

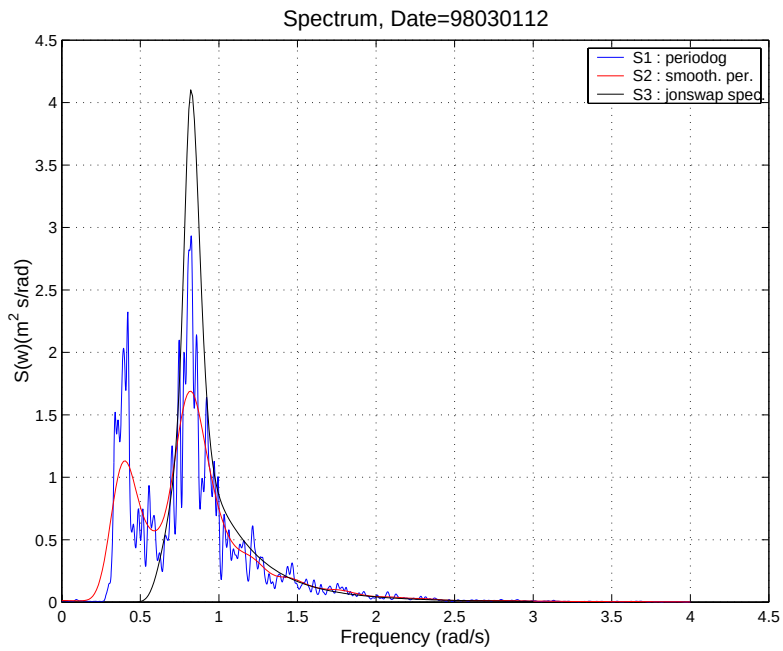

FIGURE 3.3 : Spectrum for sea state 2

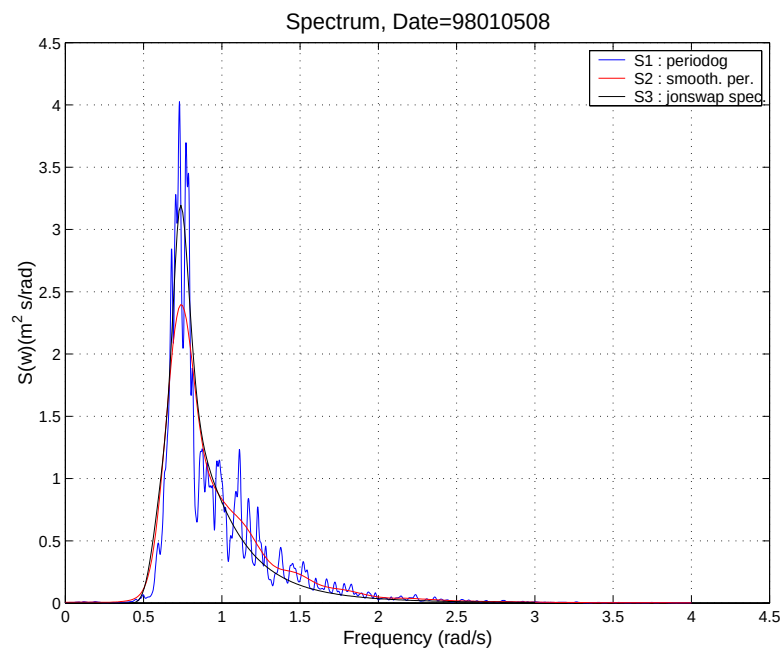

Sea State 1

Empirical wave (crest) height-period

Large differences can be observed between the 3 empirical distributions (1) $(h_z / 2, t_z/2)$, (2) $(hc/2, t_c/2)$ and (3) (h_{Ac}, t_{Ac}), see figures 3.4, 3.5 and 3.6.

The distribution (3) (h_{Ac}, t_{Ac}) has bigger crests than (1) (h_z, t_z) and (2) (h_c, t_c). The median of both crests and period distribution from (2) are smaller than the one from distributions (1) and (3). The variance of distribution (3) is larger than the 2 other ones, especially for periods.

Estimation of wave height-period with parametric models.

Half wave heights are well approximated by the two parametric models, see figures 3.7 and 3.8.

Periods are not well approximated. Small periods (<3s) are underestimated by both models. The Longuet Higgins approximation overestimates large periods (>6s).

The wave steepness is overestimated by both models.

Estimation of crest height-period (3) (h_{Ac}, t_c) with parametric models.

Parametric models do not fit the (3) (h_{Ac}, t_c) distribution because of small periods which are underestimated, see figure 3.9.

FIGURE 3.4 : Comparison of the 3 height-period distributions

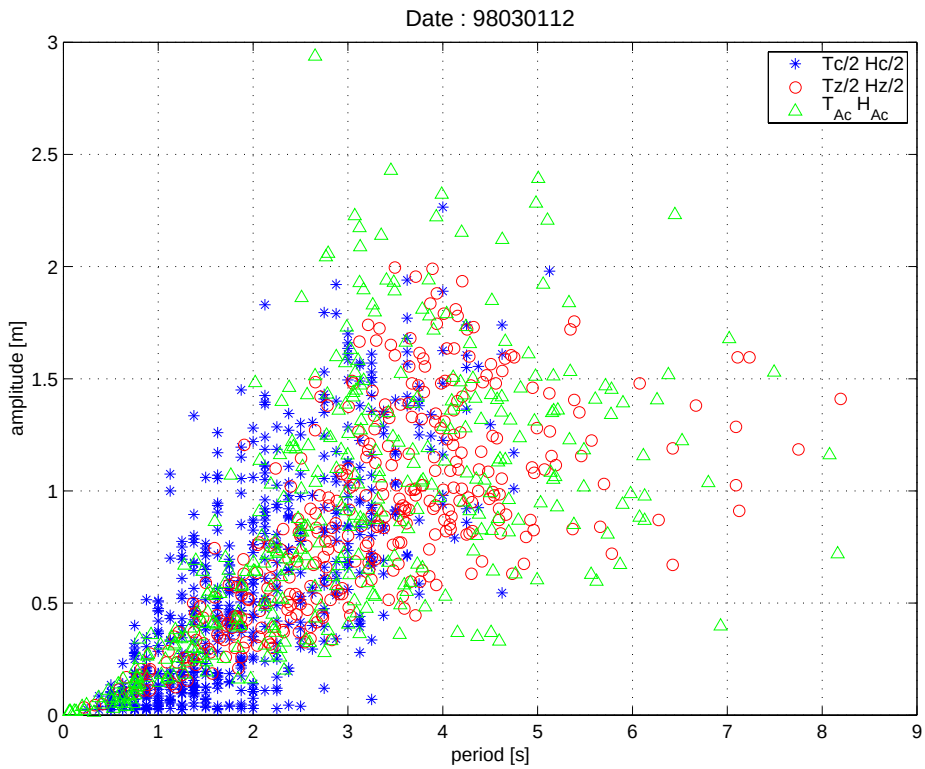

FIGURE 3.5 : Empirical crests for H_{Ac} > 0.5 m

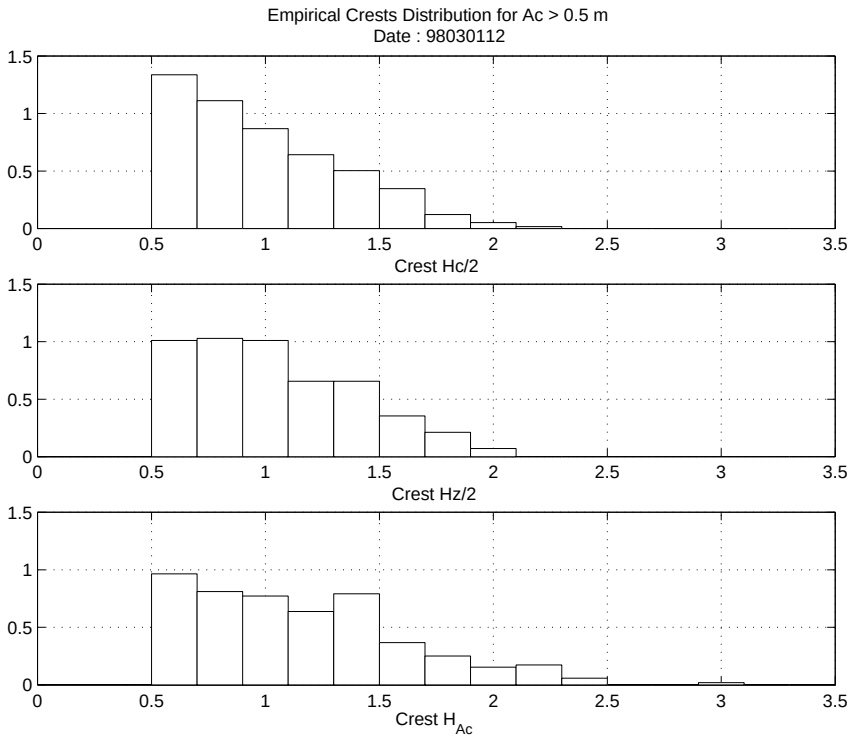

FIGURE 3.6 : Empirical periods for H_{Ac} > 0.5 m

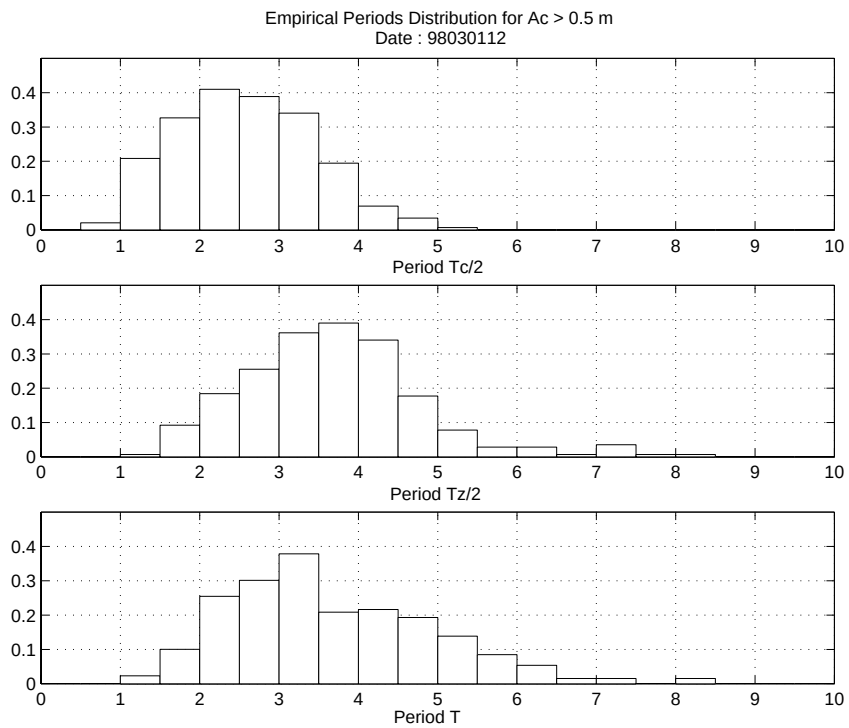

FIGURE 3.7 : Longuet-Higgins estimation of (1) (hz/2,tz/2)

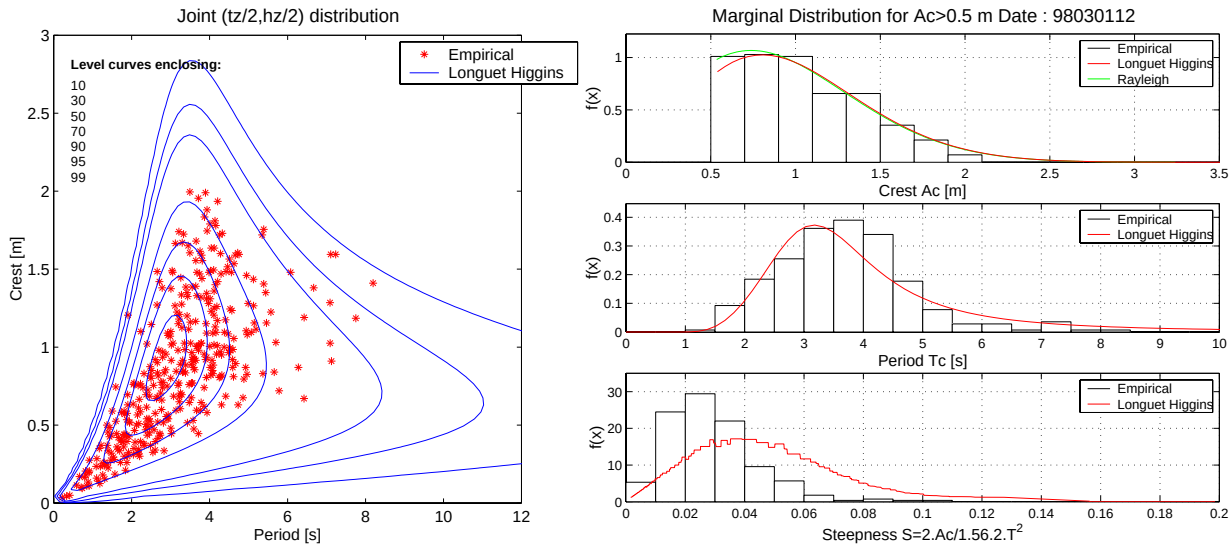

FIGURE 3.8 : Cavanié estimation of (2) (hc/2,tc/2)

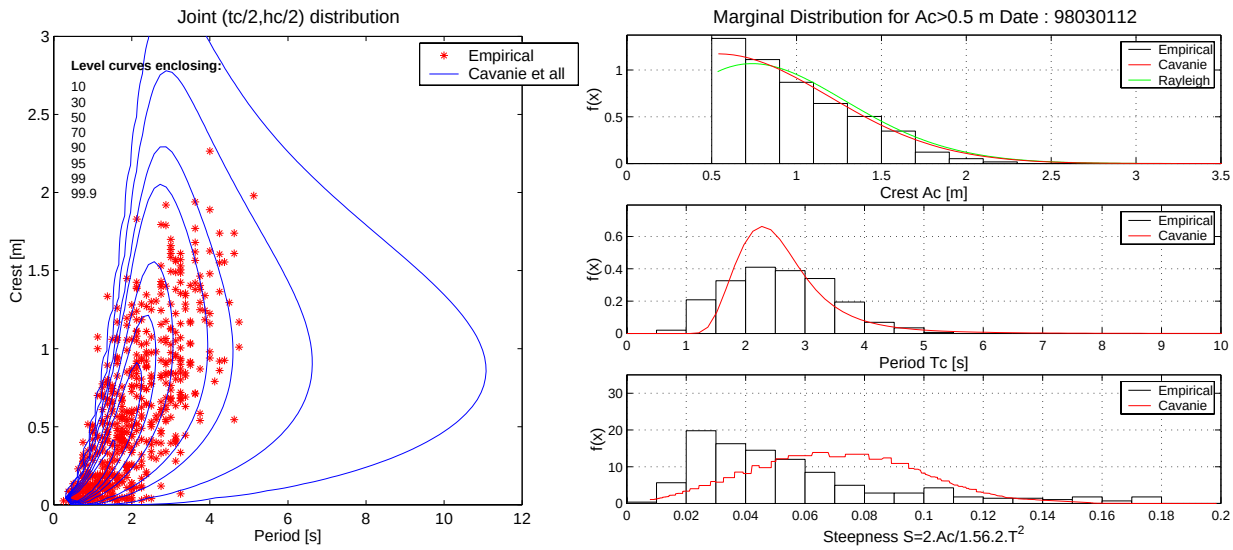

The *g* transformation (see “Lindgren and Rychlik model”, page 23) is useful to respect the asymmetry between crests and troughs. Effects of this transformation are shown in figure 3.10; it increases the estimated crests in both models, and the fit of the parametric model to the marginal crest distribution is then improved. Estimated periods are not affected by this transformation.

Estimation of crest height-period (3) (h_{Ac},t_c) with Lund model.

The Lund model is very accurate even for small crests, see figure 3.11.

Marginal estimates of both crests and periods deduced from the joint estimation are presented in figures 3.12 and 3.13. They both fit very well the empirical distributions of crests and periods. Marginal crest distributions are compared to the transformed Rayleigh distribution. The transformation g used, see page 23, is the non linear one.

The steepness estimation fits the corresponding empirical distribution well, see figures 3.12 and 3.13.

FIGURE 3.9 : Estimation of (3) (h_{Ac},t_c) with parametric models

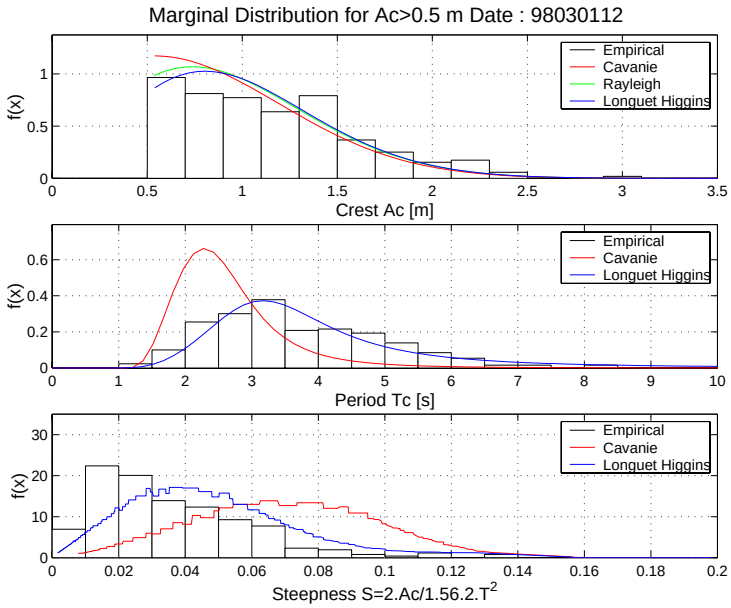

FIGURE 3.10 : Estimation of (3) (h_{Ac},t_c) with transformed parametric models

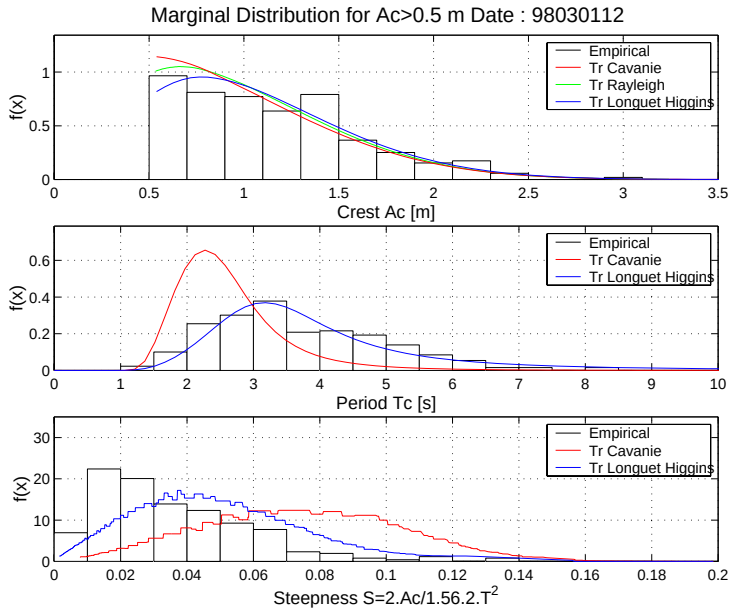

The spectrum used is the non smoothed periodogram. The estimate is computed for a specified number of points in a grid [crest periods] * [crest heights]. We denote by T=[0 11 41], H=[0 3.5 31] the grid with 41 values of periods equally spaced between 0 and 11 seconds and 31 values of crest heights between 0 and 3.5m. This notation is also used later in the report

To get the following approximation, the grid we have chosen is T=[0 11 41], H=[0 3.5 31]. The time required is 700s. NIT equals 1. The parameter NIT defines the dimensionality of the computed integral.

Accuracy could be increased by increasing NIT but the computing time would be longer.

FIGURE 3.11 : Estimation of (3) (h_{Ac},t_c) with Lund model

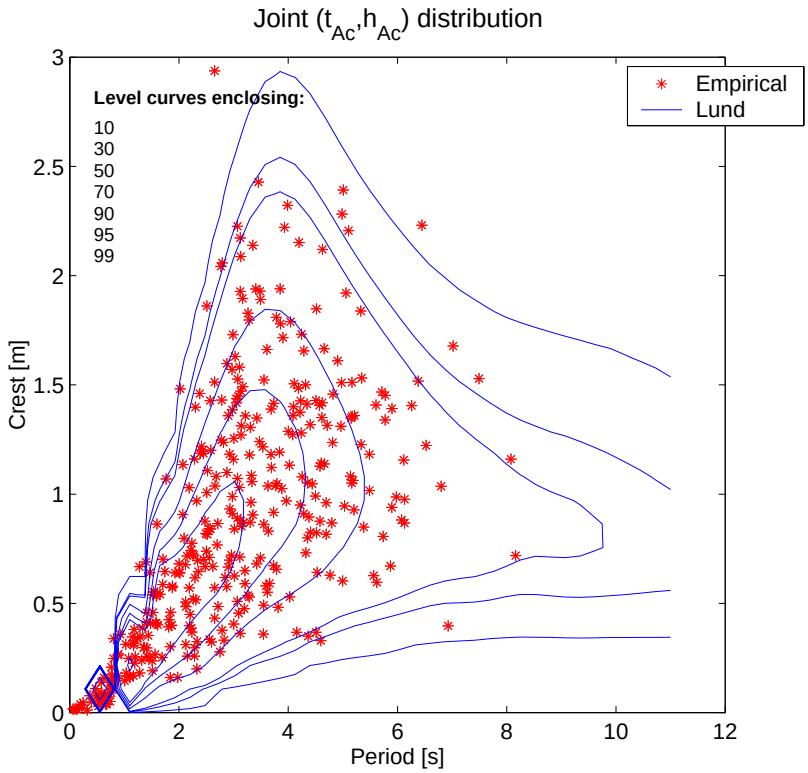

FIGURE 3.12 : Estimation from the joint distribution, (fig 3.11) for all A_c

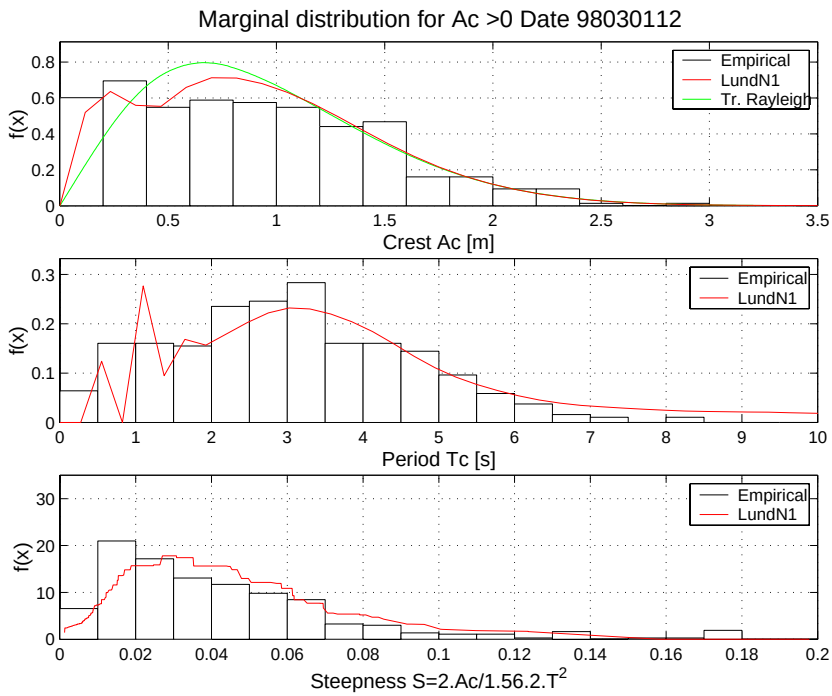

FIGURE 3.13 : Estimation from the joint distribution, (fig 3.11) for A_c > 0.5m

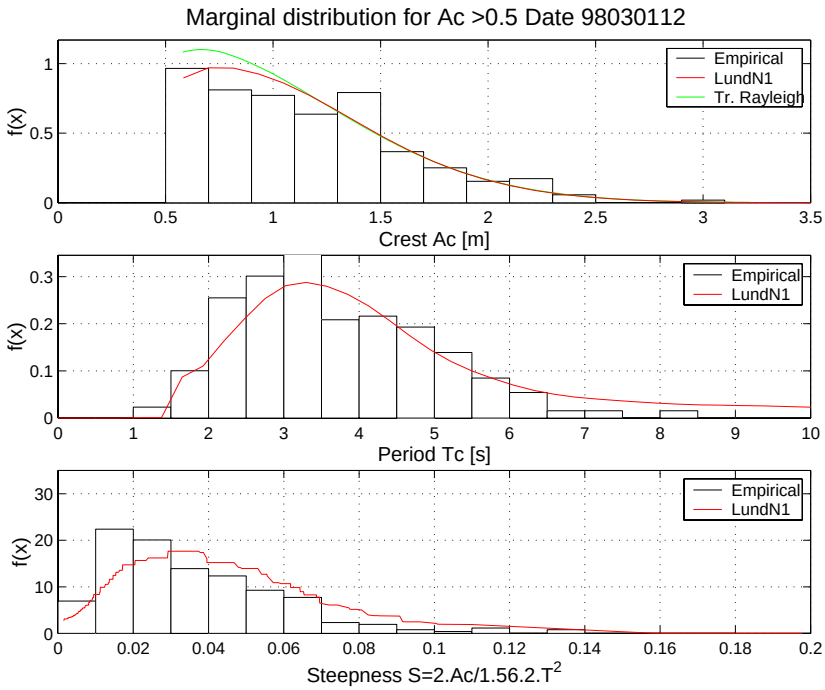

To reduce further the computing time, the estimate has been computed with different grids and different values of thresholds.

Computation for A_c > h: T=[0 11 41], (see notation page 29)

(1) H=[0 3.5 31] Computing time: 700s
(2) H=[0.5 3.5 31] Computing time: 785s
(3) H=[0.5 3.5 21] Computing time: 538s
(4) H=[1 3.5 21] Computing time: 576s
(5) H=[1 3.5 11] Computing time: 304s

If the crests of interest are bigger than 1m, an accurate estimation of the joint (3) (h_{Ac},t_c) can be obtained in 5min.

In order to see whether the time required could be reduced again by using a simpler spectrum shape or an other *g* transformation, the sensitivity of the Lund model is analysed.

Sensitivity: The three spectra we consider are the non smoothed periodogram (S1), the smoothed periodogram (S2), the Jonswap spectrum (S3). It is important to note that for this sea state, the Jonswap spectrum does not represent the second peak, which is non negligible in the real spectrum.

The marginal period distribution is dependent on the exact spectral shape and the cut-off frequency, see figure 3.14. The marginal crest distribution is not.

The two g transformations considered in figure 3.15 are the linear one, and the non linear and non parametric one (see “Lindgren and Rychlik model”, page 23).

The use of parametric *g* transformation has not been tested for the moment.

FIGURE 3.14 : Lund Model: Sensitivity to the exact spectral shape

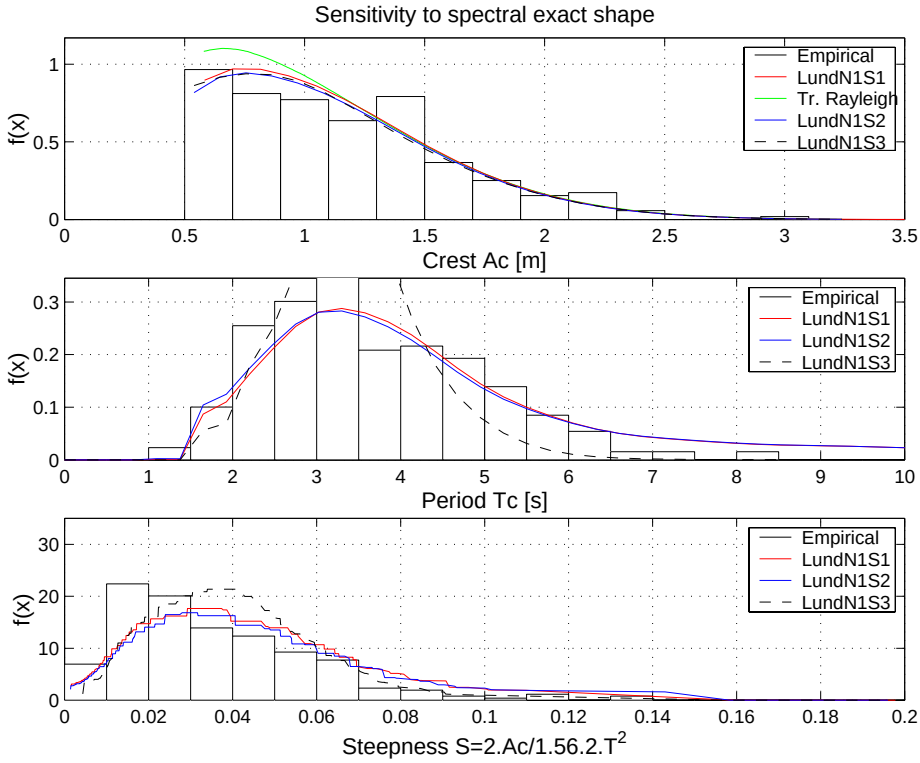

FIGURE 3.15 : Lund Model: Sensitivity to the *g* transformation

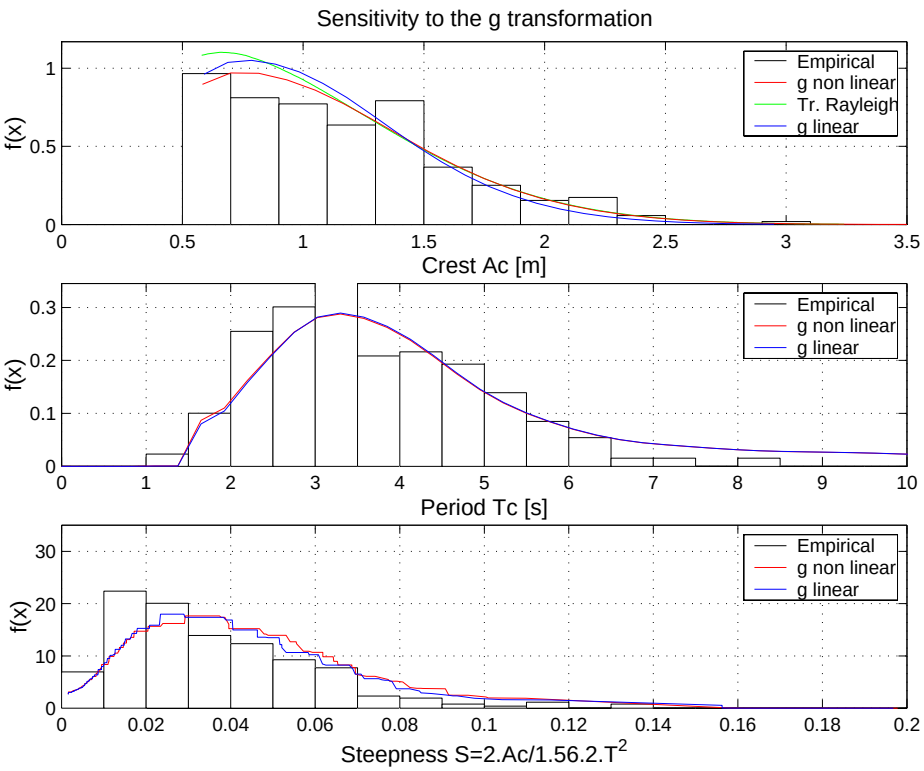

The use of the Jonswap spectrum for this sea state does not lead to accurate results. A parametric spectrum could be used but it has to reproduce the double peak of this spectrum.

Results with a suitable parametric spectral shape:

Both models from Guedes Soares [8] and Occhi Hubble [16] have been tested to approximate the double peak spectrum. The fitted spectral shapes are presented on figure 3.16.

As can be observed on figure 3.17, the estimation of (3) (h_{Ac},t_c) remains accurate if a parametric spectrum, estimated either with the Guedes Soares or with the Ochi Hubble model are used. For this sea state the results obtained with the spectrum fitted with Guedes Soares model are slightly better than the one obtained with Occhi Hubble model

Estimation of crest height - wavelength (4) (h_{Ac},L_c)

The empirical crest lengths L_c are obtained from the spatial spectrum. The height h_{Ac} is the maximum vertical distance between the up-crossing and the following down-crossing. The crest length L_{Ac} is the distance between this up-crossing and the following down-crossing. The empirical crest lengths TL_c are deduced from the periods by applying the dispersion relation.

Figures 3.18 and 3.19 present the two empirical wavelength distributions. There are no large differences between those two distributions.

There are two ways of getting an estimate of the joint distribution (4) (h_{Ac},L_c):

1. the estimate is computed from a spatial spectrum.

2. the estimate is deduced from the estimate of (3) (h_{Ac},t_c) using the dispersion relation.

The only model considered for this joint crest height - crest length distribution is Lund model.

Estimate from spatial spectrum:

The accuracy of the Lund Model in estimating the distribution (4) (h_{Ac},L_c) is not as good as the estimate (3) (h_{Ac},t_c), see figure 3.20.

To get this estimate, the grid was L=[0 100 41], H=[0 3.5 31], the parameter NIT equaled 3, and the time required is 25000s. If we take NIT equals 2, the time is 4800s but the fit is not as good.

The parameter NIT defines the dimensionality of the computed integral. Higher NIT is required to get approximations of long waves, but that also takes long computing time. The problem is that we keep high frequencies in the spectrum and then it would be best to use different grids in different regions since the density is almost singular (small L_c and A_c are difficult to integrate).

The time required is too long to make this estimate operational.

This situation could be improved in three ways; first, compute the joint density (L_c,A_c) for a limited region, compute only the marginal wavelength distribution, or cut off high frequencies in the spectrum.

FIGURE 3.16 : Fitted Spectral Shape

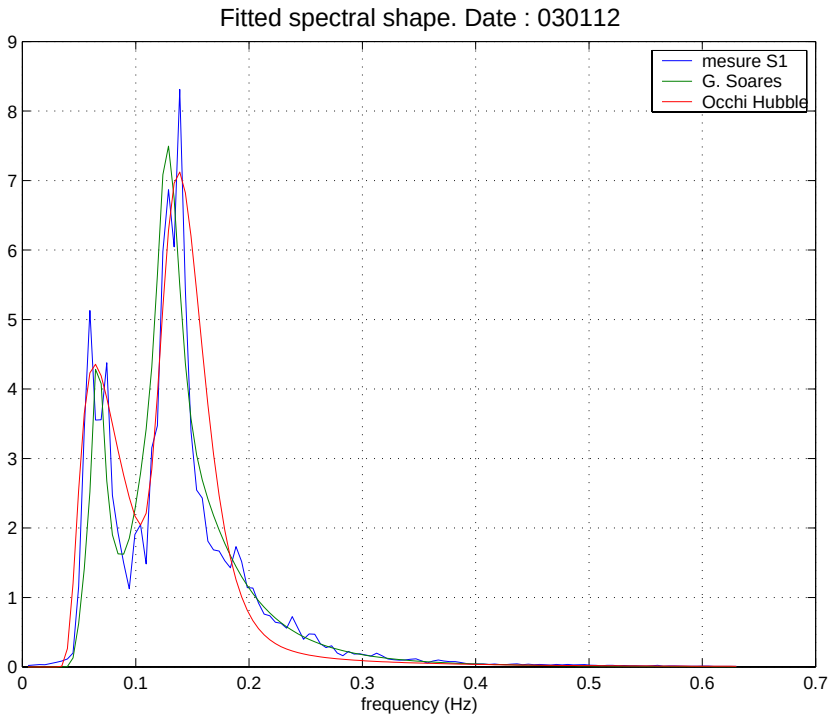

FIGURE 3.17 : Results with the fitted spectral shape

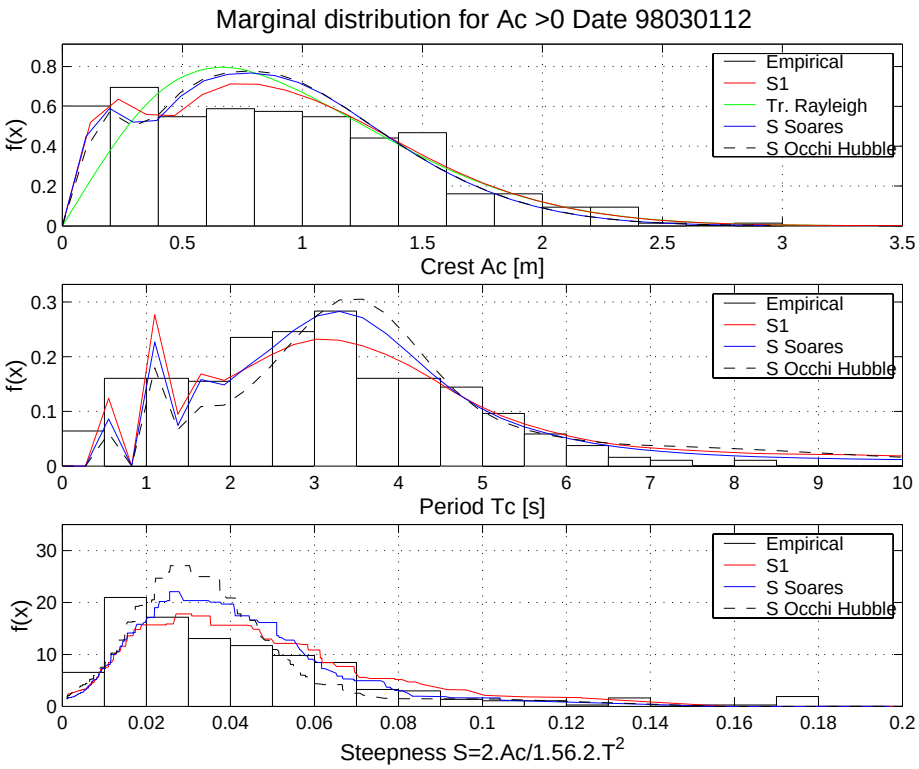

FIGURE 3.18 : Empirical wavelength distribution

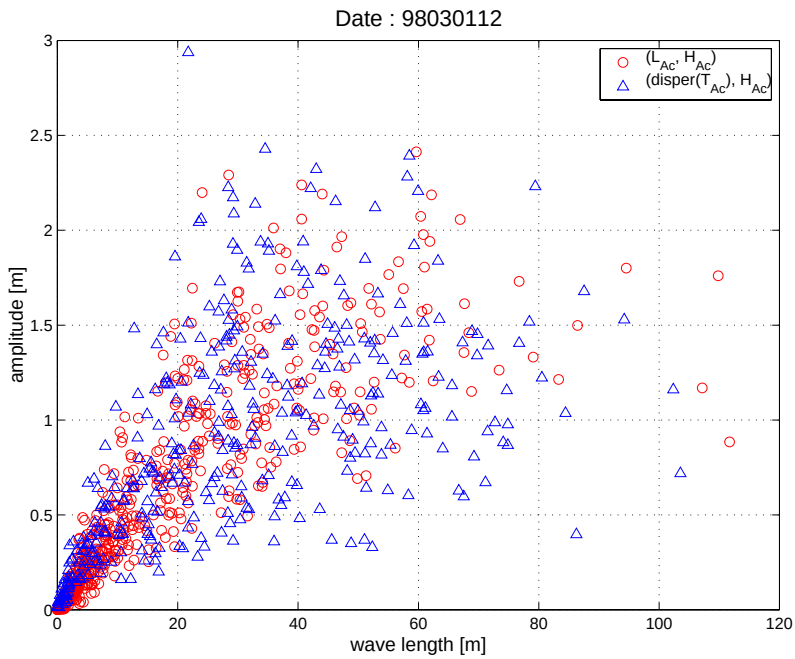

FIGURE 3.19 : Marginal empirical wavelength distribution, for Ac>0.5m

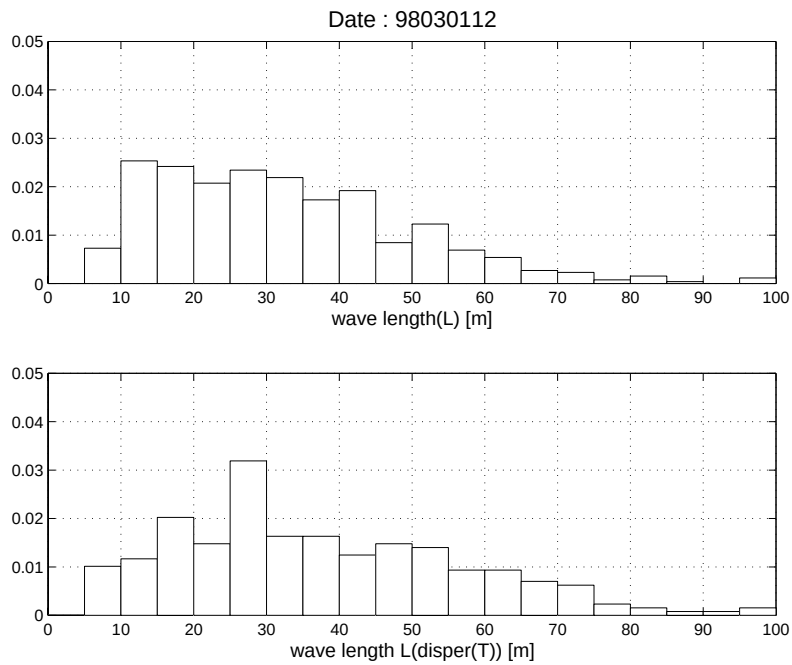

Compute only the marginal wavelength distribution: The marginal crest length distribution can be very well approximated by Lund model.

Figure 3.21 presents the sensitivity of the model to the grid considered, see the note on page 29.

Case 1. grid L=[0 120 81], time required 4300s and the accuracy is very good even for small crests (figure top and bottom left).

Case 2. grid L=[0 20 81], time required 435. This estimate is only relative to small crests but that shows how accurate the model can be (figure bottom right).

Case 3. grid L=[0 120 41], time required 972s, the accuracy is not good for small crests (figure top right).

FIGURE 3.20 : Estimation of wavelength from spatial spectrum

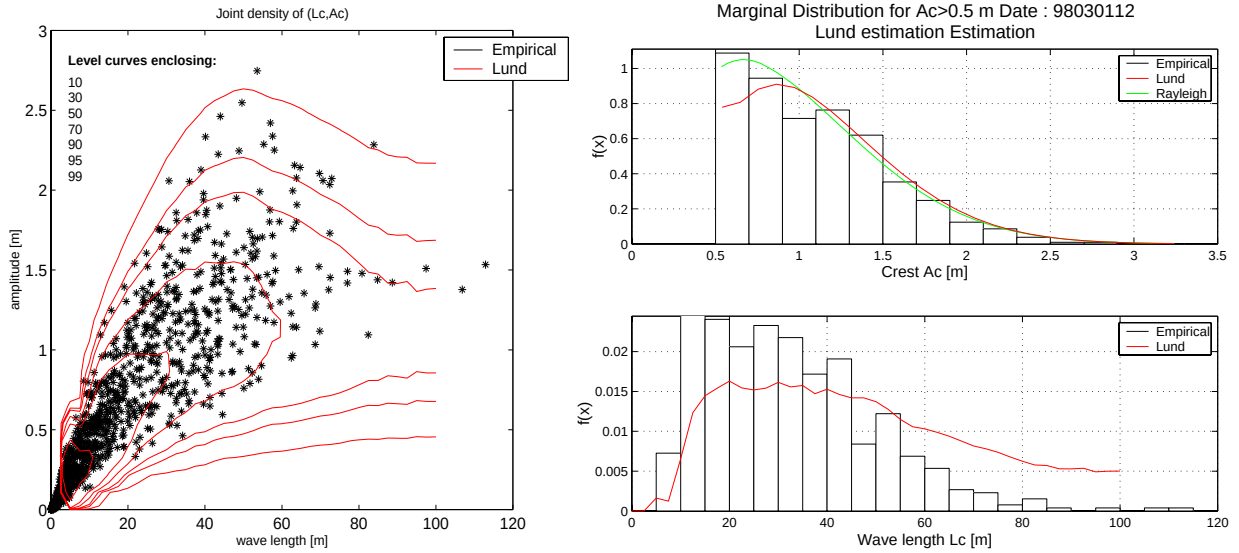

FIGURE 3.21 : Marginal wavelength distribution

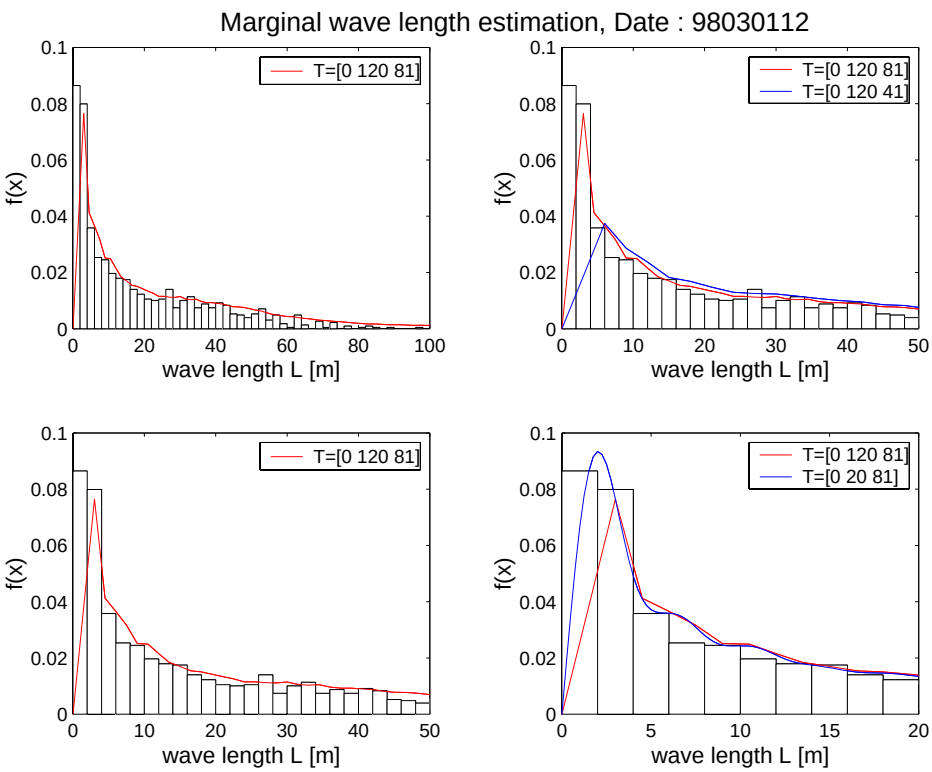

In case 3, the time consumed, 972s, is satisfactory but the small crests are not well estimated. If small crests can be neglected, it will be suitable to cut off high frequency in the spectrum to decrease computing time.

Cut off high frequency in the spectrum: The spectrum S1 has been cut to 2.5 Rad/s (Scut), and the empirical density is calculated on the non filtered data. Figure 3.22 presents the results:

- top figure: estimation with Scut: no difference depending on the grid.
- bottom figure: estimation with the large grid and S1 and Scut: for wavelengths longer than 40m. The difference is not important.

FIGURE 3.22 : Cut off high frequency in the spectrum

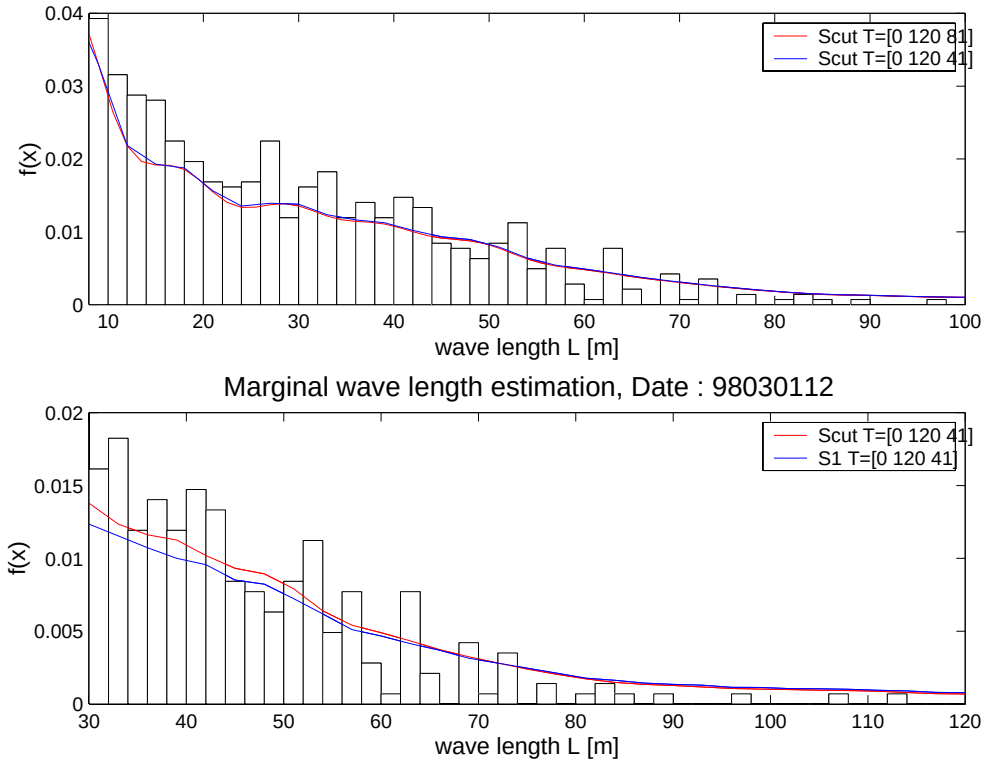

Since the time required by using Scut spectrum is less important, it is more suitable to use it. A very accurate estimation of wavelengths between 10 and 120m can be obtained in 800s.

As we said before, the joint estimate of (4) (h_{Ac},L_c) with the Lund model is not as accurate and as fast as for (3) (h_{Ac},t_{Ac}). Nevertheless a very accurate model can be obtained with a satisfactory time consumption for the marginal wavelength distribution. If small crests can be neglected, this time can be reduced by cutting high frequencies in the spectrum.

Estimate deduced by using dispersion relation

The estimate obtained from the estimate we had for (3) (h_{Ac},t_{Ac}) by using the dispersion relation gives satisfactory results, see figure 3.23. Large wavelengths are slightly overestimated.

The important advantage of this method is that it does not require extra computing time if the estimation of (3) (h_{Ac},t_{Ac}) has been computed.

Comparison between the two methods

Comparison of the two estimates of (4) (h_{Ac},L_c), computed from the spatial spectrum or deduced from the estimate we had for (3) (h_{Ac},T_{Ac}) are presented on figures 3.24 and 3.25.

FIGURE 3.23 : Estimation of wavelength deduced from estimated period *T*

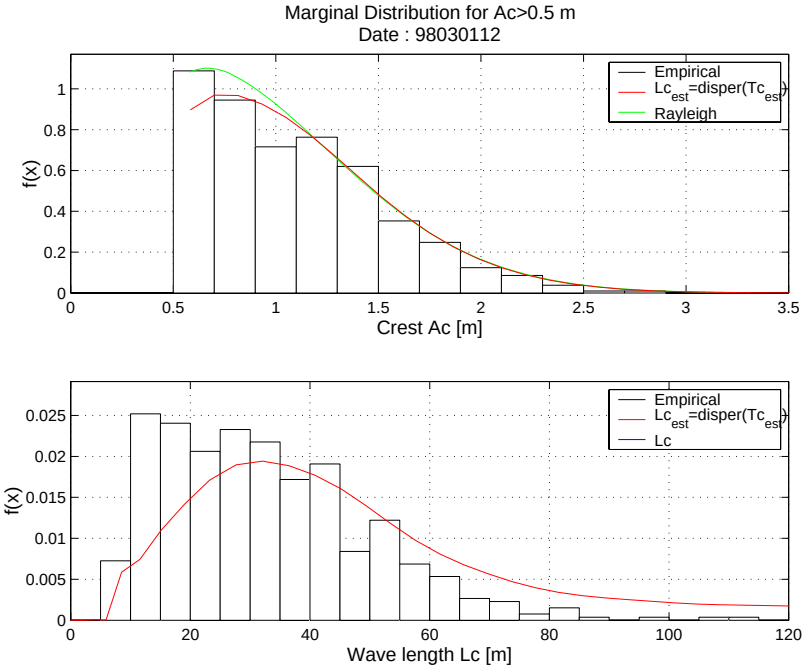

The estimate of (4) (h_{Ac},L_c) deduced from the one obtained for (3) gives satisfactory results and does not require more computer time than the one needed to estimate (3) (h_{Ac},T_{Ac}).

The estimate obtained from the spatial spectrum is not as good but it is important to note that this estimate could be much more accurate if the parameter NIT (see “Estimate from spatial spectrum:”, page 33) was increased. Some further tests need to be done to keep the computing time reasonable.

Conclusion relative to sea state 1

The joint (3) (h_{Ac},t_{Ac}) has been well approximated by the Lund model with a satisfactory time of 700s. Estimates are very accurate with the use of the non smoothed periodogram and the non parametric *g* transformation. The estimate remains accurate if a suitable parametrized spectrum is used but care needs to be taken with the spectral estimate as the joint distribution (3) (h_{Ac},t_{Ac}) is very dependent on it.

The joint distribution (3) (h_{Ac},t_{Ac}) is then accurately estimated for this sea state from the reduced parameters used in the spectral modelling.

To get a fast estimate of (4) (h_{Ac},L_c), it is advisable for the moment to deduce the estimate from the estimate we had for (3) using the dispersion relation. By using this method, the accuracy is good even if large wavelengths are slightly overestimated. The time required is the same as the time required to get the estimate of (3) (h_{Ac},t_{Ac}), i.e. 700s.

With the model using the spatial spectrum, the estimate can be computed with the desired high accuracy but the time required for the moment can be very long and sometimes un-acceptable for a laptop computer.

Some ways to get high accuracy with acceptable computation time are to compute only marginal densities or to cut off high frequencies in the spectrum.

FIGURE 3.24 : Estimation of (4) (h_{Ac},L_c) with the 2 methods

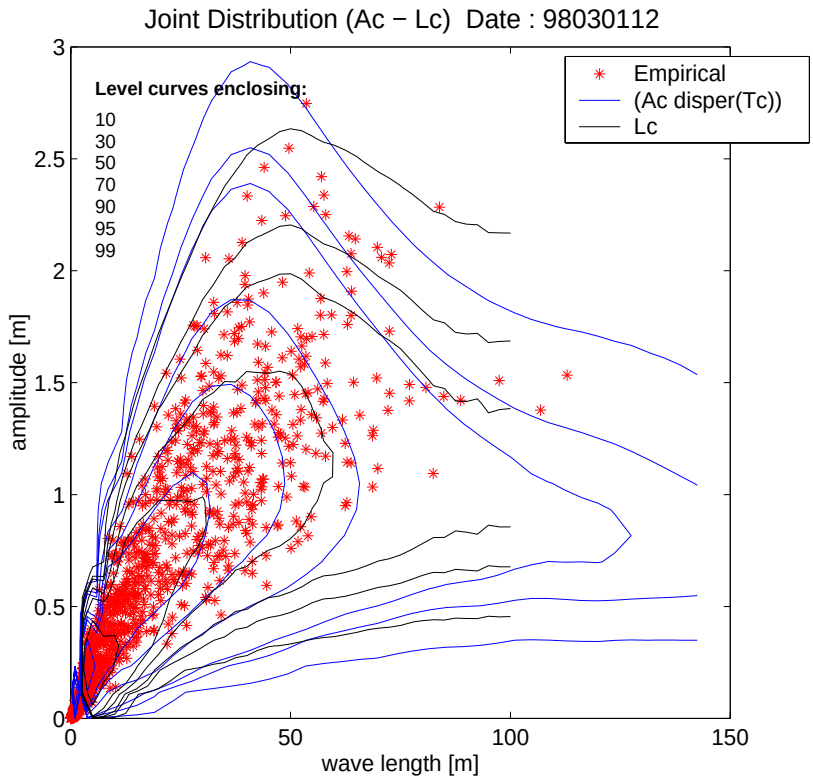

FIGURE 3.25 : Marginal estimation of (4) (h_{Ac},L_c) with the 2 methods

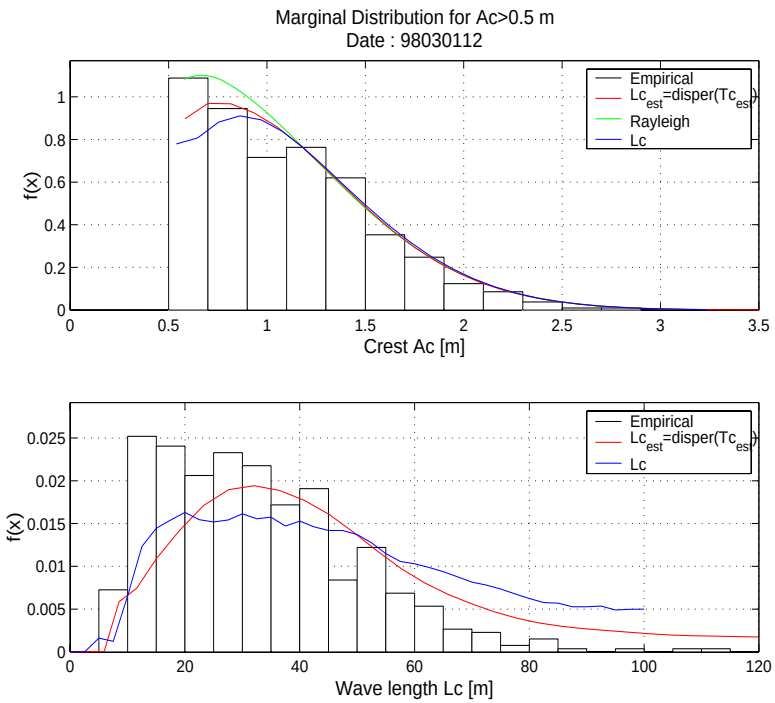

Sea State 2: more narrow-band spectrum

Empirical wave (crest) height-period

The significant wave height of this sea state is larger than in the previous one. Maximum crest heights relative to the three distributions (1) $(h_z/2, t_z/2)$, (2) $(hc/2, t_c/2)$, (3) (h_{Ac}, t_{Ac}) are then bigger than the maximum crests in the previous sea state, see figure 3.26. As it has been seen for sea state 1, the three crest height-period distributions are not the same. Maximum crests of the distribution (3) (h_{Ac}, t_{Ac}) are higher and longer than the ones given by the two other distributions.

FIGURE 3.26 : Comparison of the 3 height-period distributions

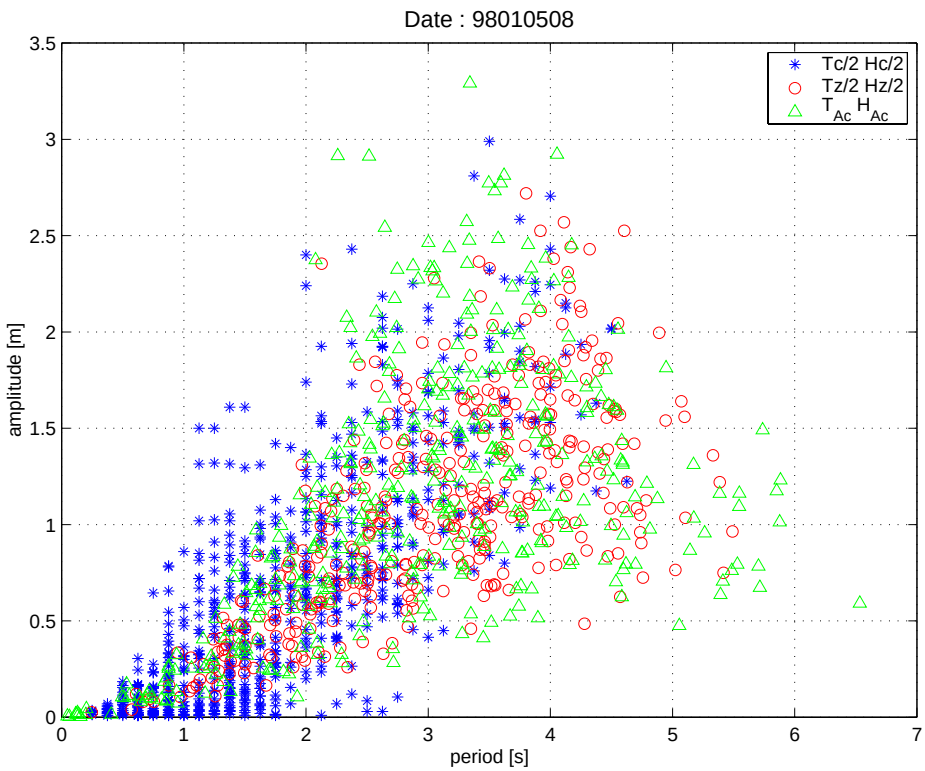

Estimation of wave height-period with parametric models.

The same remarks as the ones made for sea state 1 can be made here. Half wave heights are well approximated by the two parametric models, see figure 3.27 and 3.28. Small periods are not. They are underestimated in both case. The wave steepness is thus overestimated by both models.

Estimation of crest height-period (3) (h_{Ac}, t_c) with parametric models.

The accuracy of those models in estimating the joint (3) (h_{Ac}, t_c) distribution is not satisfactory. The steepness is overestimated by both models, see figure 3.29.

Estimation of crest height-period (3) (h_{Ac}, t_c) with Lund model.

As for sea state 1, the Lund model gives a very accurate estimate, see figure 3.30. Marginal estimates of both crests and periods deduced from the joint distribution are presented in figures 3.31 and 3.32. The estimated steepness distribution fits the empirical one well.

The time required to get this estimate is 500s, less than for the first sea state because of the narrower bandwidth of the spectrum.

This time is satisfactory and could be reduced by considering only waves larger than a level h as it has been explained for the first sea state (see “Estimation of crest height-period (3) (h_{Ac},t_c) with parametric models”, page 26).

FIGURE 3.27 : Longuet-Higgins estimation of (1) ($h_z/2$,$t_z/2$)

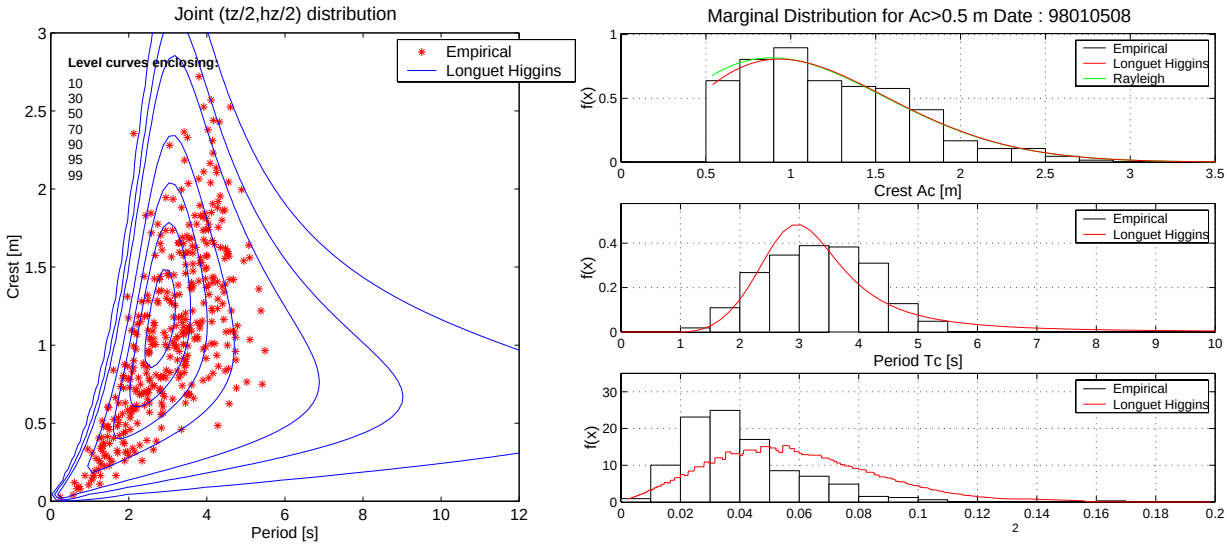

FIGURE 3.28 : Cavanié estimation of (2) ($h_c/2$,$t_c/2$)

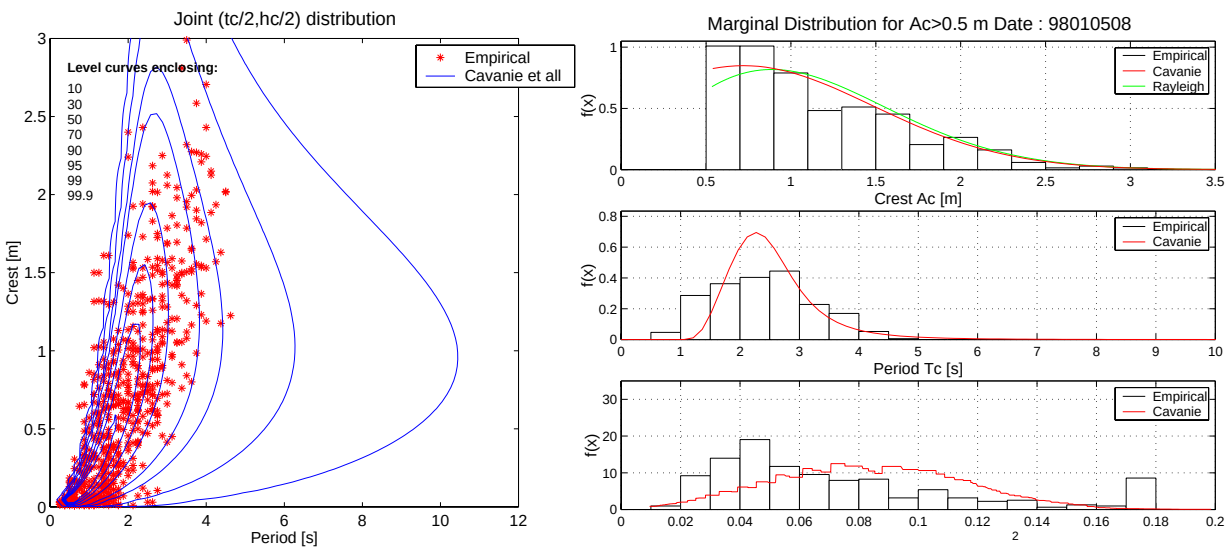

FIGURE 3.29 : Estimation of (3) (h_{Ac},t_c) with parametric models

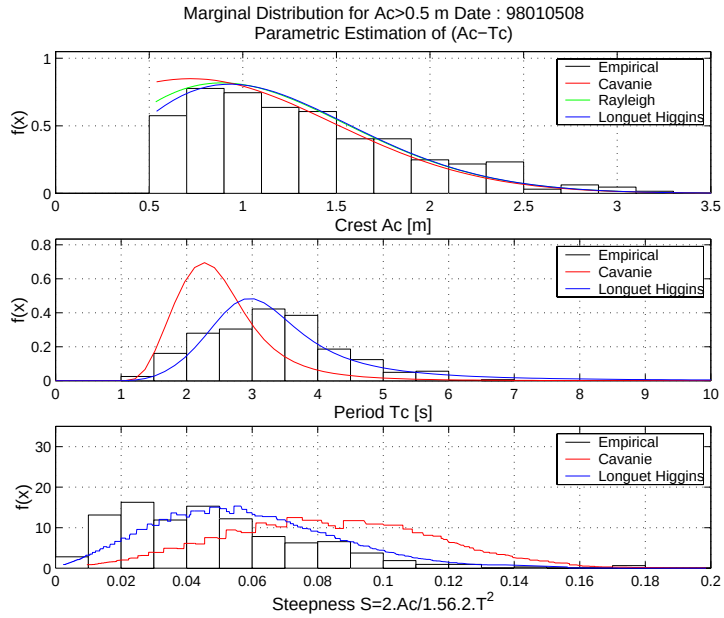

FIGURE 3.30 : Estimation of (3) (h_{Ac},t_c) with Lund models

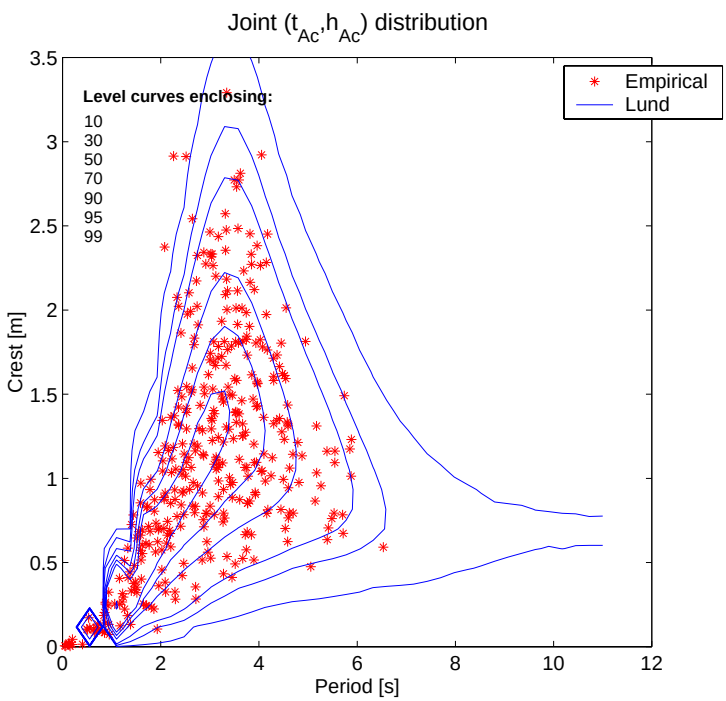

FIGURE 3.31 : Estimation from the joint distribution (fig 3.30), for all A_c

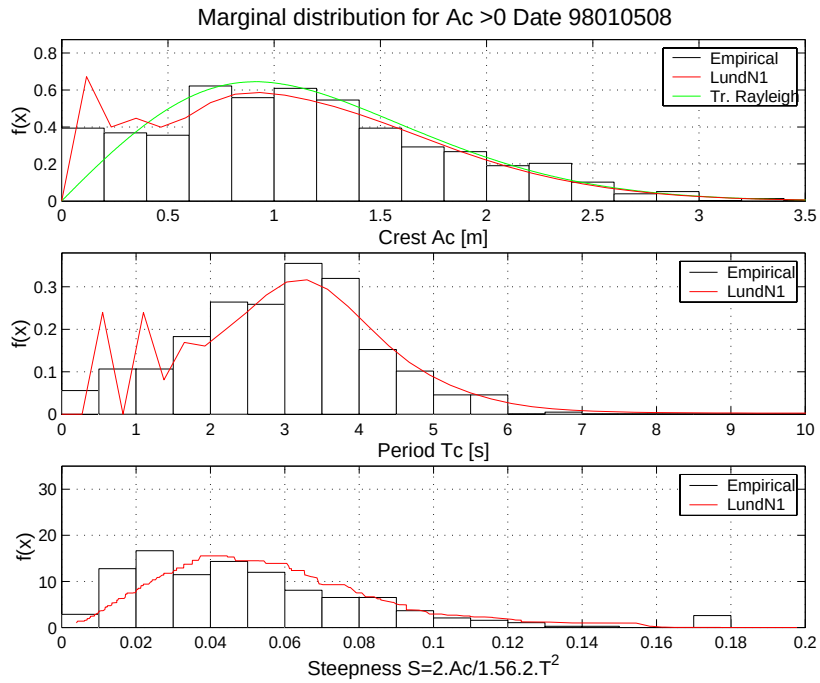

FIGURE 3.32 : Estimation from the joint distribution (fig 3.30), for A_c > 0.5m

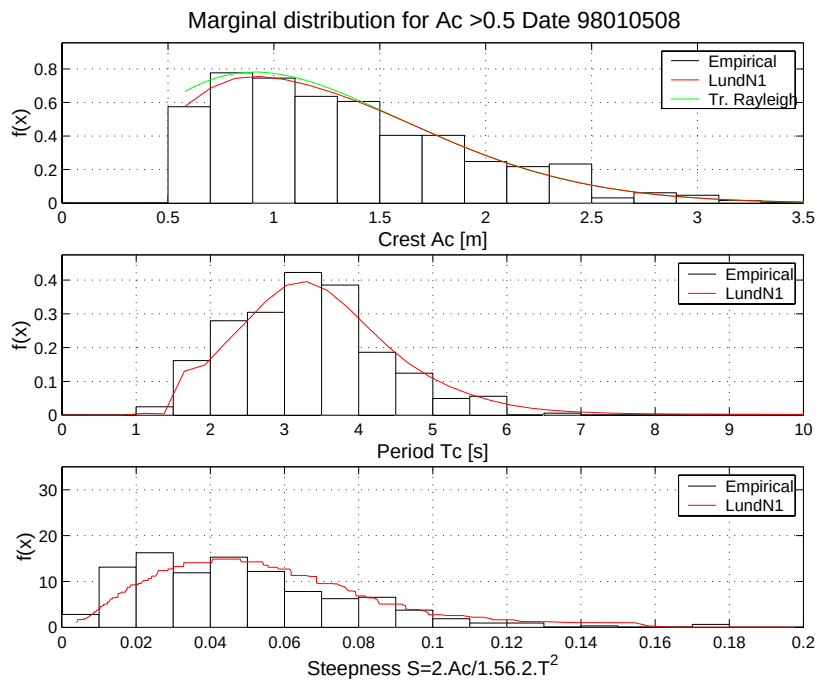

Estimation of crest height-wavelength (4) (h_{Ac},L_c)

The empirical crest length will be either L_c, obtained from the spatial spectrum or TL_c deduced from periods by applying the dispersion relation. Results are presented in figures 3.33 and 3.34. For this sea state, some differences appear between the empirical marginal distributions L_c and TL_c. In particular, the median of TL_c is bigger than the one of L_c

FIGURE 3.33 : Empirical wavelength distribution

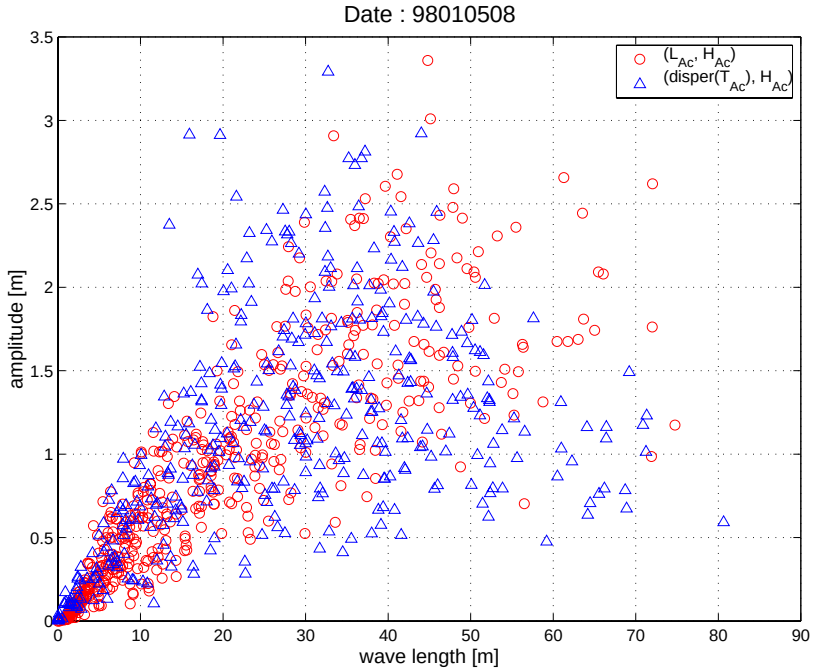

FIGURE 3.34 : Marginal empirical wavelength distribution, for Ac>0.5m

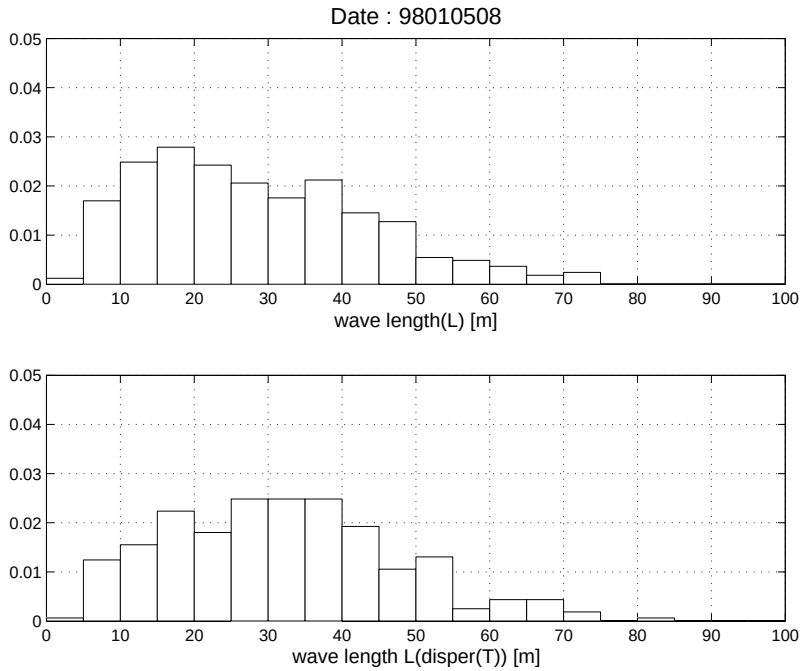

Results relative to the estimates of (4) (h_{Ac},L_c) in sea state 2 are presented in figures 3.35 and 3.36. Estimates of (4) (h_{Ac},L_c) have been computed according to two different methods (see “Estimation of crest height - wavelength (4) (h_{Ac},L_c)”, page 33):

1. estimation from spatial spectrum (blue line)
2. estimation deduced from the estimate we had for (3) (h_{Ac},t_{Ac}) (red line)

For this sea state, the estimate obtained from the spatial spectrum is slightly more accurate than the one deduced from the estimate we had for (3) (h_{Ac},t_{Ac}), see figure 3.36. Since the computing time is very long to get this estimate (2.10^4s), we will keep on advising for the moment to get the estimate by using the estimate we had for (3) and the dispersion relation.

With the method using the spatial spectrum, the accuracy of wavelength can be improved and the only problem is the time which can become very long.

FIGURE 3.35 : Estimation of (4) (h_{Ac},L_c), comparison of the 2 methods

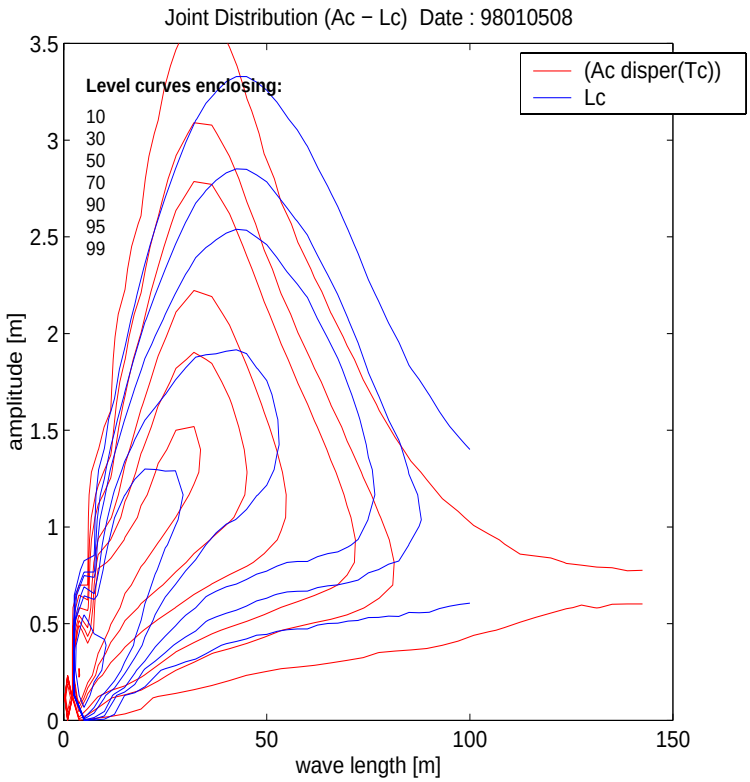

Conclusion relative to the sea state 2

This second sea state was different from the previous one, with a higher significant wave height and a spectrum not so broad banded.

We have obtained comparable results with a very good accuracy of the Lund model for the distribution (3) (h_{Ac},t_{Ac}) and with a satisfactory computing time of 8 minutes to estimate the whole joint density. This time can be reduced if the smallest crests are neglected.

For the joint distribution (4) (h_{Ac},L_c), the use of the spatial spectrum leads to accurate results but the time required can be very long if the desired accuracy is too high. The estimate of (4) (h_{Ac},L_c) deduced from the one we had for (3) (h_{Ac},t_{Ac}) by using the dispersion relation gives good results.

Conclusion

We have shown in this report that the joint distribution (3) (h_{Ac},t_{Ac}) can be well approximated by the Lund model. Results from parametric models are not satisfactory and that can be explained by the choice of the sea states which are not narrow-banded and even double peaked for the first sea state.

To get a fast estimation of the distribution (4) (h_{Ac},L_c), it is advisable not to use the spatial spectrum but to deduce the estimation from the one we had for (3) (h_{Ac},t_{Ac}). The time required to get an accurate estimate of both (3) (h_{Ac},t_{Ac}) and (4) (h_{Ac},L_c) is then around 700s (depending of the bandwidth of the spectrum). If time is not a problem, an estimate can be computed with the desired high accuracy.

The best estimates are obtained when the information used is the spectrum, the non smoothed periodogram and the non parametric g transformation (see “Lindgren and Rychlik model”, page 23).

Nevertheless, the aim of this work is to find a way to get those estimates for the desired large number of sea states and one solution for that is to use parametric shapes of spectra and of g transformation.

It has been seen that the estimates of the joint (3) distribution (h_{Ac},t_{Ac}) remain accurate when a suitable model is used to deduce a parametric spectral shape. Further tests need to prove the accuracy of the estimates with the use of a parametric *g* transformation. Then, accurate estimates of the joint distributions (3) (h_{Ac},t_{Ac}) and (4) (h_{Ac},L_c) could be obtained from g transformation and spectral shape parameterized by sea states parameters. So, the computation of the distributions on a reduced discretized space of the sea state parameters would permit to get an estimation of the joint distribution for any sea state case.

FIGURE 3.36 : Estimation of (4) (h_{Ac},L_c), comparison of the 2 methods

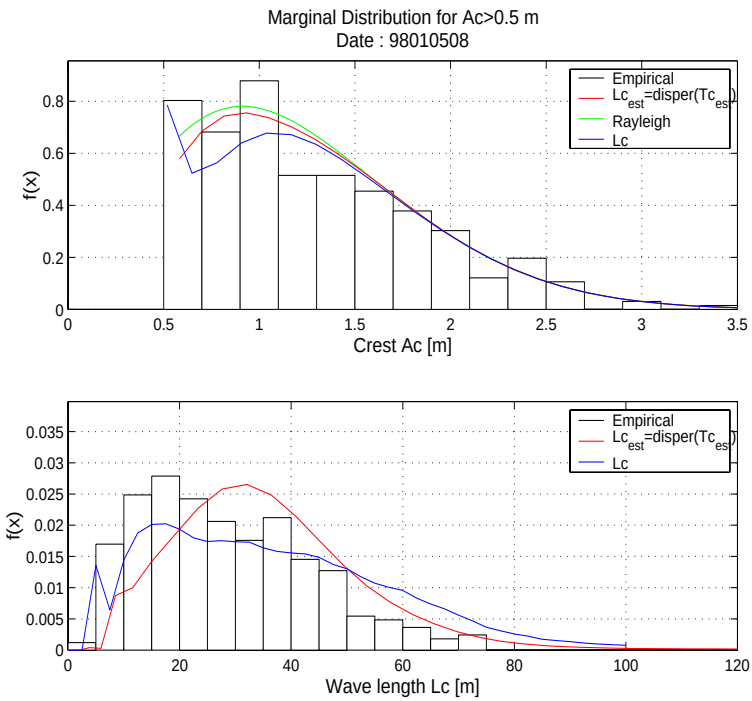

CHAPTER 4

Sensor measurements comparison

Marc Prevosto
Benjamin Moreau
George Z. Forristall

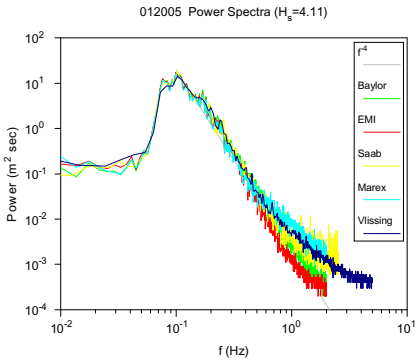

One of the main objectives of the WACSIS project was the intercomparison of different sensors used to measure the wave and crest heights. In this project we are particularly interested in the ability of a sensor to give the statistics of the crest heights as exactly as possible.

We will first explain the different types of comparison tools we will use in the sequel of this report to compare the crest height statistics, before using them in this chapter to compare the different sensors.

Tools of crest height statistics comparison

The crest height statistics can be compared, either inside each sea states or cumulatively over all the WACSIS common data base. In the latter case, to compare the sensors we are obliged to consider the same dates for all the sensors, and this could cause a drastic change in the available data when considering, for example, EMILASER (see “Intersection of sensors data base”, page 11).

Two types of plots will be used all along this report:

Rayleigh Normalised Empirical Distribution

Under the hypothesis of linear waves, the crest height distribution could be considered to follow a Rayleigh law, with its coefficient calculated from the H_s.

$$P(C > c) = \exp\left(-8\frac{c^2}{H_s^2}\right) = F_C(c) \qquad \textbf{(EQ 4.1)}$$

Starting from a sample of crest heights $\{c_1, c_2, \ldots c_n\}$, we can calculate the empirical distribution of the crest height by

$$\hat{P}(C > c) = 1 - \frac{1}{n}\left(\sum_{i=1}^{n} \mathbf{1}_{]-\infty, c[}(c_i)\right) = \hat{F}_C(c) \qquad \textbf{(EQ 4.2)}$$

that is to say, $\hat{P}(C > c)$ is the rate of crest heights higher than c.

Then a crest height ratio (call CHR in the sequel) can be defined as

$$c_R(p) = \frac{\hat{F}_C^{-1}(p)}{F_C^{-1}(p)} \qquad \textbf{(EQ 4.3)}$$

An example of the plot of this crest height ratio is given in figure 4.1.

FIGURE 4.1 : Example of crest height ratio plot, 19th of January 20:00

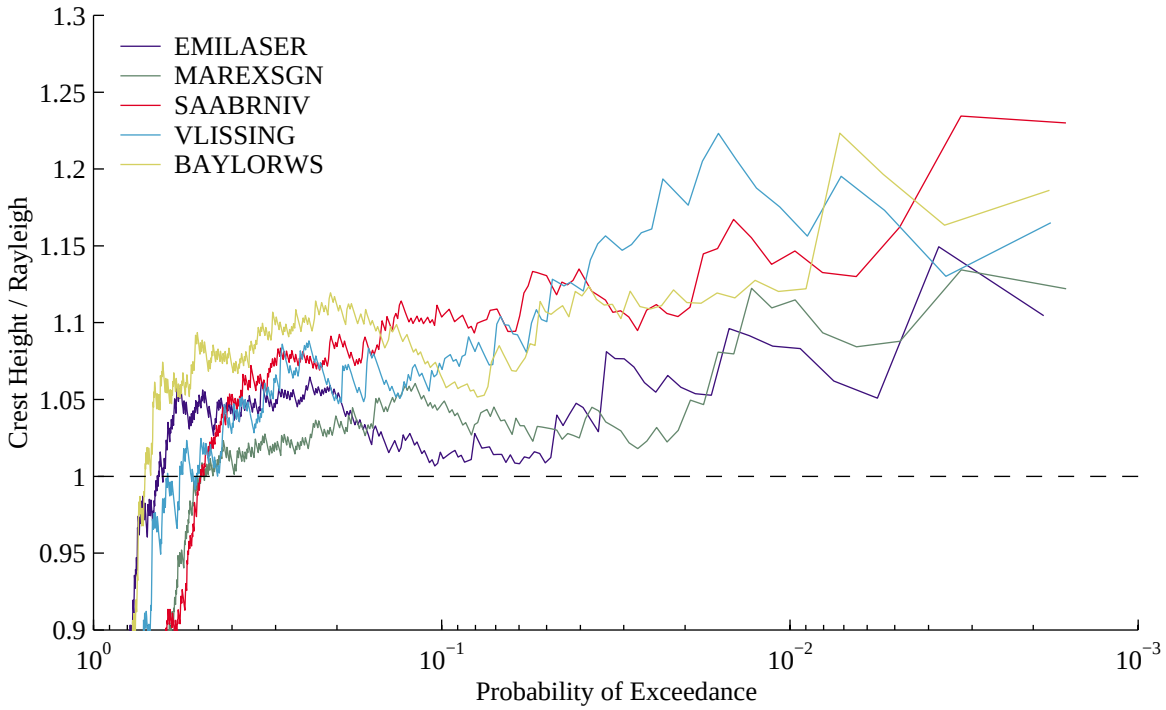

Empirical number of exceedances

The empirical number of exceedances is roughly calculated on the samples as

$$N(C > c) = n - \sum_{i=1}^{n} \mathbf{1}_{]-\infty,\, c[}(c_i) \qquad \textbf{(EQ 4.4)}$$

In this case the approximate number of crests n will be indicated (as this number could be different for the different curves in the same plot) in the abscissa caption, as well as the number of 20 min. time series used to build the sample. An example corresponding to the same samples as figure 4.1 is given in figure 4.2.

FIGURE 4.2 : Example of number of exceedances plot, 19th of January 20:00

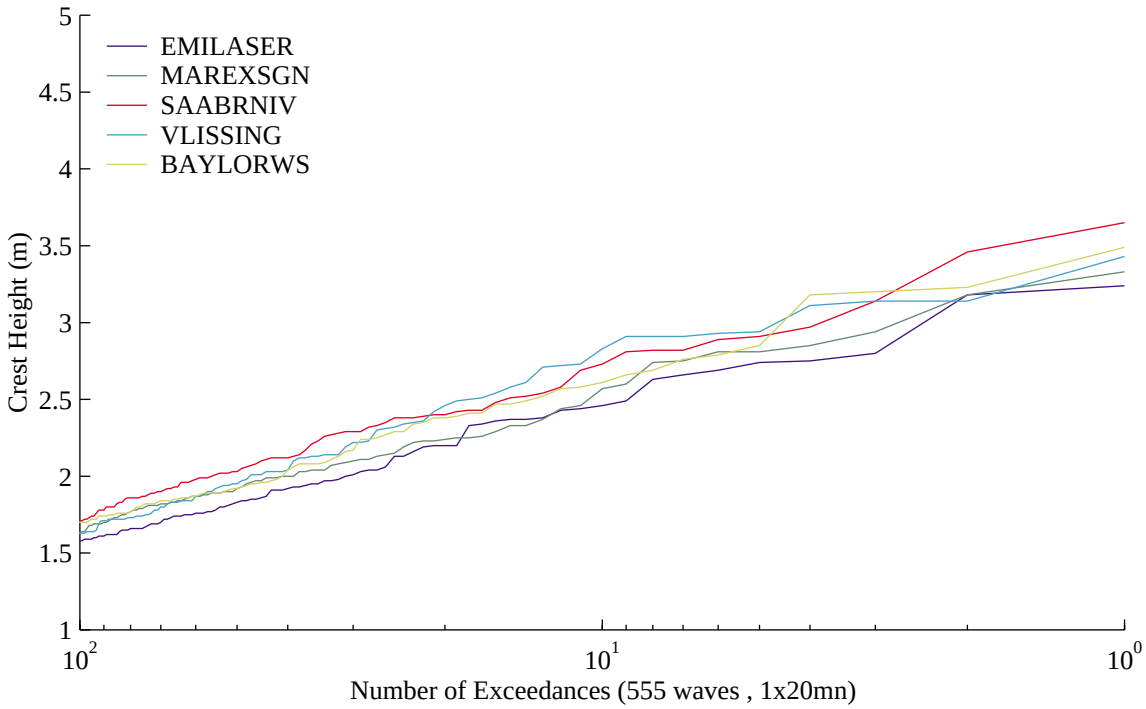

Of course the plot of the Rayleigh Normalised Empirical Distribution amplifies the differences between the samples and is sensitive to the number of waves of the sample, which could be due, as we will see, to noise or small high frequency waves.

Wave measurements with the S4

Crest heights from inverted pressure measurements

The classical way to obtain the wave elevation time series from the dynamic pressure measurements is to apply a linear transfer based on linear harmonic waves model.

When the linear elevation is

$$\eta(t) = a\sin(-\omega_0 t) \qquad \textbf{(EQ 4.5)}$$

the linear pressure (in equivalent meter) at depth z is, with h the water depth,

$$p(t, z) = \frac{\cosh k_0(z+h)}{\cosh k_0 h} a\sin(-\omega_0 t) \qquad \textbf{(EQ 4.6)}$$

Unfortunately, the transfer function $\frac{\cosh k_0(z+h)}{\cosh k_0 h}$ decreases very strongly with depth when the wave number k_0 is high, i.e. for the short wavelengths. So, for the high frequency components the pressure amplitude is under the sensor noise level,

and then, when we apply the inverse transfer function, the noise is enhanced. In our case the S4 is located between -10.5 m and -13.5 m, depending of the water depth. This situation produces, for example, a ratio of attenuation of 100 between a wave component at 8 seconds and a wave component at 3 seconds. In looking at the comparison between the spectral density of a BAYLORWS measurement and inverted S4PRVELO pressure measurement (figure 4.3), this effect of noise enhancement is very clear. The inverted pressure measurement has to be lowpass filtered up to 0.22 Hz to avoid the noise effect. Although the agreement between the two spectral densities is quite good between 0.08 Hz and 0.22 Hz, this drastic filtering modifies, without considering any nonlinear effects, the crest heights produced by the inverse transformation of the pressure measurements. In figure 4.4, the effect of the filtering is shown on a BAYLORWS time series. The filtered BAYLORWS and inverted S4PRVELO pressure measurement are generally in good agreement, but the pressure measurements unfortunately underestimate strongly the crest heights. So, no comparison of crest height statistics has been made in considering pressure measurements in the sequel of this report.

FIGURE 4.3 : Spectral densities, BAYLORWS vs inverted S4PRVELO

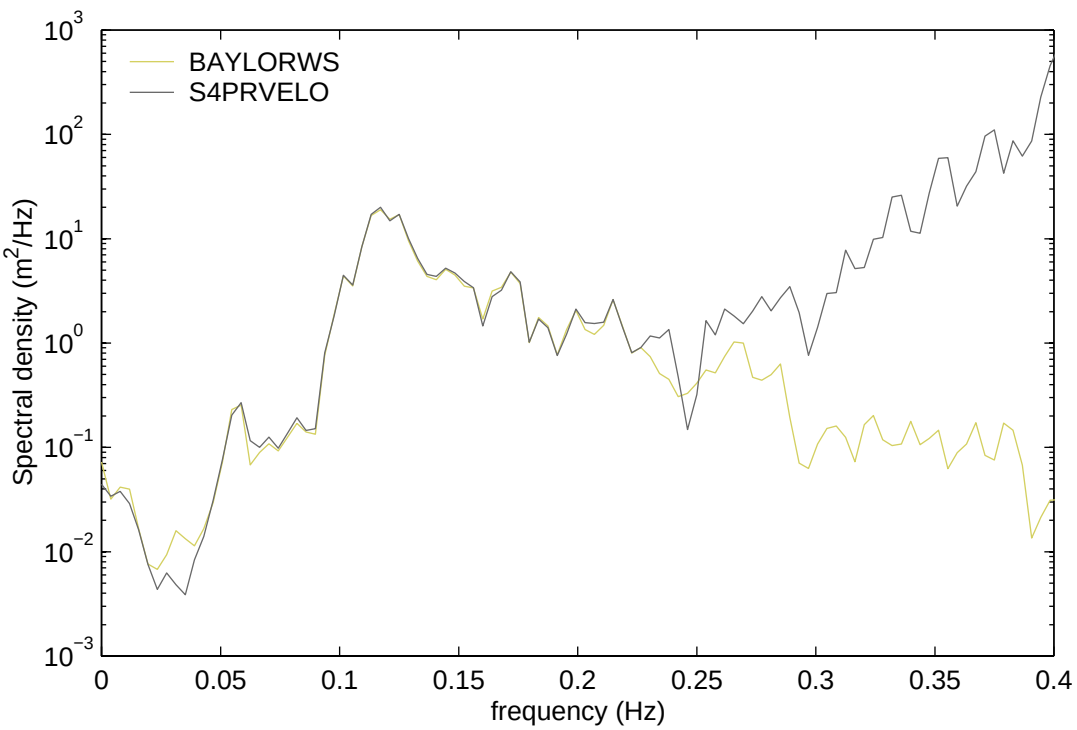

FIGURE 4.4 : **Surface elevation, effect of filtering**

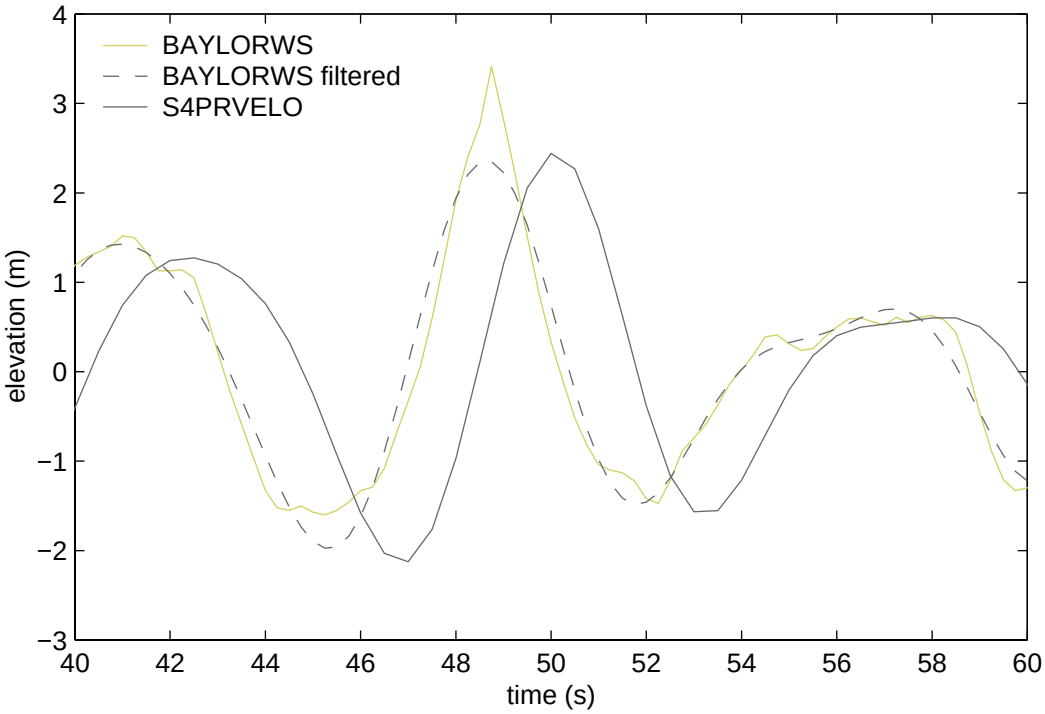

Directional information from pressure plus orbital velocities

The measurement of the particle velocities by S4PRVELO permits us to extract from its measurements directional information as has been done from WAVERGHR (see “Waverider directional information”, page 11). The direction at the peak frequency is given in figure 4.5, where the directional information is calculated from 1 hour (when available) for WAVERGHR and 20 min. for S4PRVELO (that explains the higher dispersion for this latter). It is clear that it exists a shift between the two sensors. If we correct the S4 results by substracting 30 degrees (figure 4.6), the directions are now in agreement, apart for the time series before mid December (marked with a star). In fact, the communication cable of the S4 broke in mid December, and after the repair the S4 was located in a position shifted compared to its previous one. When comparing the directions given by WAVERGHR with the directions estimated visually from the video, it is obvious that the directions given by WAVEGHR are good. So it seems that the measurement of the heading of S4PRVELO by its compass was perturbed by nearby steel structures and the perturbation was different before and after the break due to different locations.

The calculation of the rms directional spreading from the two sensors (figure 4.7) shows that S4PRVELO gives higher spreading than WAVERGHR. On this parameter the bad heading correction has no effect. A lot of possibilities could explain this discrepancy between the two sensors, for example the effect on the S4 of the interference by the platform members. But the underestimation from the Waverider is, in some way, coherent with back-front crest asymmetry and crest-trough symmetry observed in [1], which seems to prove that the mooring of the buoy reduces the buoy excursions which tighten the mooring.

FIGURE 4.5 : Peak direction

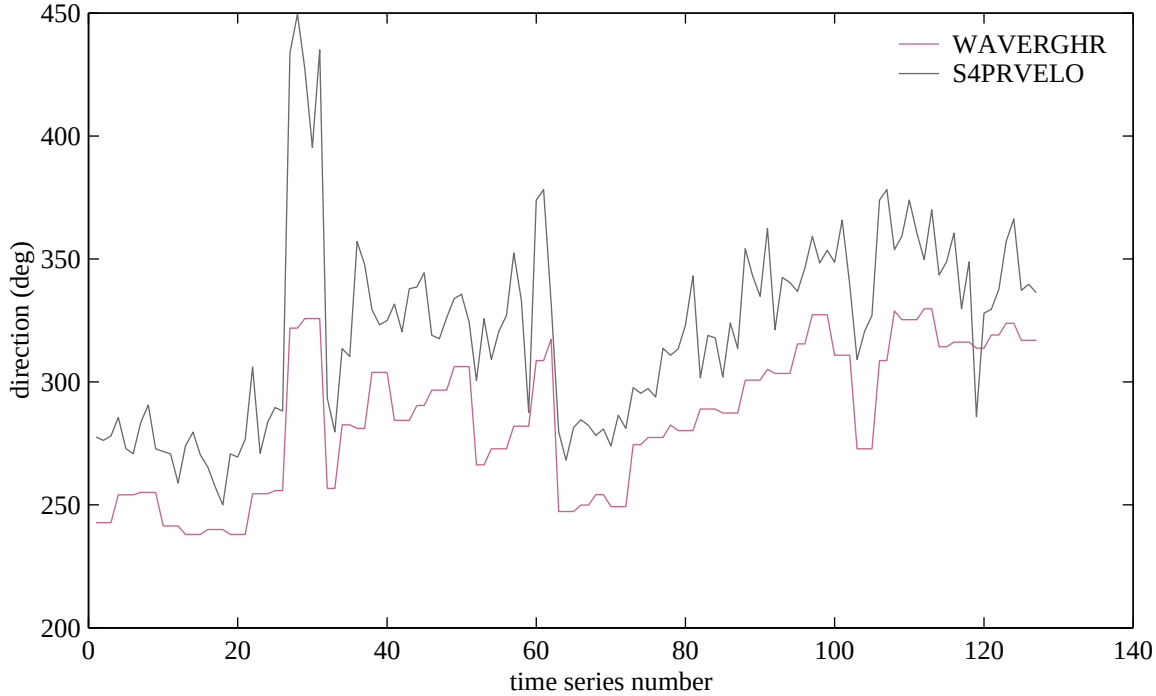

FIGURE 4.6 : Peak direction, S4PRVELO shifted -30 deg.

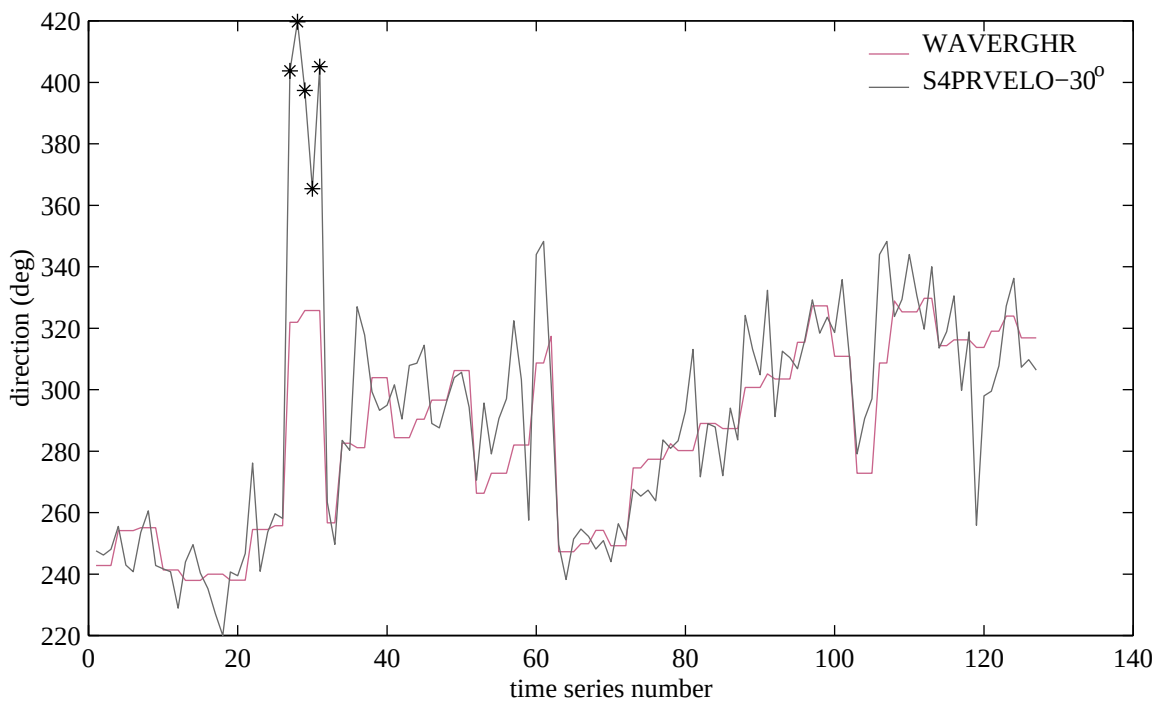

FIGURE 4.7 : Peak rms directional spreading

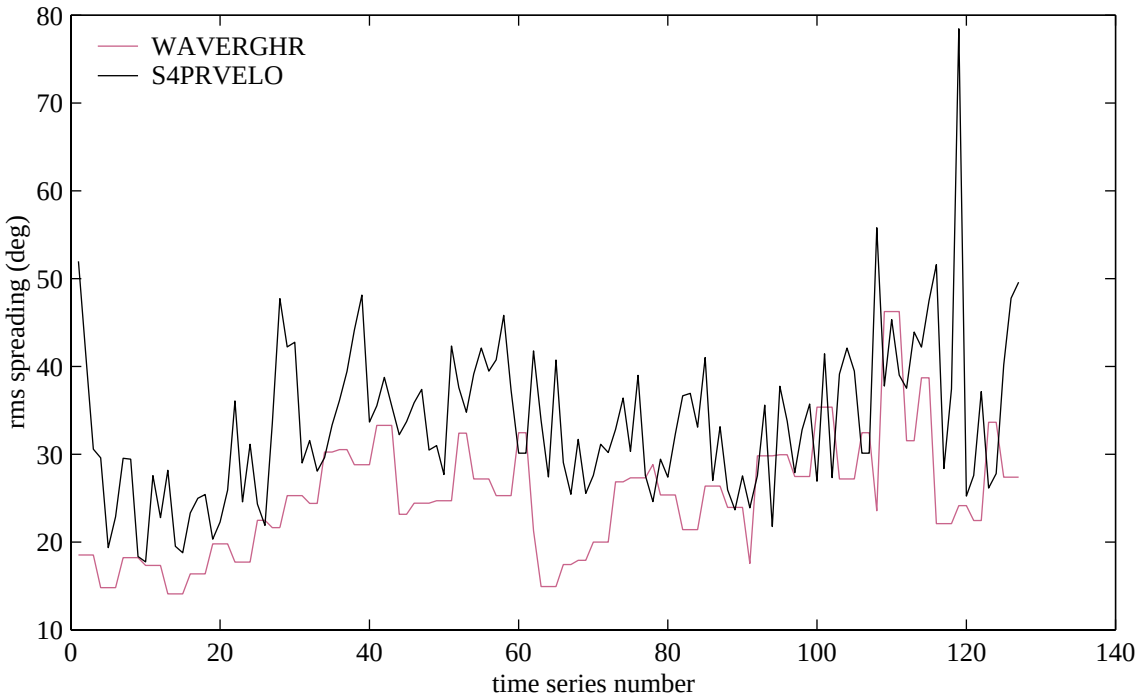

Power spectra from the wave sensors

Figures 4.8-4.11 show examples of the spectra from the various wave sensors displayed on log-log scales. The spectra are very similar near the peak and through the energy containing frequencies, but differ considerably at high frequencies. The faint gray line in the figures has a slope of -4. Although there remains some debate whether the high frequency tail of the gravity wave spectrum behaves as f^{-4} or f^{-5}, but there is no doubt that the true wave spectrum does not curve above f^{-4} at high frequencies. The Marex and Saab radars have the highest noise level, generally followed by the Vlissingen, Baylor, and EMI gauges. The noise levels stay roughly the same while the energy containing part of the spectrum decreases with decreasing significant wave height. The excess energy there must be due to some form of electronic noise, possibly exaggerated by aliasing from frequencies above the Nyquist frequency. All of the sensors were recorded as either the digital signal provided by the sensor or by directly digitizing analog signal from the sensor without any further filtering. It is likely that the sensors provide some form of internal filtering, but the details are not known to us. In any case, the measurements above about 0.5 Hz appear to be unreliable.

FIGURE 4.8 : Power spectra from 20 January 1998 at 0500

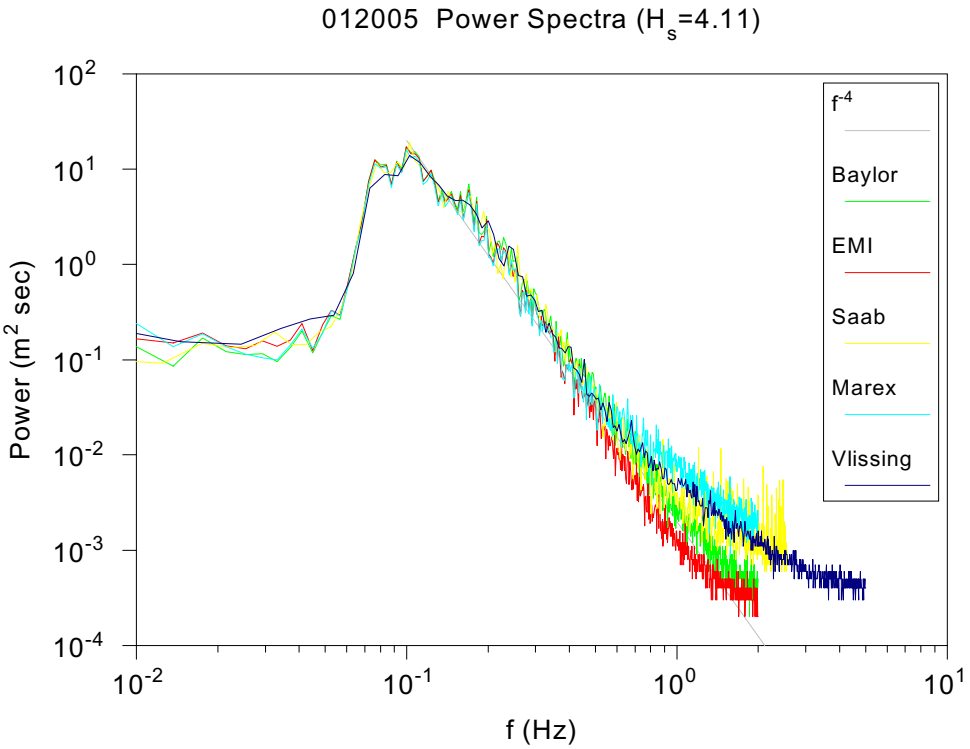

FIGURE 4.9 : Power spectra from 13 April 1998 at 1400

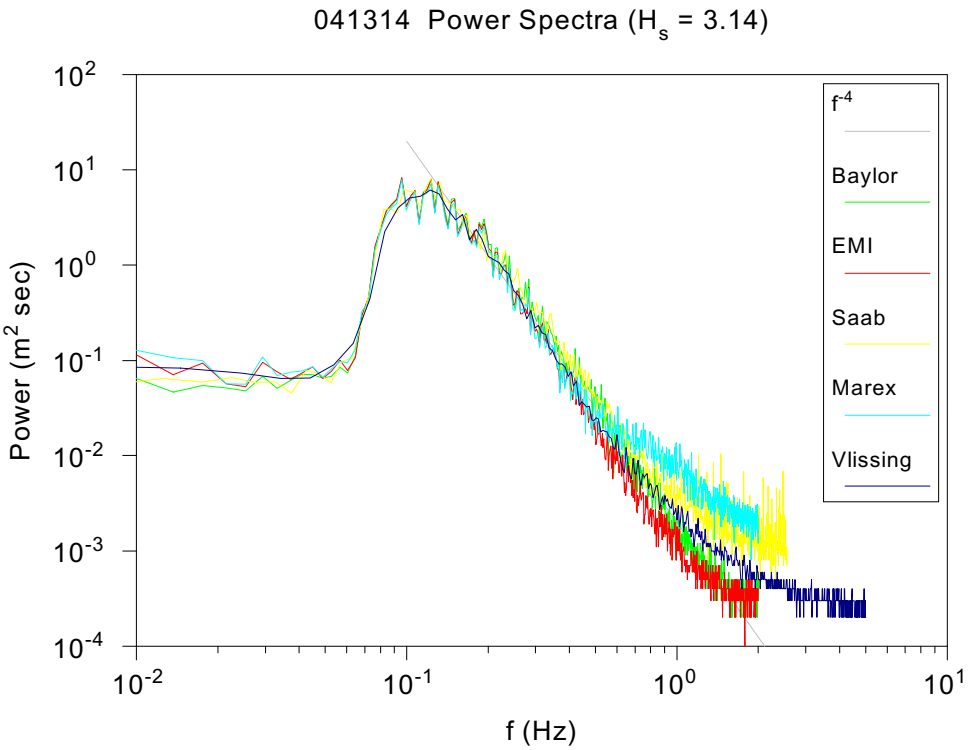

FIGURE 4.10 : Power spectra from 19 January 1998 at 1000

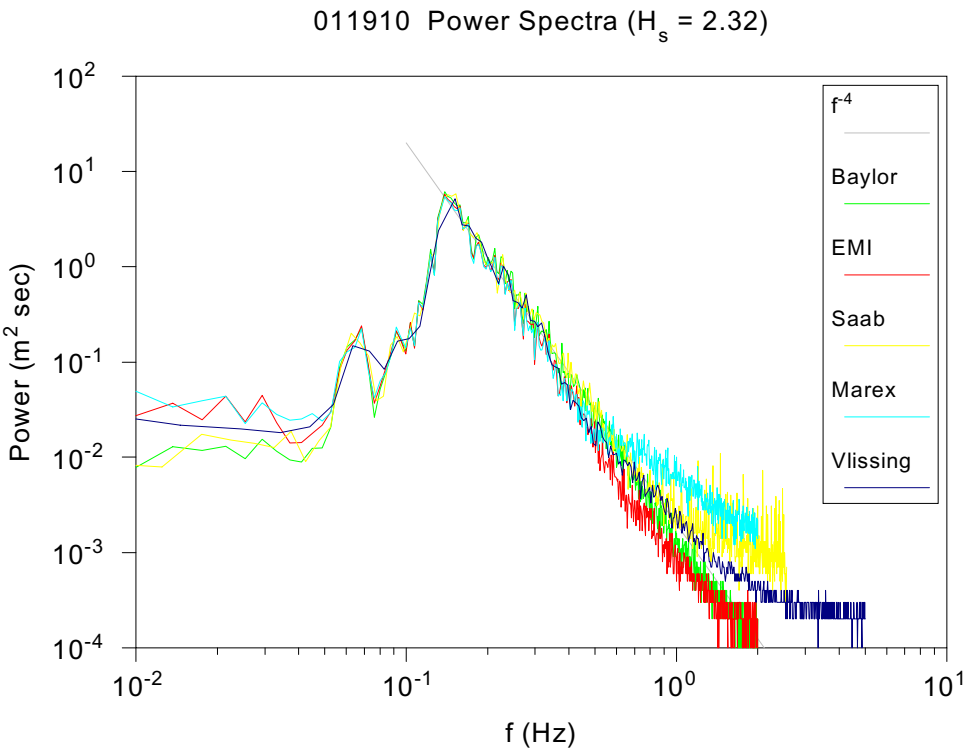

FIGURE 4.11 : Power spectra from 11 April 1998 at 0200

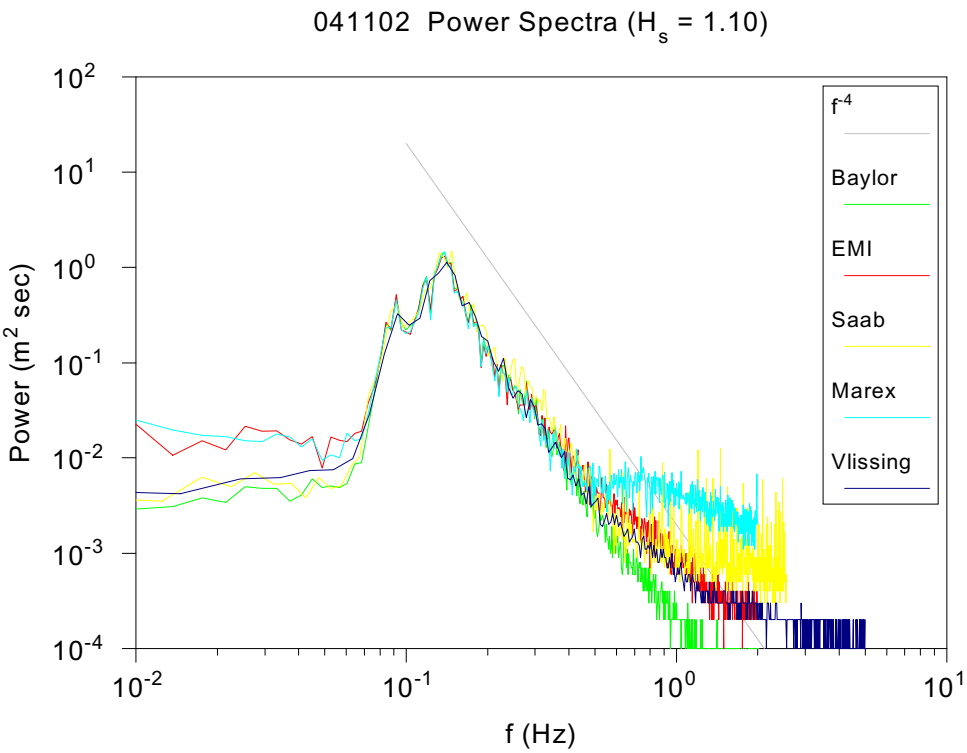

Effects of the cut-off and sampling frequencies

The different sensors measure the wave surface elevation with different sampling frequencies and different anti-aliasing cut-off frequencies. These different frequencies could create differences between the statistics of crest. Lowpass anti-aliasing filters remove the shorter wavelength components and so could change the total number of waves or the slightly change the height of the crests. The sampling of course underestimates the crest heights because the larger the sampling interval, the stronger the probability to miss the maximum of the crest. We have analysed hereafter some of the effects of both cut-off and sampling frequencies

Effects of the cut-off frequency

We consider here the EMSVWB data base (see “Intersection of sensors data base”, page 11). We have not considered the complementary dates with low H_S. We apply to the measurements a lowpass filter (using a ideal rectangular window in the frequency domain). The cut-off frequency is given the values 4Hz, 2Hz, 1Hz and 0.5Hz, without changing the sampling frequency. Of course when the sampling frequency of the sensor is lower than two times the cut-off frequency, no filter is applied.

Number of waves. A wave by wave analysis is applied on each resulting time series. The total number of waves depending of the cut-off frequency is given in table 4.1. On the raw data the number of waves given by EMILASER is 15% lower than given by MAREXSGN or SAABRNIV. The biggest effect of filtering is on these latter two sensors with a decrease higher than 10% between the raw data and the filtered data at 0.64Hz.

TABLE 4.1 : Number of waves vs cut-off frequency

Cut-off frequency	EMILASER	MAREXSGN	SAABRNIV	VLISSING	WAVERGHR	BAYLORWS
Raw	21527	24751	24741	23109	21602	22726
2 Hz			24002	23037		
1 Hz	21299	22387	22620	22461		22563
0.64 Hz	21156	21333	22126	22007	21602	22196
0.5 Hz	20984	21021	21755	21602	21351	21807

Significant wave height. If we calculate a linear regression between the Hs given by the raw data and the Hs obtained from the filtered data (table 4.2) the variation of the coefficient of the regression is very weak. The maximum of variation is 0.8% for MAREXSGN.

TABLE 4.2 : Significant wave height vs cut-off frequency

Cut-off frequency	EMILASER	MAREXSGN	SAABRNIV	VLISSING	WAVERGHR	BAYLORWS
Raw	1.000	1.000	1.000	1.000	1.000	1.000
2 Hz			1.000	0.999		
1 Hz	1.000	0.997	0.998	0.998		1.000
0.64 Hz	0.999	0.994	0.997	0.997	1.000	0.999
0.5 Hz	0.998	0.992	0.995	0.995	0.998	0.997

Crest height ratio. The date 01/19/20:00 is chosen here to look at the effect of cut-off frequency on the crest height ratio (figures 4.12 to 4.16). The sea state parameters are Hs = 3.3m and T_{02} = 6.3s. The crest height statistics have been calculated in gathering one hour of data.

It should be noticed that if the number of waves decreases due to the elimination of small waves, then the empirical probability of high crest heights would increase. This induces then an increase of the CHR (crest height ratio (EQ 4.3)). This effect should be important mainly for MAREXSGN and SAABRNIV.

For all the sensors, the filtering actually induces a slight decrease of the CHR of the higher waves. The effect of the filters in removing small ripples on the crest of the high waves must thus be more important than the effect of reducing the number of waves. For the sensors with a great effect of the filtering on the number of waves (MAREXSGN, SAABRNIV), the modification on the low probability levels is however very clear, showing that the change in the number of waves is mainly due to the filtering of the little waves.

FIGURE 4.12 : Effect of cut-off frequency, EMILASER crest height ratio

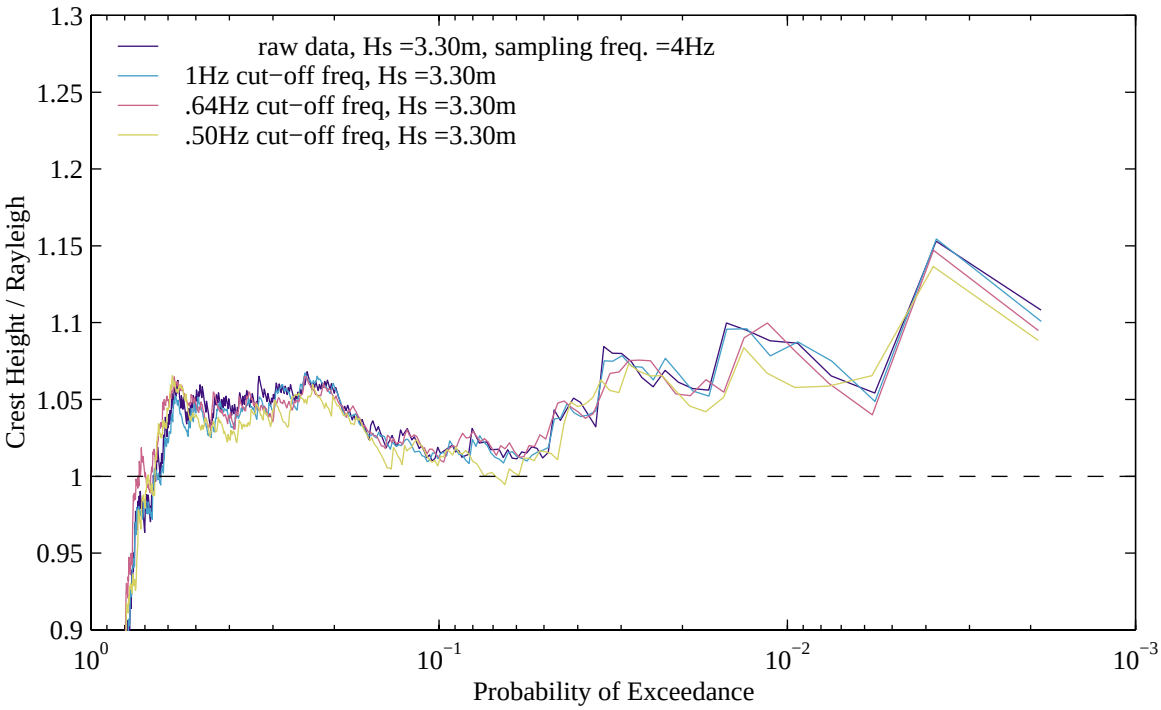

FIGURE 4.13 : Effect of cut-off frequency, MAREXSGN crest height ratio

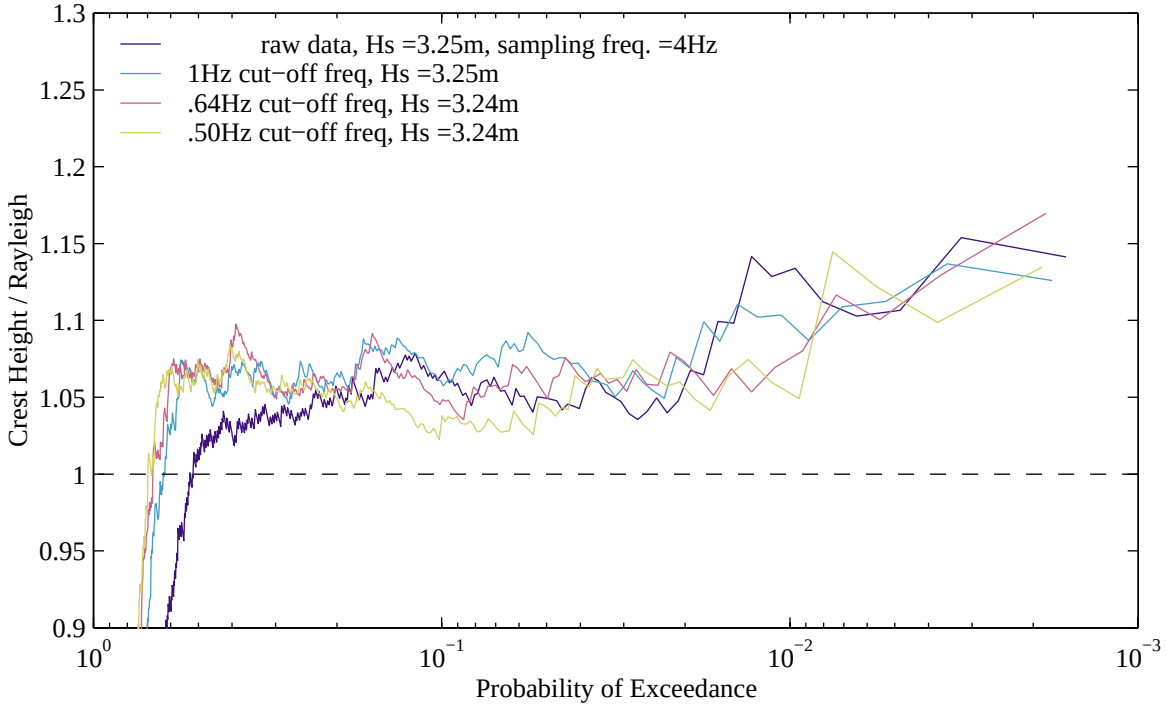

FIGURE 4.14 : Effect of cut-off frequency, SAABRNIV crest height ratio

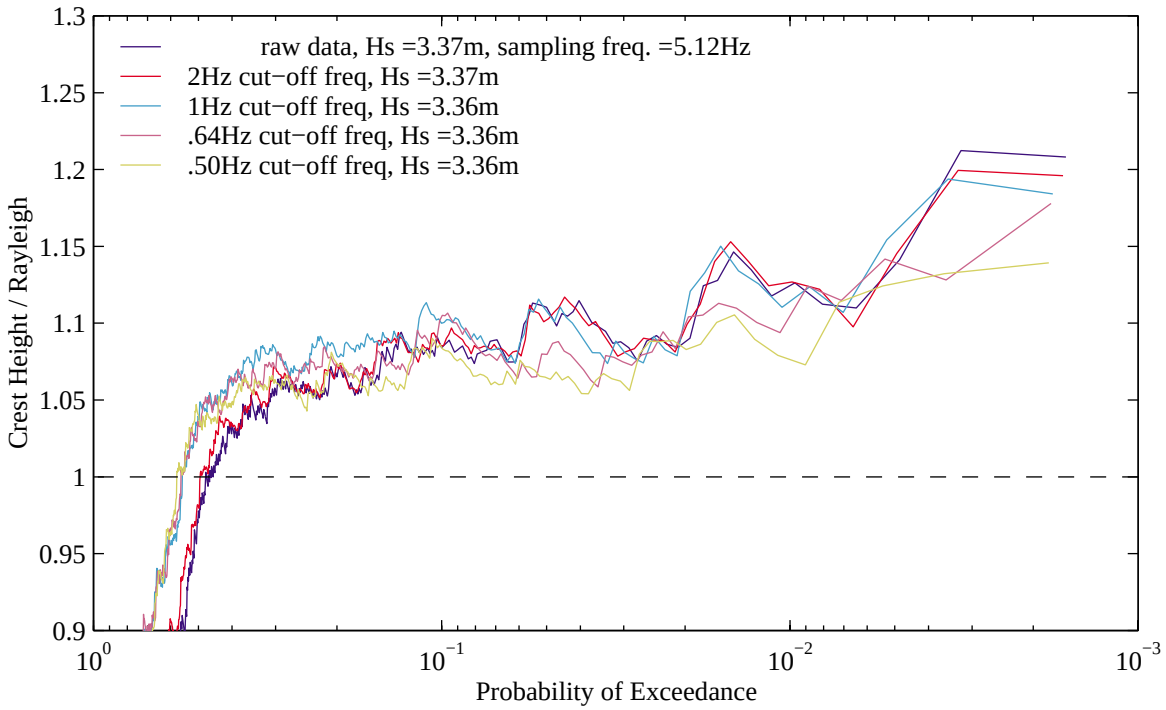

FIGURE 4.15 : Effect of cut-off frequency, VLISSING crest height ratio

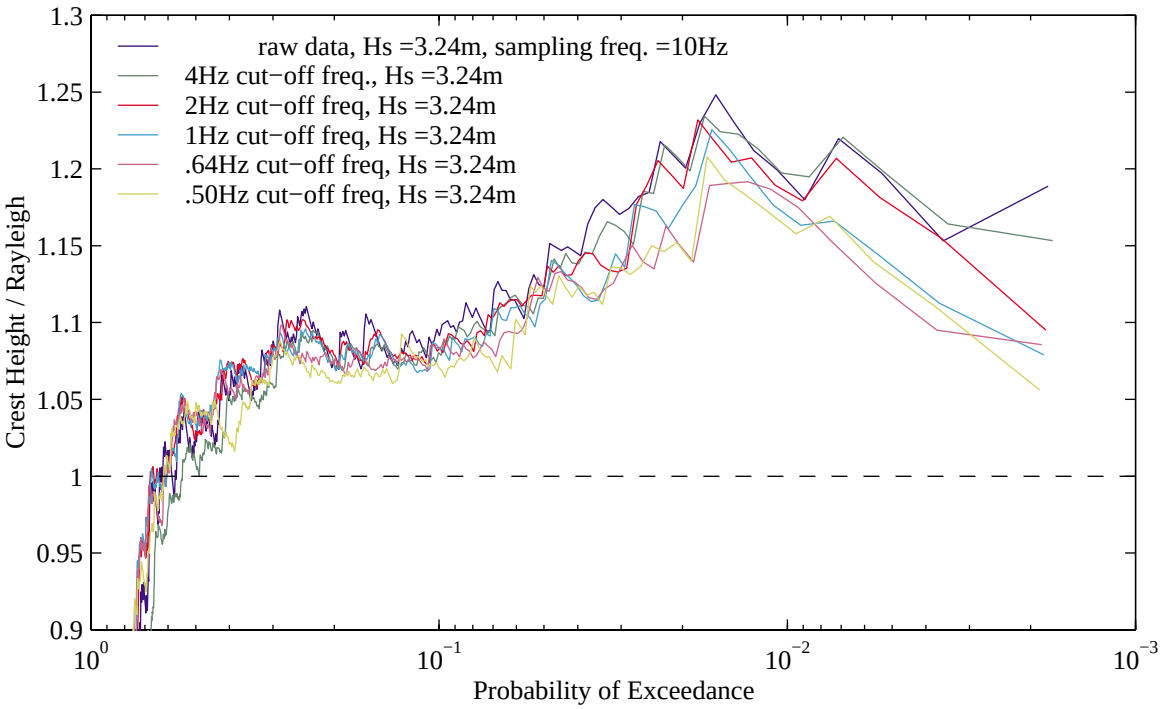

FIGURE 4.16 : Effect of cut-off frequency, BAYLORWS crest height ratio

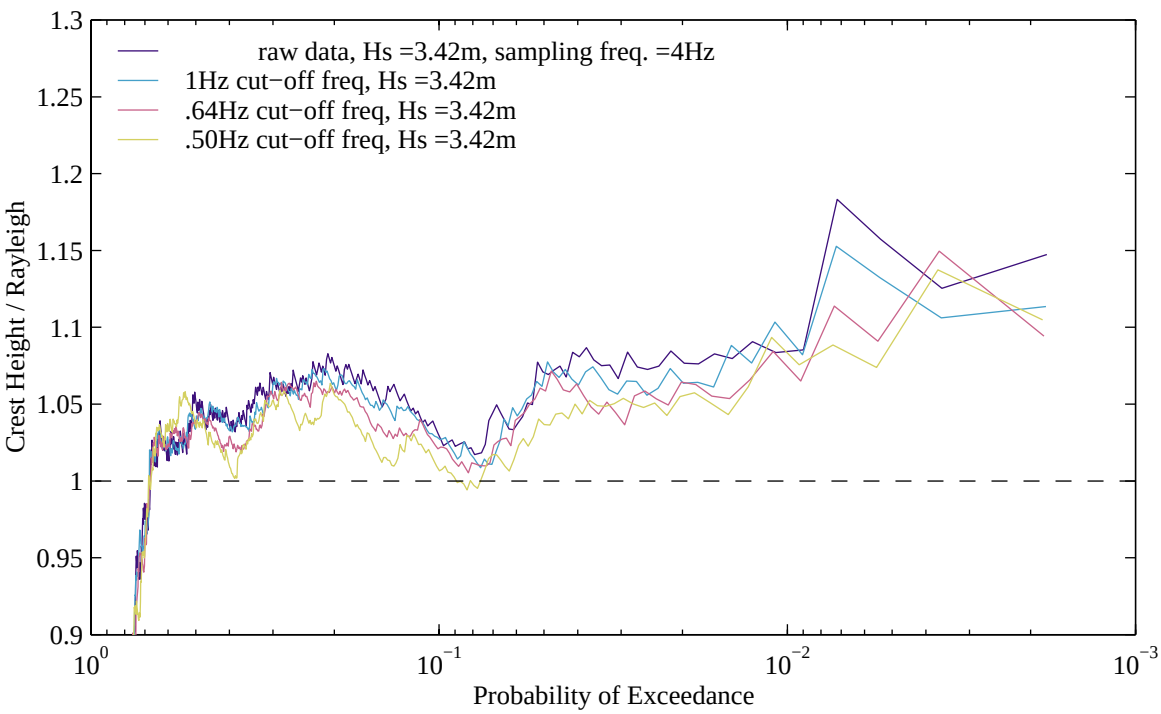

Effect of the sampling frequency

To analyse the effects of the sampling frequency, we consider again the same EMSVWB data base. Then we change the sampling frequency by first applying a lowpass filter (anti-aliasing filter) with a cut-off frequency equal half the sampling frequency. When the sampling frequency is higher than the raw sampling frequency (which is only the case for WAVERGHR) an oversampling procedure is applied.

Number of waves. In comparison with a simple lowpass filter, the differences on the number of waves is insignificant (table 4.3).

TABLE 4.3 : **Number of waves vs sampling frequency**

Sampling frequency	EMILASER	MAREXSGN	SAABRNIV	VLISSING	WAVERGHR	BAYLORWS
Raw	21527	24751	24741	23109	21602	22726
4 Hz			23726	22692	22301	
2 Hz	21074	21759	22185	21953	22062	22196
1 Hz	20278	20264	20883	20753	20999	20920

Significant Wave height. As it could be foreseen, the sampling frequency has no effect on the significant wave height (table 4.4). The total energy is only determined by the lowpass filter applied before sampling.

TABLE 4.4 : **Significant wave height vs sampling frequency**

Sampling frequency	EMILASER	MAREXSGN	SAABRNIV	VLISSING	WAVERGHR	BAYLORWS
Raw	1.000	1.000	1.000	1.000	1.000	1.000
4 Hz			1.000	0.999	1.000	
2 Hz	1.000	0.997	0.998	0.999	1.000	1.000
1 Hz	0.998	0.992	0.995	0.995	0.998	0.997

Crest height ratio. Even though it has no effect on the total energy, the effect of the sampling frequency on the crest heights is very important. As mentioned earlier the decimation causes underestimation of the crest heights. In the following plots of the CHR (figures 4.17 to 4.21) the underestimation is very clear when the sampling frequency is 1 Hz (dash-dotted line) compared to the effect of the simple lowpass filter (straight line). With this value of sampling frequency the crest statistics are close to those given by a linear hypothesis. The 2 Hz sampling also introduces a slight underestimation, perhaps clearer for other dates.

FIGURE 4.17 : Effect of sampling frequency, EMILASER crest height ratio

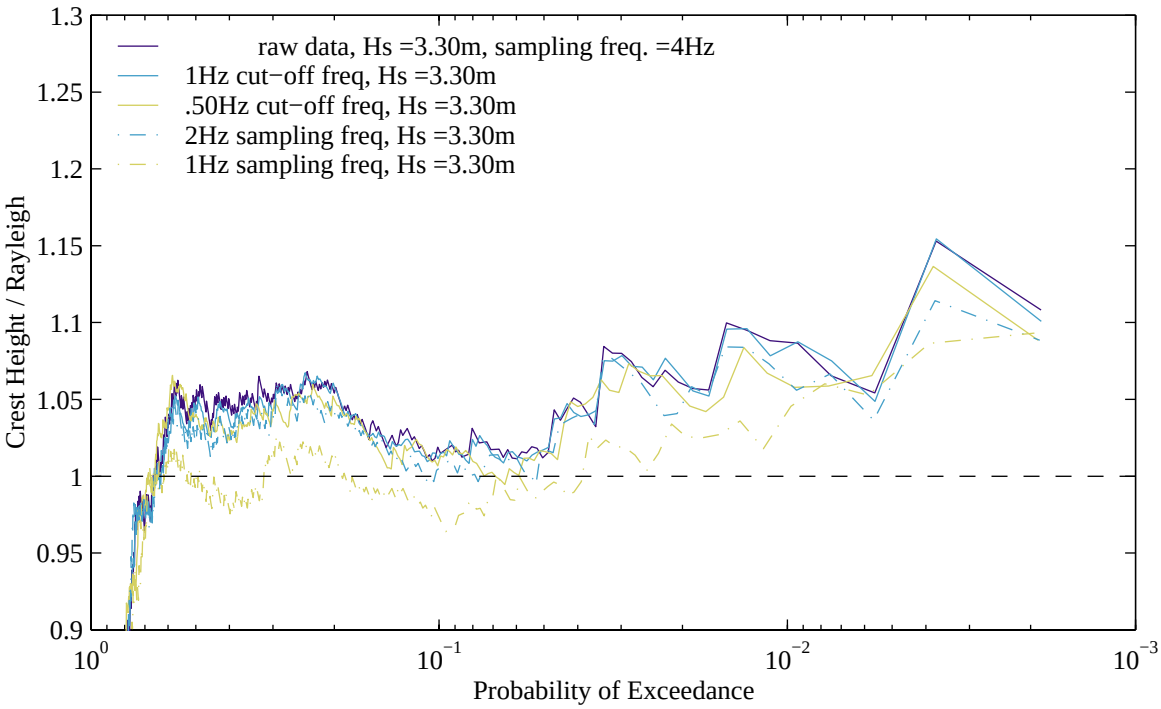

FIGURE 4.18 : Effect of sampling frequency, MAREXSGN crest height ratio

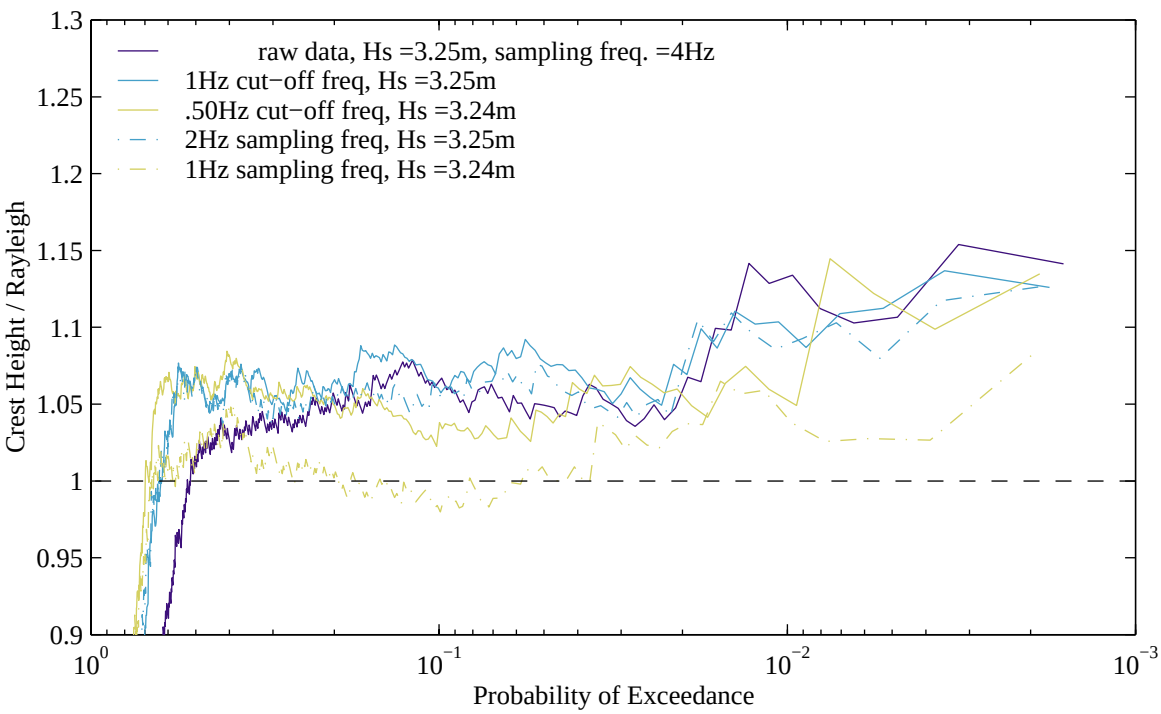

FIGURE 4.19 : Effect of sampling frequency, SAABRNIV crest height ratio

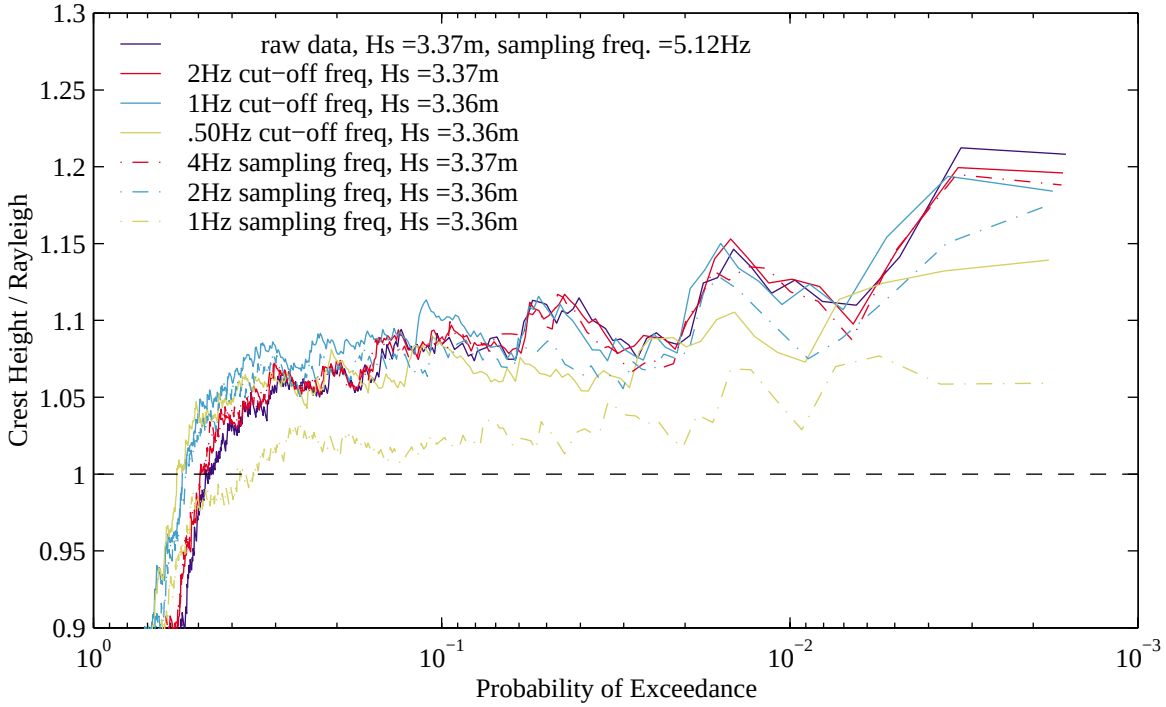

FIGURE 4.20 : Effect of sampling frequency, VLISSING crest height ratio

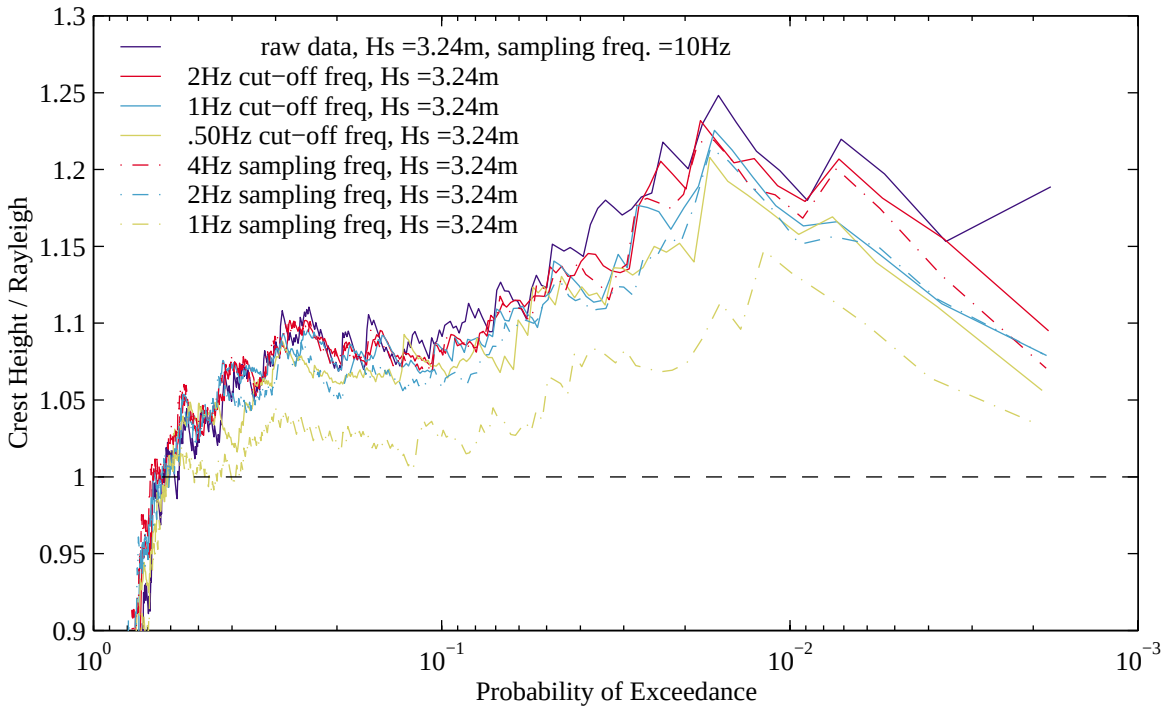

FIGURE 4.21 : Effect of sampling frequency, BAYLORWS crest height ratio

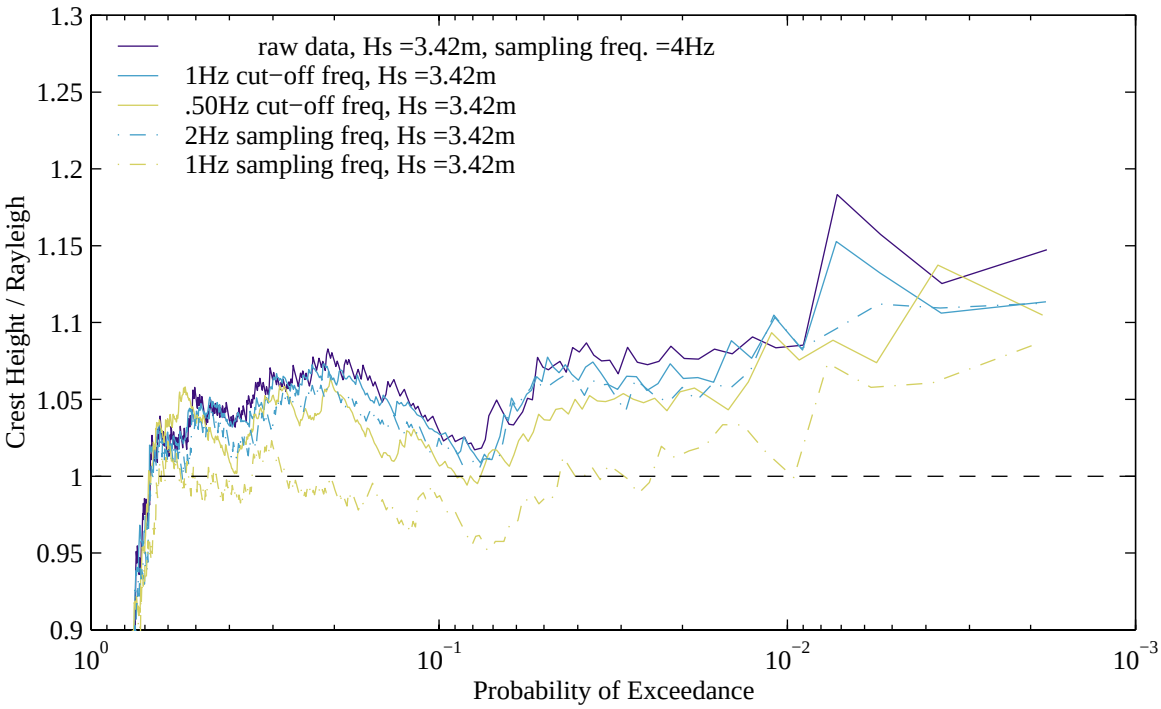

In conclusion, differences in the crest height statistics between the raw measurements of the sensors should not be due to the sampling frequency if it is equal to or higher than 4 Hz. This is the case for all the sensors, apart from WAVERGHR (1.28 Hz) and S4PRVELO (2 Hz). Lowpass filters with cut-off frequencies lower than 2 Hz progressively slightly decreases the CHR.

Gain correction

The problem of the gain correction is a difficult problem because no sensor can be considered as a reference. The WACSIS common data base has been constructed so that, at each date, sea state directional information was available from the Waverider. At this step we choose then the Hs given by the one-hour directional information from the Waverider as a reference. We will see later that it is not a perfect one. But for the aim of intercomparison of the sensors an absolute reference is not important. For the other sensors we use the Hs calculated from the measurements after applying a lowpass filter with a cut-off frequency at 0.64 Hz, the same as the Waverider measurements.

The coefficients of the linear regression between WAVERGHR and each sensor calculated from the larger data base intersection of the pair of sensors are given in table 4.5. The maximum number of time series is 360. It is important to notice that if we use the largest data base common to all the sensors (162 time series), which

does not contain the very severe sea states, the regression coefficients are different (table 4.6), and correspond to the ones given in [1].

TABLE 4.5 : Gain correction

	EMILASER	MAREXSGN	SAABRNIV	VLISSING	WAVERGHR	BAYLORWS
# of time series	232	325	327	353	292	325
regression coefficient	0.992	0.964	1.005	0.960	0.997	1.012

TABLE 4.6 : Gain correction, EMSVWB data base

	EMILASER	MAREXSGN	SAABRNIV	VLISSING	WAVERGHR	BAYLORWS
regression coefficient	0.995	0.971	1.017	0.980	0.999	1.024

Comparisons of crest height ratios

Comparison of crest height statistics from the sensors for individual sea states is difficult due to the different locations of the sensors and to the great variability in time and space of the wave field in wind sea conditions. This point will be verified with simulations in a later section, “Effect of the distance between sensors”, page 92.

By combining several hours of data with similar wave heights we can study the eliminate some of the sampling variability in single data records while still being able to see variations due to different ranges of wave heights. Since the crest height ratios are normalized by the significant wave height of the sensor during each record, there are no difficulties with combining records with different significant wave heights or with different sensors measuring slightly different significant wave heights during a sea state.

Figures 4.22 - 4.30 show the crest height ratios of all of the data in increments of 0.5 m in significant wave height. Some of the categories include relatively few hours of data. For example, Figure 4.22 includes 4 hours of data from the sensors other than the EMI and only 1 hour of data from the EMI. The statistical variability in this figure is thus very high, but the results in most of the other figures are rather robust. For example, Figure 4.23 for wave heights between 4.0 and 4.5 m includes data from 17 hours of data from most of the sensors.

Generally speaking, the Vlissingen gauge shows the highest crests, followed by the Saab radar. For significant wave heights greater than 3.0 m, the Marex radar records a few crests which are very high, to the extent that they are off the scale of the graphs. These very high crests, which we believe to be noise of some kind, are not seen when the significant wave height is less than 3.0 m. The EMI laser generally shows the lowest crest heights. The Baylor wave staff usually shows crest which are a few percent higher than the EMI.

These figures show very clearly that the crest height ratio increases with increasing significant wave height. This fact illustrates the fundamental non-linearity of the heights of wave crests. In theory, many other factor such as wave steepness and the degree of directional spreading could influence the crest height ratio, but for this data set, we found that the range of those variables was small, and the crest height ratios could be ranked almost entirely by the significant wave height.

FIGURE 4.22 : Crest height ratios for significant wave heights between 4.5 and 5.0 m.

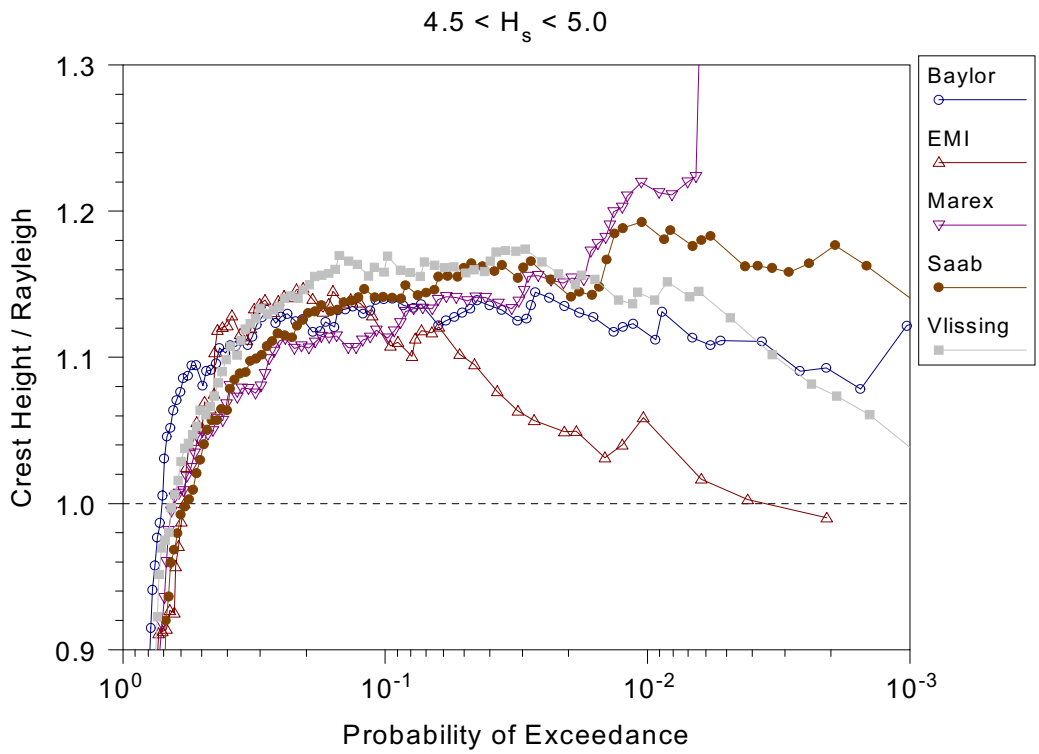

FIGURE 4.23 : Crest height ratios for significant wave heights between 4.0 and 4.5 m.

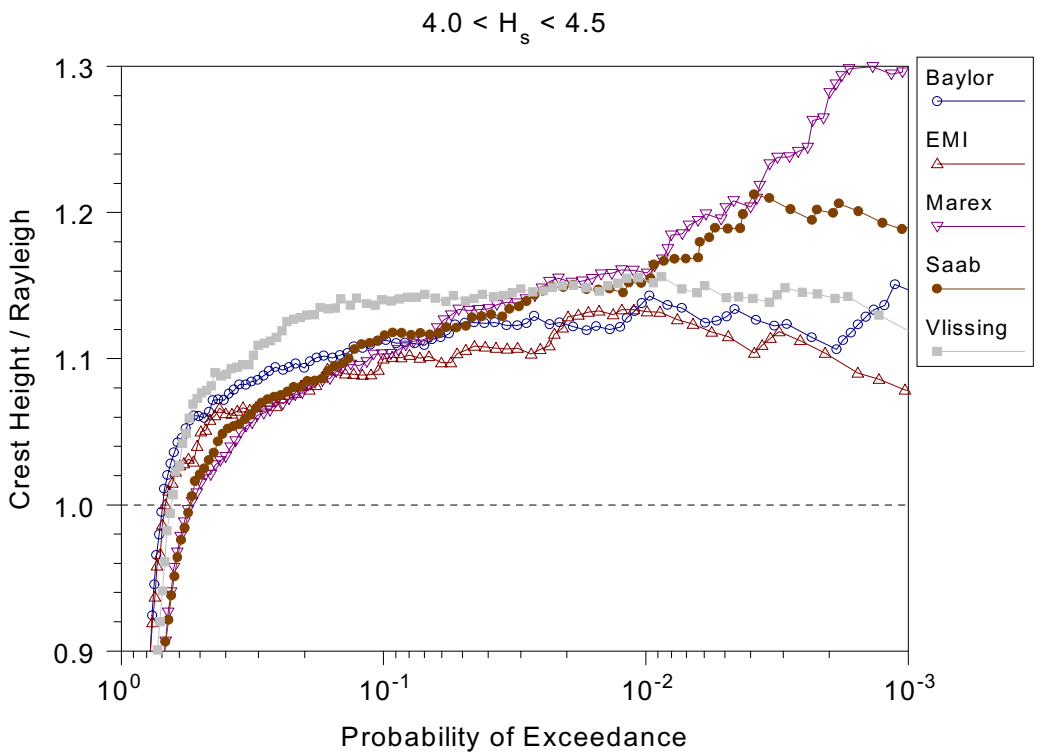

FIGURE 4.24 : Crest height ratios for significant wave heights between 3.5 and 4.0 m.

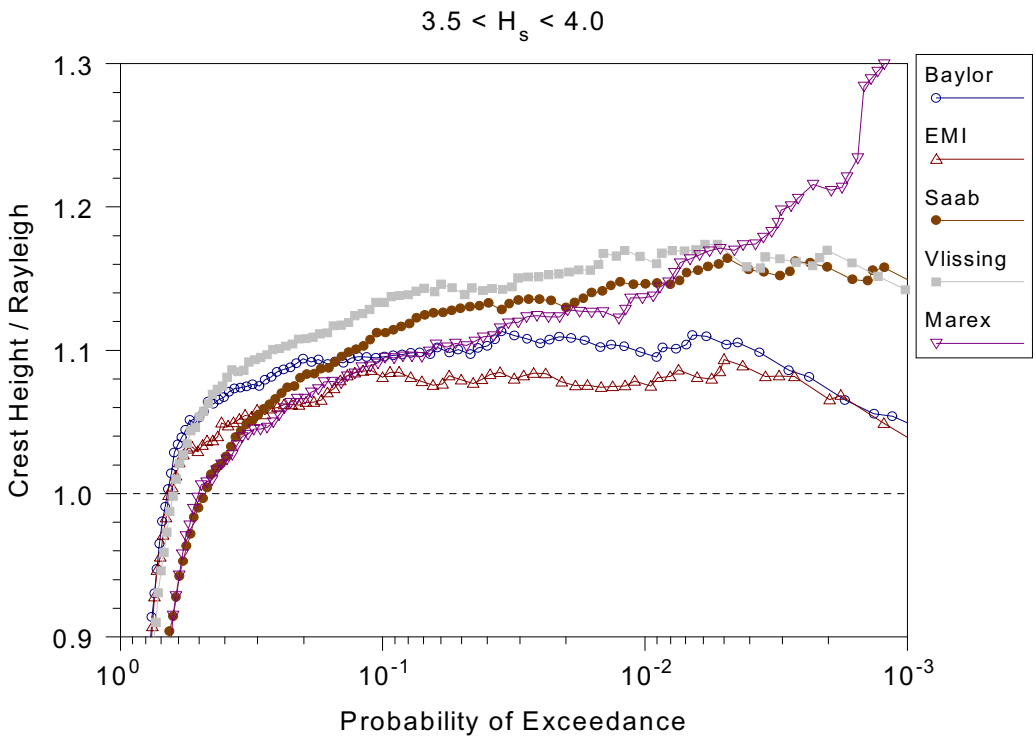

FIGURE 4.25 : Crest height ratios for significant wave heights between 3.0 and 3.5 m.

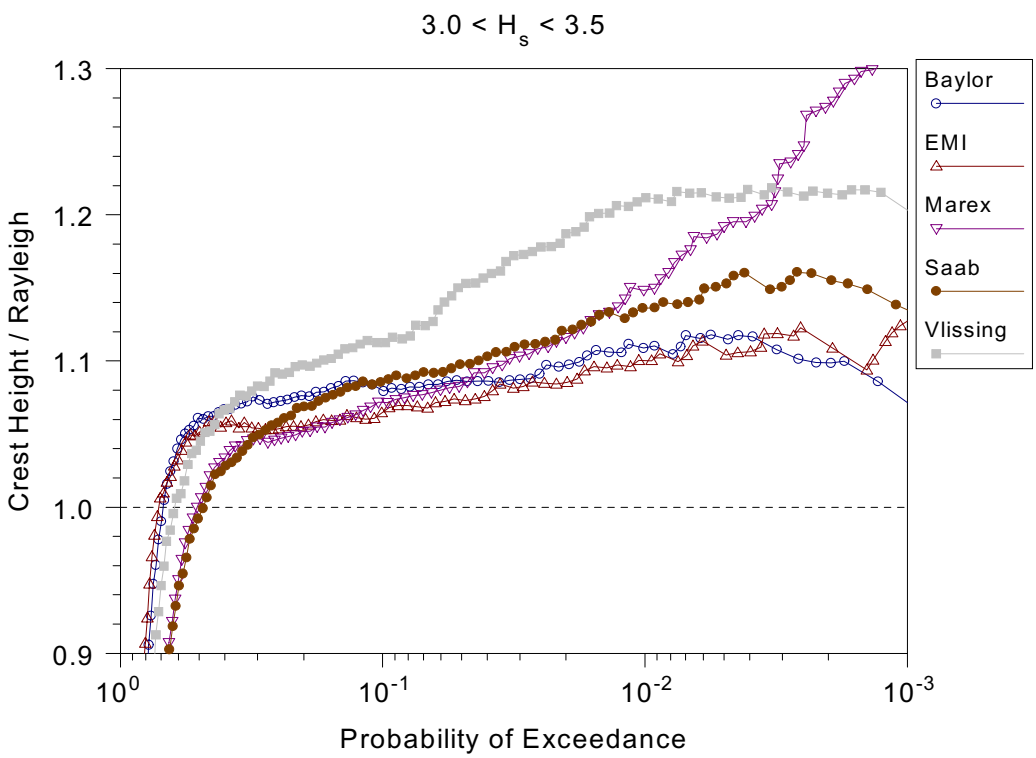

FIGURE 4.26 : Crest height ratios for significant wave heights between 2.5 and 3.0 m.

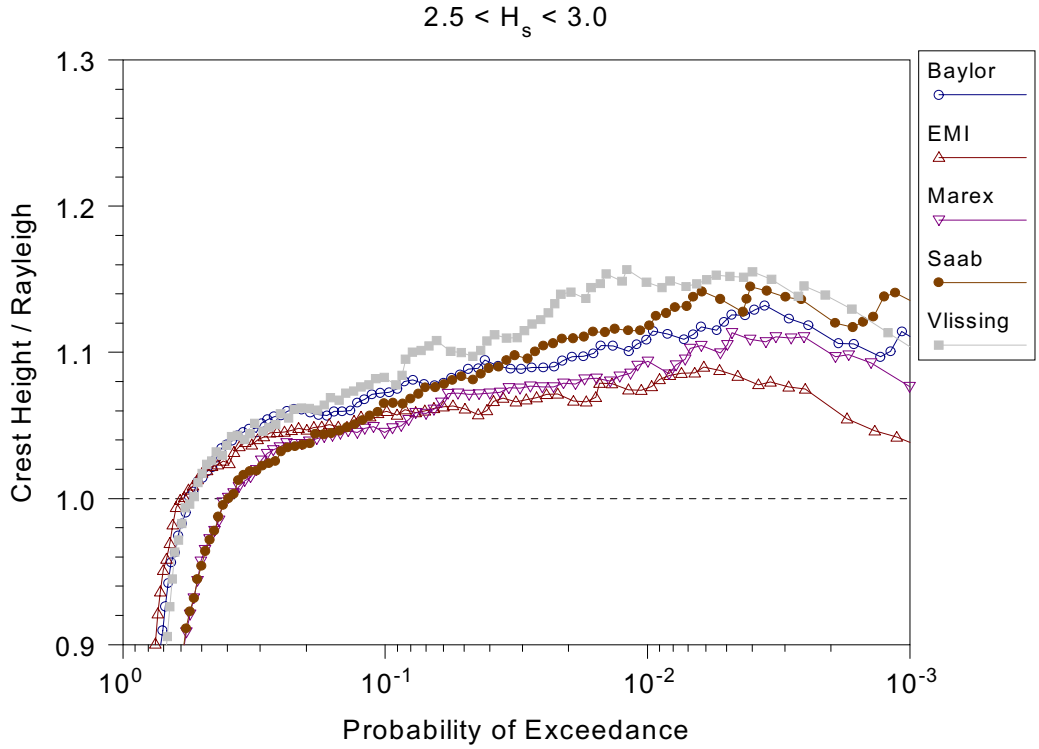

FIGURE 4.27 : Crest height ratios for significant wave heights between 2.0 and 2.5 m.

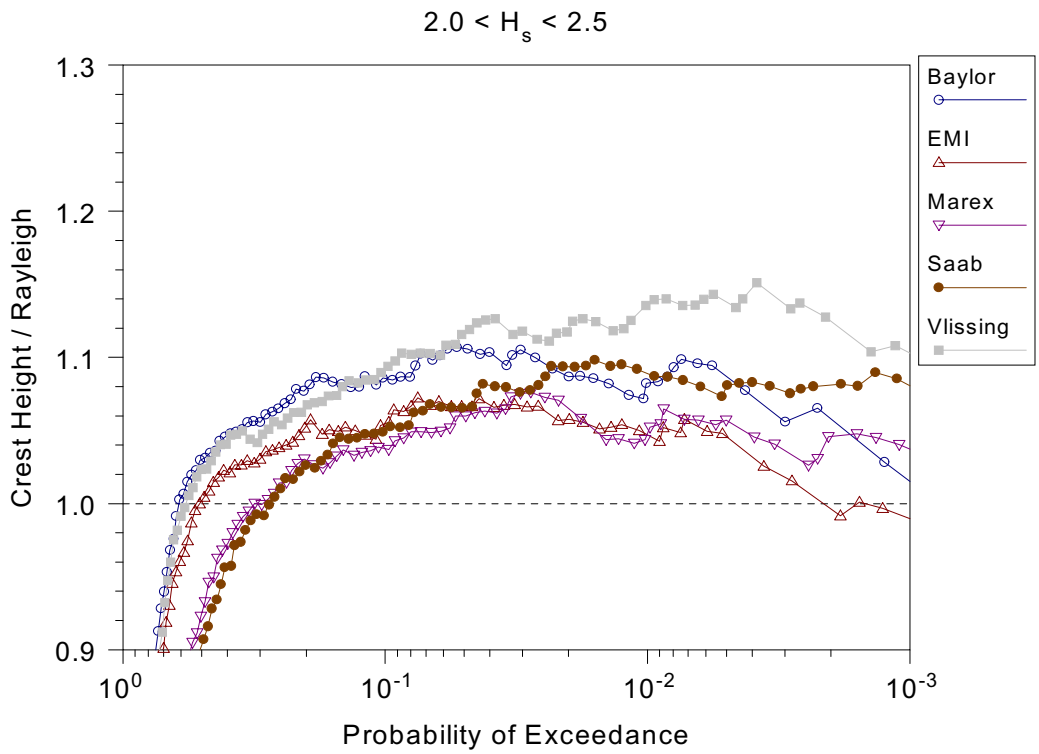

FIGURE 4.28 : Crest height ratios for significant wave heights between 1.5 and 2.0 m.

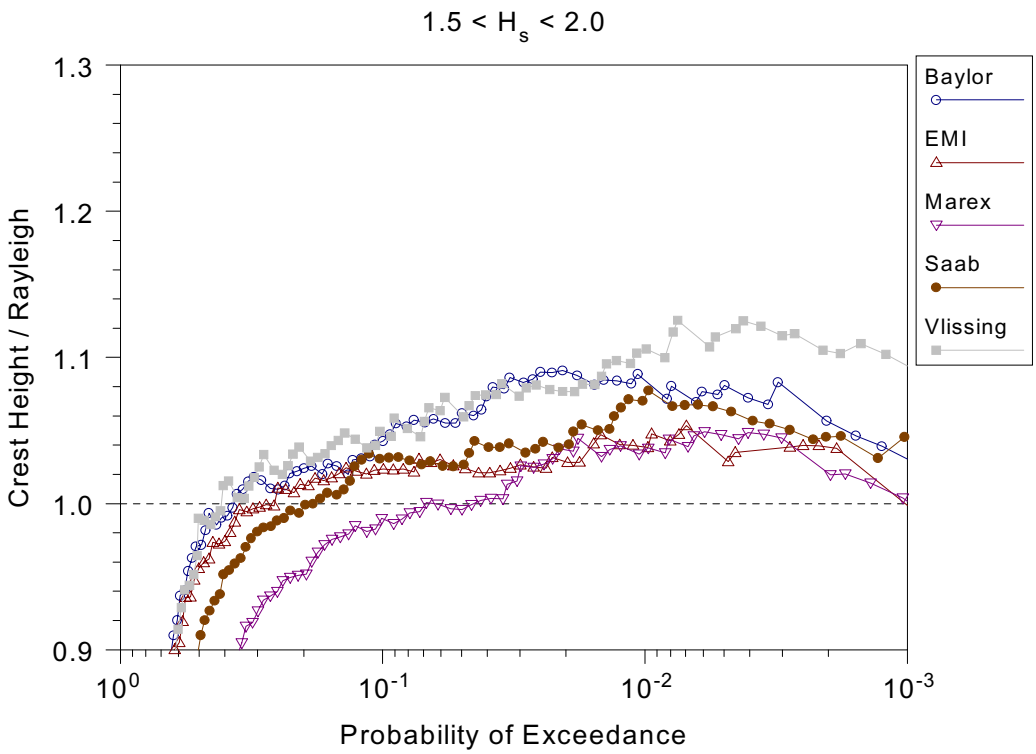

FIGURE 4.29 : Crest height ratios for significant wave heights between 1.0 and 1.5 m.

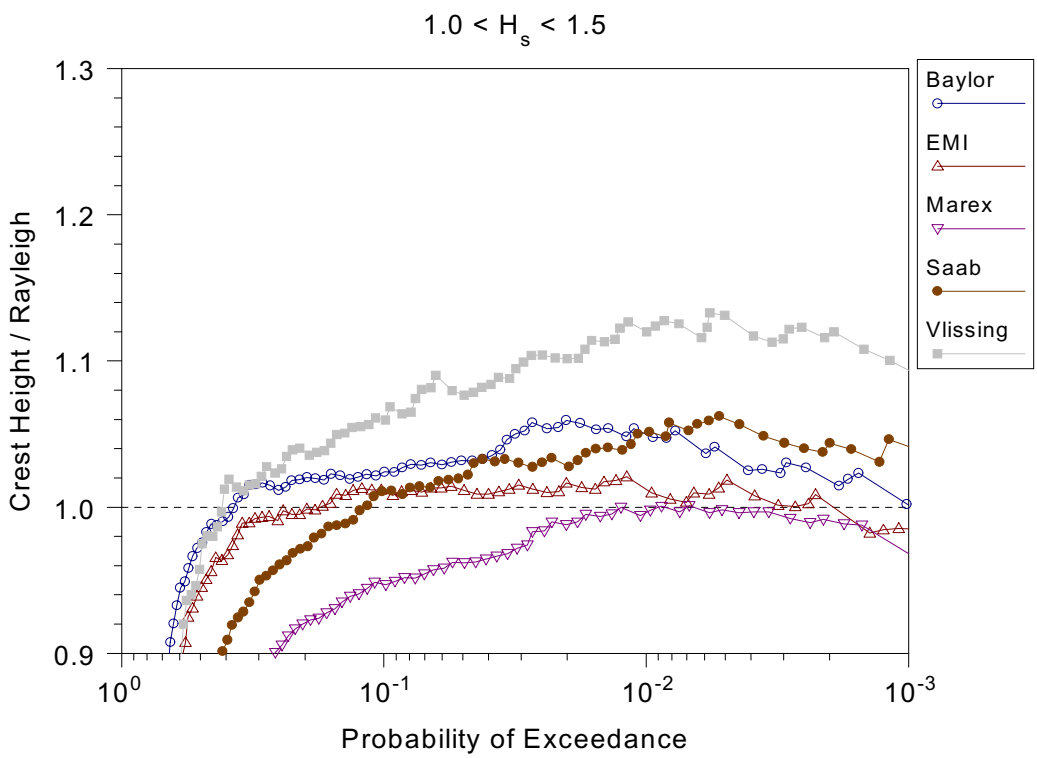

FIGURE 4.30 : Crest height ratios for significant wave heights between 0.5 and 1.0 m.

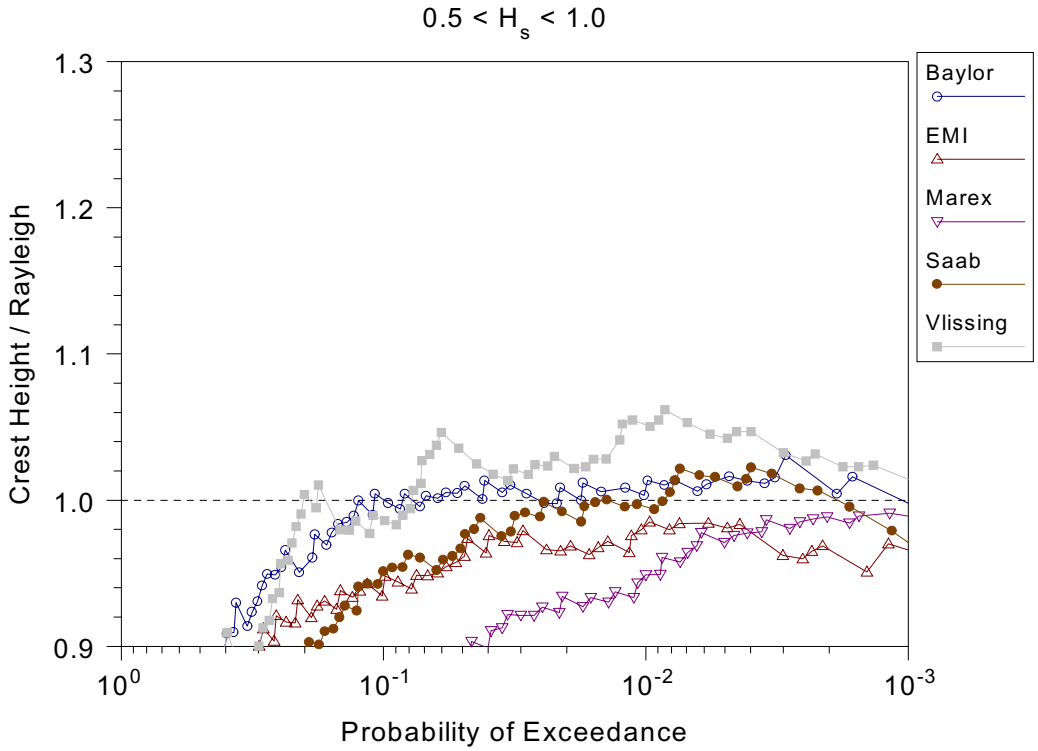

Statistics of crests all-over campaign

The analysis of the waves accumulated over all of the campaign furnishes another precise tool of comparison. Due to the poor sampling of severe sea states in the EMILASER data base, we have analysed separately two data bases, one without EMILASER (called MSVB) and a second one with only EMILASER and BAYLORWS (called EB).

The gain corrections indicated in table 4.5 have been applied and the number of exceedances has been calculated from the raw data and on the filtered data. Filtered here means a sampling frequency equal to 4 Hz and a lowpass filter at 0.64 Hz (a frequency of 0.64 Hz corresponds to a wavelength of 3.8m).

In the MSVB data base using raw data (figure 4.31), we observe clear differences between the sensors, BAYLORWS giving the lower levels of crest height (Crest height levels for an exceedance number of 100 are given in table 4.7). Due to a great number of spikes in the data (see [1]), a very strong overestimation of the crest heights by MAREXSGN appears over 4m.

When the data are filtered (figure 4.32), we observe a decrease of the crest heights from all the sensors. The decrease is greater for VLISSING (30cm at 100 exceedance number) than for BAYLORWS (16cm) or SAABRNIV (20cm).

The results from the EB data base show a slight difference in the raw data (figure 4.33) between BAYLORWS and EMILASER, and the filtered data (figure 4.34)

shows a decrease of the crest heights from both the sensors, higher for BAYLORWS (14 cm at 100 exceedance number) than for EMILASER (7 cm).

Considering only the filtered results which include components with wavelengths up to 3.8 m, it appears that VLISSING, BAYLORWS and EMILASER give very close results, SAABRNIV overestimates, and MAREXSGN is contaminated by noise spikes even after the filtering.

FIGURE 4.31 : MSVB Crest levels, Raw data

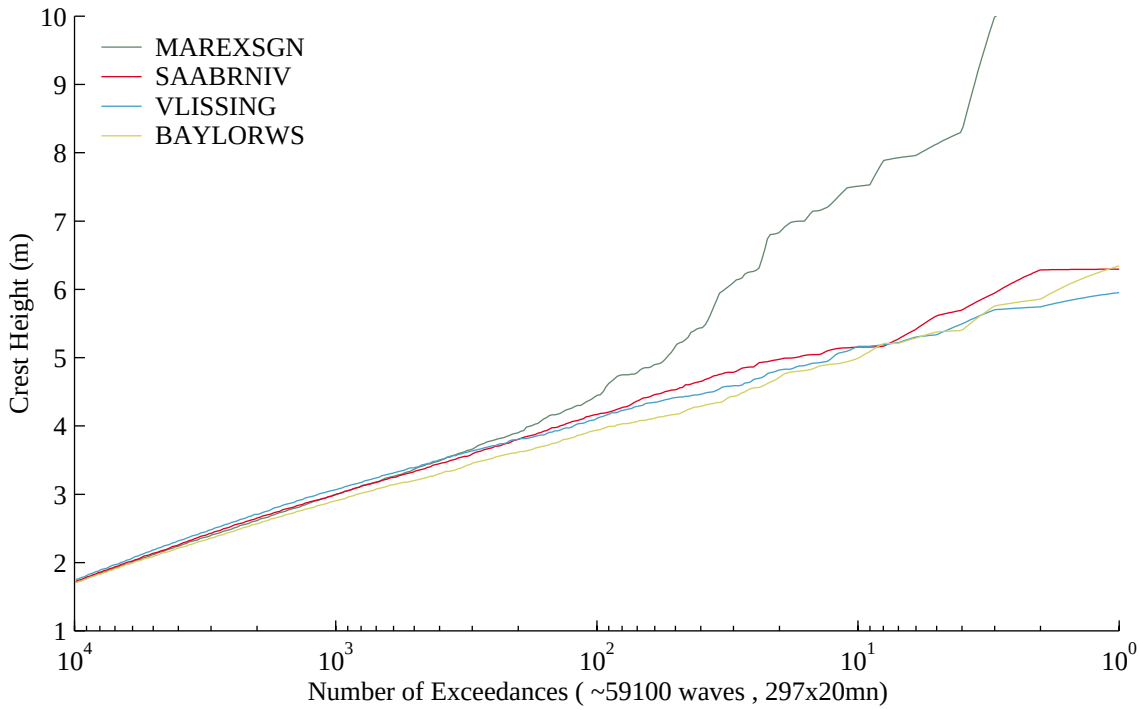

FIGURE 4.32 : MSVB Crest levels, Filtered data

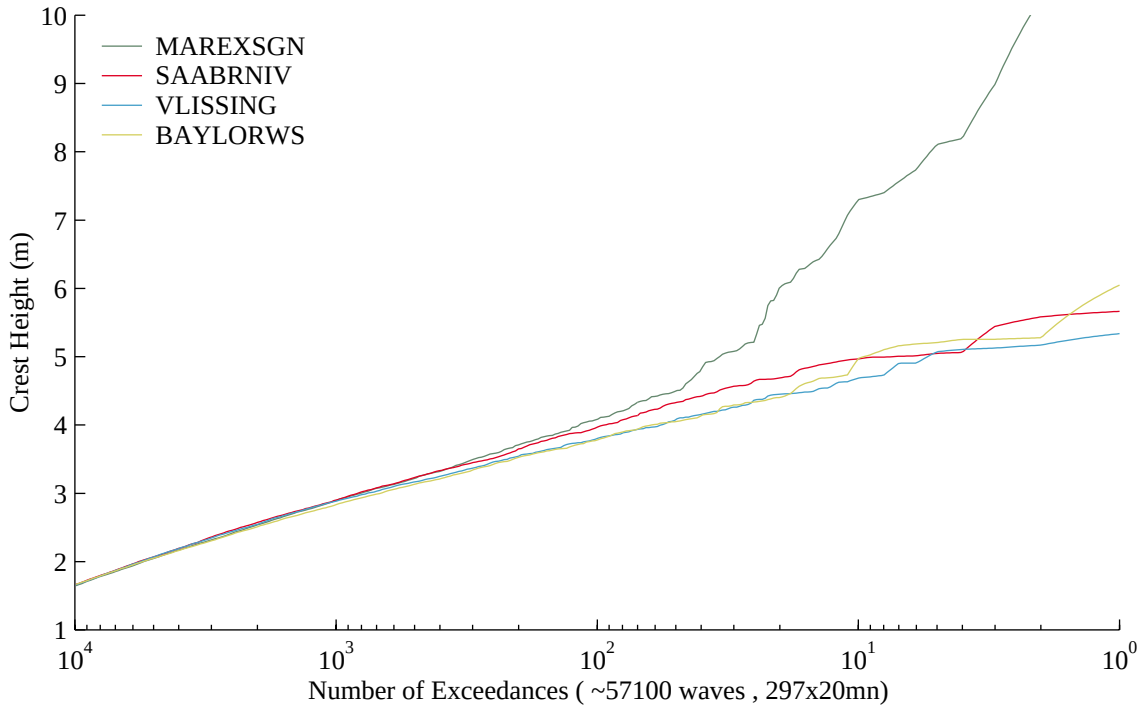

FIGURE 4.33 : EB Crest levels, Raw data

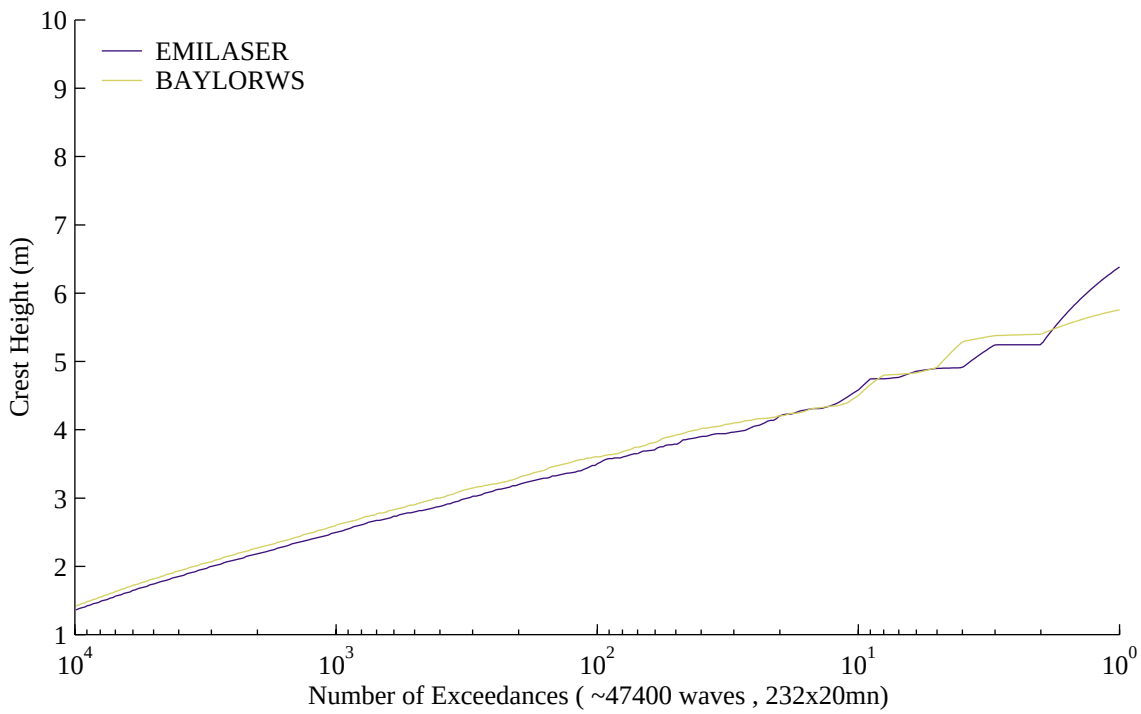

FIGURE 4.34 : EB Crest levels, Filtered data

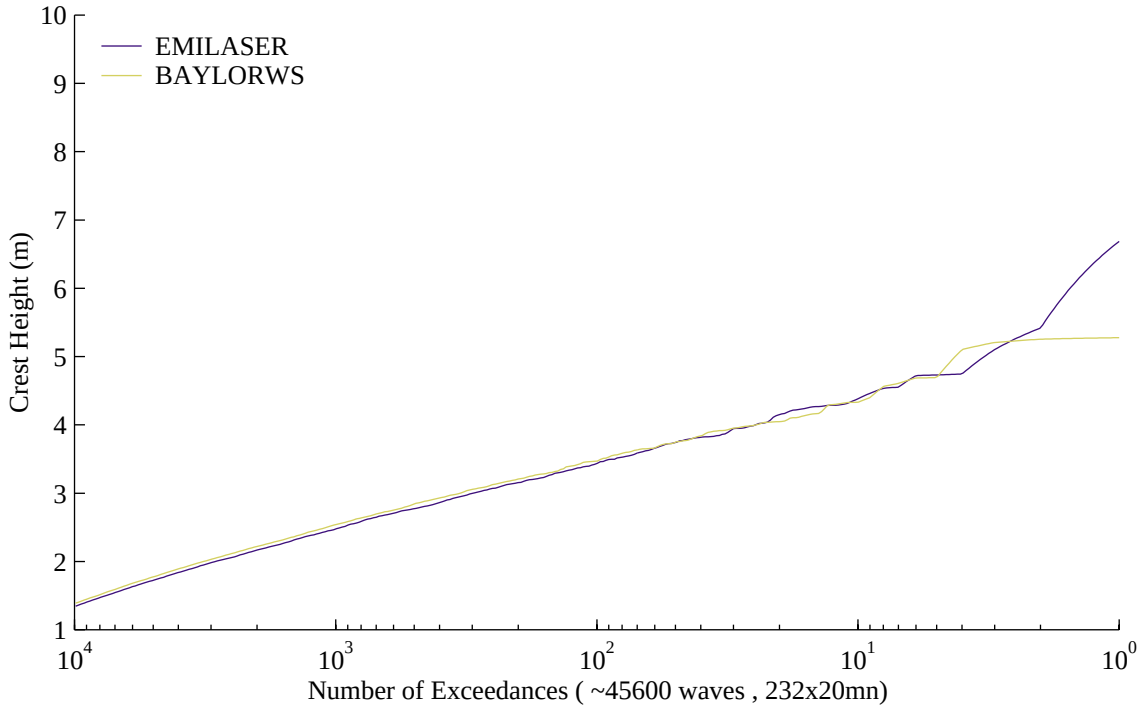

Statistics of troughs all-over campaign

The same analyses on the troughs are very instructive (figure 4.35 to 4.38, table 4.7).

First, apart for some high levels due to spikes on the data, all the sensors give very close results. However some problems seem to remain on MAREXSGN. And secondly the filtering has practically no effect on the trough heights (< 4cm), apart from the spikes.

This also probably proves that the gain correction was correctly well applied.

FIGURE 4.35 : MSVB Trough levels, Raw data

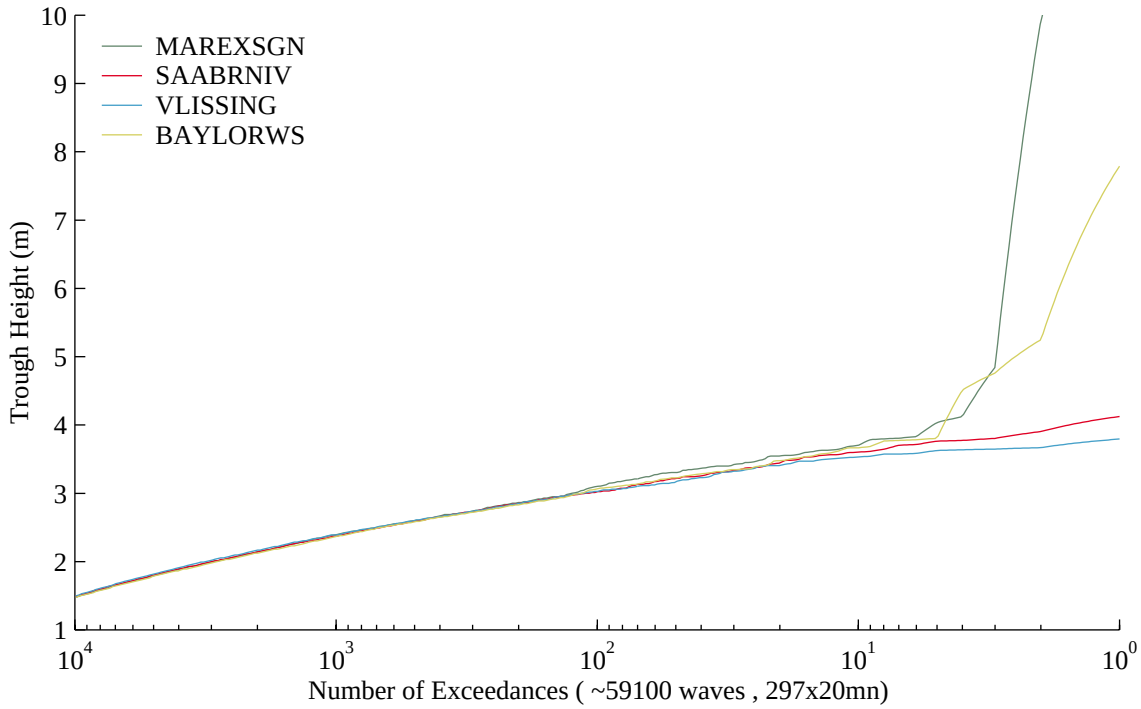

FIGURE 4.36 : MSVB Trough levels, Filtered data

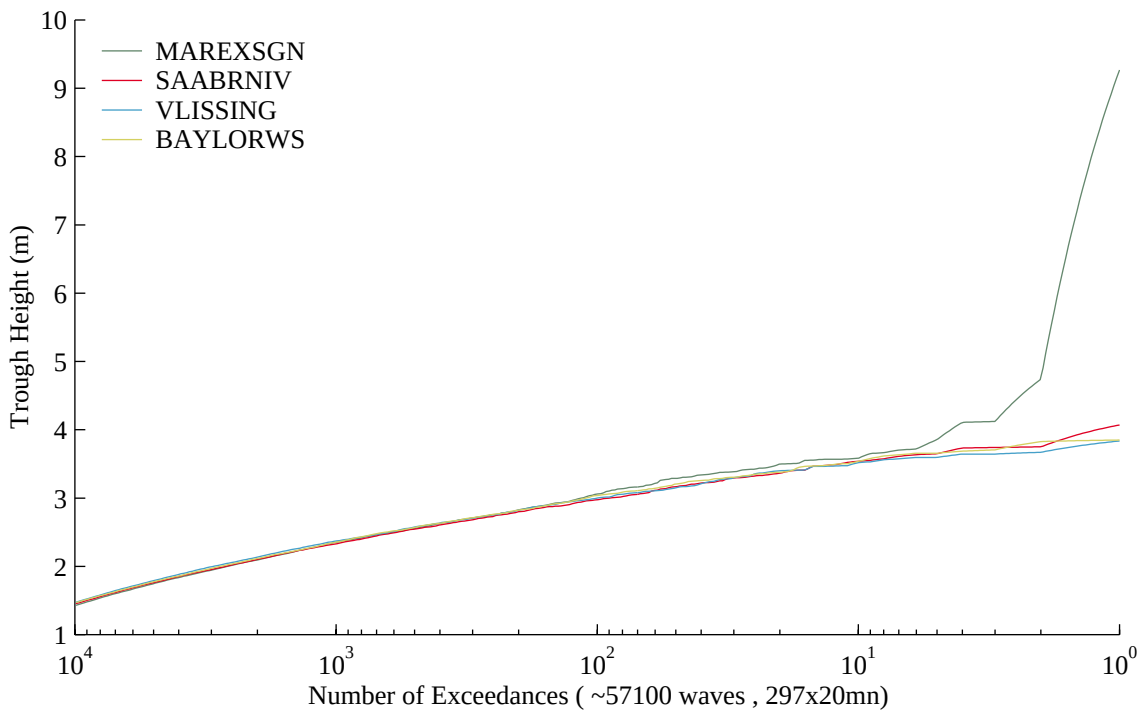

FIGURE 4.37 : EB Trough levels, Raw data

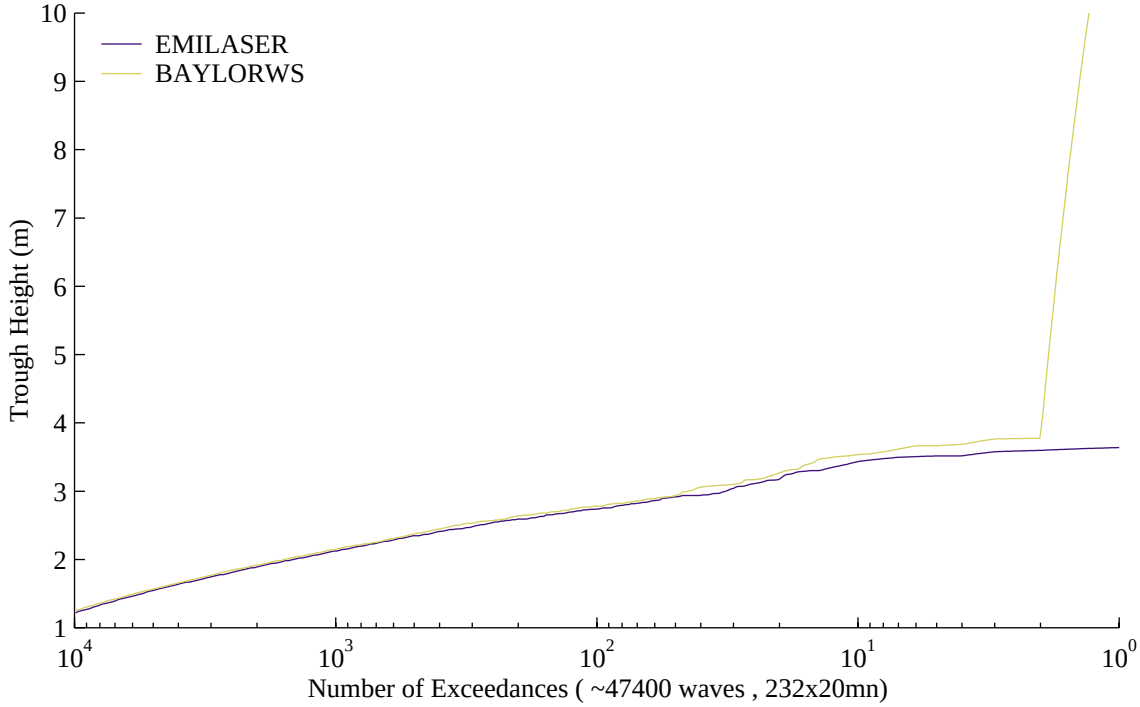

FIGURE 4.38 : EB Trough levels, Filtered data

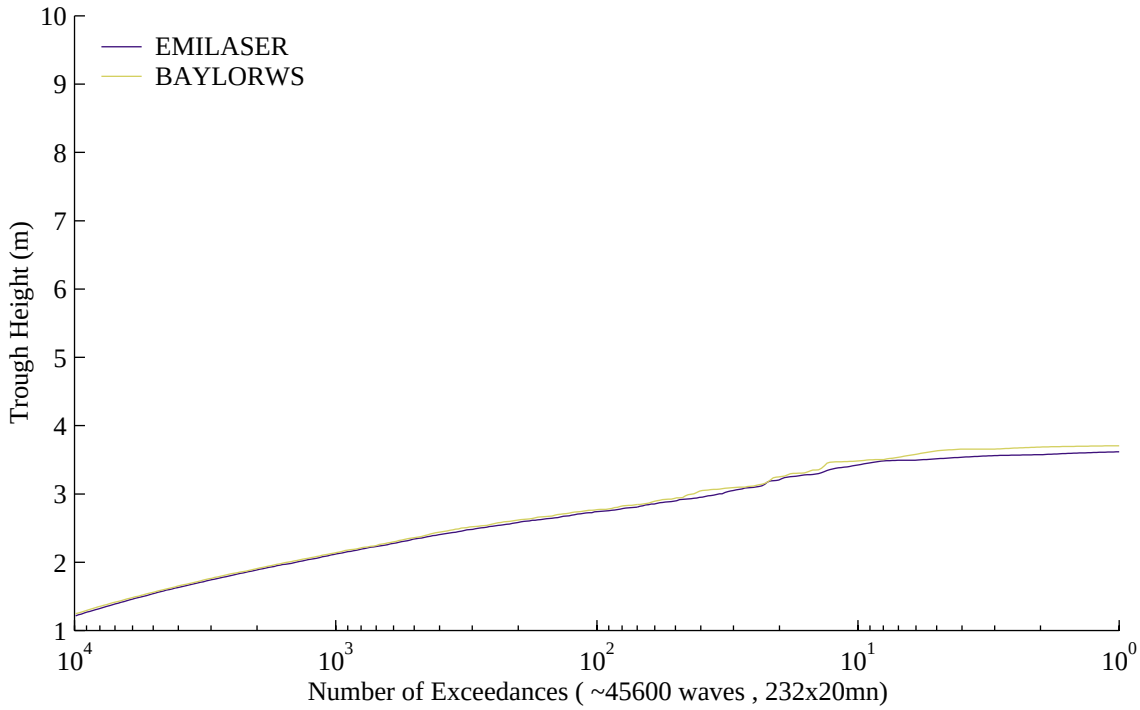

TABLE 4.7 : Crest and trough levels (m) for Exceedance Number equal 100

			EMILASER	MAREXSGN	SAABRNIV	VLISSING	BAYLORWS
Crest	MSVB	Raw		4.45	4.17	4.11	3.94
		Filtered		4.08	3.97	3.80	3.78
	EB	Raw	3.51				3.61
		Filtered	3.44				3.47
Trough	MSVB	Raw		3.10	3.02	3.03	3.07
		Filtered		3.06	2.98	3.00	3.04
	EB	Raw	2.74				2.78
		Filtered	2.74				2.77

Conclusion

The comparison of the crest height statistics between the different sensors shows that the raw data of the sensors gives different crest statistics. This is not true for the troughs.

If we observe in detail typical crest shapes measured by VLISSING (figure 4.39), little waves riding on crests appear very often. This phenomena is rarely or never observed on the troughs. The frequency of these little waves are roughly between 0.5Hz to 0.3Hz. Their very high frequency and significant amplitude must be due to a modulation effect that enhances riding wave on the crest and reduce it on the trough. When the data is filtered to 0.64Hz, these little waves disappear and the crest height decreases.

The differences of measurement principle, and the different filtering induced in space and time, render with more or less fidelity these little waves. This explains in great part the decrease of crest height observed in the previous figures and in table 4.7.

When the data are filtered to 0.64 Hz, to include only long waves, VLISSING, BAYLORWS and EMILASER give very close results. However, when the short waves are filtered out, SAABRNIV still overestimates the crest heights and MAREXSGN is too much perturbed by spikes to be compared with the other sensors.

FIGURE 4.39 : VLISSING crest details, raw data (blue), filtered data (green)

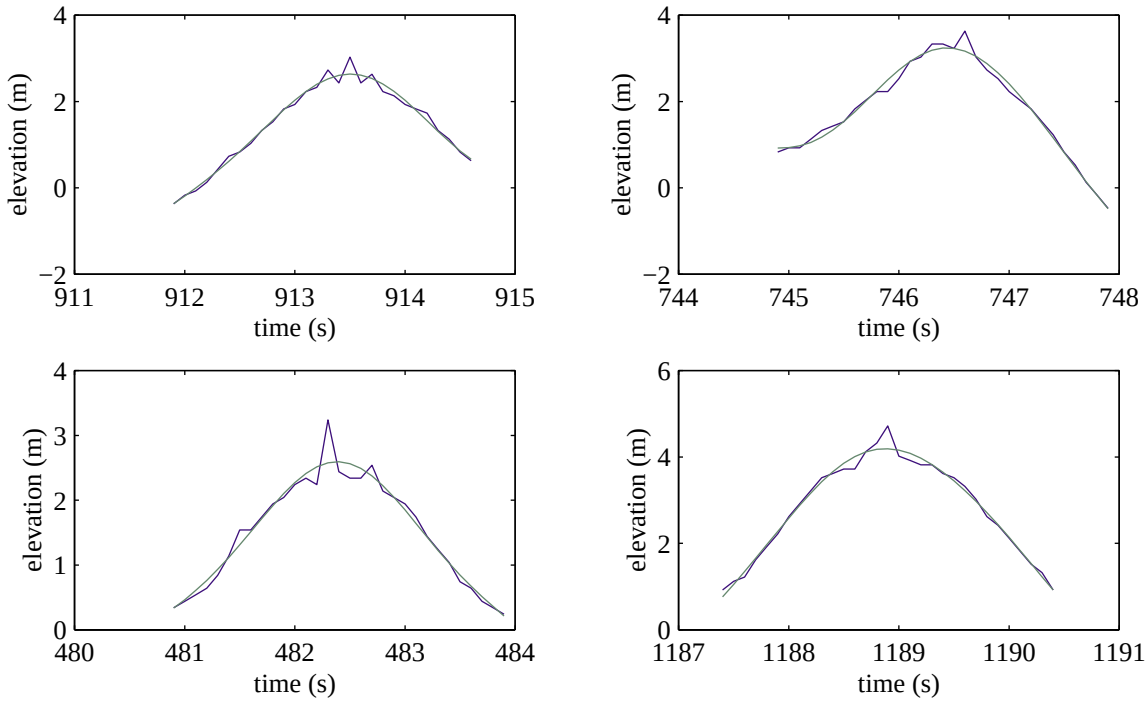

CHAPTER 5

Simulation methods
Effect of simulation parameters

Marc Prevosto
Benjamin Moreau
George Z. Forristall

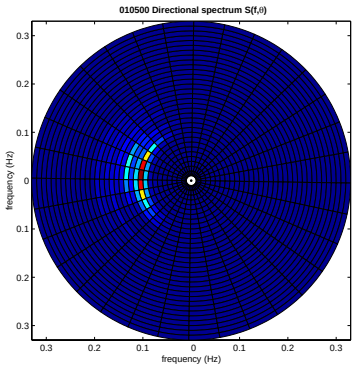

In order to compare crest statistics given by second order models of wave kinematics with the measurements and to fit parameterized models of crest heights, we have used simulation methods for the elevation of the free surface. The formulas are based on the irregular wave version of the second order Stokes expansion. They were calculated for infinite water depth by Longuet-Higgins [15] and the calculations were extended to intermediate water depth by Sharma and Dean [24]. These models will be described in the first part of this chapter.

The calculations were coded independently at Shell and Ifremer. Comparisons showed that the programs gave exactly the same answers when the same input parameters and discretizations were used, but there are many details which can influence the accuracy of the results. It is necessary to understand as well as possible the effects of the angular and frequency discretization, the angular and frequency truncation, the water depth and the source of the input spectrum. These different points are tackled in the second part of the chapter.

Models of wave surface elevation

The nonlinear model of the elevation process is the superposition of two processes:

$$\eta(t) = \eta_1(t) + \eta_2(t) \qquad \textbf{(EQ 5.1)}$$

The first order (linear) part $\eta_1(t)$ of this model is a directional Gaussian process (superposition of Airy waves in different directions of propagation with random phases and amplitudes):

Linear part

$$\eta_1(t) = \sum_{\theta, f} b(\theta, f)\sin(2\pi f) + c(\theta, f)\cos(2\pi f) \qquad \textbf{(EQ 5.2)}$$

with b and c Gaussian random variables defined by

$$\mathbb{E}(b(\theta, f)^2) = \mathbb{E}(c(\theta, f)^2) = S(\theta, f)d\theta df, \quad \textbf{(EQ 5.3)}$$

and $\mathbb{E}(b(\theta_i, f_j)c(\theta_k, f_l)) = 0$ **(EQ 5.4)**

where $S(\theta, f)$ is the directional spectral density.

$\eta_1(t)$ can be re-written

$$\eta_1(t) = \sum_{\theta, f} a(\theta, f)\sin(2\pi f + \phi(\theta, f)) \quad \textbf{(EQ 5.5)}$$

with now $a(\theta, f)$ a Rayleigh random variable and $\phi(\theta, f)$ a uniform random variable in [-π,π], with

$$\mathbb{E}(a(\theta, f)^2) = 2S(\theta, f)d\theta df \quad \textbf{(EQ 5.6)}$$

and $a(\theta_i, f_j)$, $\phi(\theta_k, f_l)$ independent variables. **(EQ 5.7)**

Using equations 5.2-5.4 or equations 5.5-5.7 includes the proper variability of the spectral amplitudes and so of the Gaussian process

2nd order directional - 3D

The 2nd order Stokes expansion based on this linear part is

$$\begin{aligned}\eta_2(t) = &\sum_{\theta_i, f_j, \theta_k, f_l} a(\theta_i, f_j)a(\theta_k, f_l)T^D(\theta_i, f_j, \theta_k, f_l)\cos(2\pi(f_j - f_l) + (\phi(\theta_i, f_j) - \phi(\theta_k, f_l))) \\ &+ \sum_{\theta_i, f_j, \theta_k, f_l} a(\theta_i, f_j)a(\theta_k, f_l)T^S(\theta_i, f_j, \theta_k, f_l)\cos(2\pi(f_j + f_l) + (\phi(\theta_i, f_j) + \phi(\theta_k, f_l))) \\ &- c_{\eta_2}\end{aligned} \quad \textbf{(EQ 5.8)}$$

where c_{η_2} is a constant to ensure that $\mathbb{E}(\eta_2(t)) = 0$.

The two 2nd order transfer functions T^S and T^D of course depend of the water depth. Their expressions are given in appendix 5.1.

2nd order uni-directional - 2D

If now we consider a uni-directional wave train in which all the components propagate in the same direction, we obtain, of course, the same linear part of the elevation, but a different second order part.

$$\eta_1(t) = \sum_{\theta, f} a(\theta, f)\sin(2\pi f + \phi(\theta, f)) = \sum_f a_u(f)\sin(2\pi f + \phi_u(f)) \quad \textbf{(EQ 5.9)}$$

$$\eta_2(t) = \sum_{f_j, f_l} a_u(f_j)a_u(f_l)T_u^D(f_j, f_l)\cos(2\pi(f_j - f_l) + (\phi_u(f_j) - \phi_u(f_l)))$$
$$+ \sum_{f_j, f_l} a_u(f_j)a_u(f_l)T_u^S(f_j, f_l)\cos(2\pi(f_j + f_l) + (\phi_u(f_j) + \phi_u(f_l)))$$
$$- c_{\eta_2}$$

Non-linear narrowband - 2D

A simplified model of 2nd order uni-directional waves is obtained if the spectral density is sufficiently narrow to consider the 2nd order transfer functions as constant. In this case,

$T_u^D(f_j, f_l)$ (resp. $T_u^S(f_j, f_l)$) are considered constant and equal to $T_{nb}^D(f_m)$, (resp. $T_{nb}^S(f_m)$), with

$$T_{nb}^D(f_m) = \lim_{\substack{f_j \to f_m \\ f_l \to f_m}} T_u^D(f_j, f_l) \text{ and } T_{nb}^S(f_m) = \lim_{\substack{f_j \to f_m \\ f_l \to f_m}} T_u^S(f_j, f_l) \qquad \textbf{(EQ 5.10)}$$

which gives for the second order part

$$\eta_2(t) = T_{nb}^D(f_m)\sum_{f_j, f_l} a_u(f_j)a_u(f_l)\cos(2\pi(f_j - f_l) + (\phi_u(f_j) - \phi_u(f_l)))$$
$$+ T_{nb}^S(f_m)\sum_{f_j, f_l} a_u(f_j)a_u(f_l)\cos(2\pi(f_j + f_l) + (\phi_u(f_j) + \phi_u(f_l))) \qquad \textbf{(EQ 5.11)}$$
$$- T_{nb}^D(f_m)\sum_{f_j} a_u^2(f_j)$$

if $\eta_1(t)$ is considered as a product of an amplitude and a phase time function, $\eta_1(t) = A(t)\cos(\Omega(t))$, where the amplitude and instantaneous frequency are slowly varying, the unidirectional narrowband second order part becomes

$$\eta_2(t) = T_{nb}^D(f_m)A^2(t)$$
$$+ T_{nb}^S(f_m)A^2(t)\cos(2\Omega(t)) \qquad \textbf{(EQ 5.12)}$$
$$- \frac{1}{8}H_s^2 T_{nb}^D(f_m)$$

The formulas for T_{nb}^D and T_{nb}^S are given in appendix 5.2.

Simulation method

The simulation method consists of calculating the formulas of the 2nd order transfer function, drawing $b(\theta, f)$ and $c(\theta, f)$ from the linear part (EQ 5.2) and calculating the 2nd order part taking into account all the interactions between the components. The draw of b and c coefficients depends of the directional spectral density of the sea-states.

Directional spectrum

The Waverider used during the WACSIS campaign furnished directional information (see “WACSIS Web site”, page 16), which does not completely describe the directional spectrum. To complete this information we have to choose a model of shape of directional spreading.

We have used for that the Longuet-Higgins (Mitsuyasu) $\cos^{2s}$ model

$$S(f, \theta) = S(f)H(f, \theta) \qquad \textbf{(EQ 5.13)}$$

with

$$H(f, \theta) = A(s(f))\cos^{2s(f)}\left(\frac{\theta - \bar{\theta}(f)}{2}\right) \qquad \textbf{(EQ 5.14)}$$

The Waverider furnishes the point spectrum $S(f)$ and the variations with frequency of the mean direction $\bar{\theta}(f)$ and of the spreading coefficient $s(f)$.

Truncation of the spectrum

As it is explained in [4] (Chen, 1994), the non-linear interactions between long and short waves are very badly calculated with a Stokes expansion and for better accuracy it is better to introduce a modulated wave-mode approach. This approach results in a so-called hybrid model [30]. This approach may be necessary in the computation of the kinematics in the crest, but in the case of free-surface elevation, a simpler method can be used to avoid the poor convergence of the Stokes expansion for the calculation of the non-linear interactions between long and short waves. It consists merely in a truncation of the spectral density, thus removing very long and short waves from the nonlinear interactions. This will also reduce the time of computation.

To reduce the computation time we have also truncated the spectrum in direction, removing from the 2nd order calculation the directions in which the contribution to the total energy was very low (figure 5.2).

Effect of simulation parameters

The accuracy of the simulation depends on some parameters which have to be determined carefully to avoid bias in the comparison between the simulations and the measurements.

Discretization of the directional spectrum

The interval [-π,+π] has been regularly discretized into 255, 127, 63, 31, 15, 7, 3, or 1 sectors (figure 5.4). The case with 1 sector corresponds to the 2D case. The comparison of the crest height ratio for these different discretizations (figure 5.5) shows that, for a typical sea state at the WACSIS site, 31 sectors are needed to accurately simulate the effect of spreading on the nonlinear interactions.

FIGURE 5.1 : Spectral truncation

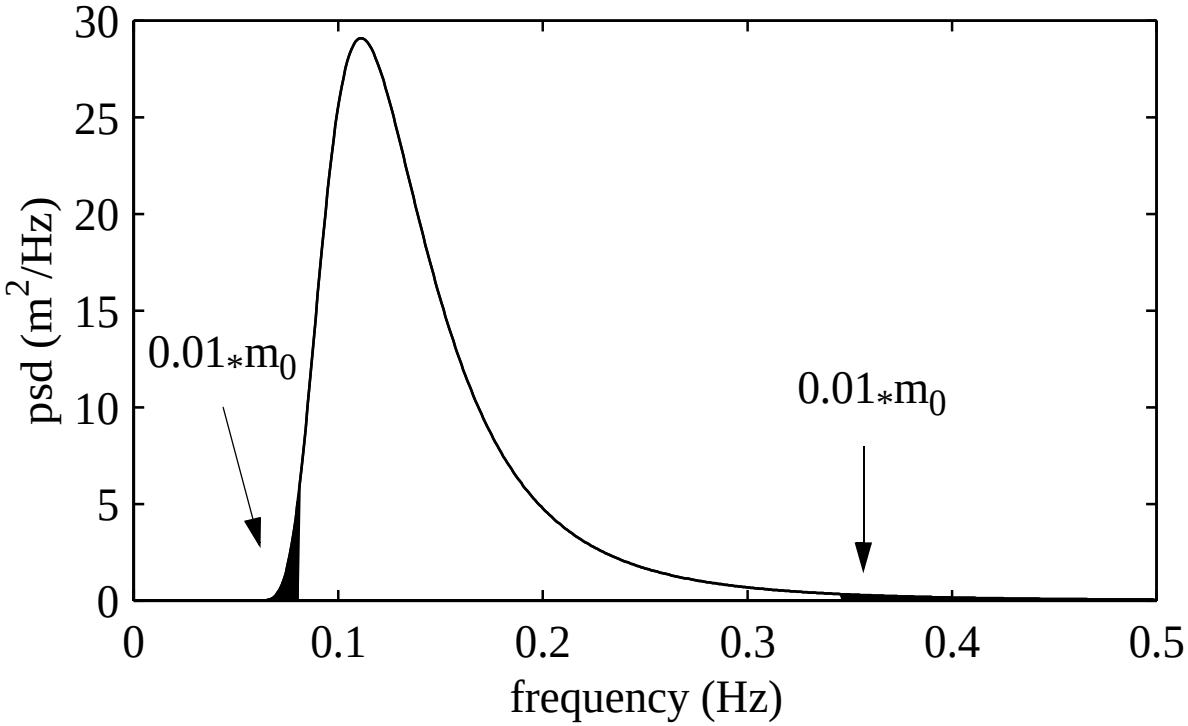

Frequency truncation

The effect of frequency truncation is quite different in amplitude for the 2D (figure 5.6) and the 3D (figure 5.7) case. Four percentages of truncation have been tested: 1%, 2%, 5%, 10%. The percentages indicated correspond to the amount of energy removed from each side of the peak frequency, starting from the lowest and the highest frequencies (see figures 5.1).

The crest height ratio has been calculated from 100 hours of simulations corresponding to the sea state of January the 5th 00:00. Compared to the case without truncation the truncation of 1% increases the crest heights to a great extent in the 2D case and slightly in the 3D case. In observing the time series it is clear that the case without truncation generates waves with unphysical shapes due, as said previously, to the very bad convergence of the short-long waves interactions. In removing 1% energy of the shorter waves and 1% energy of the longer waves we remove a very small part of the nonlinear interactions but avoid the relatively large error of convergence of their interactions (especially for 2D). When the rate of truncation is increased, removing a greater part of the nonlinear interactions, we decrease the crest heights.

FIGURE 5.2 : Directional truncation

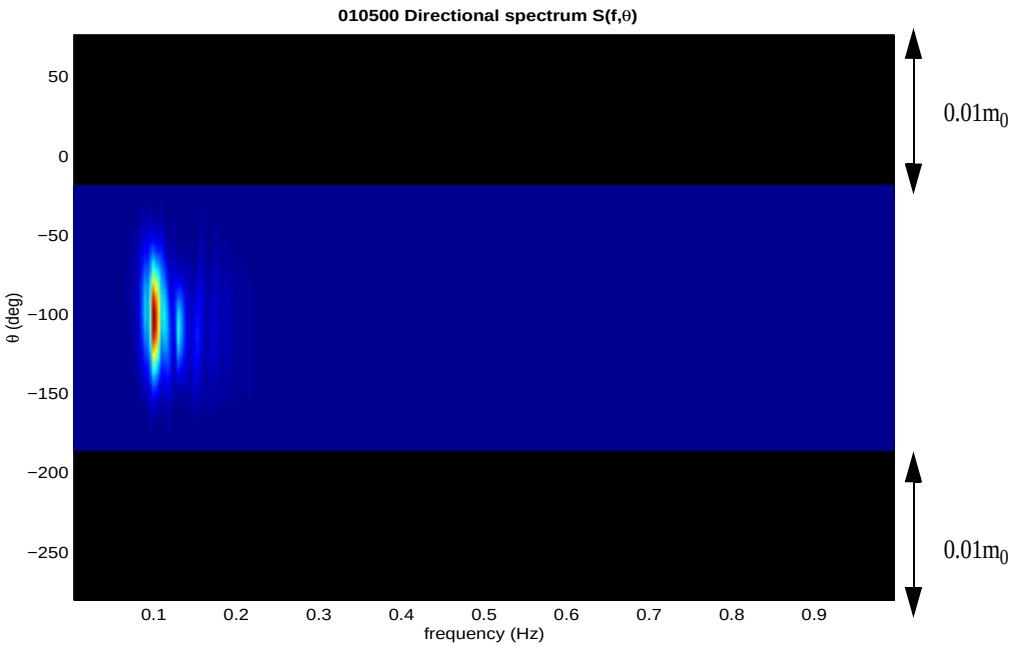

FIGURE 5.3 : Spectral plus directional truncation

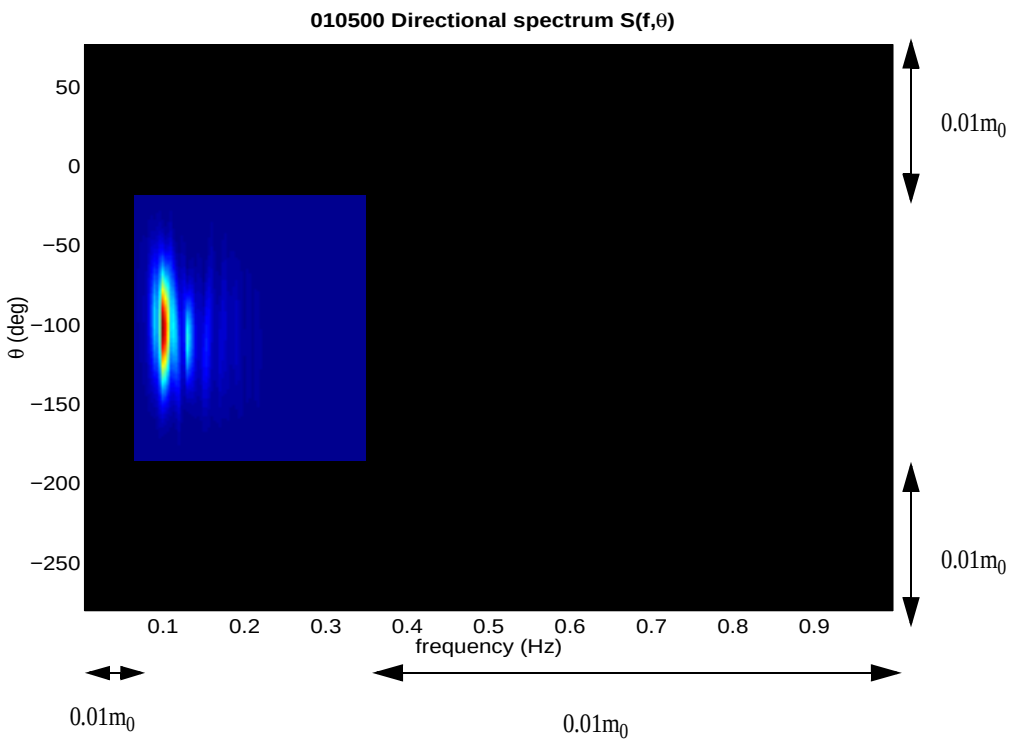

FIGURE 5.4 : Directional discretization

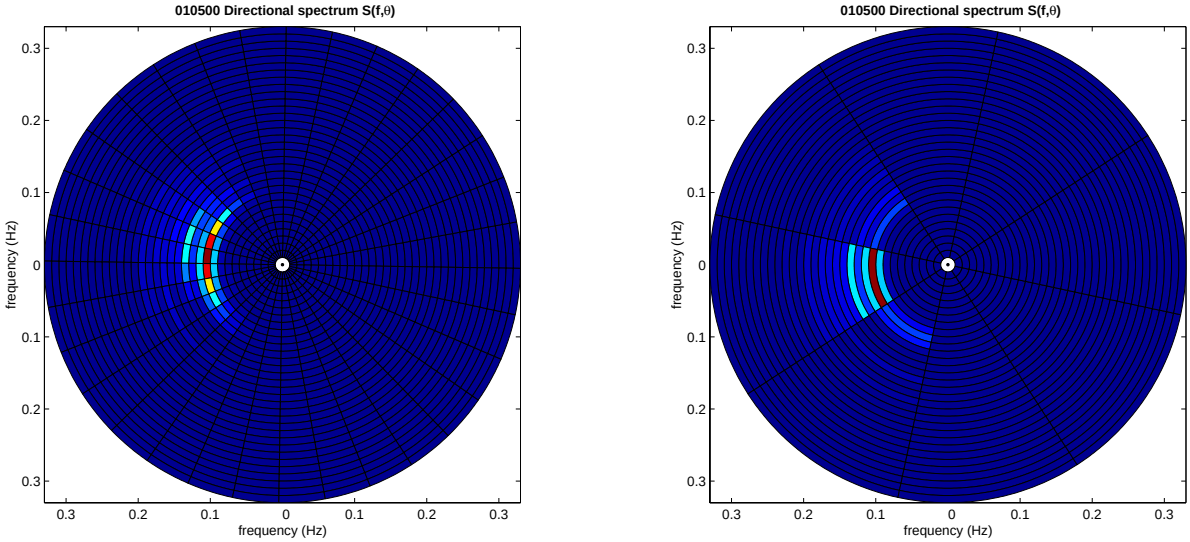

32 sectors **8 sectors**

FIGURE 5.5 : Effect of directional discretization

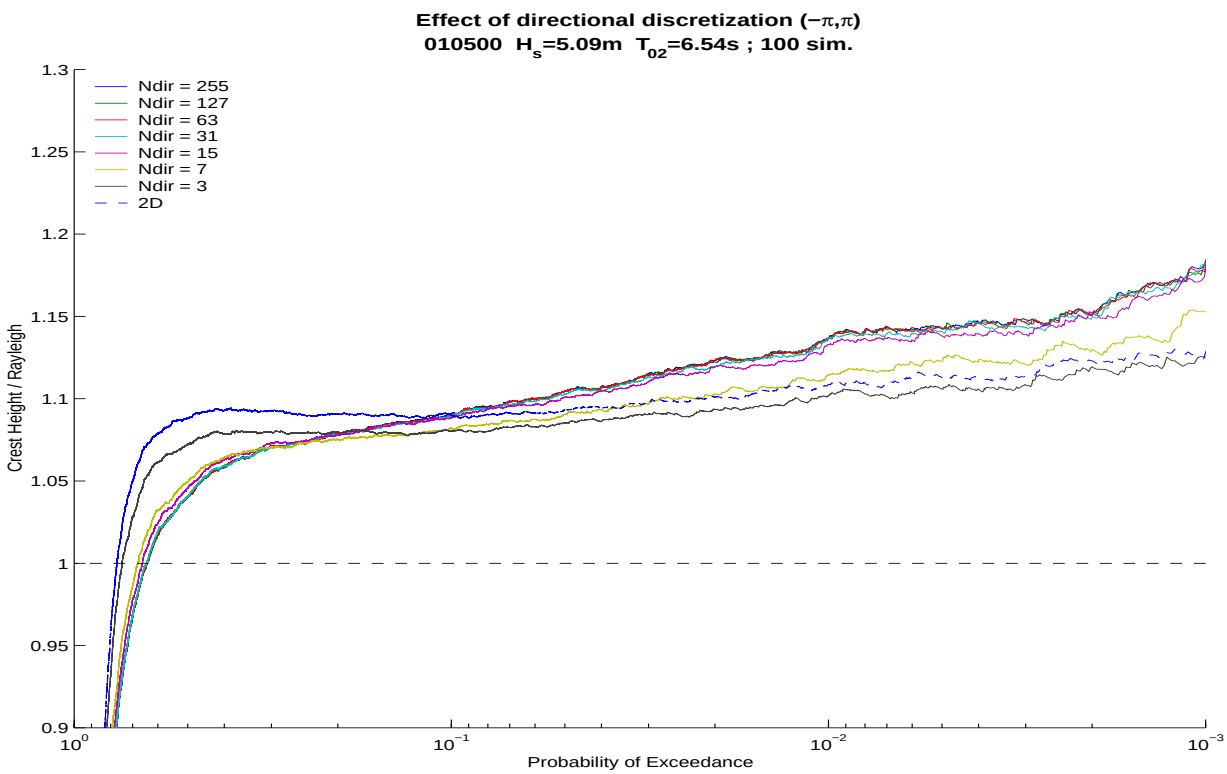

In fact in the actual sea states, either we are close to a 2D situation, which corresponds to long-crested waves (swell), and in this case the spectrum is relatively narrow and so the problem of short-long waves interactions is avoided, or we are in a short-crested waves situation (wind sea), clearly 3D, where the short-long waves interactions present due to a broader spectrum do not seem to create real problems. Thus, the frequency truncation does not seem so critical in practice, but a rate of 1% has been used for all the simulations in this report.

Angular truncation

When the percentage of truncation in direction increases, the crest heights decrease as they did for the frequency truncation. The percentage indicated on the plots (figure 5.8) corresponds to the percentage of total energy which was removed on each side of the mean direction of the peak frequency. That is to say for a rate of 5%, 10% of the energy is removed for the calculation of the second order part. The 1% truncation seems a good choice which has little effect on the crest ratios, and it corresponds for typical direction spreading in the WACSIS data to removing half the number of angular sectors.

Water depth

When the waves propagate on intermediate water depth (in fact it is the dimensionless ratio of water depth to wavelength which is critical) the kinematics and the wave elevation are modified. As can be seen from the second order transfer functions, the nonlinear interactions are also modified by a change in the water depth. The tide and the storm surge induce variations of the mean water level at the site, and we have to know if it is important to take these variations into account. At the WACSIS site, the range of water depth is 16.4m-20m.

The effect on the crest height ratio is significant, but again the amplitude of the effect is quite different in the 2D case (figure 5.9) and in the 3D case (figure 5.10). The modifications are quite important in the 3D case, which corresponds to the actual cases, and so an accuracy of the order of 0.1m is necessary (at the WACSIS site and for the average wavelengths encountered) in the mean water level to accurately calculate the crest height statistics.

FIGURE 5.6 : Effect of frequency truncation on 2D simulations

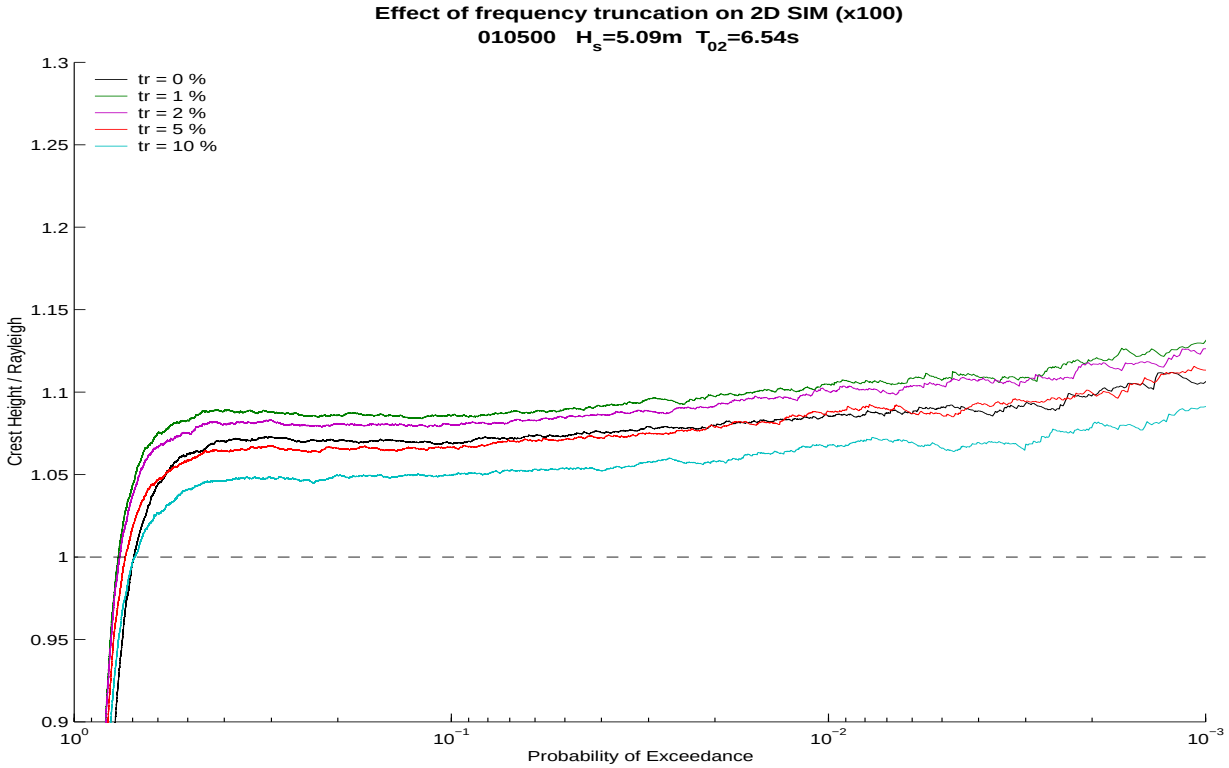

FIGURE 5.7 : Effect of frequency truncation on 3D simulations

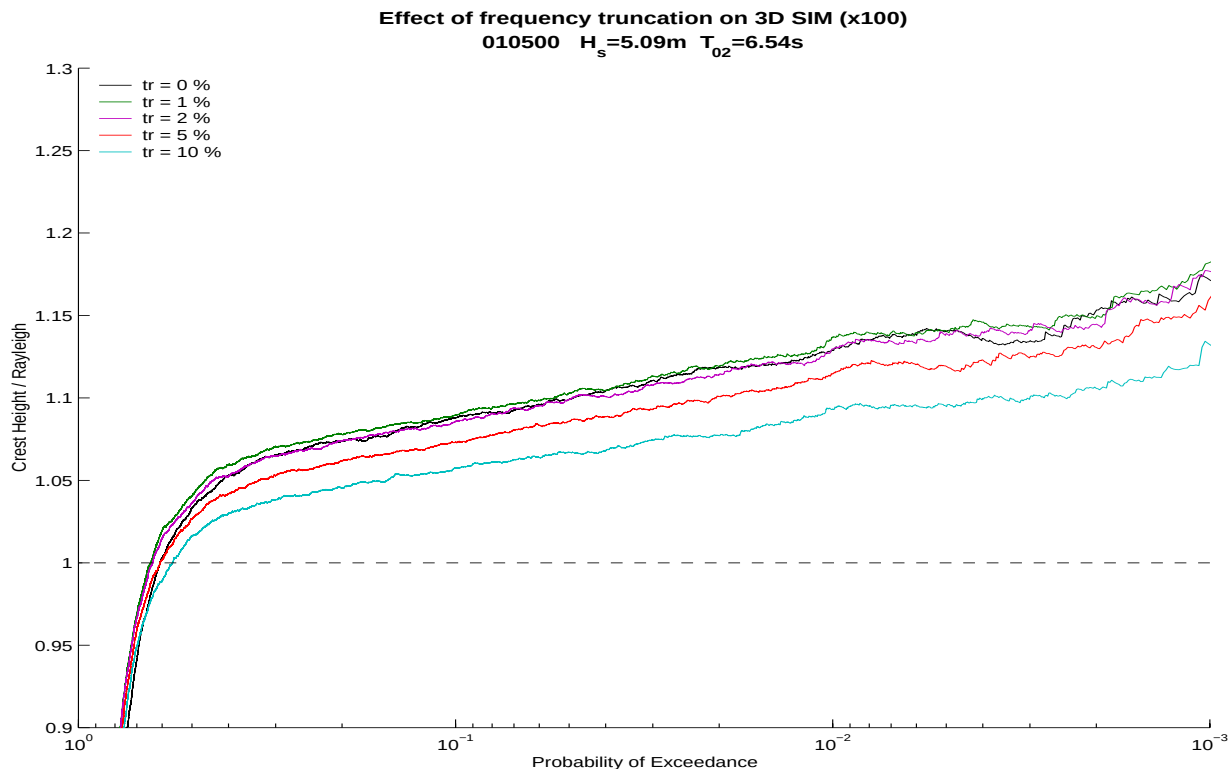

FIGURE 5.8 : Effect of directional truncation

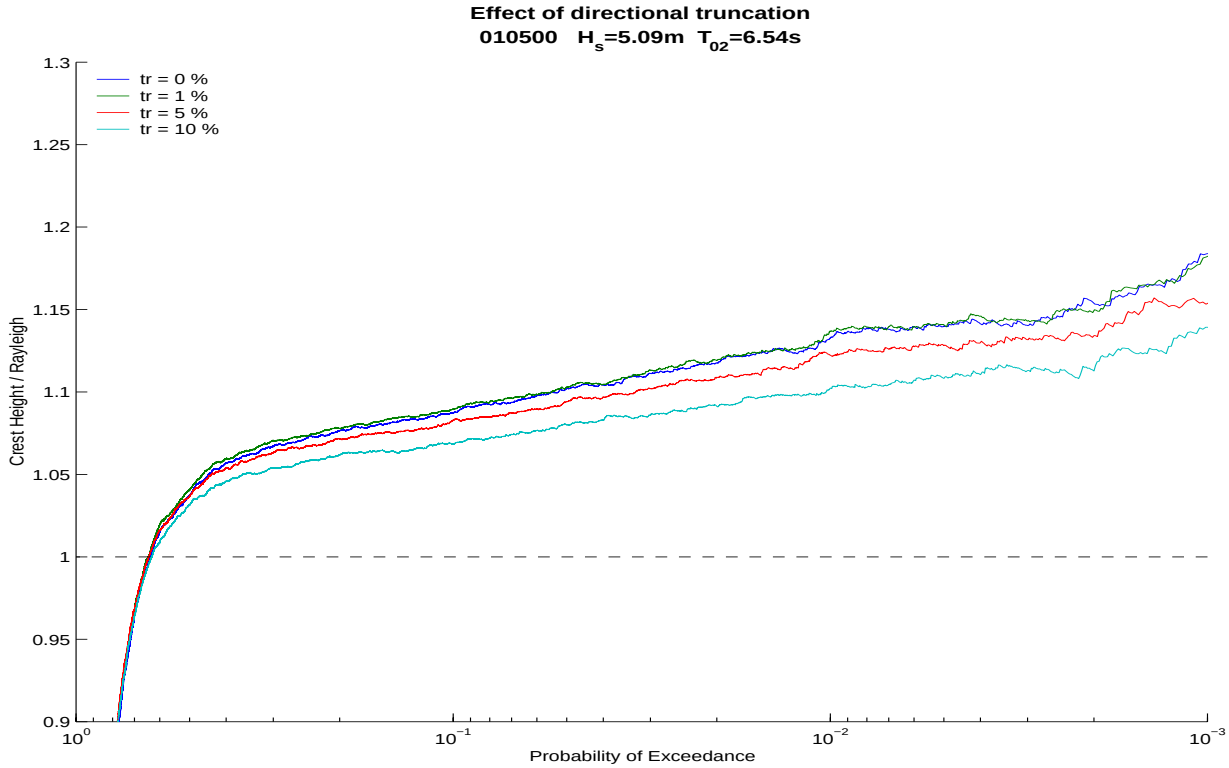

FIGURE 5.9 : Effect of water depth on 2D simulations

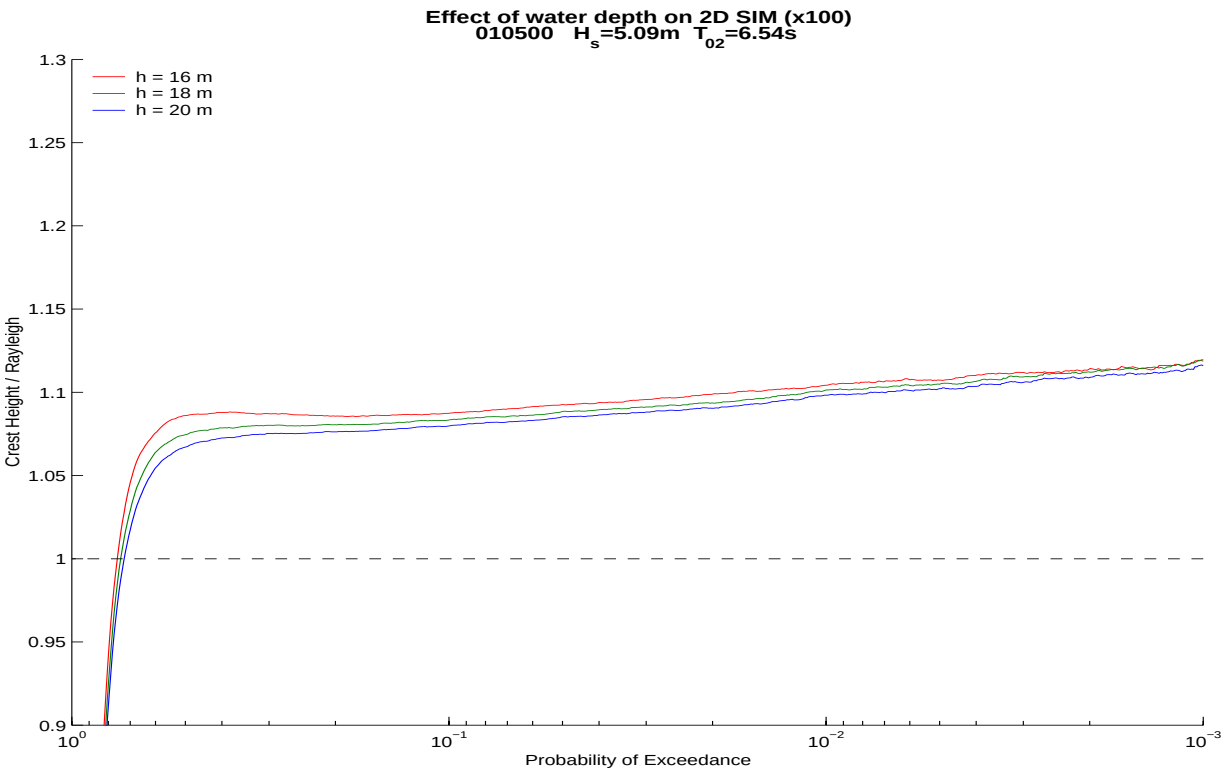

FIGURE 5.10 : **Effect of water depth on 3D simulations**

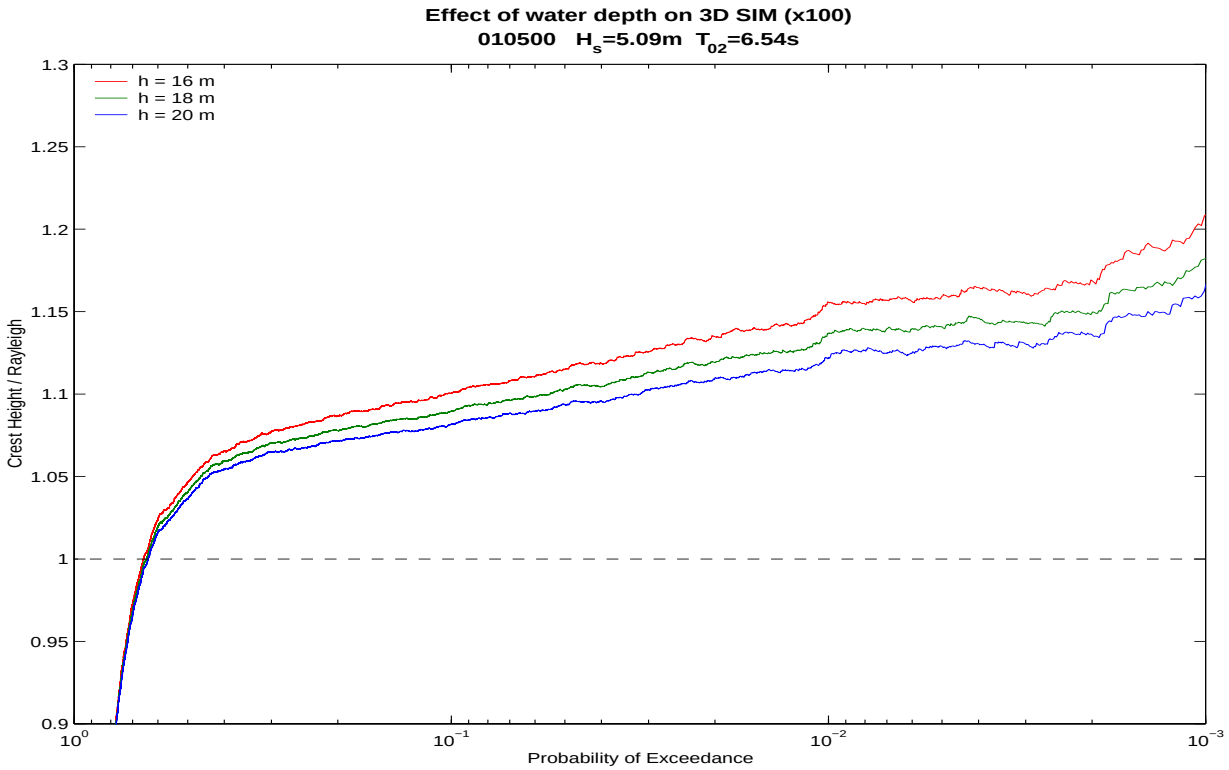

Point spectrum

The primary information of the kinematics simulation is the directional spectrum. This spectrum is decomposed into a point spectrum and a directional distribution (EQ 5.13). For future site studies it is interesting to know if the sensor which will furnish the point spectrum is important or not. As it is well known, a buoy of free-floating type, due to the principle of measurement, does not measure bounded waves in infinite depth, and only partially (theoretically) in finite depth. Other sensors like lasers or wave staffs fortunately measure well the bounded waves. As the spectral density used in our models is considered as being the spectrum of the free waves (EQ 5.2 and 5.3), if the spectrum used comes from EMILASER or BAYLORWS and so contains also the energy of the bounded waves, then there is an inconsistency in the calculations. It is important to know what effect this inconsistency has on the crest height statistics.

Thousands equivalent years of WACSIS campaign (i.e., a thousand hours of simulations for each hour in the WACSIS data base) have been simulated starting from the point spectra of WAVERGHR, EMILASER and BAYLORWS. The comparison of the number of exceedances of crest height levels in figure 5.11 and 5.12 shows that the weak energy of the bounded waves treated as energy of free waves when using EMILASER or BAYLORWS spectra does not significantly change the crest height statistics.

But we have to be cautious because these results are obtained after applying to the sensors a gain correction which includes the effect of the energy of the bounded waves. This effect on Hs will be seen from the simulations to be of the order of 1%. Thus it seems that considering a spectra including bounded waves energy will change the crest heights at the same order of magnitude.

FIGURE 5.11 : Effect of point spectrum, WAVERGHR vs BAYLORWS

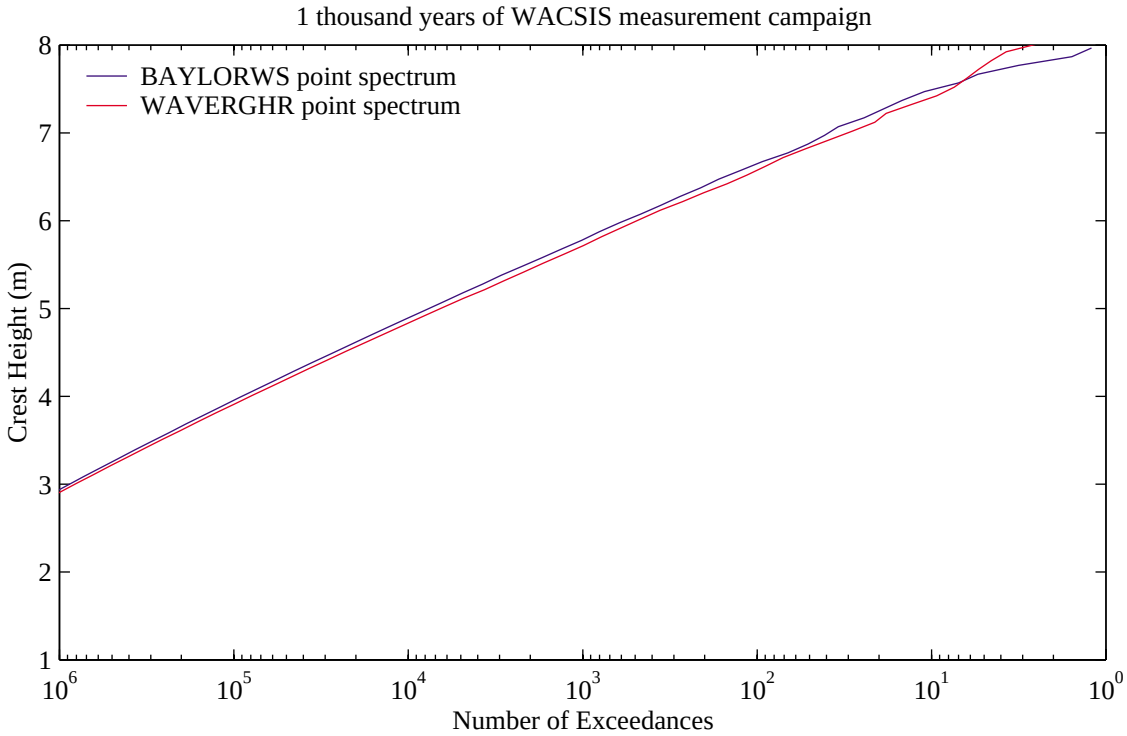

FIGURE 5.12 : Effect of point spectrum, WAVERGHR vs EMILASER

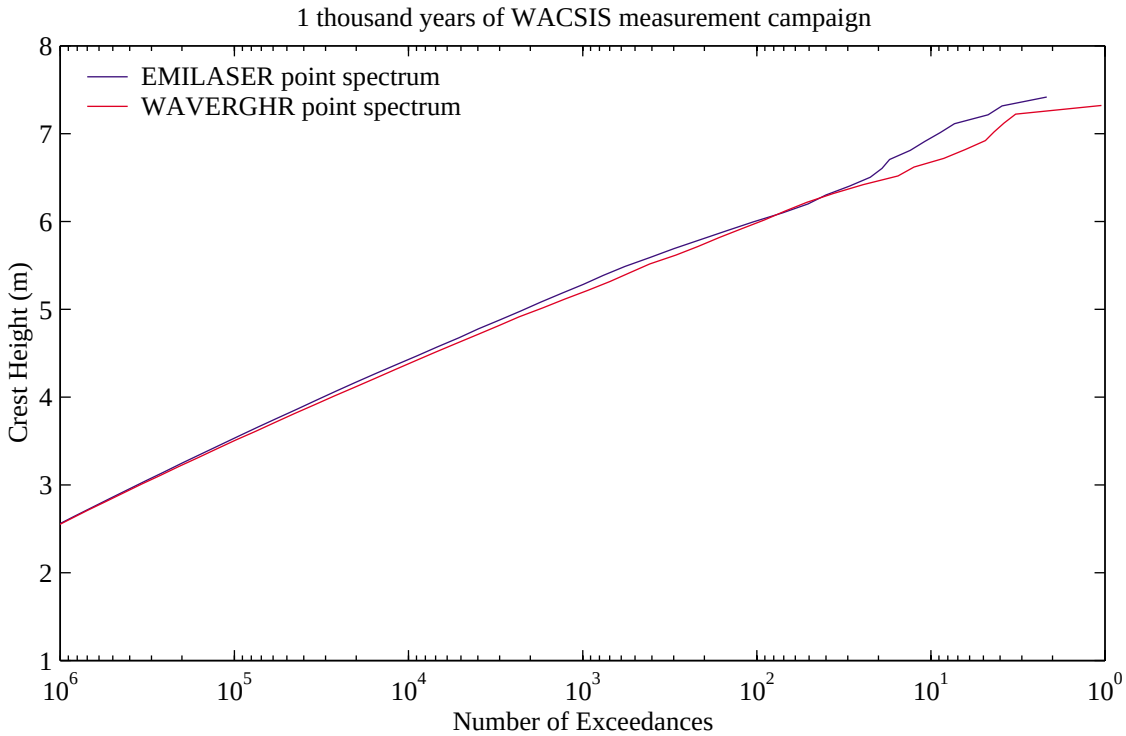

Conclusion

Simulations based on irregular waves with second order Stokes expansions have been studied using the characteristics of the sea states encountered during the WACSIS campaign. A simple technique of frequency truncation has been used to avoid the short-long waves interaction problem. The truncations in the angular and frequency domains have been optimised. The effect of variations of water depth has been shown to be well taken into account. All these elements will be important to compare as pertinently as possible the measurements to the simulations in the sequel of this report.

Appendix 5.1: 2nd order transfer function

$$T(\theta_i, f_j, \theta_k, f_l) = \frac{1}{2g}\left(2(\omega_j + \omega_l)D(\vec{\mathbf{k}_i}, \vec{\mathbf{k}_k}) + \omega_j\omega_l + \omega_j^2 + \omega_l^2 - \frac{g^2\vec{\mathbf{k}_i} \bullet \vec{\mathbf{k}_k}}{\omega_j\omega_l}\right) \quad \textbf{(EQ 5.15)}$$

with

$$\vec{\mathbf{k}_i} = k_j\vec{\mathbf{d}_i}\ ,\ k_j = \left|\vec{\mathbf{k}_i}\right|\ ,\vec{\mathbf{d}_i} = \cos\theta_i\vec{\mathbf{x}} + \sin\theta_i\vec{\mathbf{y}}\ ,(2\pi f_j)^2 = \omega_j^2 = gk_j\tanh k_j h \quad \textbf{(EQ 5.16)}$$

$$\vec{\mathbf{k}_k} = k_l\vec{\mathbf{d}_k}\ ,\ k_l = \left|\vec{\mathbf{k}_k}\right|,\vec{\mathbf{d}_k} = \cos\theta_k\vec{\mathbf{x}} + \sin\theta_k\vec{\mathbf{y}}\ ,(2\pi f_l)^2 = \omega_l^2 = gk_l\tanh k_l h \quad \textbf{(EQ 5.17)}$$

and

$$D(\vec{\mathbf{k}_i}, \vec{\mathbf{k}_k}) = \frac{2(\omega_j + \omega_l)(g^2\vec{\mathbf{k}_i} \bullet \vec{\mathbf{k}_k} - \omega_j^2\omega_l^2) + g^2(k_j^2\omega_l + k_l^2\omega_j) - \omega_j\omega_l(\omega_j^3 + \omega_l^3)}{2\omega_j\omega_l((\omega_j + \omega_l)^2 - g\left|\vec{\mathbf{k}_i} + \vec{\mathbf{k}_k}\right|\tanh\left|\vec{\mathbf{k}_i} + \vec{\mathbf{k}_k}\right|h)} \quad \textbf{(EQ 5.18)}$$

$$D(k\vec{\mathbf{d}_i}, \omega, k\vec{\mathbf{d}_k}, -\omega) = 0 \quad \textbf{(EQ 5.19)}$$

The difference transfer function $T^D(\theta_i, f_j, \theta_k, f_l)$ corresponds to $T(\theta_i, f_j, \theta_k, -f_l)$ and the sum transfer function $T^S(\theta_i, f_j, \theta_k, f_l)$ corresponds to $T(\theta_i, f_j, \theta_k, f_l)$.

The offset coefficient is

$$c_{\eta_2} = \int_K \frac{k}{\sinh 2kh} S(\vec{\mathbf{k}})d\vec{\mathbf{k}} \quad \textbf{(EQ 5.20)}$$

Appendix 5.2: Narrow-band non-linear transfer coefficients

In the formulas below, $\kappa = k_m h$ is the dimensionless depth.

where $(2\pi f_m)^2 = gk_m\tanh k_m h$ **(EQ 5.21)**

The expressions for vertical displacement, Eulerian (fixed point) measurements are, in finite or infinite water depth (see [19] for more formulas):

$$T_{nb}^D(f_m) = c_{diff}(\kappa)k_m\ ,\ T_{nb}^S(\kappa) = c_{sum}(\kappa)k_m \quad \textbf{(EQ 5.22)}$$

with $c_{diff}(\kappa) = \dfrac{Q(\kappa) + \kappa(1 - (\tanh\kappa)^2)}{Q(\kappa)^2 - 4\kappa\tanh\kappa}$ $\quad c_{diff}(\infty) = 0$ **(EQ 5.23)**

and $c_{sum}(\kappa) = \dfrac{1}{4}\left(\dfrac{2 + (1 - (\tanh\kappa)^2)}{(\tanh\kappa)^3}\right)$ $\quad c_{sum}(\infty) = \dfrac{1}{2}$ **(EQ 5.24)**

where $Q(\kappa) = \tanh\kappa + \kappa(1 - (\tanh\kappa)^2)$ $\quad Q(\infty) = 1$ **(EQ 5.25)**

CHAPTER 6

2nd order simulations Comparison with measurements

Marc Prevosto
Benjamin Moreau
George Z. Forristall

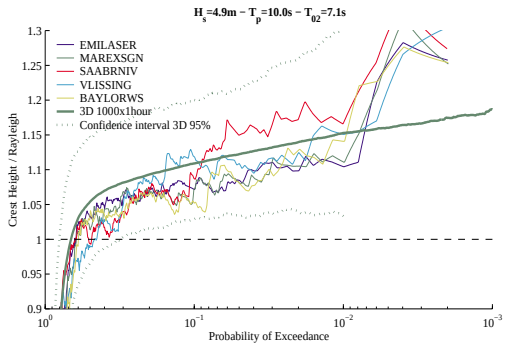

The problem which now is posed is to know if the simulations furnish crest statistics comparable to the measurements. But, as the different sensors give different crest statistics as has been seen in a previous chapter, a second issue should be answered: do the simulations validate the results obtained by one or more sensors?

Gain correction

The gain correction which has been calculated for the sensors comparison (see “Gain correction”, page 63) was based on a comparison between the Hs given by the sensors and the Hs given by the Waverider. In fact, as it will be seen later (“Waverider”, page 100) the Waverider measurements give crest statistics which are very close to those given by a linear assumption. So, when comparing the measurements (which normally include the nonlinearities) with the simulations (which include the 2nd order nonlinearities), it is better to calculate the gain correction so that the statistics of Hs are the same from the measurements and from the nonlinear simulations. In fact, this will not change the relative gain between sensors, but will give more coherent comparisons with the simulations. The new gain corrections are given in table 6.1.

TABLE 6.1 : Gain correction from simulation

	EMILASER	MAREXSGN	SAABRNIV	VLISSING	WAVERGHR	BAYLORWS
# of time series	232	325	327	353	292	325
regression coefficient	0.984	0.956	0.999	0.954	0.997	1.004

Inside sea state statistics

Analyses of specific dates

Comparisons have been made between the CHR (EQ 4.3) calculated from the sensor measurements and that calculated from a thousand simulated one-hour time

series. Six dates have been chosen to cover different sea state situations. These hours are the 3rd of January at 00:00 and 23:00, the 5th of January at 00:00, the 4th of January at 00:00, the 19th of January at 20:00 and a low Hs sea state on the 20th of January at 22:00. 2D and 3D simulations have been generated, and the confidence interval at 95% calculated from the thousand CHR estimators of the 3D simulations. The results are given in figure 6.1 and 6.2, and in appendix 6.1. The raw and filtered (f_{samp} = 4Hz, $f_{cut\text{-}off}$ = 0.64Hz) measurements have been considered. The simulations correspond to the filtered case, and as shown in Chapter 2, the measurements appear to be contaminated by noise at frequencies above 0.64Hz. These curves show a great dispersion of the CHR between sensors, but more or less always in the confidence interval (in the filtered case). This great inside-sea-state dispersion does not allow an accurate comparison between the measurements and the simulation.

Effect of the distance between sensors

Synthetic time series corresponding to measurements at the location of the sensors have been generated with the 3D simulator. Starting with a random draw of the linear components, for example at the EMILASER location, we have linearly propagated these components to the locations of each the other sensors (see “Sensor locations”, page 4) and then calculated the second order parts. Each simulation was for the same single hour.

If we compare the filtered data in figure 6.2 with the simulations at the locations of the measurements which are shown in figures 6.3 and 6.30-6.34, the simulations give results more centred around the 3D “exact” value. Some bias between simulations and measurements in figure 6.2 could be due to the fact that the actual sea state is different from the estimated sea state description coming from the Waverider measurements and not exactly stationary for one hour.

The dispersion between sensors due to the distance between the sensors also exists in the simulations. This fact confirms that part of the difference between VLISSINGEN and SAABRNIV and the other sensors is due to their distant location from them. But in general the dispersion is greater in the measurements than in the simulations. And if we look at the 95% confidence interval on the CHR calculated on one hour, the measurements tend to fill a large part of this interval as if they were more independent than what is given by the simulation. This could be due to the simplified linear propagation used in the simulations, to structural effects on the local wave fields and of course to the different spatial integrations and sensor principles, but also to the directional spreading model used in $\cos^{2s}$ that perhaps generates longer wave crests than in reality.

Comparisons of crest height ratios

As noted in the chapter on sensor comparisons, it is difficult to come to any firm conclusions by considering the data in individual sea states. Therefore, as before, we have combined several hours of data with similar wave heights in order to eliminate some of the sampling variability in single data records while still being able to see variations due to different ranges of wave heights. Since the crest height ratios are normalized by the significant wave height of the sensor during each record, there are no difficulties with combining records with different significant wave heights.

FIGURE 6.1 : 5th of January 00:00, comparison simulation - raw data

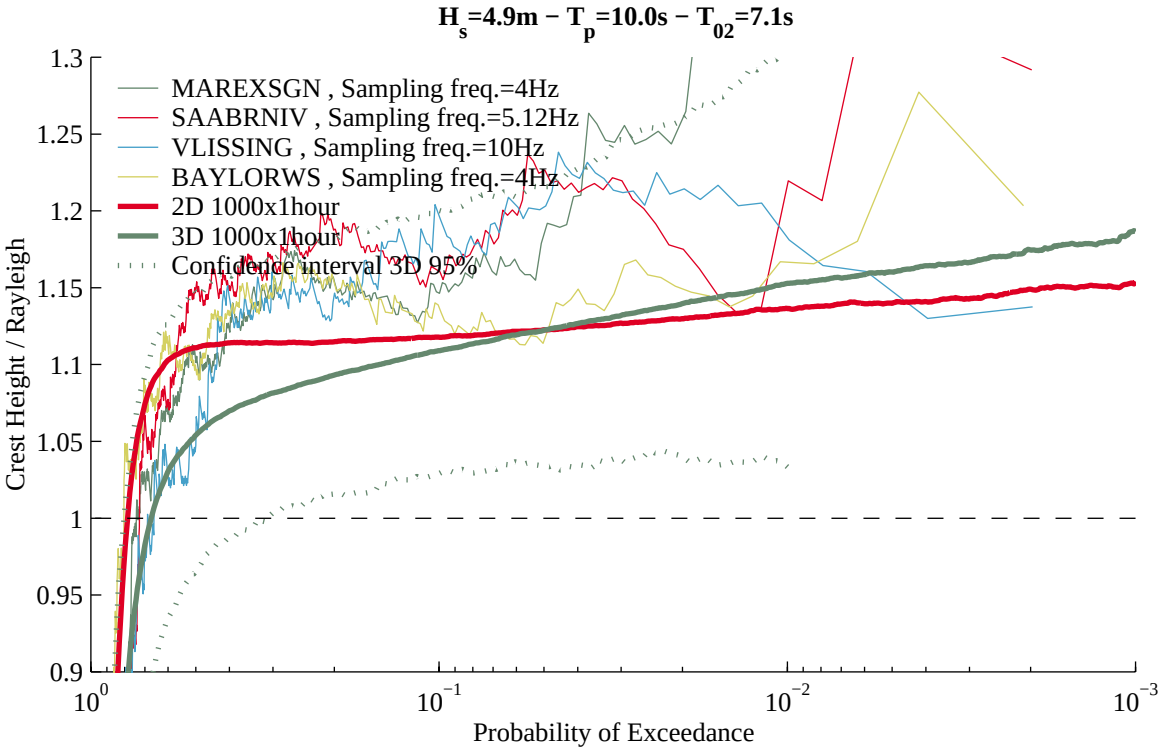

FIGURE 6.2 : 5th of January 00:00, comparison simulation - filtered data

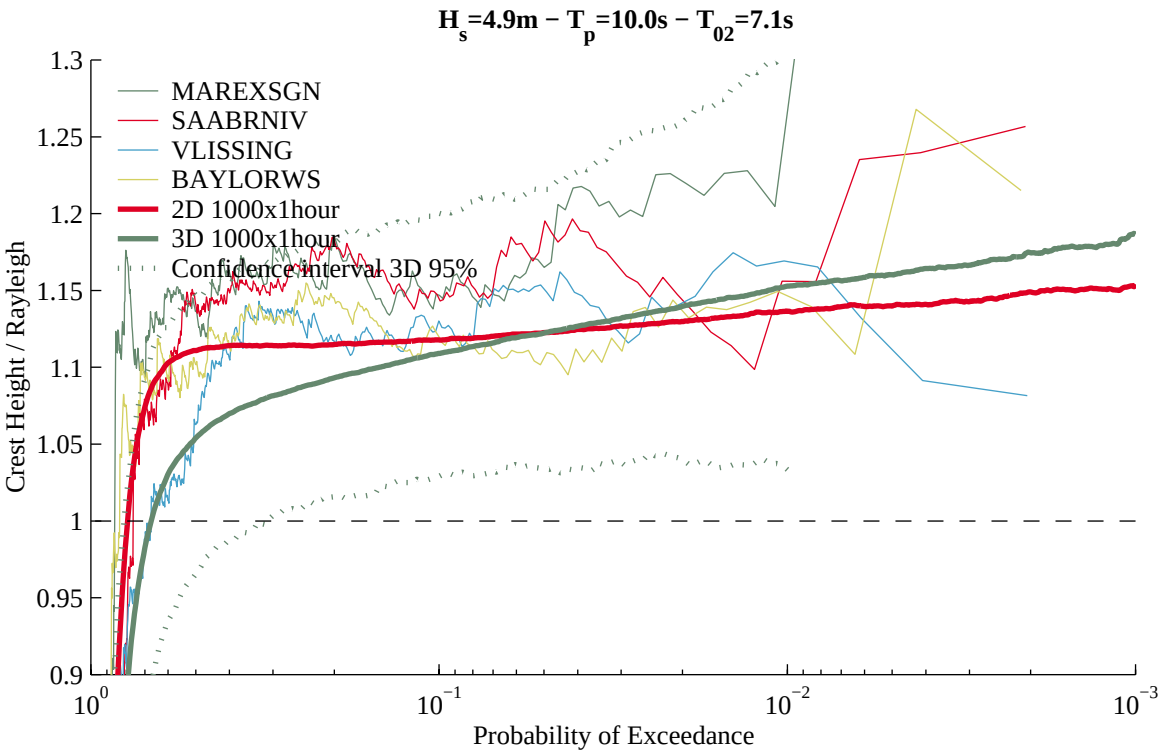

FIGURE 6.3 : 5th of January 00:00, simulation comparison between sensors

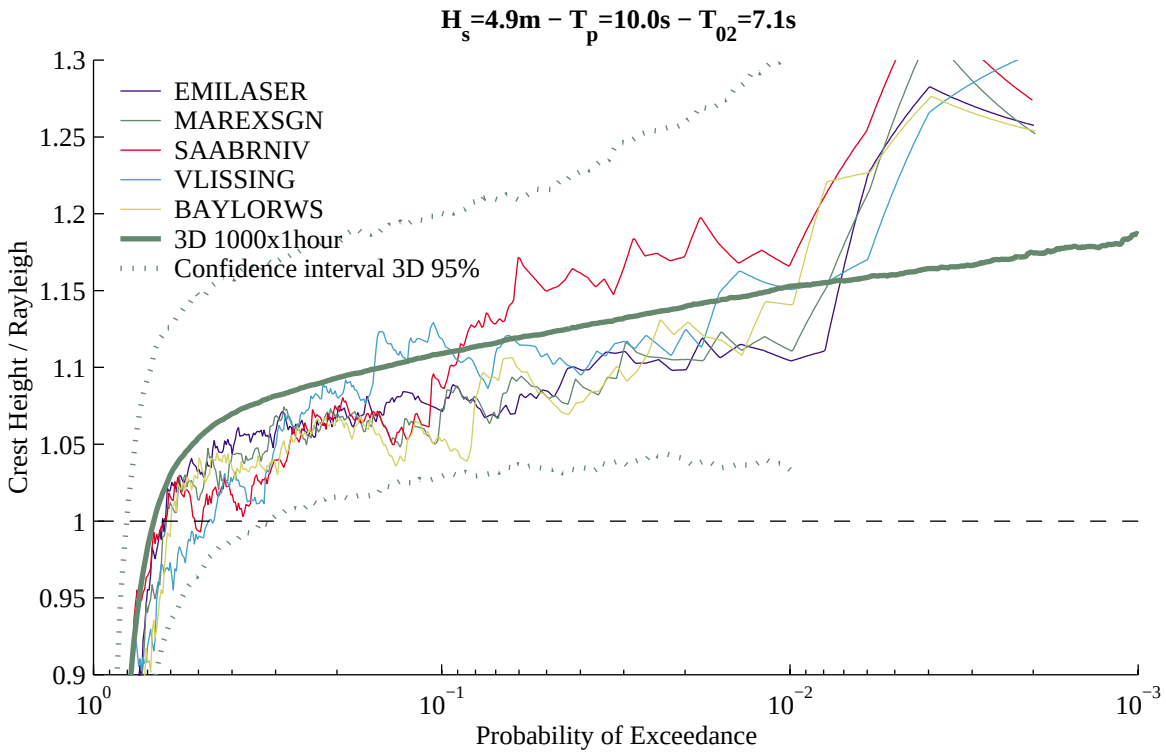

Figures 6.4 - 6.5 and 6.7 - 6.13 show the crest height ratios of all of the data in increments of 0.5 m in significant wave height. The measurements have all been filtered at 0.64 Hz using a boxcar filter. The simulations are from 1000 repetitions using the directional wave spectrum measured by the Waverider.

For significant wave heights greater than about 3.0 m, the filtered measurements divide into two groups, with the measurements from the Saab and Marex radars being slightly higher than those from the Baylor, EMI, and Vlissingen instruments. Even after the filtering, there are some large noise spikes in the Marex data. The Baylor, EMI and Vlissingen instruments agree very closely with the simulations while the radars are a few percent higher. As noted in the chapter on simulations, the three dimensional (directionally spread) simulations give slightly higher crest heights for these conditions. It is instructive to note that the filtered trough depths are nearly identical for all of the sensors, as shown in Figure 4.36 for the entire campaign and in Figure 6.6 for significant wave heights between 4.0 and 4.5 m. Apparently the sensors react differently to crests than to troughs.

For the lower wave height ranges, the measurements are grouped closer together with a mean just slightly higher than the simulations. For the lowest waves, the Vlissing step gauge is noticeably higher than the other instruments, presumably because of its discrete resolution.

FIGURE 6.4 : Comparison of crest height ratios of filtered measurements and second order simulations for significant wave heights over 4.5 m.

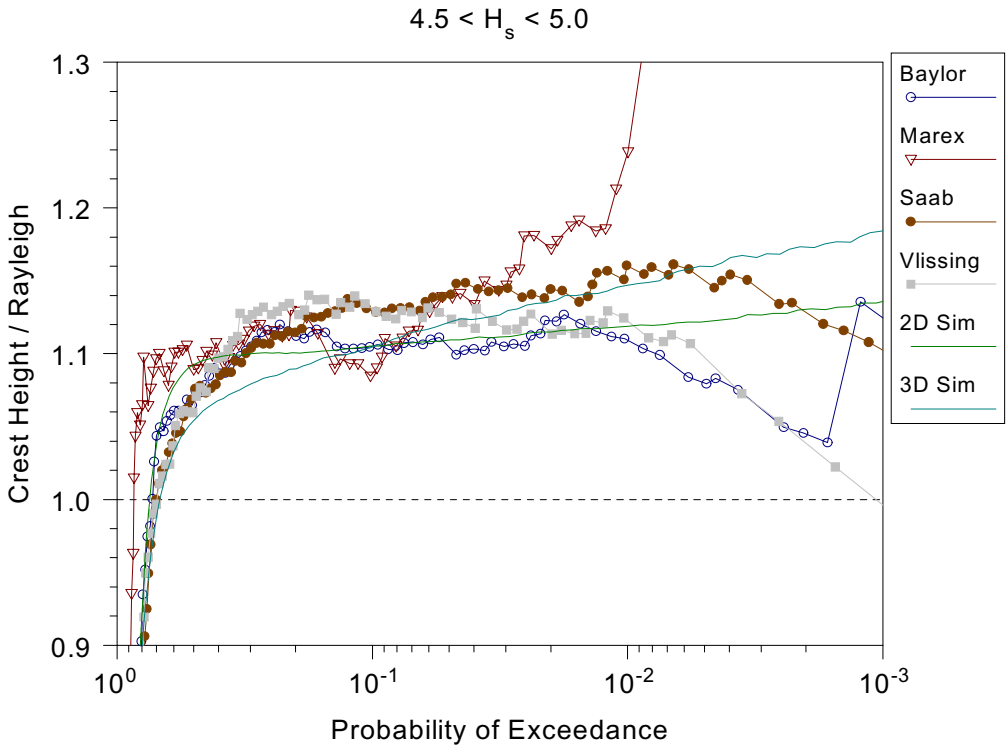

FIGURE 6.5 : Comparison of crest height ratios of filtered measurements and second order simulations for significant wave heights between 4.0 and 4.5m.

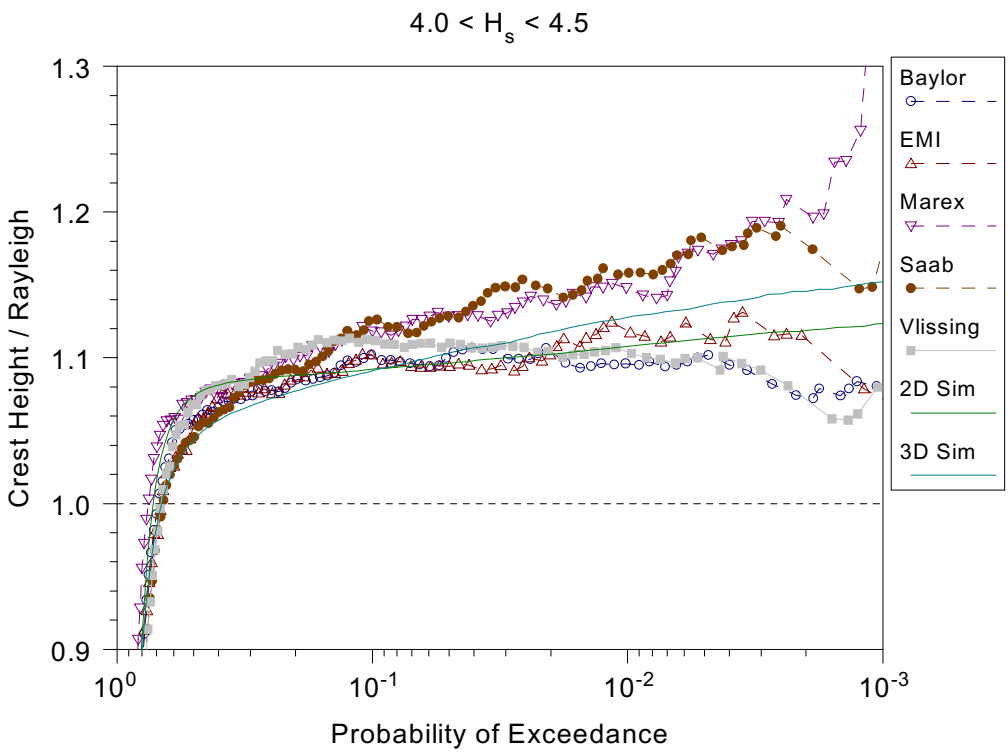

FIGURE 6.6 : Trough depth ratios of filtered measurements for significant wave heights between 4.0 and 4.5m.

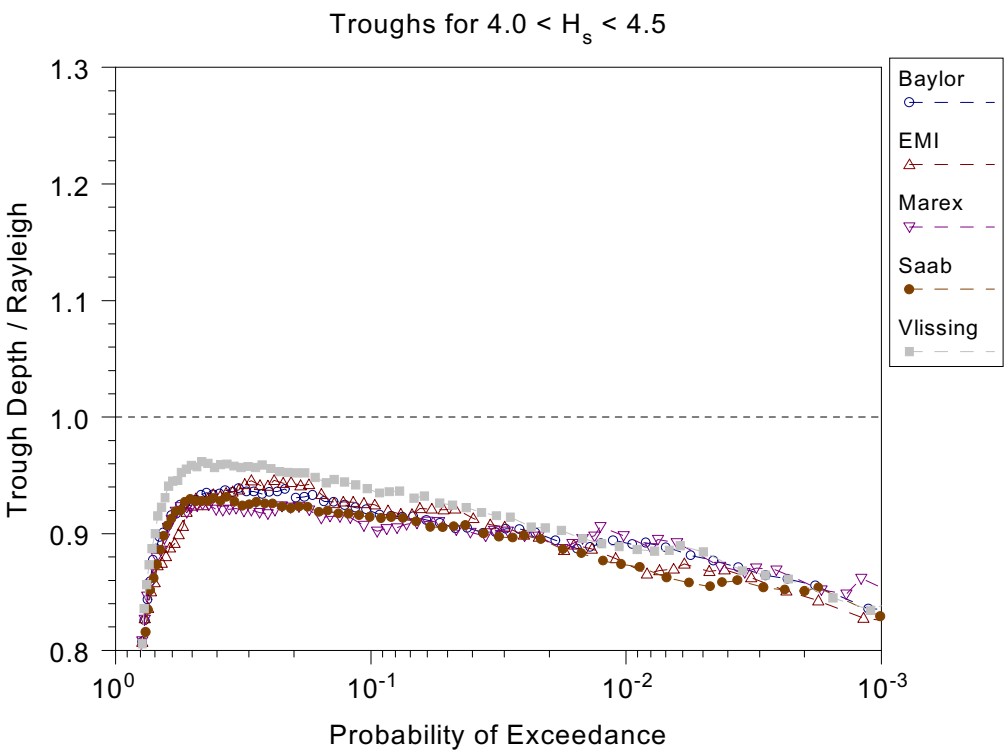

FIGURE 6.7 : Comparison of crest height ratios of filtered measurements and second order simulations for significant wave heights between 3.5 and 4.0m.

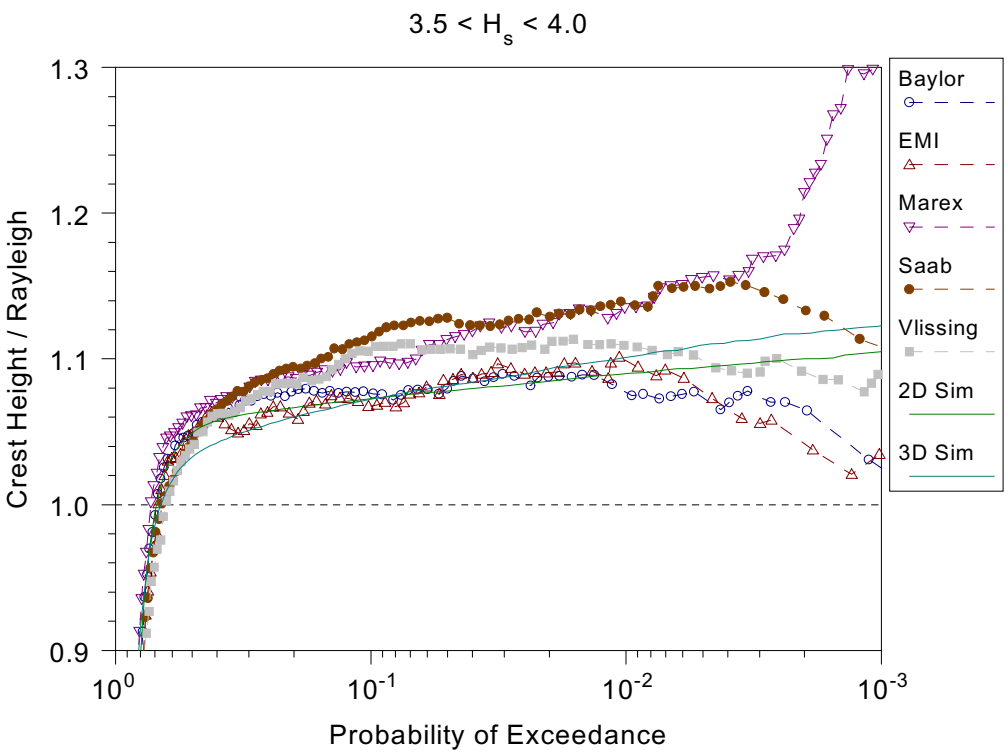

FIGURE 6.8 : Comparison of crest height ratios of filtered measurements and second order simulations for significant wave heights between 3.0 and 3.5m.

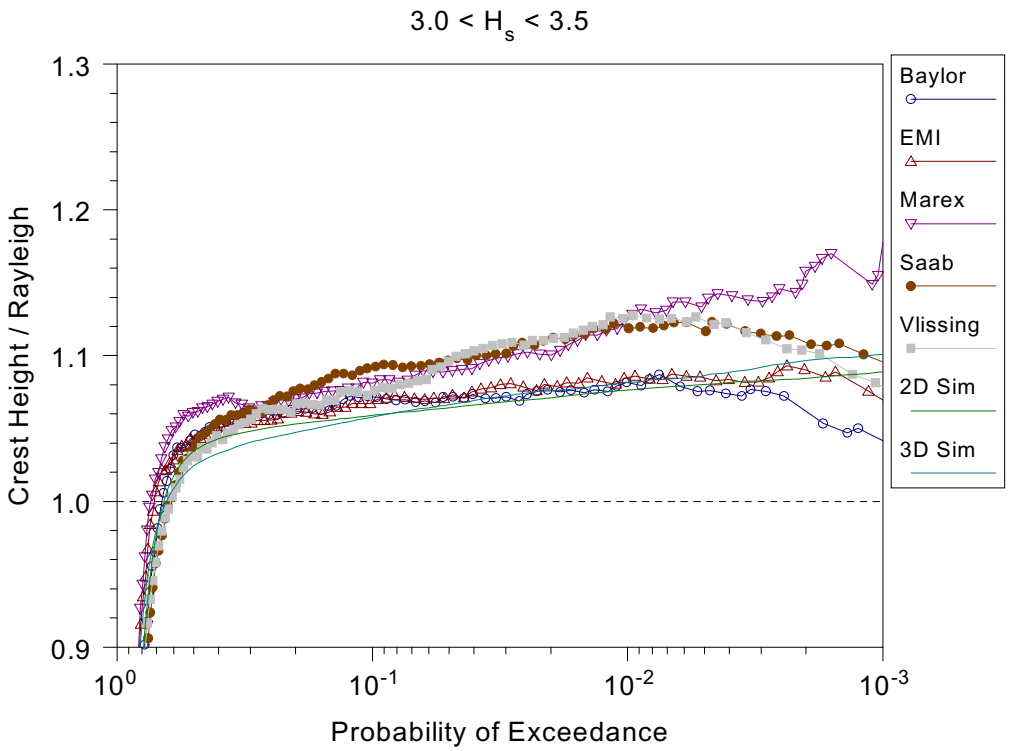

FIGURE 6.9 : Comparison of crest height ratios of filtered measurements and second order simulations for significant wave heights between 2.5 and 3.0m.

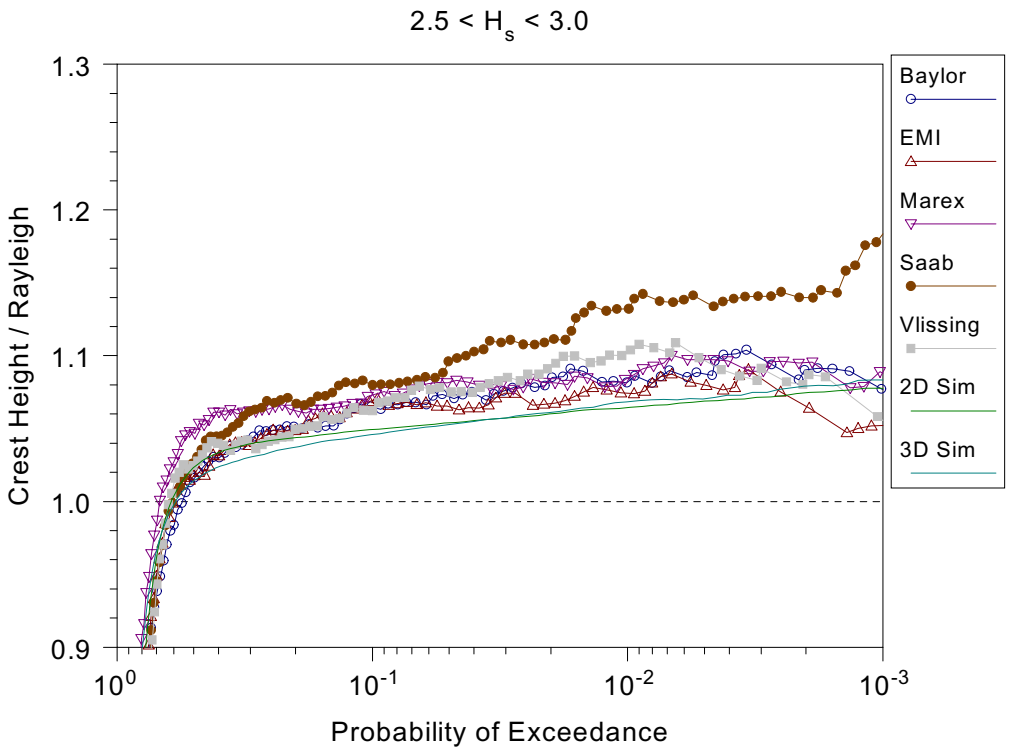

FIGURE 6.10 : Comparison of crest height ratios of filtered measurements and second order simulations for significant wave heights between 2.0 and 2.5m.

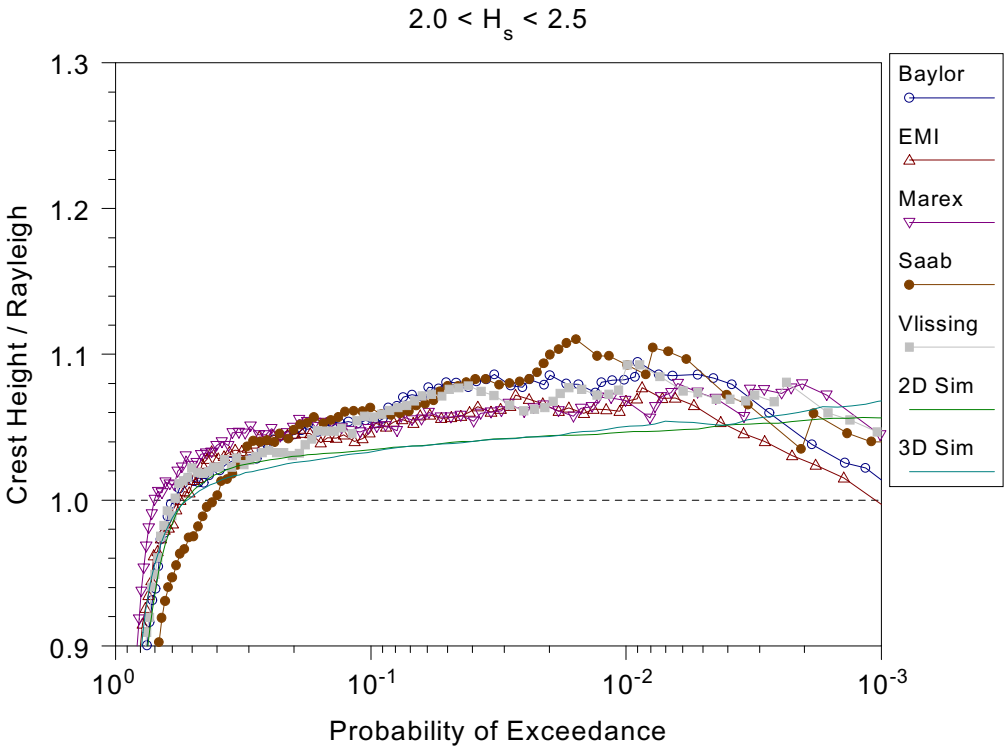

FIGURE 6.11 : Comparison of crest height ratios of filtered measurements and second order simulations for significant wave heights between 1.5 and 2.0m.

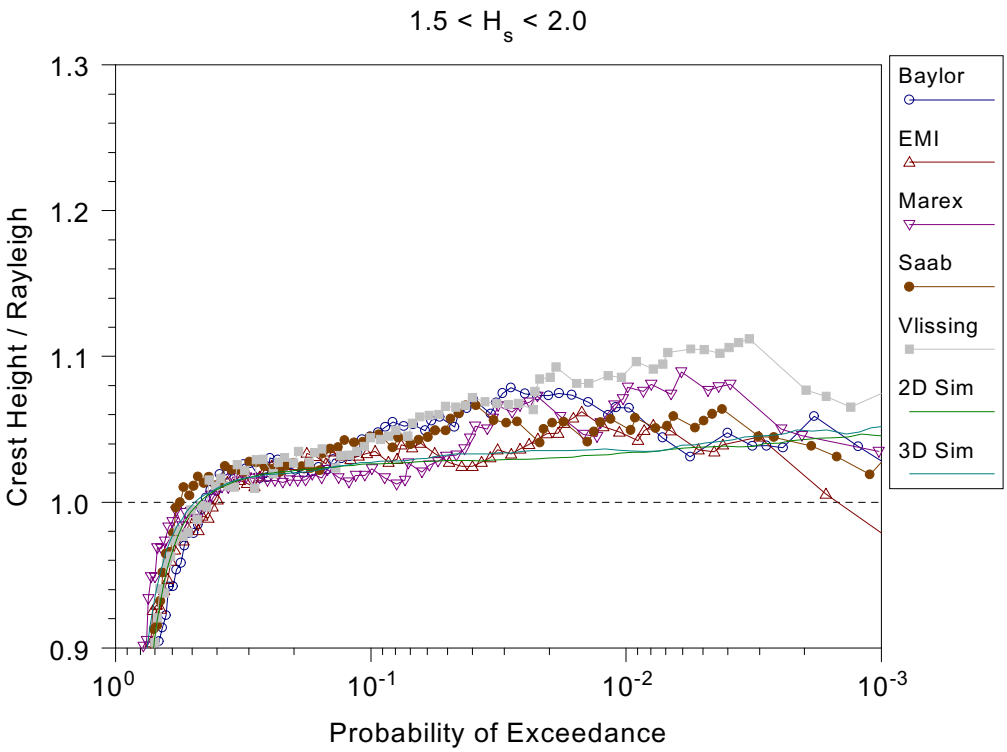

FIGURE 6.12 : Comparison of crest height ratios of filtered measurements and second order simulations for significant wave heights between 1.0 and 1.5m.

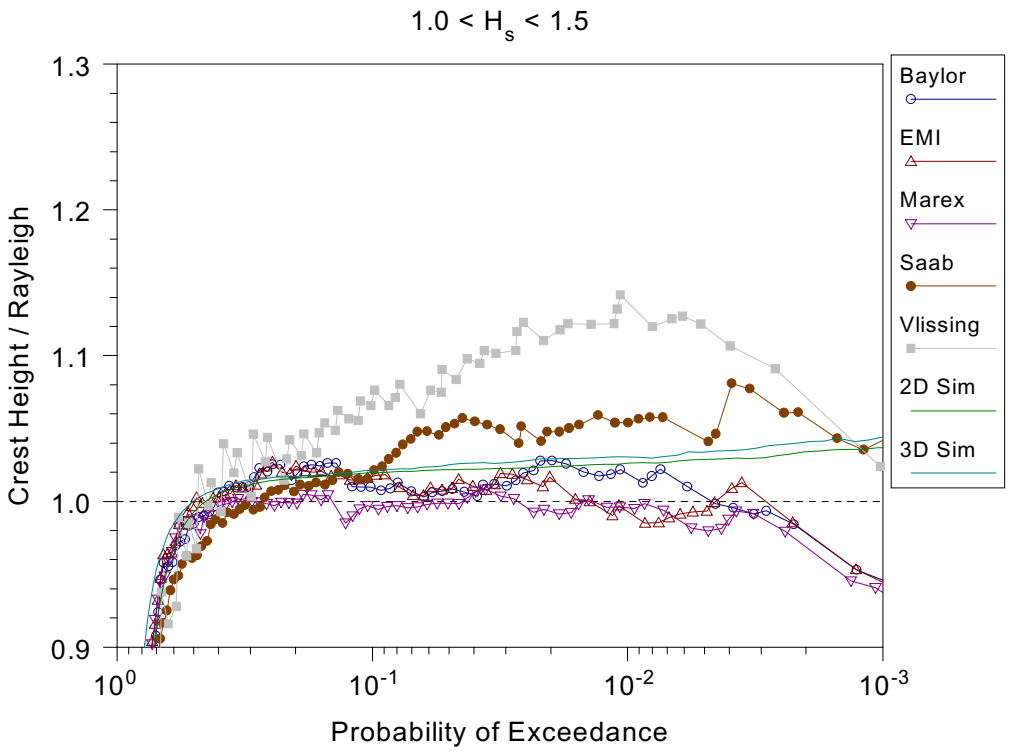

FIGURE 6.13 : Comparison of crest height ratios of filtered measurements and second order simulations for significant wave heights between 0.5 and 1.0m.

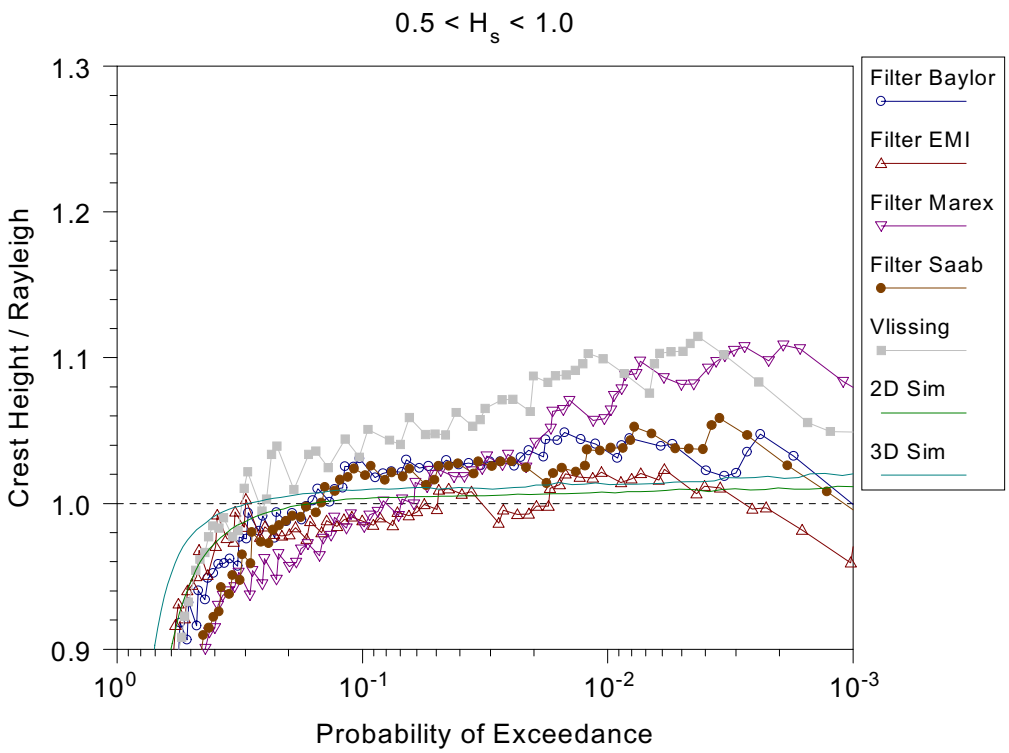

Crest height distribution all-over campaign

The analysis of waves accumulated over all of the campaign gives another precise tool of comparison, as it did for comparing the sensors in Chapter 4. Again, due to the poor sampling of severe sea states in the EMILASER data base, we have analysed separately two data bases, one without EMILASER (called MSVB) and a second one with only EMILASER and BAYLORWS (called EB).

The gain corrections indicated in table 6.1 have been applied and the number of exceedances have been calculated from the raw data and from the filtered data. As before filtering means a sampling frequency of 4Hz and a lowpass filter at 0.64Hz.

Confidence interval. In an another part, we have simulated 1000 WACSIS campaigns by simulating for each 20 min. sea state of the WACSIS data base 1000 time series. The simulated time series were 1024 points long (17 min.), so for comparison we used only the first 17 minutes of the measured time series. This has permitted us to calculate a median number of exceedances and the 95% confidence interval of the number of exceedances if calculated on one campaign (as is the case from the measurements).

Filtered data. First let us look at the comparison with the filtered data. (i.e. data with the same sampling and cut-off frequencies as the simulations). In the MSVB data base (figure 6.15), VLISSINGEN and BAYLORWS give very close results inside the confidence interval. On the EB data base (figure 6.16), EMILASER and BAYLORWS give again close results inside the confidence interval. So the simulations are in good agreement with three sensors. Compared to these three sensors, SAABRNIV is at the border of the confidence interval, slightly overestimating the crest levels compared to the simulations.

Raw data. It is clear in looking at the comparisons of the simulations with the raw data (figures 6.17 and 6.18), that the simulations, taking no account of the wave frequency components higher than 0.64Hz, underestimate the crest levels, particularly compared to VLISSINGEN which measures short waves up to 5Hz.

Waverider. When looking at the results obtained from WAVERGHR (figure 6.19), it is clear that as it is well known in deep water, the buoy gives crest height statistics very close to those obtained from the linear hypotheses.

Conclusion

Simulations of the wave elevation with a second order irregular 3D model give statistics of crest height similar to three of the sensors when we consider only wave components up to 0.64Hz. The power spectra from the sensors indicate that the measurements are very likely to be contaminated by noise above this frequency. Furthermore, the WAVERGHR spectra used for simulations give energy of the linear part only up to 0.64Hz.

The SAABRNIV and MAREXSGN radar gauges gave crest heights somewhat higher than the simulations even after the measurements were filtered. It is possible that part of the reason for this difference is a combination of the hydrodynamics of short waves riding on long waves and the way that radar sensors respond to the short waves. The conventional perturbation expansion which we have used for our simulations is not accurate when high frequency waves are carried far from $z = 0$ by the large low frequency waves. For short waves riding on long waves, it is more appropriate to expand the free surface boundary conditions at the long wave

surface rather than at the undisturbed surface. This technique, discussed by Zhang et al. (1999) [31] is called a phase modulation solution.

Figure 6.14, taken from Zhang et al. (1999), is an example of the difference between the conventional and phase modulation solutions for a long wave with a frequency of 0.0742 Hz and a short wave with a frequency of 0.1991 Hz. The abscissa of the figure is the phase of the long wave. The conventional and phase modulated solutions are completely different in character. The conventional solution has highest amplitudes and shortest wave lengths at the zero crossings of the long wave, while the phase modulated solution has its largest amplitude at the crest of the long wave (this is particularly clear in the VLISSING measurements, figure 4.39). Thus a simulation based on the phase modulation technique would probably give slightly higher crests than our simulations if high frequency waves were included.

FIGURE 6.14 : Conventional and phase modulation solutions for a short wave on a long wave. First order solution (solid line), conventional second order solution (dashed line), phase modulation solution (line with dots)

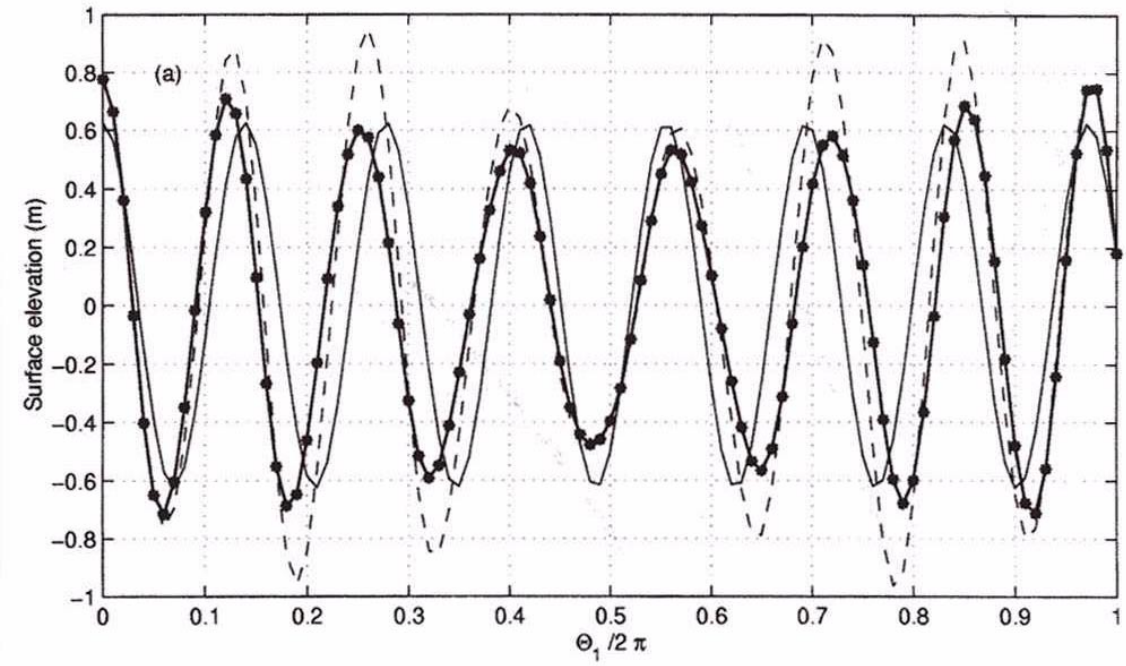

Since the high frequencies were poorly measured they have been filtered out of our comparisons. It is possible, however, that the some effect of the high frequency waves remains in the radar measurements due to their relatively large footprints. If a radar senses the highest point in its footprint and if the wavelength of the short waves is comparable to the size of the footprint, then the high frequency waves will be aliased into lower frequencies and not removed by the filter. We have not been able to confirm that the radars actually do sense the highest point in their footprints, so this explanation is still speculative.

More accurate measurement and simulation of wave components with frequencies above 0.64Hz might possibly increase the crest height ratios slightly. For most purposes, however, the difference would not be important since those components have very short wavelengths and thus do not affect engineering structures. Thus in the severe, but not extreme, sea states encountered during the campaign, we conclude that our second order model gives accurate predictions for the heights of crests.

FIGURE 6.15 : MSVB Crest levels, Filtered data vs simulations

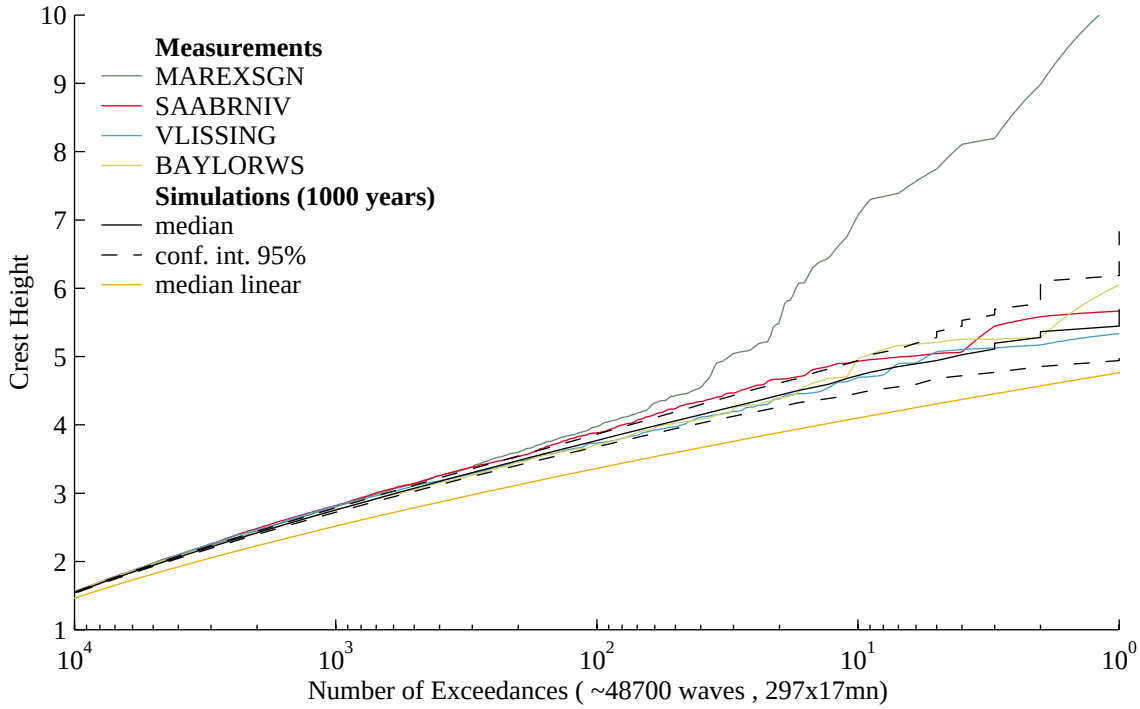

FIGURE 6.16 : EB Crest levels, Filtered data vs simulations

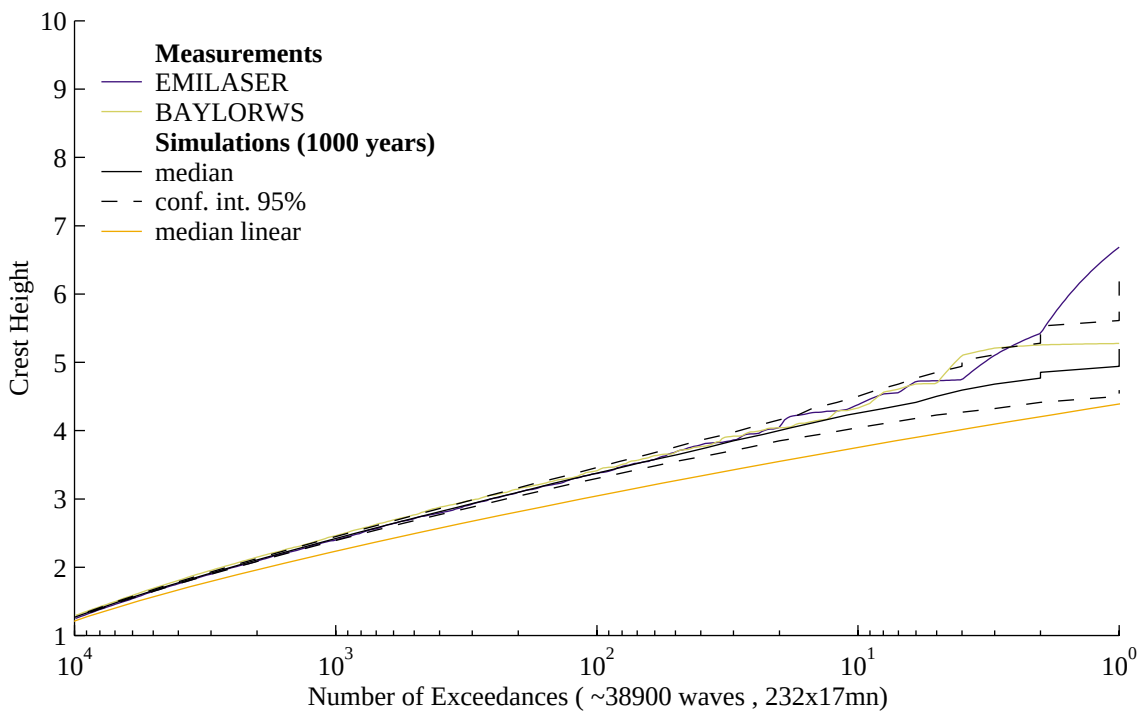

FIGURE 6.17 : MSVB Crest levels, Raw data

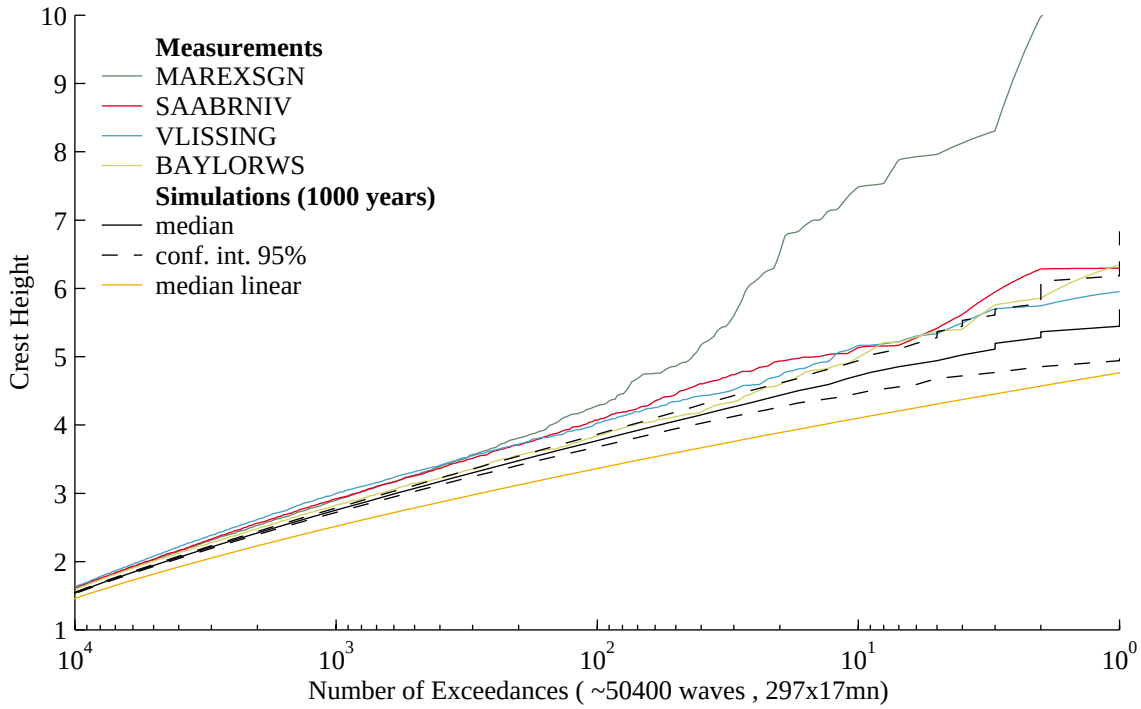

FIGURE 6.18 : EB Crest levels, Raw data

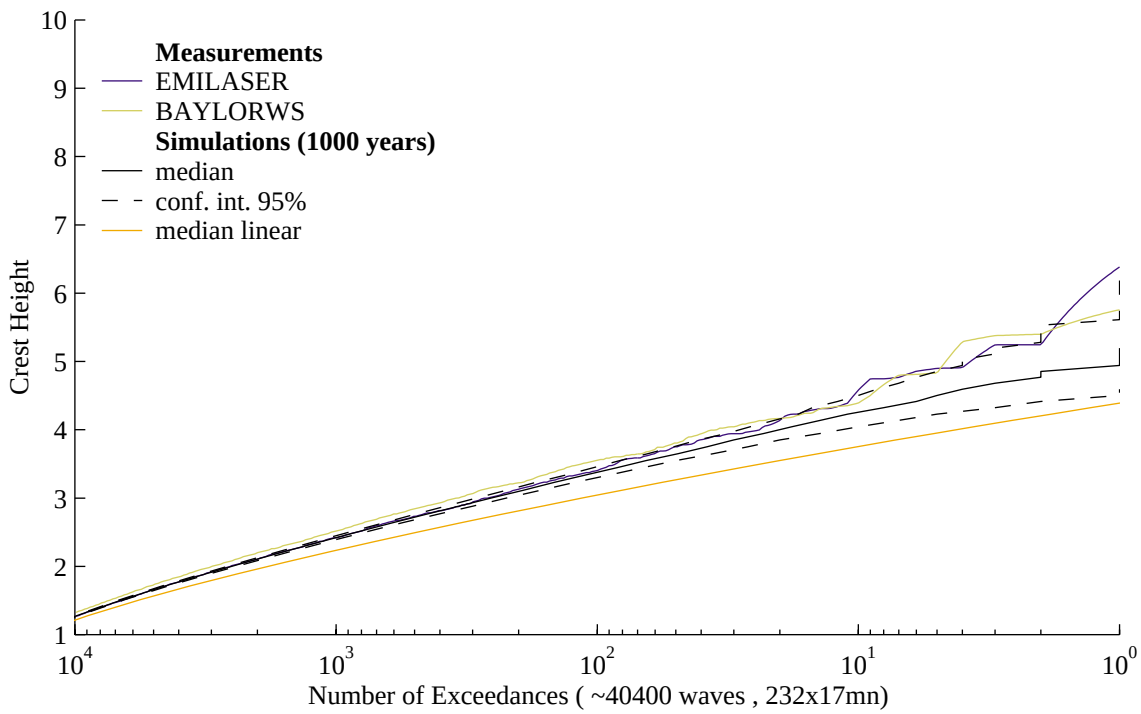

FIGURE 6.19 : W Crest levels, Filtered data

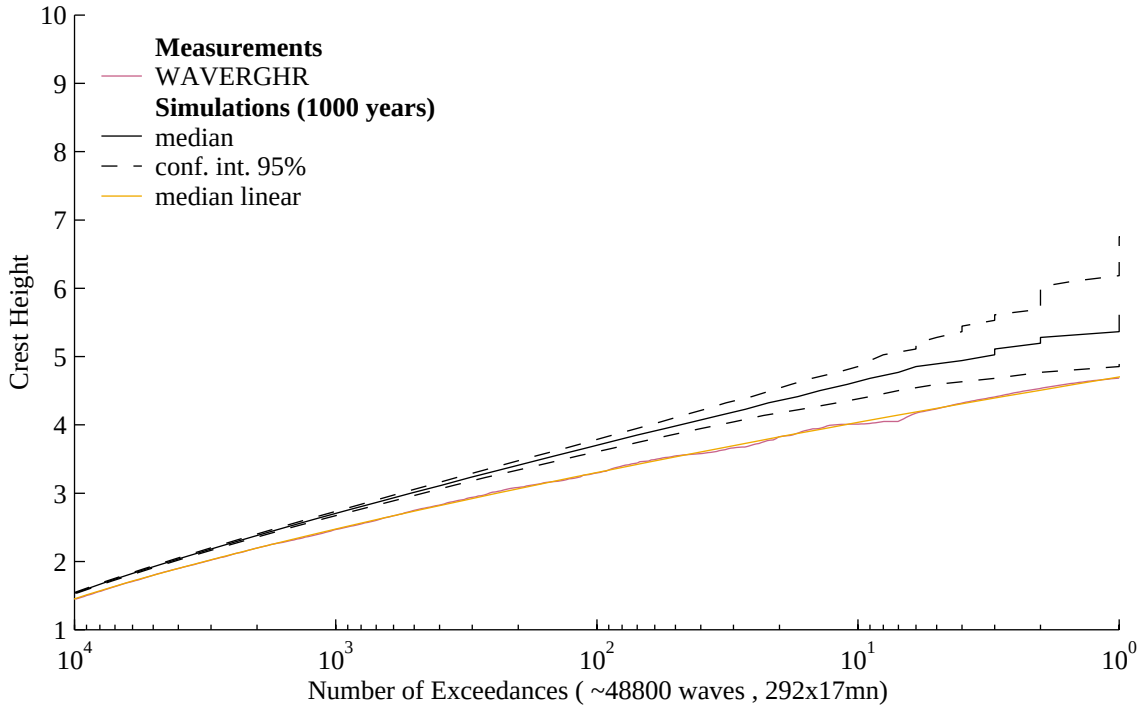

Appendix 6.1: Crest Height Ratio on some dates

FIGURE 6.20 : 3rd of January 17:00, comparison simulation - raw data

H_s=3.7m − T_p=8.0s − T_{02}=6.0s

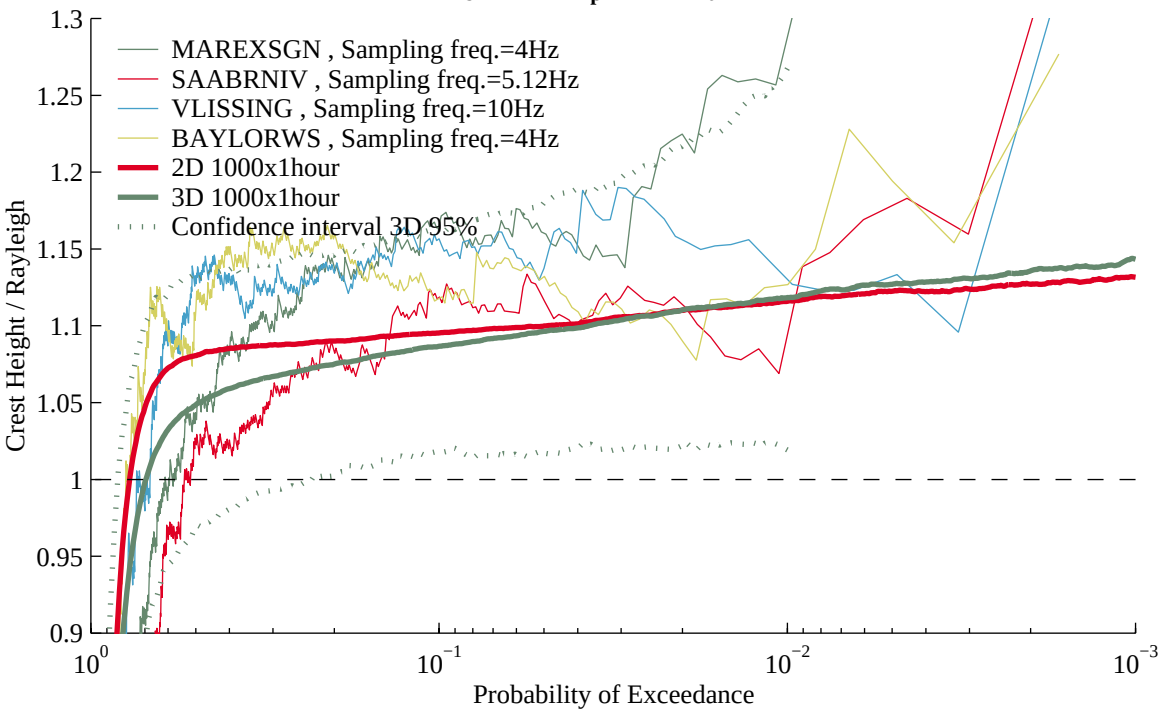

FIGURE 6.21 : 3rd of January 17:00, comparison simulation - filtered data

H_s=3.7m − T_p=8.0s − T_{02}=6.0s

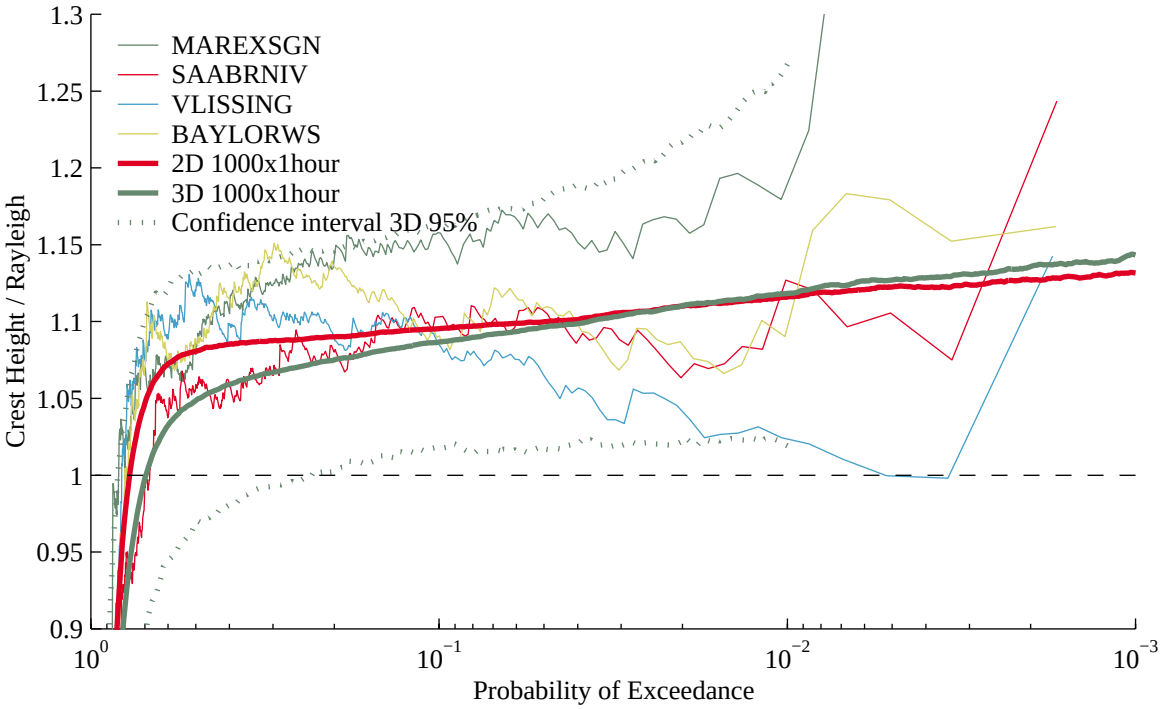

FIGURE 6.22 : 3rd of January 23:00, comparison simulation - raw data

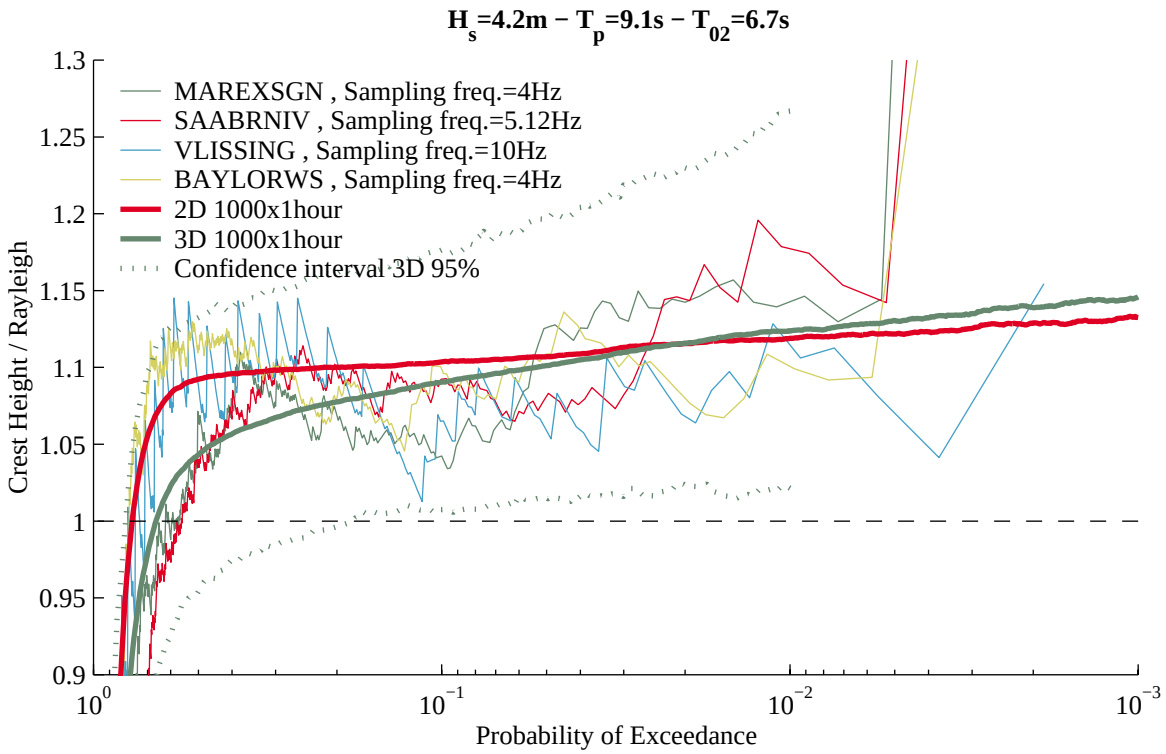

FIGURE 6.23 : 3rd of January 23:00, comparison simulation - filtered data

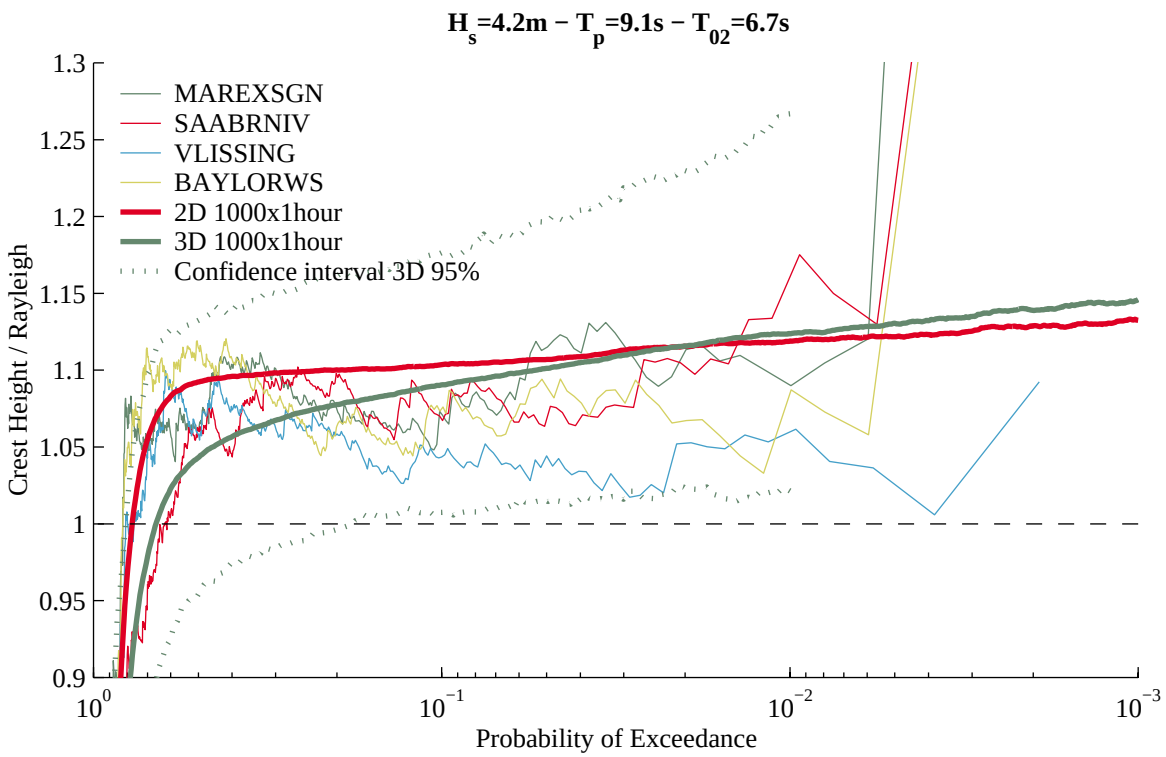

FIGURE 6.24 : 4th of January 00:00, comparison simulation - raw data

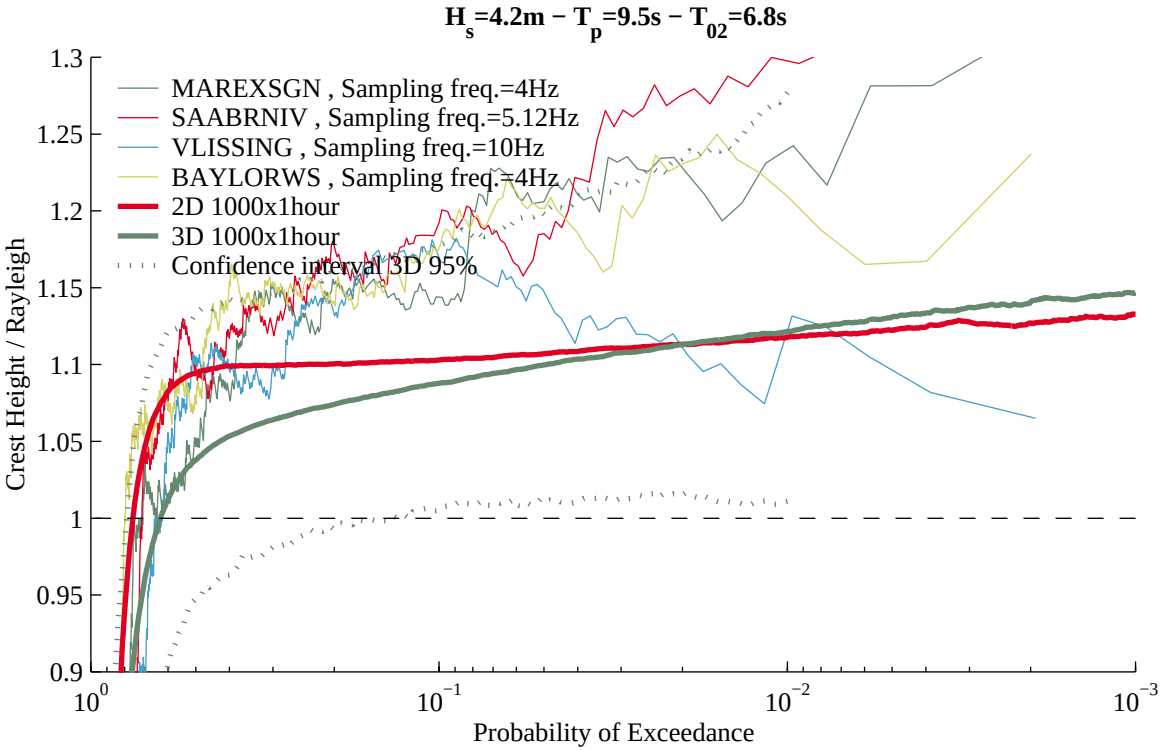

FIGURE 6.25 : 4th of January 00:00, comparison simulation - filtered data

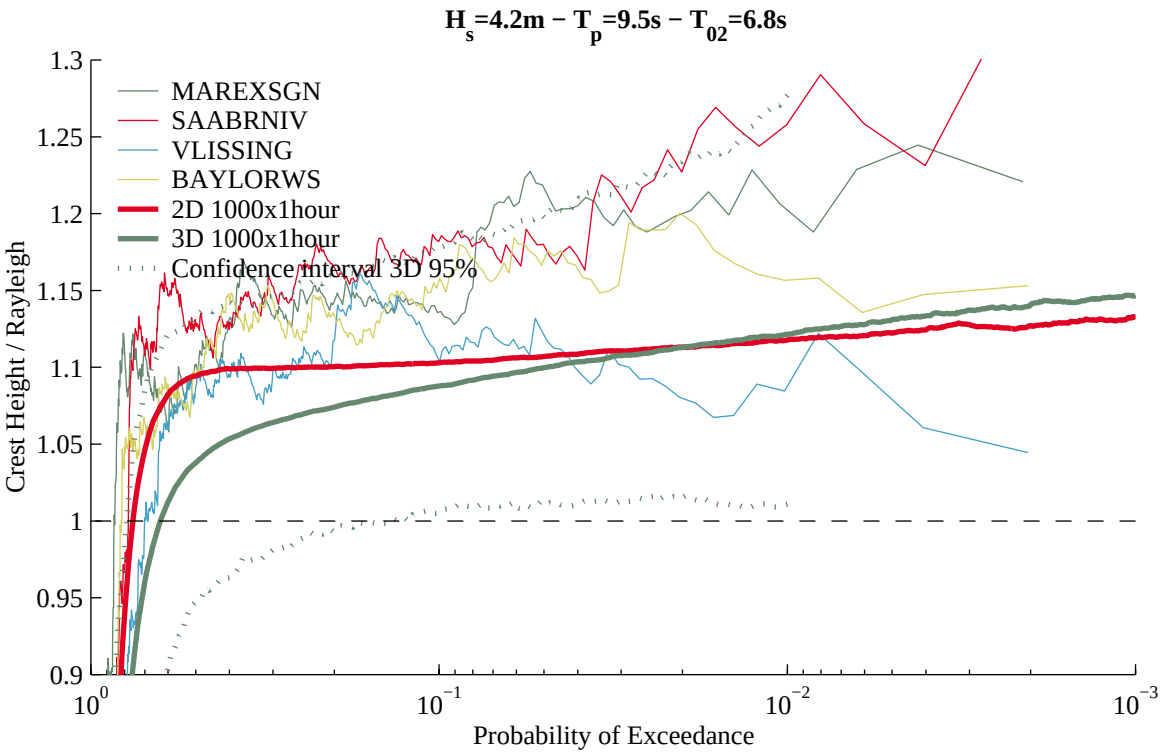

FIGURE 6.26 : 19th of January 20:00, comparison simulation - raw data

H_s=3.3m − T_p=10.5s − T_{02}=6.3s

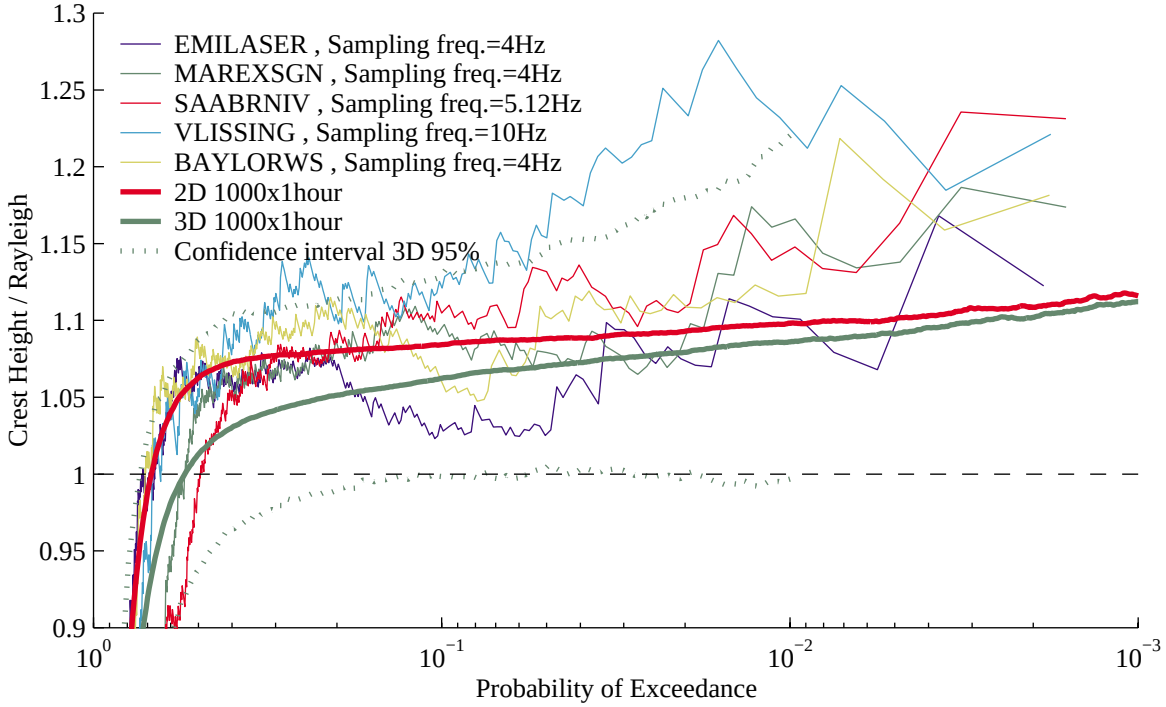

FIGURE 6.27 : 19th of January 20:00, comparison simulation - filtered data

H_s=3.3m − T_p=10.5s − T_{02}=6.3s

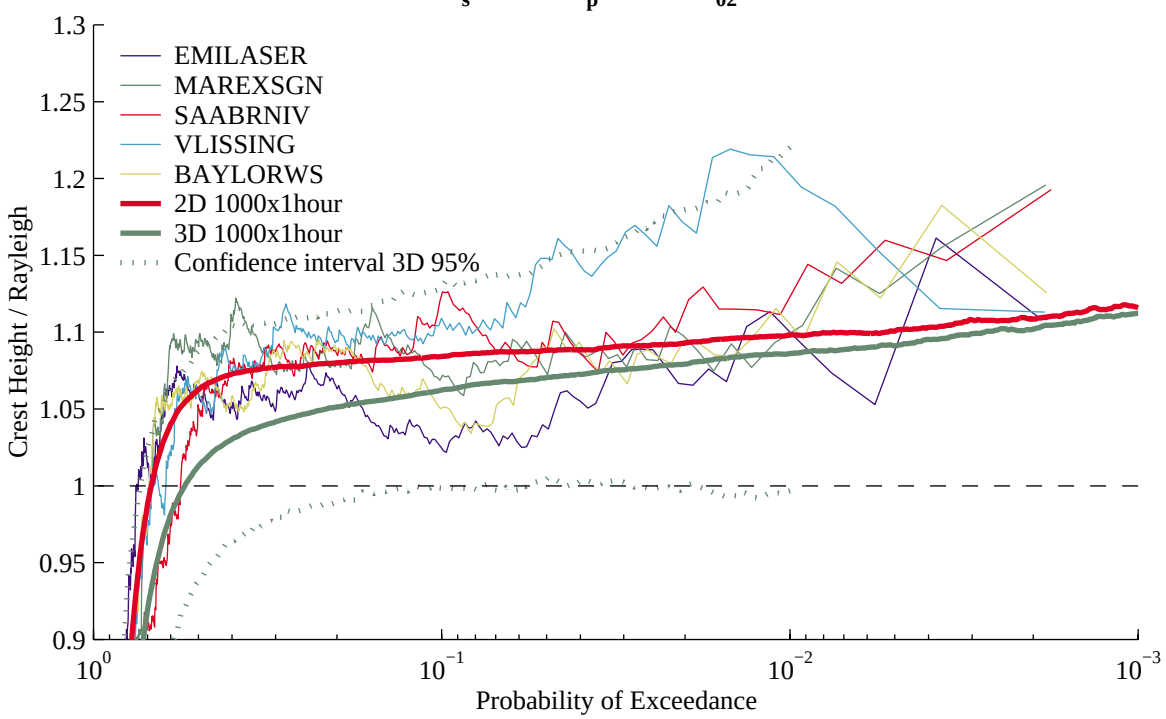

FIGURE 6.28 : 20th of January 22:00, comparison simulation - raw data

H_s=1.6m − T_p=10.0s − T_{02}=5.4s

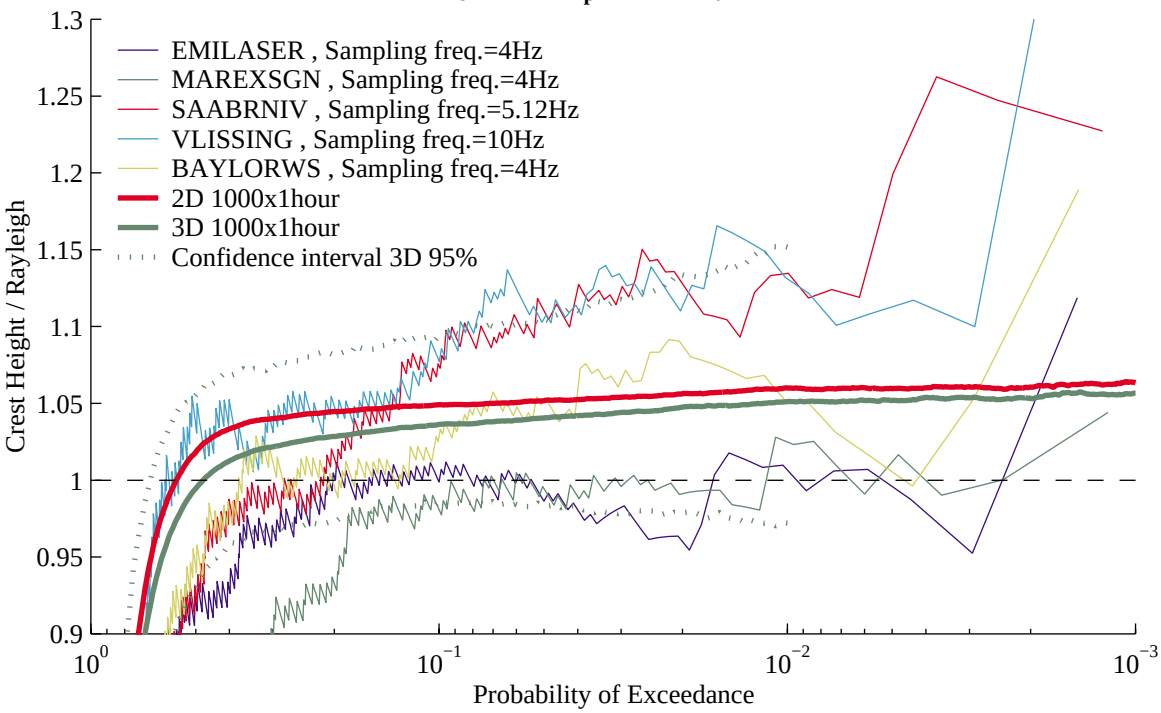

FIGURE 6.29 : 20th of January 22:00, comparison simulation - filtered data

H_s=1.6m − T_p=10.0s − T_{02}=5.4s

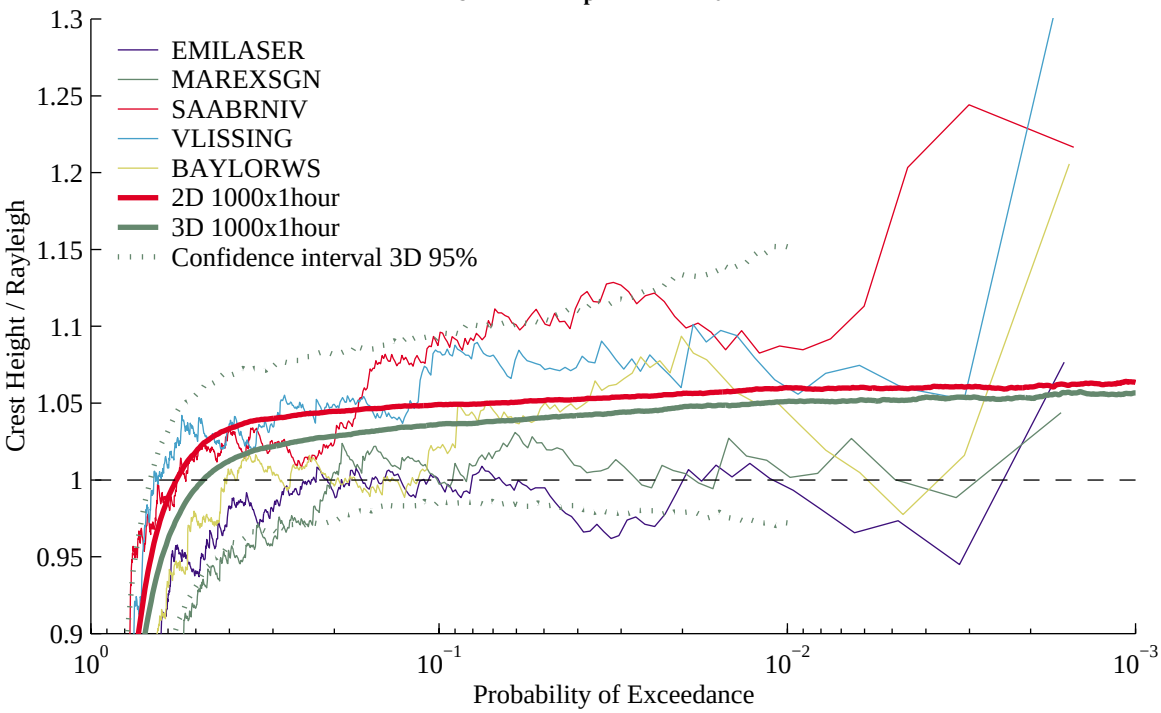

Appendix 6.2: Simulation - Comparison between sensors

FIGURE 6.30 : 3rd of January 17:00, simulation comparison between sensors

H_s=3.7m − T_p=8.0s − T_{02}=6.0s

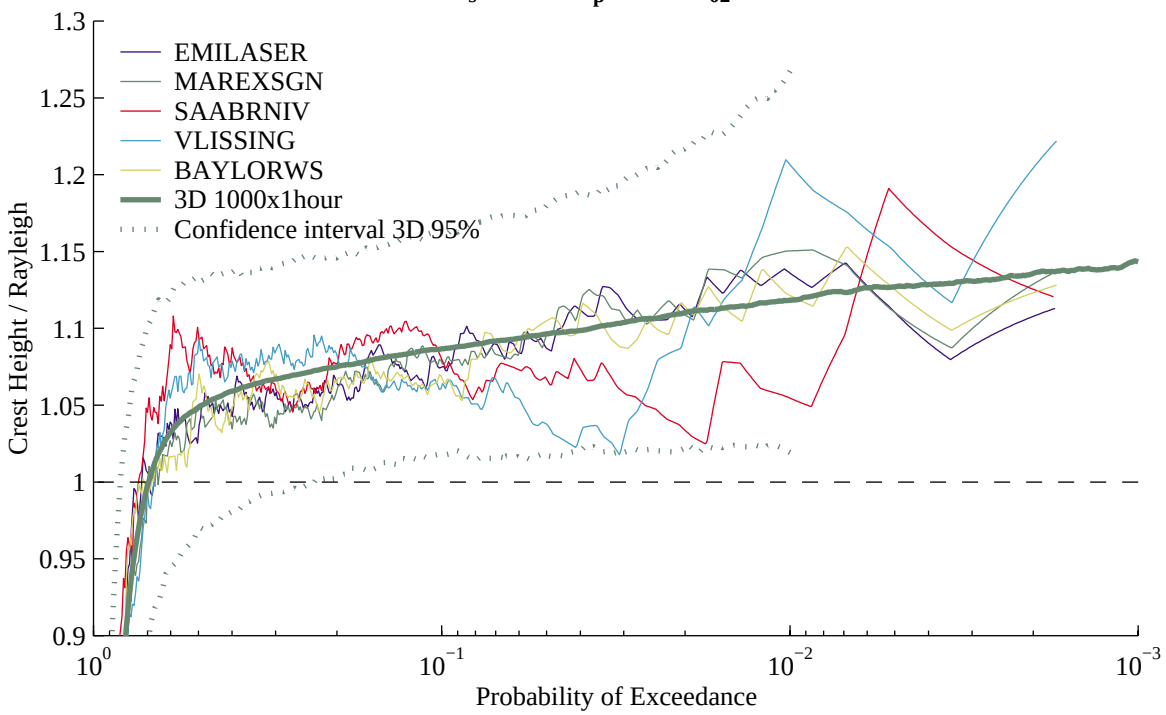

FIGURE 6.31 : 3rd of January 23:00, simulation comparison between sensors

H_s=4.2m − T_p=9.1s − T_{02}=6.7s

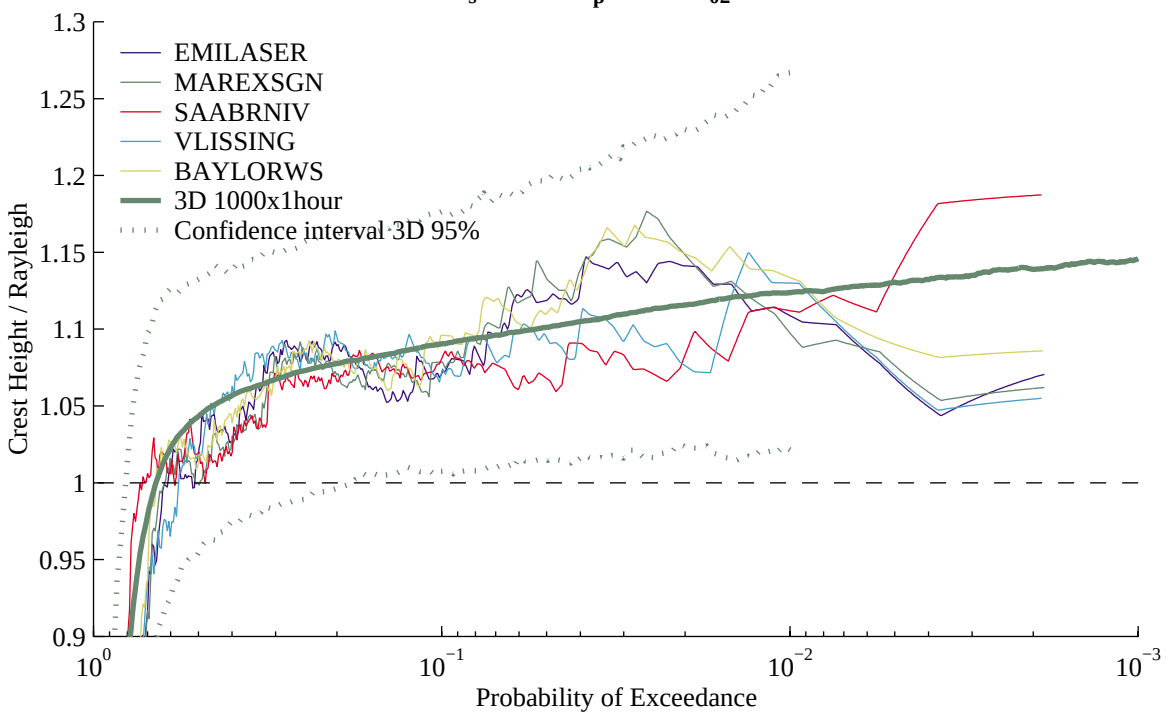

FIGURE 6.32 : 4th of January 00:00, simulation comparison between sensors

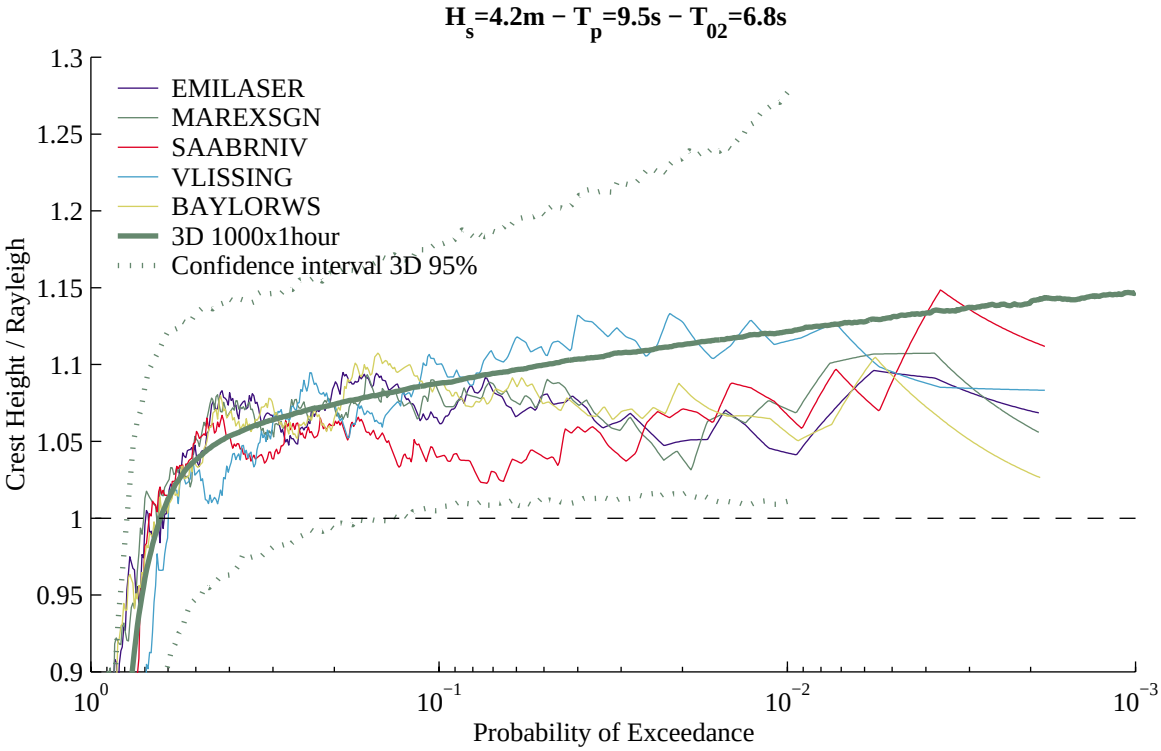

FIGURE 6.33 : 19th of January 20:00, simulation comparison between sensors

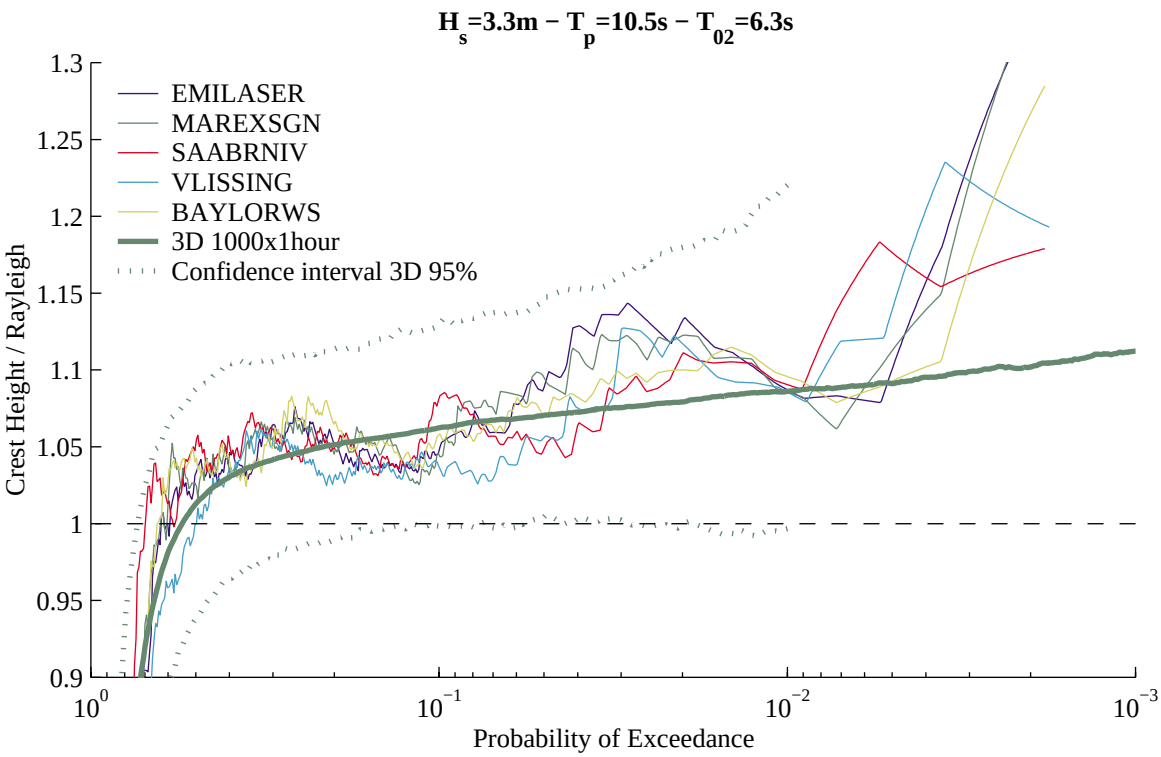

FIGURE 6.34 : 20th of January 22:00, simulation comparison between sensors

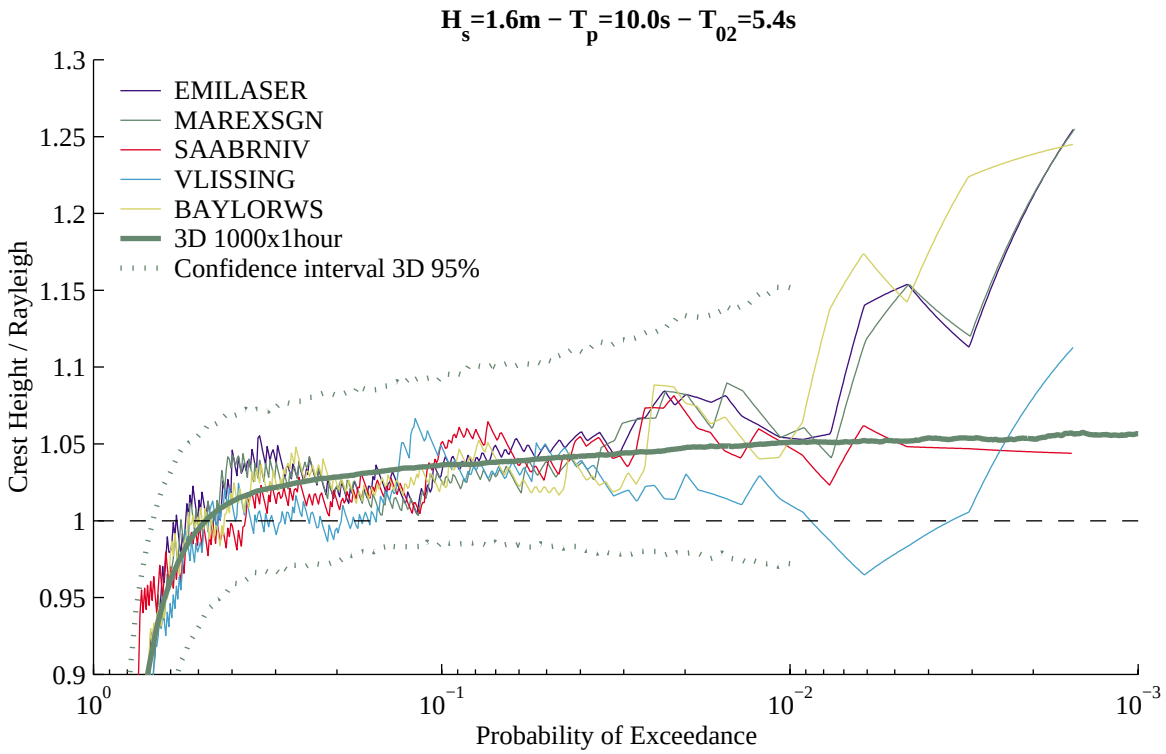

CHAPTER 7

Models of distribution Comparison with simulations

Marc Prevosto
George Z. Forristall

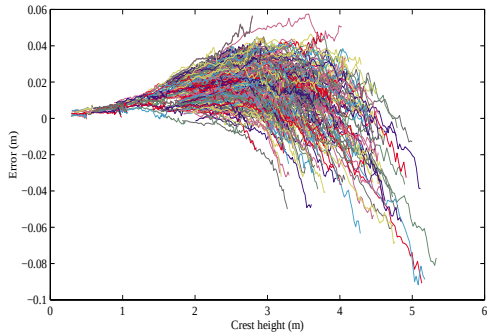

The methodologies to furnish statistics of waves inside a sea state starting from spectral information are of different kinds. They can be based on theoretical considerations, e.g. Transformed Gaussian process method [22] or First Order Reliability Method (FORM) [26], or they can use a Monte Carlo technique. This later technique has been used in the simulation studies reported in this document.

In any case, independently of the methodology, the answers will differ depending on the model of irregular gravity waves which is taken as starting point. Even though more complex models exist like the hybrid model [30,31] or the Creamer transformation [5], the second order 3D irregular wave model described in the previous chapter shows good agreement with the measurements of crest heights on intermediate water depth made in WACSIS.

As better practical tool for engineers, simplified parametric models have been proposed. Some of these models are tested and compared with 2nd order simulations and measurements in this chapter.

Simplified parametric models - State of the art

Rayleigh model

When the sea surface elevation is considered to follow a Gaussian process model, the law of the local maxima is (see [21]):

$$f_{max>0}(\tilde{x}) = \frac{1}{\sqrt{2\pi}}\left(\varepsilon \exp\left(-\frac{\tilde{x}^2}{2\varepsilon^2}\right) + I\tilde{x}\exp\left(-\frac{\tilde{x}^2}{2}\right)\int_{-\infty}^{\tilde{x}I/\varepsilon} \exp\left(-\frac{z^2}{2}\right)dz\right) \qquad \textbf{(EQ 7.1)}$$

with $\tilde{x} = x/(\sqrt{m_0})$ the normalized amplitude and $I = \sqrt{1-\varepsilon^2}$ an irregularity coefficient with $\varepsilon = \sqrt{1-\frac{m_2^2}{m_0 m_4}}$ a bandwidth parameter (m_i the spectral moments).

The distribution in EQ. 7.1 is not really useful for engineering purposes since it counts all of the small local maxima which can occur between zero crossings. Furthermore, it depends on the fourth moment of the spectrum so it is very sensitive to the amount of energy at high frequencies. If ε tends to 0 (narrowband), then local maxima become crest global maxima and so crest heights follow a Rayleigh law. In fact for high levels and spectral bandwith of actual seas the Rayleigh law given in EQ. 7.2 approximate very well the maximum elevation between zero crossings of a Gaussian process.

$$P(C > c) = \exp\left(-8\frac{c^2}{H_s^2}\right) \qquad \textbf{(EQ 7.2)}$$

The sea surface elevation is, however, obviously non Gaussian (see e.g. [15]), and nonlinearities mainly due to the steepness of waves modify the crest heights. Other models have thus been proposed to give more accurate crest height distributions.

Regular Stokes Waves

In engineering design, crest heights are often estimated by taking the height and period of a individual wave at a specified probability level and then applying a high order regular wave theory to it. Stokes fifth order theory is commonly used for this purpose. Since such regular waves are often used as input to calculate forces on a structure, this method has the advantage of consistency. It has the disadvantage of neglecting the random and directionally spread nature of the real sea.

For the comparisons in this chapter, we estimated wave heights from the Rayleigh distribution before calculating the crest heights from Stokes fifth order theory. If the wave heights were estimated from an empirical distribution such as the one due to Forristall (1978) [6] then both the wave heights and crest heights would be lower by as much as 10%.

Haring et al.

This model is based on a nonlinear transformation of a Rayleigh law, where the transformation is dependent of the crest height normalized by water depth. It was first proposed by Jahns and Wheeler [10] and fitted later using measurements by Haring et al. [9]. The fitting used wave staff measurements in the Gulf of Mexico and Waverider measurements in the North Sea, both in relatively shallow water. The model is thus not correct for infinite depth where it tends to the Rayleigh law. The model is given by

$$P(C > c \mid H_s;d) = \exp\left(-8\frac{c^2}{H_s^2}\left(1 - 4.37\frac{c}{d}\left(0.57 - \frac{c}{d}\right)\right)\right) \qquad \textbf{(EQ 7.3)}$$

with d the water depth

Derived Narrowband models

Some other models were derived from a narrowband model of the 2D irregular second order wave model. As explained in “Non-linear narrowband - 2D”, page 79, the second order narrowband model is written

$$\begin{aligned}\eta(t) &= A(t)\cos(\Omega(t)) \\ &+ T^D_{nb}(f_m)A^2(t) + T^S_{nb}(f_m)A^2(t)\cos(2\Omega(t)) \\ &- \frac{1}{8}H_s^2 T^D_{nb}(f_m)\end{aligned} \quad \textbf{(EQ 7.4)}$$

If we consider that the envelope varies sufficiently slowly, the crest occurs at instant t_c when $\Omega(t_c) = 0$. Then the crest height given by the linear part is $A(t_c)$, and the crest height at second order is

$$A_{nonlin}(t_c) = A(t_c) + (T^D_{nb}(f_m) + T^S_{nb}(f_m))A^2(t_c) - T^D_{nb}(f_m)\frac{H_s^2}{8} \quad \textbf{(EQ 7.5)}$$

which links linear to nonlinear crest heights by a quadratic transformation:

$$C = C_{lin} + (T^D_{nb}(f_m) + T^S_{nb}(f_m))C^2_{lin} - T^D_{nb}(f_m)\frac{H_s^2}{8} \quad \textbf{(EQ 7.6)}$$

Tayfun (1980) [25], Tung and Huang (1986) [27], Kriebel and Dawson (1991) [11], and Kriebel and Dawson (1993) [12] proposed models based on such a nonlinear quadratic relation:

$$C = C_{lin} + \alpha(f_m;d)C^2_{lin} + \beta = Q(C_{lin}) \quad \textbf{(EQ 7.7)}$$

and on the Rayleigh law for the distribution of the linear crests:

$$P(C_{lin} > c \mid H_s) = \exp\left(-8\frac{c^2}{H_s^2}\right) \quad \textbf{(EQ 7.8)}$$

So, in a classical way, the distribution of the nonlinear crests is obtained by applying the inverse nonlinear transformation (EQ. 7.7).

$$P(C > c \mid H_s;f_m;d) = \exp\left(-8\frac{(Q^{-1}(c))^2}{H_s^2}\right) \quad \textbf{(EQ 7.9)}$$

The only solution of the inverse transformation is

$$C_{lin} = Q^{-1}(C) = \frac{-1 + \sqrt{1 + 4\alpha(C - \beta)}}{2\alpha} \quad \textbf{(EQ 7.10)}$$

giving

$$P(C > c \mid H_s;f_m;d) = \exp\left(-8\frac{\left(\frac{-1 + \sqrt{1 + 4\alpha(c - \beta)}}{2\alpha}\right)^2}{H_s^2}\right) \quad \textbf{(EQ 7.11)}$$

The differences between the models come from different choices of α, and different approximations of $Q^{-1}(C)$. All the previous authors take β equal to zero and coefficient of the transformation from second order <u>regular</u> Stokes wave. But unfortunately in finite water depth the irregular narrowband models do not tend to

the regular model (due to the difference terms), making the Kriebel and Dawson finite depth model not an exact one (Compare EQ. 7.14 to the sum of EQ. 5.23 and EQ. 5.24). Tung and Huang [27] made an error by taking into account in infinite water depth a low frequency part which in fact does not exist.

Kriebel and Dawson. The Kriebel and Dawson model is based on the second order regular Stokes wave model in infinite or finite depth, giving

$$C = C_{lin} + \frac{1}{2}\frac{R}{H_s}C_{lin}^2 \rightarrow C_{lin} = \left(-1 + \sqrt{1 + 2\frac{R}{H_s}C}\right)\frac{H_s}{R} \qquad \textbf{(EQ 7.12)}$$

$$\text{with} \quad \begin{aligned} R &= kH_s f_2(kd) \\ k \leftarrow T_m &= 0.95T_p \end{aligned} \qquad \textbf{(EQ 7.13)}$$

$$\text{and } f_2(kd) = \frac{\cosh kd(2 + \cosh 2kd)}{2\sinh^3 kd} - \frac{1}{\sinh 2kd} \qquad \textbf{(EQ 7.14)}$$

Kriebel and Dawson approximated the inverse transformation $Q^{-1}(C)$, first [11] at second order and later [12] with a corrected third order expansion. This induces a problem in the crest distribution when the steepness is strong. These simplifications are not necessary as we know an analytic form of the inverse transformation (EQ. 7.10). In the sequel of the report we will call the crest distribution based on equations 7.12, 7.13 and 7.14 the exact Kriebel model, and the model which uses the truncated inverse transformation the Kriebel model. The Kriebel model is given by:

$$C_{lin} = \left(1 - \frac{1}{2}R\frac{C}{H_s}\right)C \qquad \textbf{(EQ 7.15)}$$

In infinite depth the exact Kriebel and Dawson model and the Tayfun model are the same. A difference could exist which comes from the definition of T_m (EQ. 7.13).

$$P(C > c \mid (H_s, T_p)) = \exp\left(-\frac{8}{H_s^2 k^2}(-1 + \sqrt{1 + 2kc})^2\right) \qquad \textbf{(EQ 7.16)}$$

Comparisons of crest height ratios with existing models

The Stokes, Haring and exact Kriebel models are compared to the filtered measurements in Figure 7.1 through Figure 7.9. In the figure captions, the exact Kriebel model is referred to as the “Kriebel” model. As before, the measurements have had a low pass filter with a cut off of 0.64Hz applied before the crests were identified.

The three models give results which are generally quite close to each other. The crest height ratios from the models increase with increasing significant wave height as the should, but they are higher than any of the measurements for all but the smallest waves. The error is probably due to the fact that all of these model effectively concentrate all of the energy of the spectrum at the peak frequency, and the nonlinear interaction term is greatest for the self interaction. Better results could be expected from a perturbated narrow band model that accounts for the spread of the spectrum in frequency and direction.

FIGURE 7.1 : Comparison of crest height ratios of filtered measurements and models for significant wave heights between 4.5 and 5.0 m.

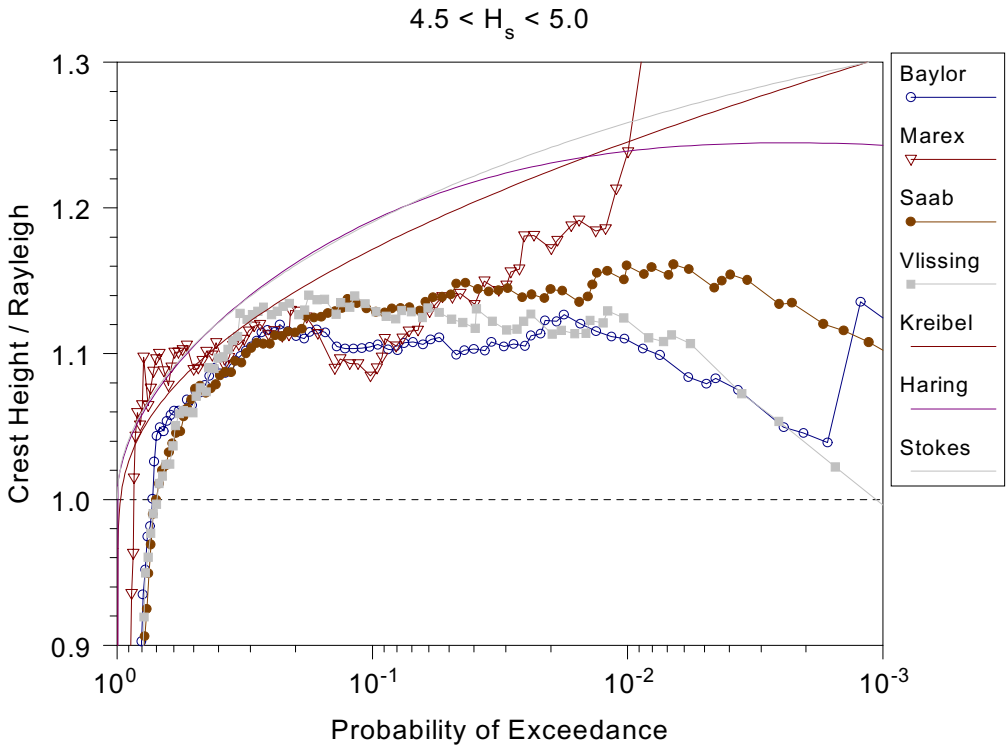

FIGURE 7.2 : Comparison of crest height ratios of filtered measurements and models for significant wave heights between 4.0 and 4.5 m.

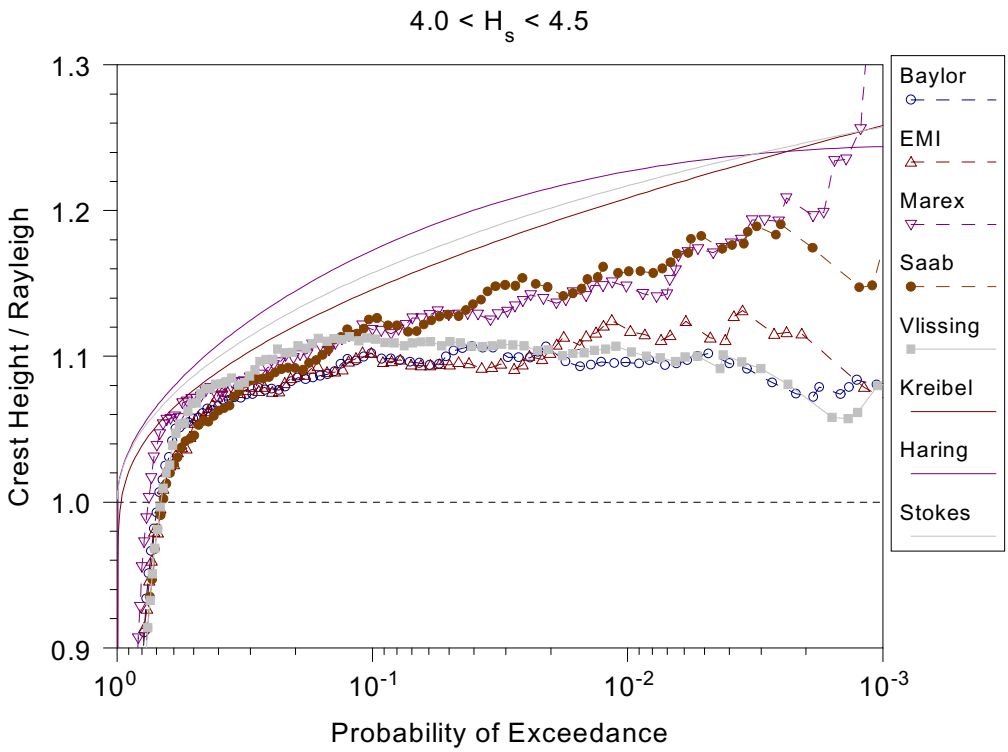

FIGURE 7.3 : Comparison of crest height ratios of filtered measurements and models for significant wave heights between 3.5 and 4.0 m.

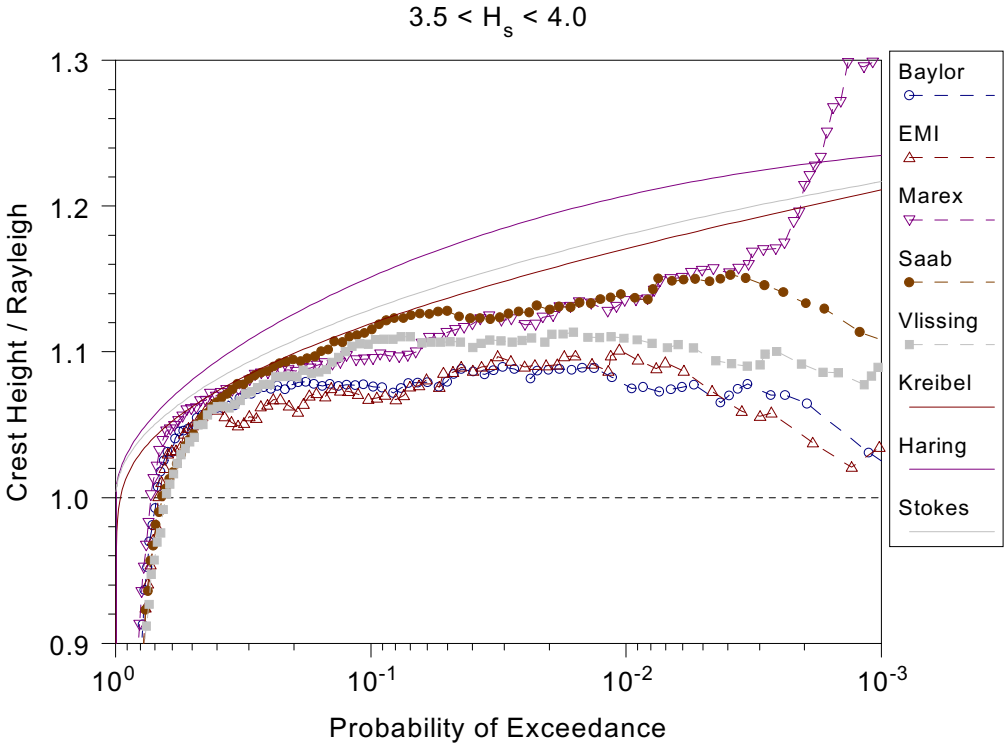

FIGURE 7.4 : Comparison of crest height ratios of filtered measurements and models for significant wave heights between 3.0 and 3.5 m.

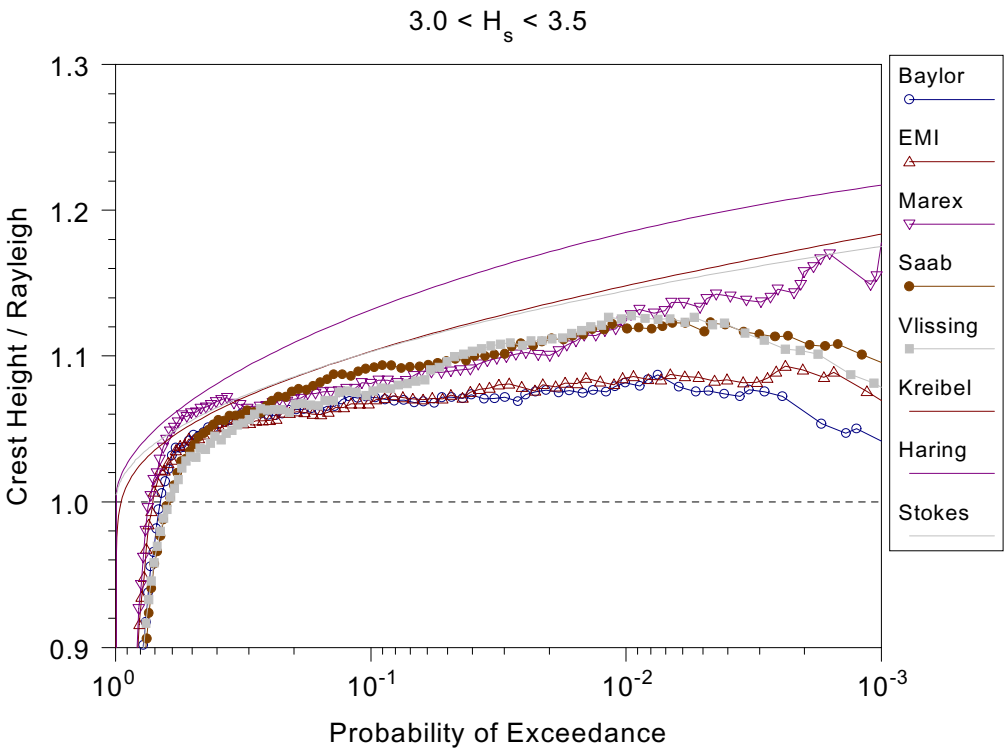

FIGURE 7.5 : Comparison of crest height ratios of filtered measurements and models for significant wave heights between 2.5 and 3.0 m.

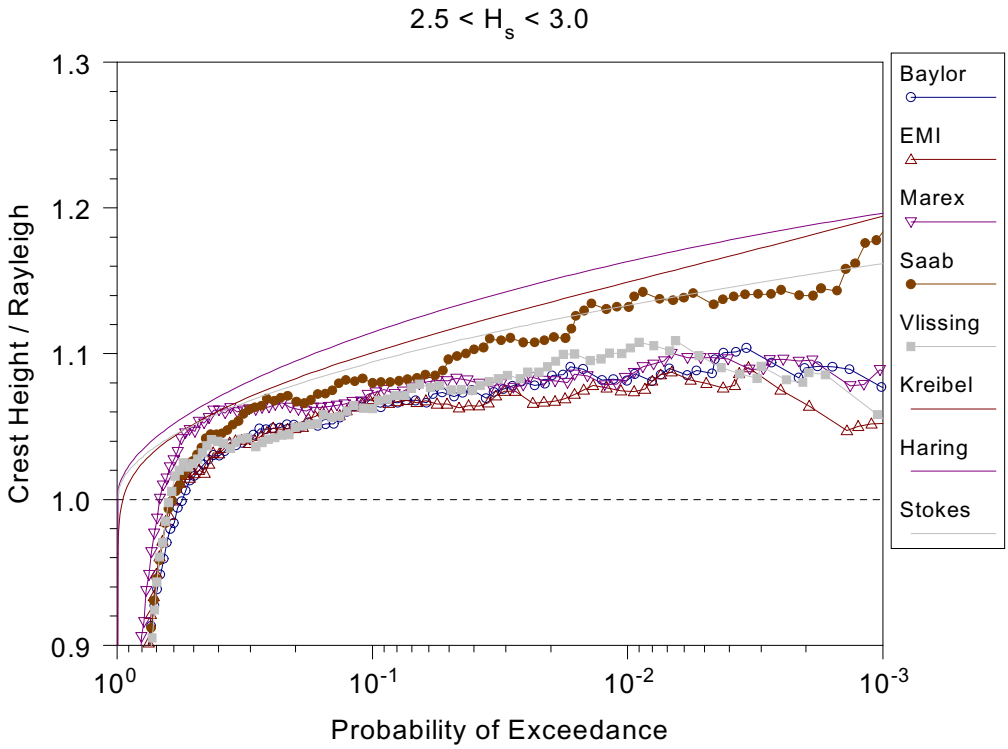

FIGURE 7.6 : Comparison of crest height ratios of filtered measurements and models for significant wave heights between 2.0 and 2.5 m.

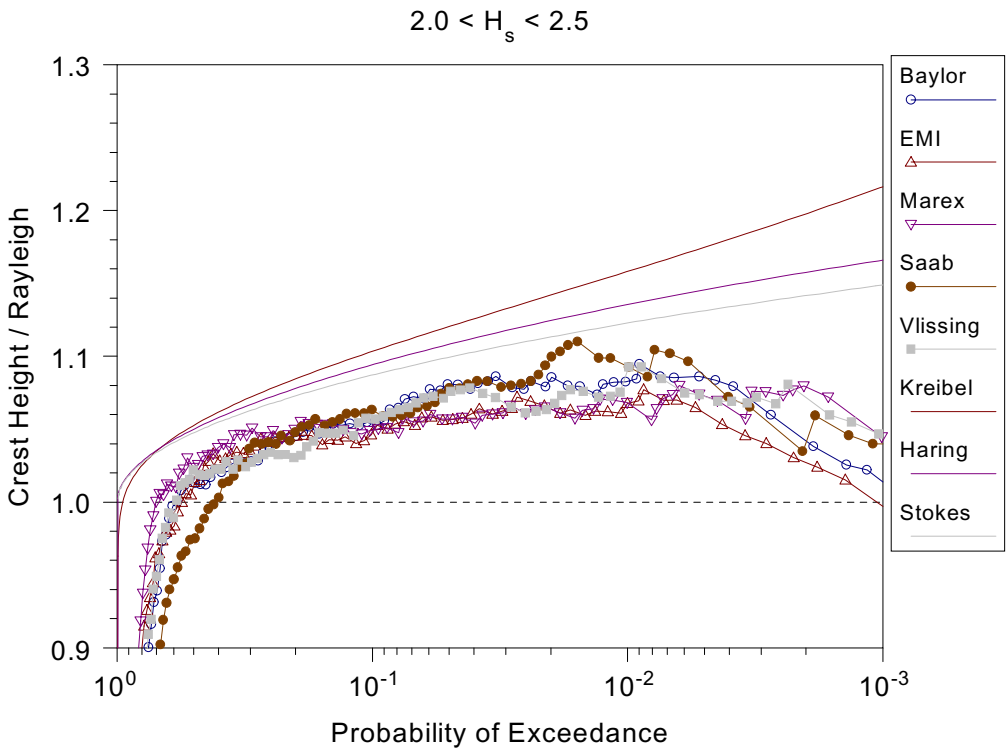

FIGURE 7.7 : Comparison of crest height ratios of filtered measurements and models for significant wave heights between 1.5 and 2.0 m.

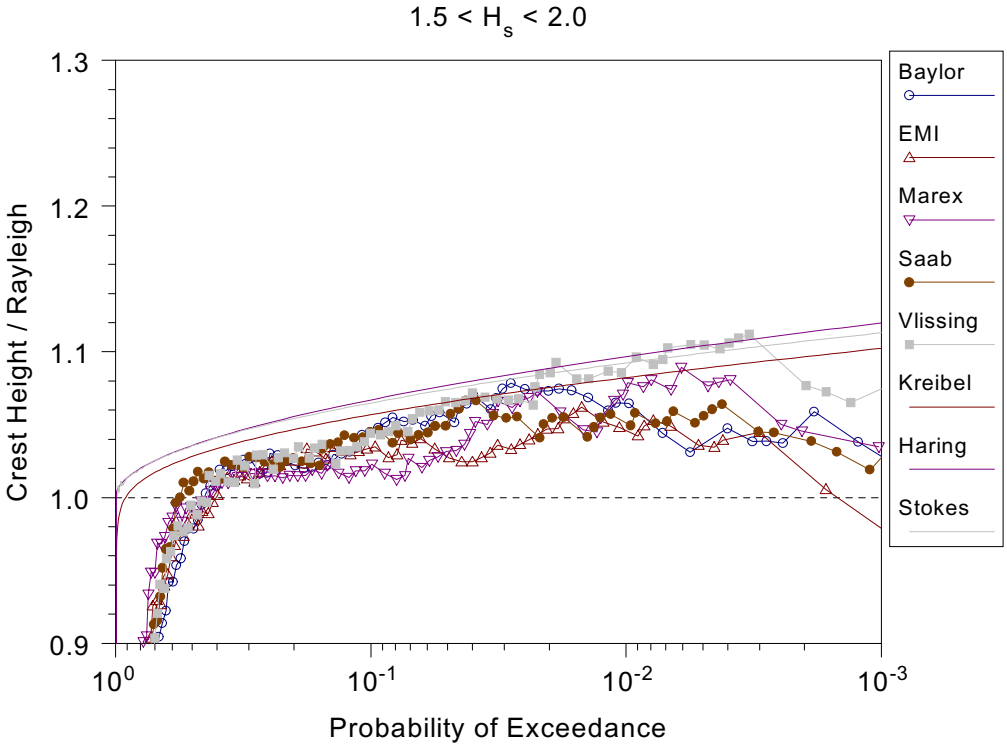

FIGURE 7.8 : Comparison of crest height ratios of filtered measurements and models for significant wave heights between 1.0 and 1.5 m.

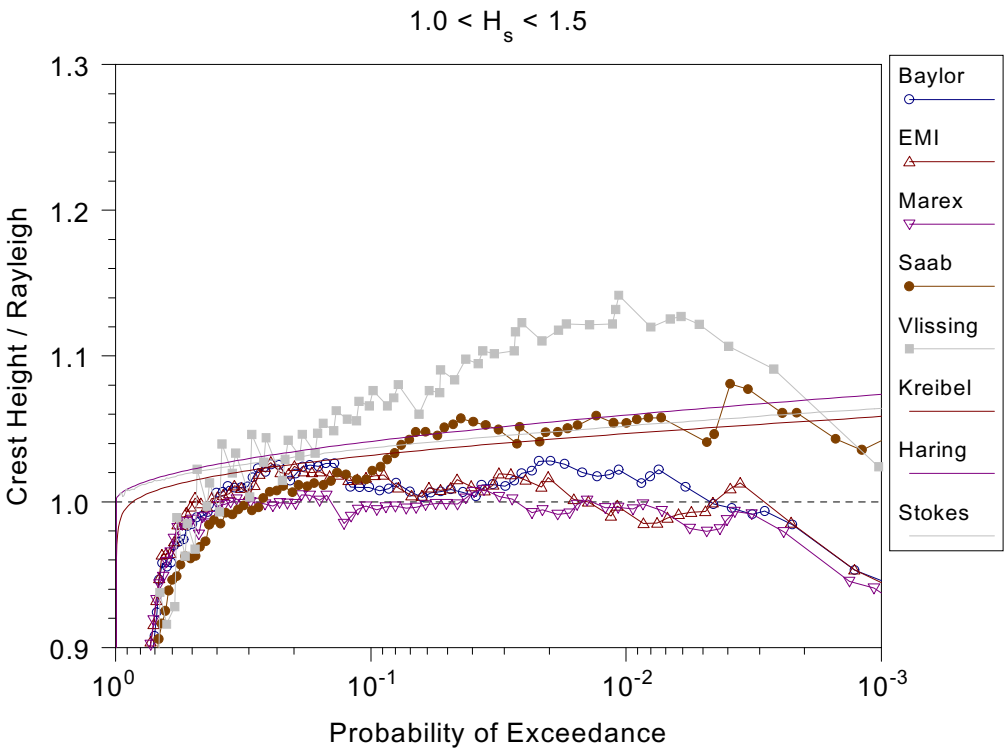

FIGURE 7.9 : Comparison of crest height ratios of filtered measurements and models for significant wave heights between 0.5 and 1.0 m.

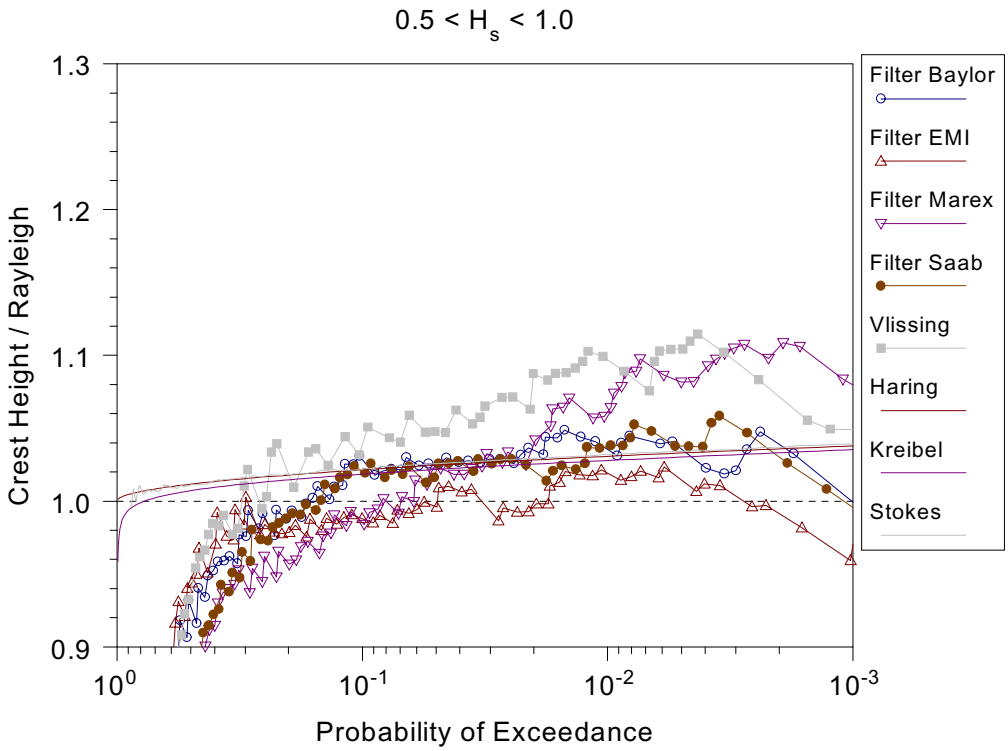

Simplified parametric models - New models

Two new models have been recently developed which take into account the 3D structure of the waves. The first one is a perturbated narrowband-derived model similar to those discussed in the previous section and the second one is a perturbated Weibull model.

Marc Prevosto model - Perturbated narrowband model

This model assumes narrowband and infinite crested waves (EQ. 7.11), but uses the exact asymptotic narrowband transfer coefficients (see appendix "Narrow-band non-linear transfer coefficients", page 90). In order to take into account spectral bandwidth and directional spreading in equation 7.6, we consider the same model but with modified H_s and f_m.

$$\tilde{H}_s = \alpha_{H_s} H_s \,,\; \tilde{f}_m = \alpha_{f_m} f_m \qquad \textbf{(EQ 7.17)}$$

In looking at different directional spectrum climatologies, including the WACSIS data base, and different water depths, the α_{H_s} and α_{f_m} formulations have been determined from simulations and theoretical considerations to be:

$$\alpha_{H_s} = 1 - \frac{1}{2}(\tanh(kd) - 0.9)\sqrt{\frac{2}{1+s}} \qquad \textbf{(EQ 7.18)}$$

where s is the power of the equivalent $\cos^{2s}$ directional distribution at the peak frequency (see EQ. 5.14), and

$$\alpha_{f_m} = \frac{1}{1.23} \text{ with } f_m = \frac{1}{T_{02}} \qquad \textbf{(EQ 7.19)}$$

The formulation of α_{H_s} has been chosen to take into account the fact that the effect of the directional spreading on the crest heights is opposite in deep and shallow water (see [20]). This model has the advantage of furnishing a unique expression both the 2D and 3D cases, and so can be adapted to all intermediate situations.

George Forristall model - Perturbated Weibull model

This model is based on a Weibull law with the two parameters written as polynomials in the steepness and Ursell number.

$$P(C > c) = \exp\left(-\left(\frac{c}{\alpha H_s}\right)^{\beta}\right) \text{ with} \qquad \textbf{(EQ 7.20)}$$

$$\alpha = \alpha_1 + \alpha_2 S_1 + \alpha_3 U_r \text{ and } \beta = \beta_1 - \beta_2 S_1 - \beta_3 U_r + \beta_4 U_r^2 \qquad \textbf{(EQ 7.21)}$$

and the steepness $S_1 = \frac{2\pi}{g}\frac{H_s}{T_{01}^2}$ and the Ursell number $U_r = \frac{H_s}{k_{01}^2 d^3}$.

Starting from simulations based on a synthetic directional spectrum data base and different water depths, two different sets of coefficients of the polynomials were fitted from 2D and 3D simulations [7].

The fit on 2D simulations gave

$$\begin{aligned} \alpha &= 1/\sqrt{8} + 0.2892 S_1 + 0.1060 U_r \\ \beta &= 2 - 2.1597 S_1 + 0.0968 U_r^2 \end{aligned} \qquad \textbf{(EQ 7.22)}$$

The fit on 3D simulations gave

$$\begin{aligned} \alpha &= 1/\sqrt{8} + 0.2568 S_1 + 0.0800 U_r \\ \beta &= 2 - 1.7912 S_1 - 0.5302 U_r + 0.284 U_r^2 \end{aligned} \qquad \textbf{(EQ 7.23)}$$

The advantage of this model is its simplicity. Of course it does not take into account variations in the directional spreading, but as it will be shown hereafter, it works well when facing realistic wind sea directional spreading.

Inside sea states comparison

These two models have been compared using a simulated data base starting from the directional spectrum data base of the WACSIS project. Three water depths were used. They were infinite water depth, 30 meters water depth and the actual water depth. On the plots (figures 7.10-7.13), each coloured line corresponds to the error between the crest heights given by the model and those obtained from simulations at the same level of probability. The plotted error could be written

$$\text{error}(c) = F_C^{-1}(\hat{F}_C(c)) - c \qquad \textbf{(EQ 7.24)}$$

where $F_C(c)$ is the distribution given by the model and $\hat{F}_C(c)$ is the empirical distribution of crest heights estimated from 1000 one hour time series, corresponding to one directional spectrum and one water depth.

As is well known the Rayleigh model always underestimates the crest heights (figure 7.10). The error in this data set reaches 80 cm. When using the narrowband model, corresponding to s = infinity in equation 7.18, the error is decreased to a range from -15 cm to 17 cm (figure 7.11). The two new models, which take account of the directional spreading reduce again the range of the error by a factor two, -8 cm to 8 cm for the Prevosto model (figure 7.12) and -9 cm to 6 cm for the Forristall model (figure 7.13).

All-over campaign comparison

We consider the number of exceedances all-over the campaign. That is to say that for each model we follow the different steps:

- choose a water depth: 1000m, 30m, Meetpost water depths 17-20m
- take a directional spectrum of the WACSIS data base and calculate parameters of the model (H_s, T_{02}, T_{01}, s)
- calculate the number of waves N during one hour of this sea state by $3600/T_{02}$ and then calculate the number of exceedances by multiplying the number of waves by the probability of exceedance given by the model N. (C > c)
- cumulate with the previous sea states

and for simulations

- choose a water depth: 1000m, 30m, Meetpost water depths 17-20m
- take a directional spectrum of the WACSIS data base and simulate 1000 one hour time series
- calculate the number of exceedances and divide it by 1000 to obtain the mean number of exceedance an hour.
- cumulate with the previous sea states

The results are given in figures 7.14-7.19. For each water depth the second of the pair of figures shows an expanded view of the heights of the highest 10 crests.

In “shallow” water (17-20m) (figures 7.14-7.15), the Kriebel model is completely wrong, the Haring and exact Kriebel models overestimate the heights, and Prevosto and Forristall models are very close to the simulations. In intermediate water depth (30m) (figures 7.16-7.17), in decreasing order the Kriebel, Haring and exact Kriebel models overestimate and the Prevosto and Forristall models agree with the simulations. In deep water (figures 7.18-7.19), all the models are very close to the simulations apart from the Haring model which gives exactly the same results as the Rayleigh model as has been explained previously.

Conclusion

Apart from the infinite water depth situation for the exact Kriebel model, the parametric models of crest distributions which were proposed in the past are not very accurate. The two new parametric models which have been recently proposed give results very close to what is obtained empirically from second order 3D irregular simulations of the WACSIS directional spectra, whatever the water depth.

The formulation of the Forristall model is simpler than the Prevosto model. But it does not take into account explicitly the directional spreading as the Prevosto model does. So the Prevosto model will be more accurate in extreme directional spreading situations (very short-crested or close to swell situations).

FIGURE 7.10 : Model vs empirical statistics - Rayleigh model

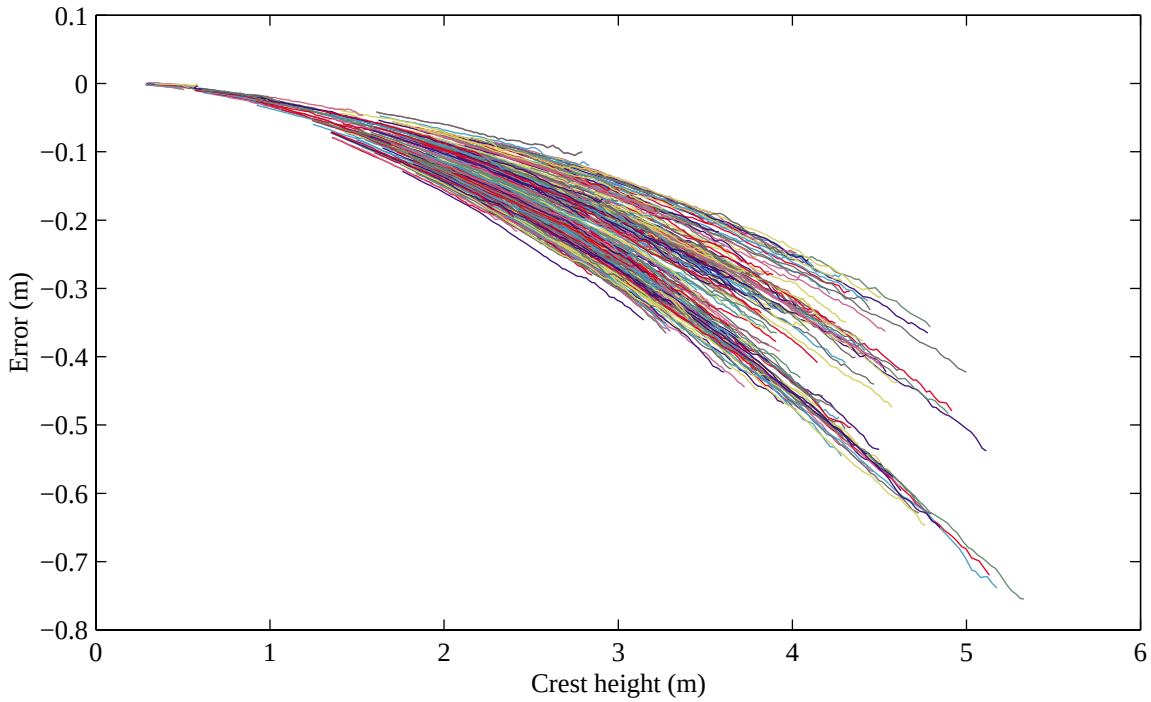

FIGURE 7.11 : Model vs empirical statistics - Narrowband model

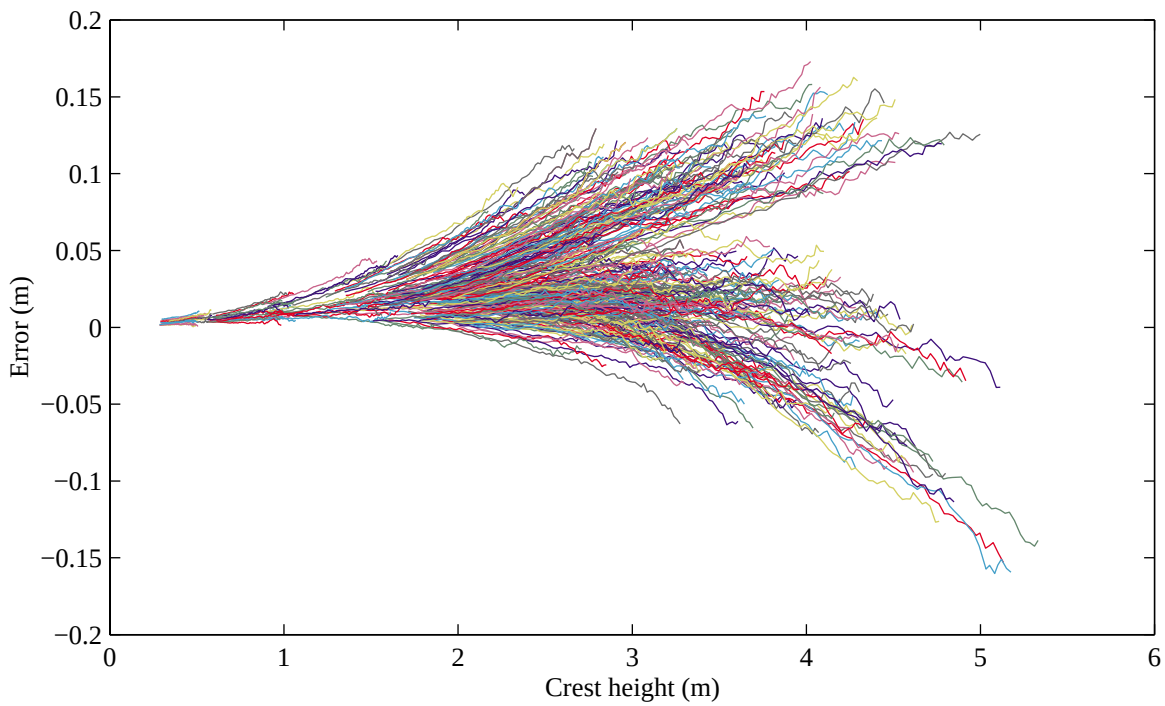

FIGURE 7.12 : Model vs empirical statistics - Prevosto model

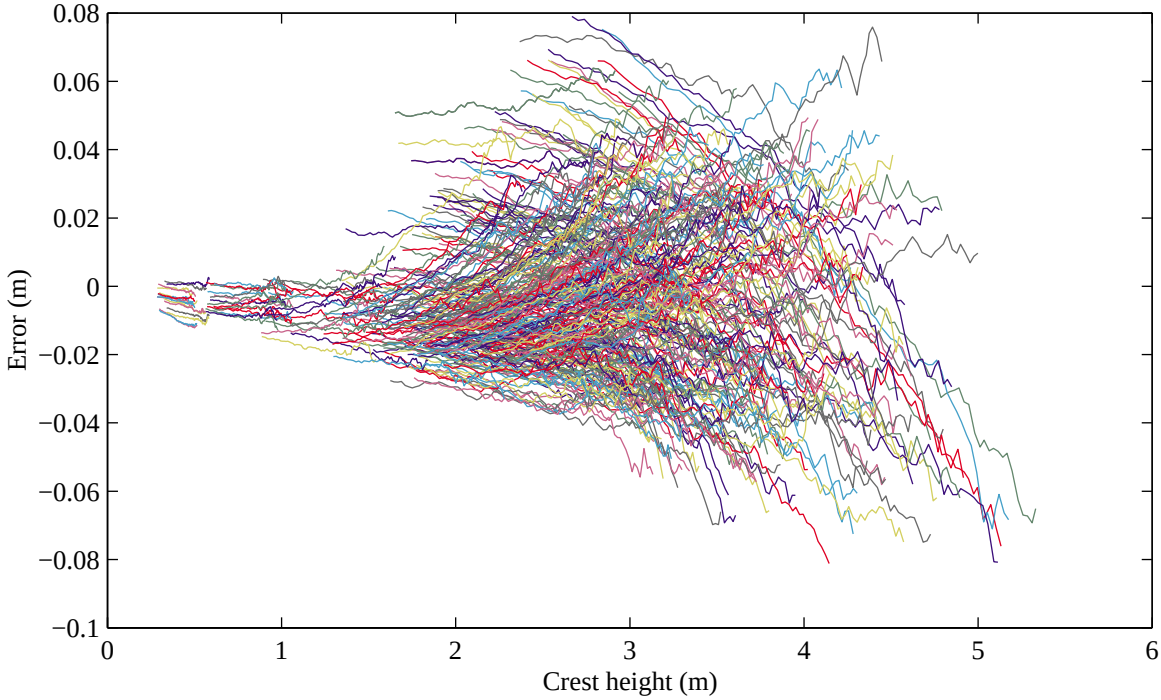

FIGURE 7.13 : Model vs empirical statistics - Forristall model

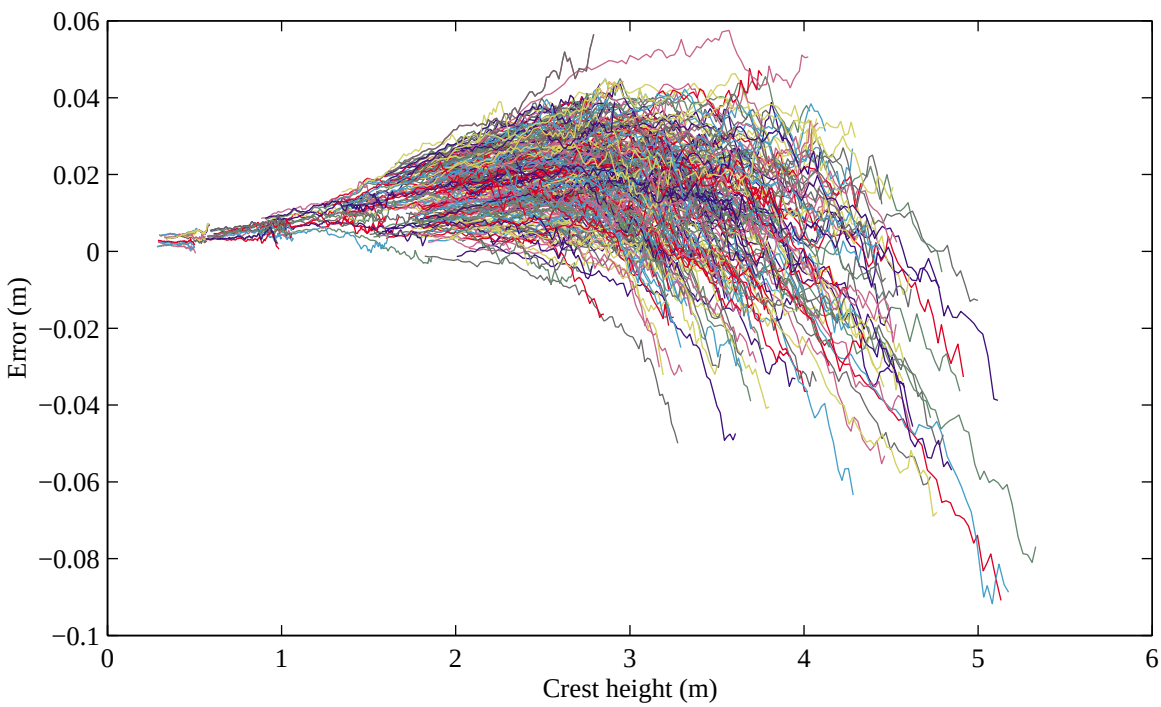

FIGURE 7.14 : Models vs empirical statistics - Meetpost water depths 17-20m

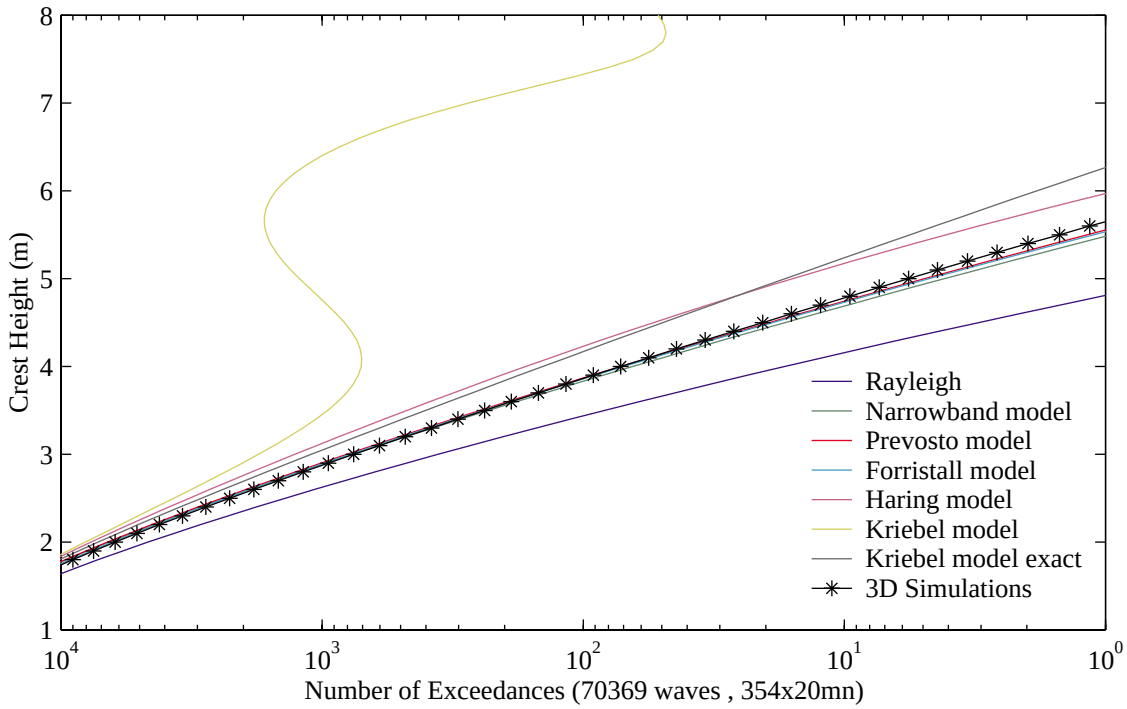

FIGURE 7.15 : Models vs empirical statistics - Meetpost water depths 17-20m

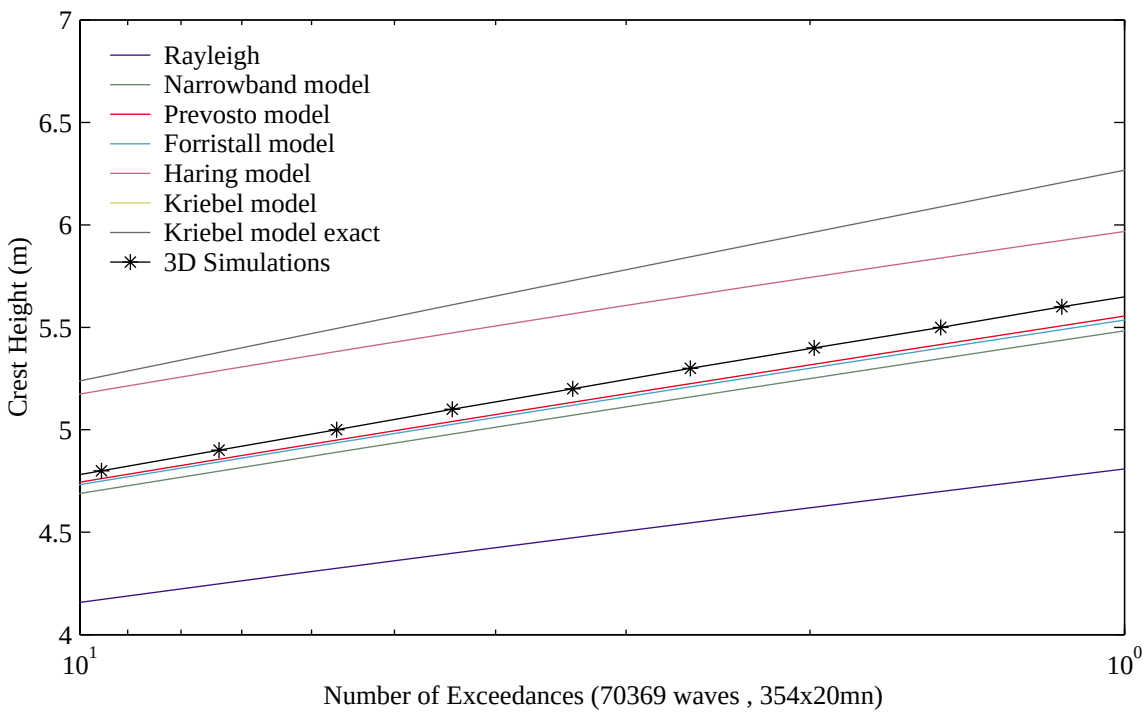

FIGURE 7.16 : Models vs empirical statistics - water depth 30m

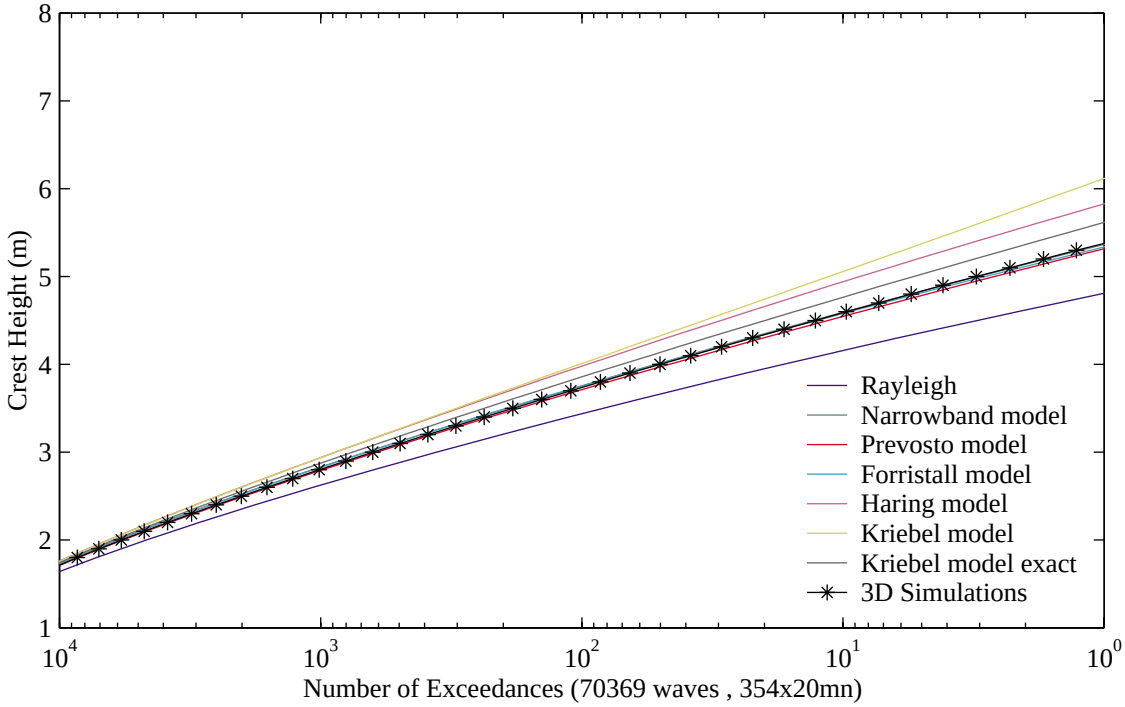

FIGURE 7.17 : Models vs empirical statistics - water depth 30m

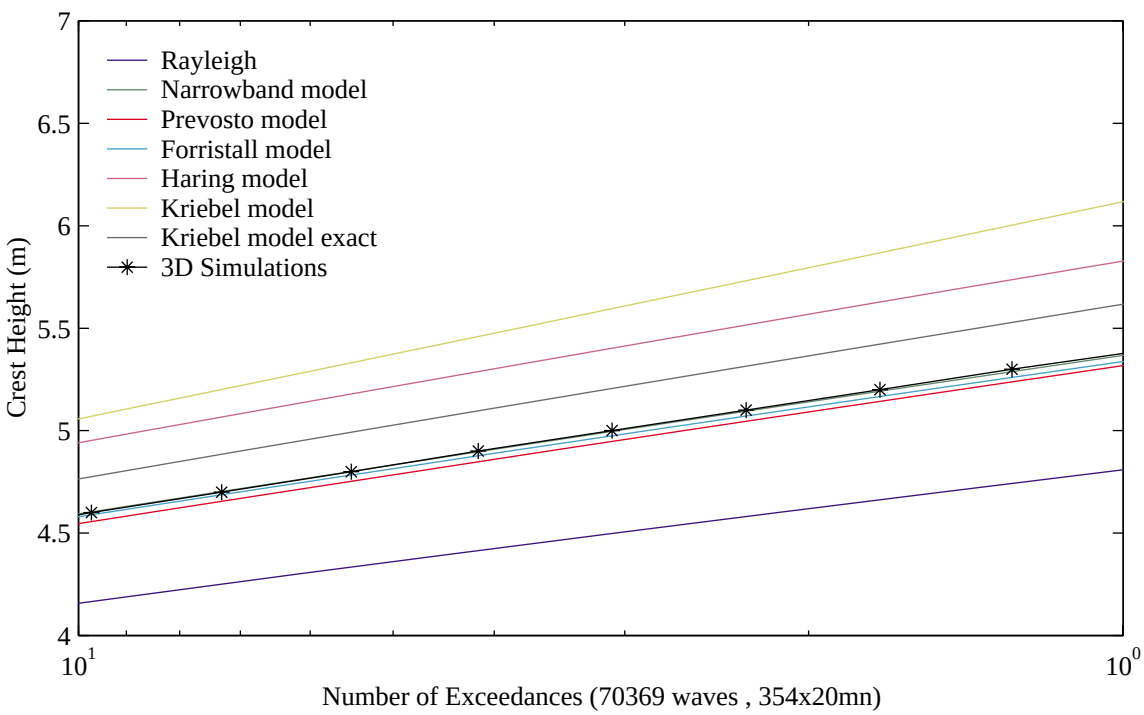

FIGURE 7.18 : Models vs empirical statistics - water depth 1000m

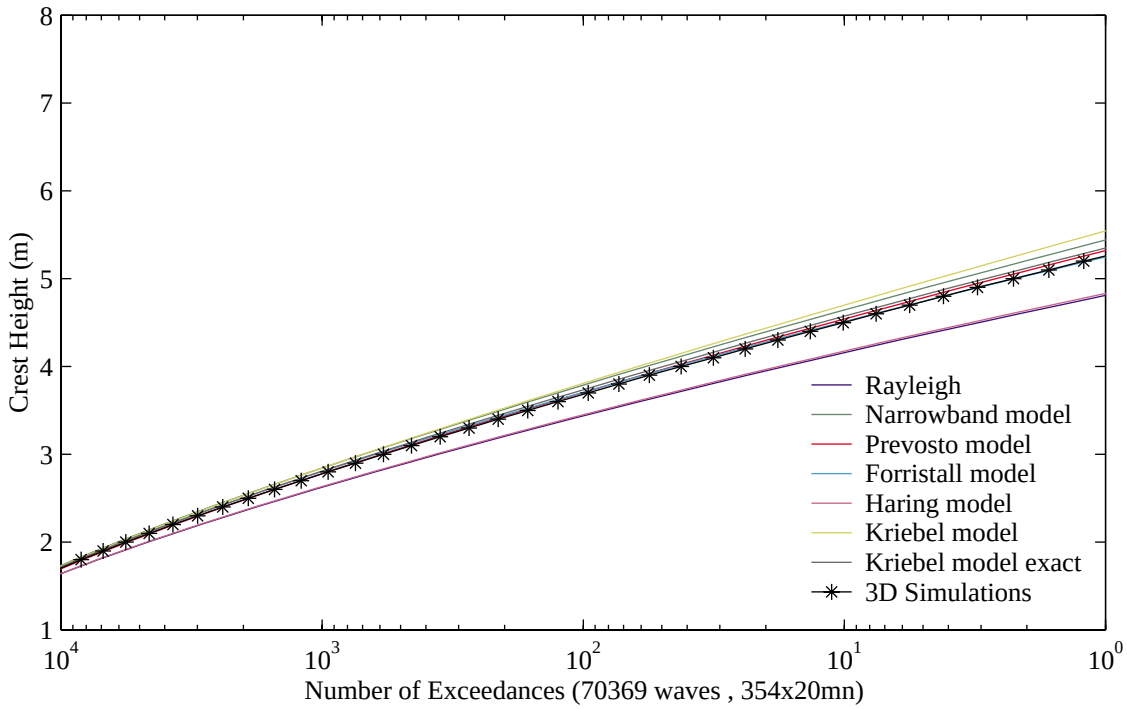

FIGURE 7.19 : Models vs empirical statistics - water depth 1000m

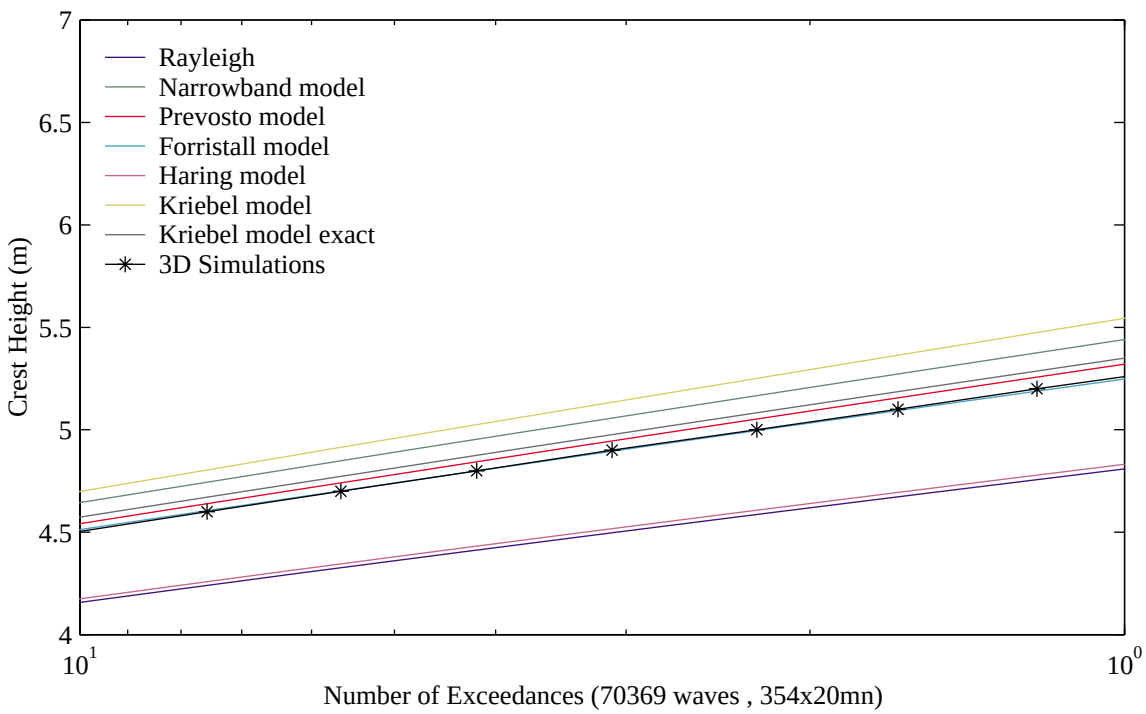

CHAPTER 8

Simplified Hs-dependent models

Marc Prevosto

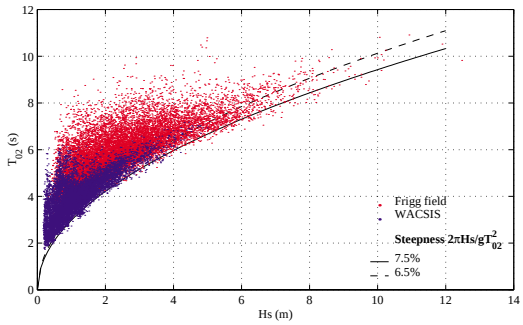

We have seen in the previous chapter that two parametric models were proposed which give very accurate results when compared to 2nd order irregular wave models. The Forristall model is pameterized by H_s and T_{01}, the Prevosto model by H_s, T_{02} and s. But very often the climatology on a site is only available for Hs, e.g. when the climatology comes from altimeter measurements. Then the issue is: are these models still usable?

Simplified Hs-dependent models

Constant steepness

Let us look at and compare the relation between Hs and T_{02} for two sites in the North Sea with different fetch and, more or less deduced, very different extreme conditions (figure 8.1). The Frigg field data, with extreme conditions corresponding to Hs around 12 meters and the WACSIS Meetpost site with extreme Hs around 5 meters, show a very similar maximum steepness limit of 7.5% which corresponds to the breaking limit. The steepness is here calculated as the deep water steepness i.e.

$$S_2 = \frac{2\pi}{g}\frac{H_s}{T_{02}^2} \qquad \textbf{(EQ 8.1)}$$

If we observe the tail (extreme Hs) of the joint distributions, for the two sites the values of (Hs,T_{02}) concentrate around a steepness of 6.5%. These points correspond in fact to pure wind seas and will contribute almost exclusively to the statistics of extreme crest heights.

If now we plot the fractiles of the steepness versus the Hs (figure 8.2), we observe again very close constant values for the extreme sea states. At the WACSIS site the median value equals 0.062 and will be used in further comparisons.

FIGURE 8.1 : T_{02} vs Hs

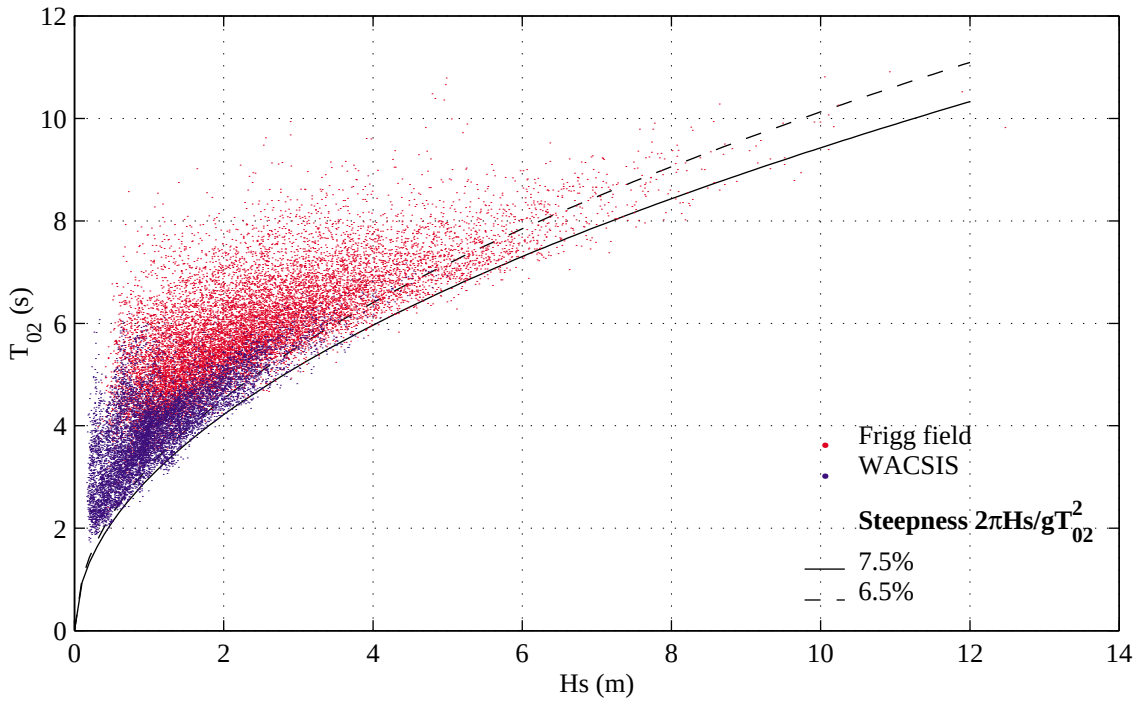

FIGURE 8.2 : Steepness fractiles vs H_s

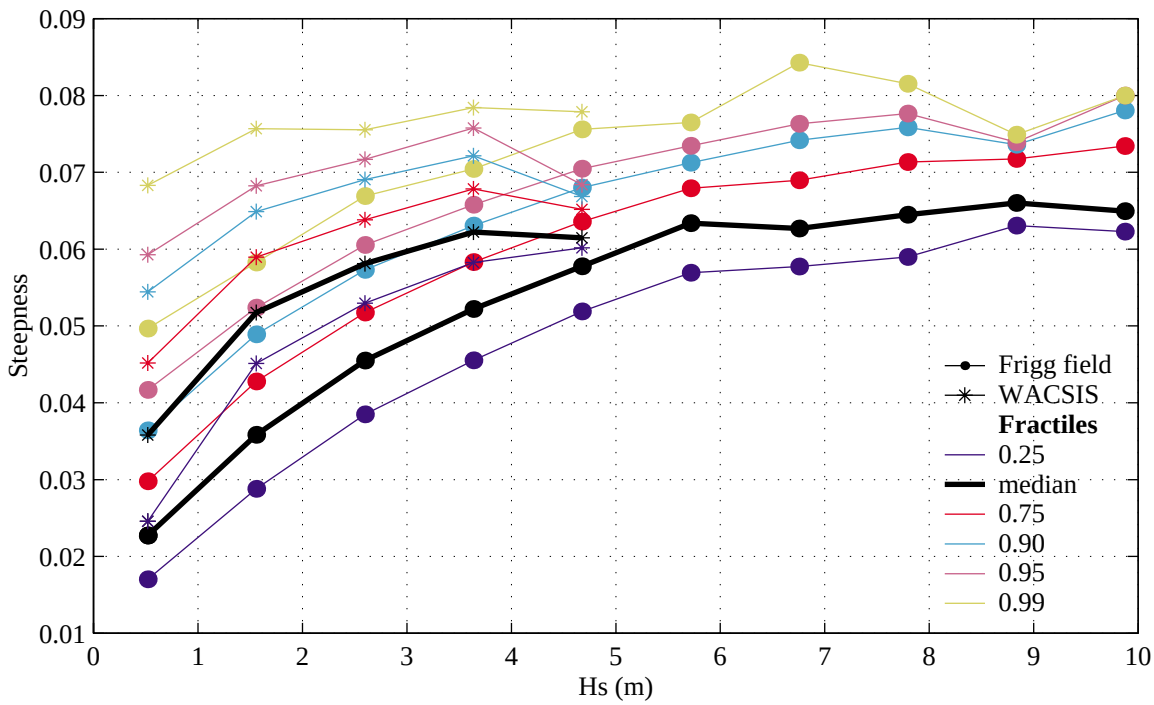

Constant directional spreading

During the WACSIS campaign the directional spreading factor s goes from 2 to 35 (figure 8.3). But for extreme sea states it goes from 5 to 20 with a mean value around 10. This mean value will be used in further comparisons

FIGURE 8.3 : Directional spreading coefficient vs Hs

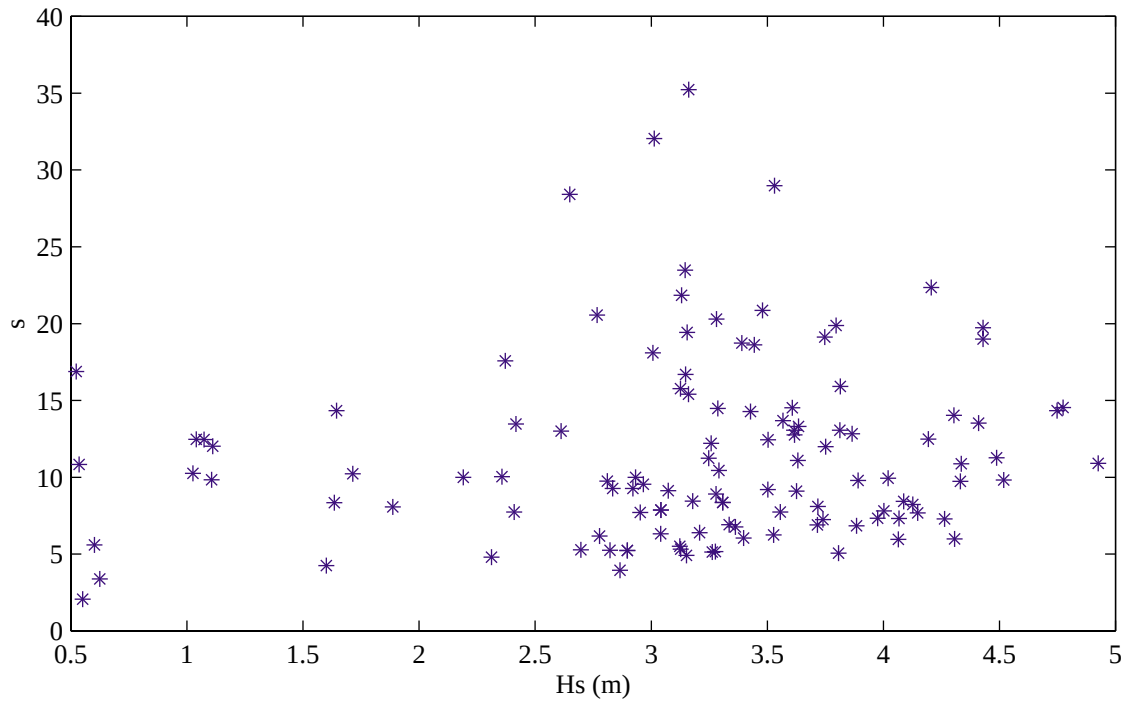

Crest heights from Hs alone

In following the same steps as explained in “All-over campaign comparison”, page 123, we have compared different simplified models with the general parametric Prevosto model.

- the Rayleigh model which uses only Hs
- the Prevosto model with a constant steepness equal to the median value of the extreme sea states (S_2 = 0.62), but using the directional spreading factor s of the data base
- the Prevosto model with the same constant steepness and the directional spreading factor s equal to a mean value (= 10) of the extreme sea state directional spreading factors.

We also compared two extreme directional spreading situations:

- the Prevosto model with the same constant steepness and the directional spreading factor s equal 1 (very spread wind sea).
- the Prevosto model with the same constant steepness and the directional spreading factor s equal 1000 (swell).

and two models with the extreme steepnesses of the WACSIS severe sea states:

- the Prevosto model with constant steepness equal 0.74

- the Prevosto model with constant steepness equal 0.44

The results for the different water depth situations are given figures 8.4-8.6. Only the zoomed plots for the number of exceedances 1 to 10 are given. In all the water depth situations the two simplified climatologies (Hs; T_{02}=sqrt(2πHs/S_2), S_2=0.062; s) and (Hs; T_{02}=sqrt(2πHs/S_2), S_2=0.062; s=10) give results very close to the model using the complete climatology (Hs; T_{02}; s).

The effect of steepness (S_2=0.044, 0.062, 0.074) is less pronounced in shallow water than in deep water. That is easily understandable, since for a given Hs, if the steepness decreases, T02 calculated from EQ 8.1 increases and so does the wave-length, increasing the bottom effect nonlinearity and thus compensating the effect of decreasing the steepness.

The opposite effect of directional spreading in shallow and deep water is also very clear. However, the difference of the magnitude of the effect is not intuitively explainable.

Crest height return values

In using the law of Hs obtained from the data of the WACSIS campaign of measurements (see “Climatology”, page 12):

$$P(H_s > h) = \exp\left(-\left(\frac{c}{\alpha}\right)^{\beta}\right) \text{ with } \begin{array}{l} \alpha = 1.265 \\ \beta = 1.494 \end{array} \qquad \textbf{(EQ 8.2)}$$

and the previous Hs-dependent model, we are able to compute the crest height law by:

$$P(C_{max} < c) = \int_0^{\infty} P(C_{max} < c \mid H_s = h) f_{H_s}(h)\,dh \qquad \textbf{(EQ 8.3)}$$

$$\text{with } P(C_{max} < c \mid H_s = h) = P(C < c \mid H_s = h)^N \qquad \textbf{(EQ 8.4)}$$

where C_{max} is the maximum crest height encountered during a sea state that we considered here of constant duration T equal 20 minutes. N the number of waves in a sea state is given by T/T_{02} where, as explained previously, T_{02} is given from H_s by a constant steepness S_2 equal 0.062 (EQ 8.1).

The crest height return value C_r corresponding to n seasons (December-May) could then be obtained by:

$$P(C_r < c) = 1 - \frac{1}{M} \qquad \textbf{(EQ 8.5)}$$

where M is the number of sea states during the n seasons.

The results are given for n equal 0.1, 1, 10, 20. The value n equal 0.1 corresponds in fact to the value which is exceeded 10 times in average during one season, and so could be in some sense compared to the WACSIS measurements empirical value.

FIGURE 8.4 : Effect of constant sea state parameters - water depth 17-20m

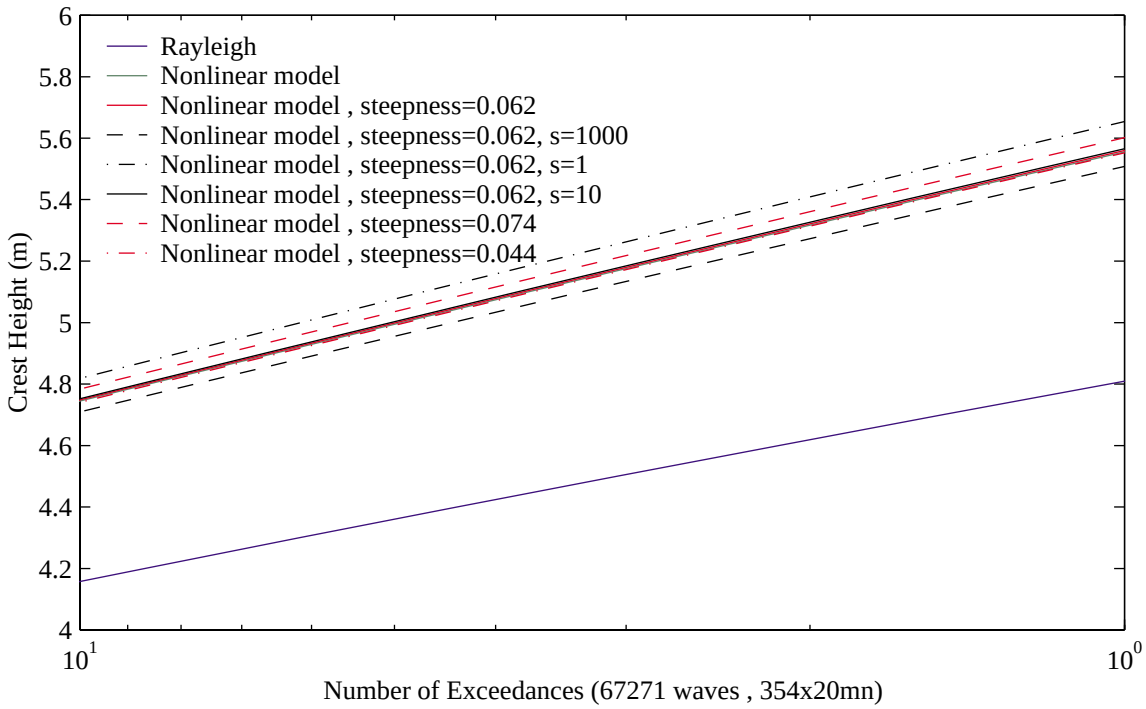

The values given by the Rayleigh model and the Hs-dependent nonlinear model are given in table 8.1. For the Hs-dependent model we have used the directional spreading factor s equal 10 and a constant water depth equal 18 m.

TABLE 8.1 : Crest height return values (m)

	Return period (in season)			
	0.1	**1**	**10**	**20**
Rayleigh	4.2	5.1	6.1	6.3
Hs-dependent	4.8	6.1	7.3	7.7

The values given for n equal 0.1 are in good agreement with the measurements (see figure 6.15, number of exceedances equal 10^1). However in the figure all the crest heights are taken into account and not only the maximum inside each sea state. For 20 seasons the underestimation of the return value by the Rayleigh distribution is higher than 20%.

Conclusion

In the context of a climatology based on WACSIS directional spectra data base, a simplified climatology based on Hs and a constant steepness equal to the median value for severe sea-states (= 0.062) and a mean directional spreading (= 10) gives the same crest statistics as that given by using the complete climatology.

FIGURE 8.5 : Effect of constant sea state parameters - water depth 30m

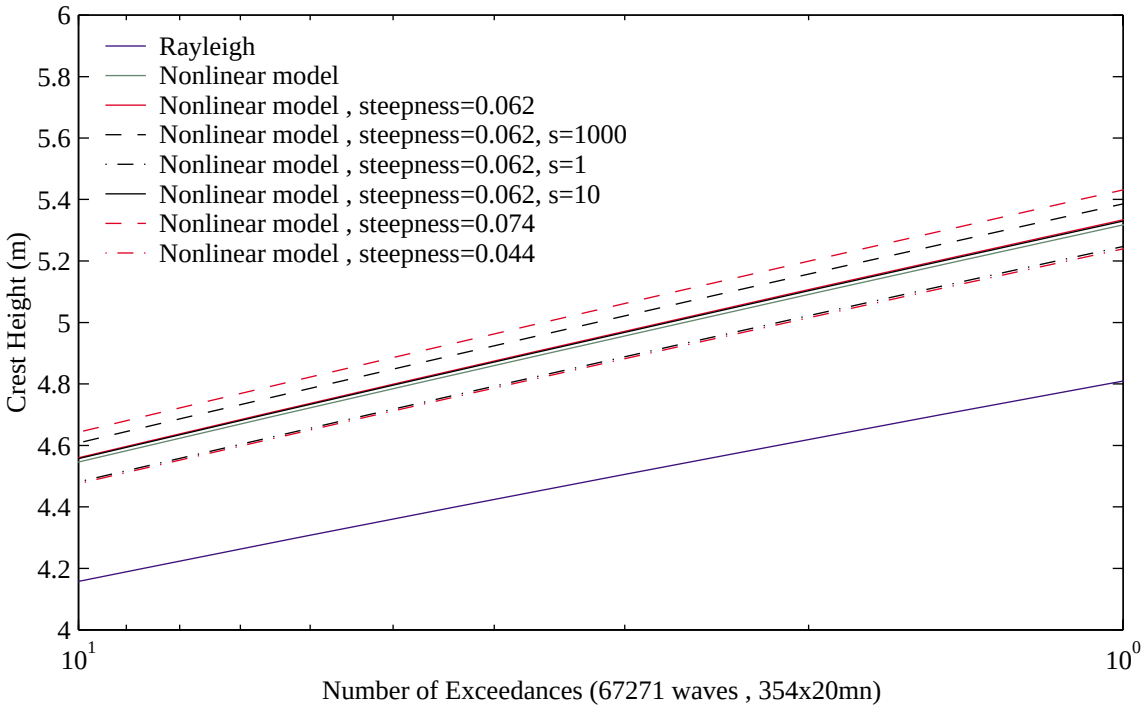

FIGURE 8.6 : Effect of constant sea state parameters - water depth 1000m

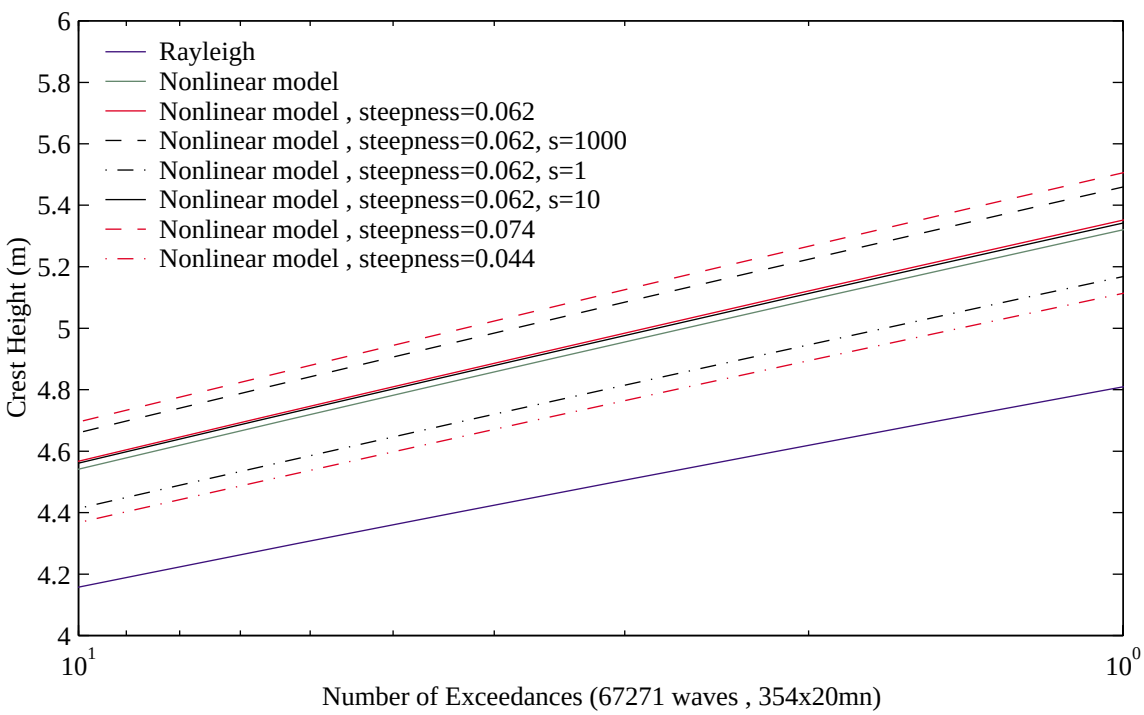

Conclusions

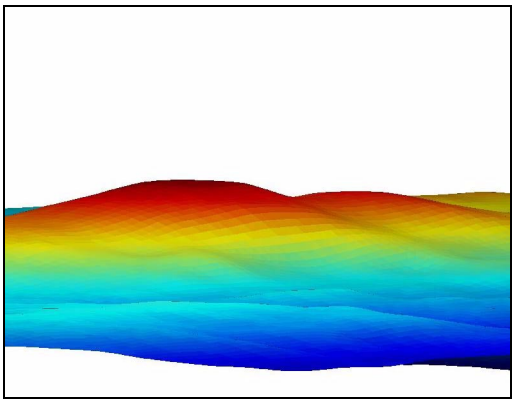

The aims of these studies have been first to construct for all the project team a common data base from the raw data collected at the Meetpost Noordwijk measurement platform. The second aim was to analyse the data base in terms of crest height-period joint distributions, intercomparison of the crest measurements by the sensors, and comparison with numerical second order irregular waves models. Finally, we have validated new crest distribution models which take into account as completely and simply as possible the nonlinear characteristics of actual spread seas.

All these studies have provided very positive answers which permit us to propose concrete conclusions for engineering purposes and future researches.

***WACSIS Common Data Base*.** Based on 120 dates, selected on criteria of severity of sea states, availability of video recordings or particular sea state characteristics, a homogeneous common data base has been constructed and distributed to all the partners of the project. Before inclusion in the data base, each time series has been detrended to remove the tide and storm surge effects. Over- and under-sampling of each time series have been added to the base to permit more extensive comparisons.

A Web site has been maintained during all the time of the WACSIS project to facilitate the exchange of information on data and meetings.

***Height-Period Joint Distributions*.** We have shown in this report that the joint distribution of crest height and crest period can be well approximated by the Lund model. The best estimates are obtained using a spectrum estimated as the non smoothed periodogram and a non parametric g transformation.

The results from Cavanié and Longuet-Higgins parametric models are not satisfactory, particularly with sea states which are not narrow-banded or double peaked.

As the aim of this study was to find a way to get estimates of joint distributions for the desired large number of sea states, one solution is to use parametric shapes of spectra and of the g transformation. It has been seen that the estimates of the joint distribution remain accurate when a suitable model is used to deduce a parametric spectral shape. Further tests are necessary for parametric *g* transformation. Then, accurate estimates of the joint distributions could be obtained from g transformation and spectral shape parameterized by sea states parameters. Then the computation of the distributions on a reduced discretized space of the sea state parameters would permit an estimation of the joint distribution for any sea state case.

Sensor measurements comparison. The comparison of the crest height statistics between the different sensors has shown that the raw data of the sensors gives different crest statistics but very close trough statistics.

Part of these differences are due to little waves with short wavelengths which are viewed differently by the sensors (different space and time filtering). When the data are filtered to 0.64 Hz, to include only long waves, the Vlissingen step gauge, the Baylor wave staff and the Thorn laser wave height sensor give very close results. However, when the short waves are filtered out, SAAB radar still overestimates the crest heights and MAREX radar is too much perturbed by spikes to be compared with the other sensors.

Simulation methods - Effect of simulation parameters. Simulations based on irregular waves with second order Stokes expansions have been studied using the characteristics of the sea states encountered during the WACSIS campaign. A simple technique of frequency truncation has been used to avoid the short-long waves interaction problem. The truncations in the angular and frequency domains have been optimised. The effect of variations of water depth has been shown to be well taken into account. All these elements have permitted us to work with wave simulators as good as possible in making comparisons with the measurements. The simulations used data given by the Waverider buoy as directional spectral information.

2nd order simulations - Comparison with measurements. Simulations of the wave elevation with a second order irregular 3D model have given statistics of crest height similar to three of the sensors: the Vlissingen step gauge, the Baylor wave staff and the Thorn laser wave height sensor, when we consider only wave components up to 0.64Hz. The power spectra from the sensors indicate that the measurements are very likely to be contaminated by noise above this frequency. Furthermore, the Waverider buoy spectra used for simulations give energy of the linear part only up to 0.64Hz.

So, in the severe, but not extreme, sea states encountered during the campaign, the second order model seems accurate. Including wave components with frequencies above 0.64Hz might possibly increase the crest height ratios slightly, but the difference would not be important for most engineering uses since those components have very short wavelengths and thus do not affect engineering structures.

Models of distribution - Comparison with simulations. Apart from the infinite water depth situation for the exact Kriebel model, the parametric models of crest distributions which were proposed in the past are not very accurate. The two new parametric models which have been recently proposed by George Forristall and Marc Prevosto give results very close to what is obtained empirically from second order 3D irregular simulations of the WACSIS directional spectra, whatever the water depth.

The formulation of the Forristall model is simpler than the Prevosto model but it does not take into account explicitly the directional spreading as the Prevosto model does. So the Prevosto model will be more accurate in extreme directional spreading situations (very short-crested or close to swell situations).

Simplified Hs-dependent models. In the context of a climatology based on WACSIS directional spectra data base, a simplified climatology based on the Hs climatology and a constant steepness equal median value for severe sea-states and a mean directional spreading has given the same crest statistics as that given in using the complete climatology. This shows that the more complex models proposed by Forristall or Prevosto could be used, if necessary, in a very simple way, but still taking into account accurately the nonlinearities of spread seas and still in agreement with the set of the three reliable sensors of the WACSIS project intercomparison.

References

[1] Barstow, S.F., Mathisen, J.P., Schølberg, P., Mørk G., Krogstad, H.E., (2001) "Intercomparison of seastate and zerocrossing parameters from the WACSIS field experiment and interpretation with video evidence," Oceanographic Company of Norway, Report OCN R-20025.

[2] Brotkorb, P. A., Johannesson, P., Lindgren, G., Rychlik, I., Ryden, J., Sjo, E., (2000) WAFO - A matlab toolbox for random waves and loads. Proceedings of the tenth ISOPE Conference, vol III.

[3] Cavanie, A., Arhan, M., and Ezraty, R., (1976). A statistical relationship between individual heights and periods of storm waves. Proceedings, BOSS'76, Trondheim, pp354-360.

[4] Chen, L., Zhang, J. (1994) "On interaction between intermediate-depth long waves and deep-water short waves", Offshore Technol. Res. Center Report, no. A5575, p. 37.

[5] Creamer, D.B., Henyey, F.S., Schult, R., Wright, J., 1989, "Improved linear representation of ocean surface waves", *J. Fluid Mech.*, vol.205, pp. 135-161.

[6] Forristall, G.Z., 1978, "On the statistical distribution of wave heights in a storm", *Journal of Geophysical Researc*h, no. 83, pp. 2353–2358.

[7] Forristall, G.Z., 2000, "Wace Crest Distributions: Observations and Second-Order Theory", *Journal of Physical Oceanography*, vol. 30, no.8, pp. 1931-1943.

[8] Guedes Soares, C., (1984), "Representation of double-peaked sea wave spectra", Ocean Engineering, vol 11, n° 2, pp 185-207.

[9] Haring, R.E., Heideman, J.C., (1978) "Gulf of Mexico rare wave return periods", *Proc. Offshore Technology Conference*, pp. 1537–1550, OTC 3230.

[10] Jahns, H.O., Wheeler, J.D., (1973) "Long-term wave probabilities based on hindcasting of severe storms", *J. Pet. Technol.*, 473–486.

[11] Kriebel, D.L., Dawson, T.H., (1991) "Nonlinear effects on wave groups in random seas", *J. Offshore Mech. Arctic Eng.*, no. 113, pp. 142-147.

[12] Kriebel, D.L., Dawson, T.H., (1993) "Nonlinearity in wave crest statistics", *Proc. 2nd Int. Symp. Ocean Wave Measurement and Analysis*, pp. 61-75.

[13] Lindgren, G. and Rychlik, I. (1982) Wave characteristic distribution for Gaussian Waves - wave-length, amplitude and steepness. Ocean Engineering, 9, pp. 411-432.

[14] Longuet Higgins, M.S. (1975) On the joint distribution wave periods and amplitude in a random wave _eld. Proc. R. Soc. A389, pp 24-258.

[15] Longuet-Higgins, M.S., (1963), "The effect of non-linearities on statistical distributions in the theory of sea waves", J. Fluid Mech., vol. 17, pp. 459-480.

[16] Occhi, M.K. and Hubble, E.N. (1976). "On six parameter wave spectra". Proc. 15th Coastal Engineering Conf., A.S.C.E., pp 321-328.

[17] Occhi, M.K. and Ahn, K. (1994) Probability distribution applicable to non Gaussian random processes. Probabilistic Engineering Mechanics, 9, 255-264.

[18] Podgorski, K., Rychlik, I., and Machado, U.E.B. (2000). Exact distributions for apparent waves in irregular seas. Ocean. engng. 27(9), 979-1016.

[19] Prevosto, M., Krogstad, H.E., Robin, A., (2000) Probability distributions for maximum wave and crest heights. Coastal Engineering, vol. 40, pp. 329-360.

[20] Prevosto, M., 1998, "Effect of Directional Spreading and Spectral Bandwidth on the Nonlinearity of the Irregular Waves", *Proc. 8th ISOPE Conf.*, vol. III, pp. 119-123.

[21] Rice, S.O., (1945) "Mathematical analysis of random waves", *Bell Syst. tech. J.*, vol. 24, pp. 46-156.

[22] Rychlik I., Johannesson P., Leadbetter M.R. (1997). Modelling and statistical analysis of ocean wave data using transformed gaussian processes. Marine structure, 10, 13-47.

[23] Rychlik, I. and the 'WAFO group' (2000) WAFO, a Matlab Toolbox for Analysis of random waves and loads, a tutorial. Dept. of Math. Stat., Lund University.

[24] Sharma, J.N., Dean R.G., (1979), "Development and evaluation of a procedure for simulating a random directional second order sea surface and associated wave forces", *Ocean Engineering Report, no. 2*0, University of Delaware, Newark.

[25] Tayfun, M.A., 1980, "Narrow-band nonlinear sea waves", *J. Geophys. Res.*, vol. 85, no. C3, pp. 1548-1552.

[26] Tromans, P.S., Taylor, P.H., 1998, “The shapes, histories and statistics of nonlinear wave crests in random seas”, *Proc. OMAE Conf.*.

[27] Tung, C.-C., Huang, N.E., 1985, "Peak and trough distributions of nonlinear waves", *Ocean Eng.*, vol. 12, no. 3, pp. 201-209.

[28] van Unen, R.F., van Beuzekom, A.A., Forristall, G.Z., Mathisen, J.-P., Starke, J., 1198, "WACSIS - Wave Crest Sensor Intercomparison Study at the Meetpost Noordwijk Measurement Platform", *Oceans’98*, Nice, France, IEEE, pp. 192-197.

[29] Winterstein, S.R. (1988) Nonlinear vibration odels for extremes and fatigue. J. Engng. Mech. ASCE, 114, No10, pp 1772-1790.

[30] Zhang, J., Chen, L., Ye, M., Randall, R.E. (1996) "Hybrid wave model for unidirectional irregular waves, Part I. Theory and numerical scheme", *Appl. Ocean Res.*, vol. 18, nos 2-3, pp. 77-92.

[31] Zhang, J., Yang, J., Wen, J., Prislin, I., Hong, K., 1999, "Deterministic wave model for short-crested ocean waves: Part I. Theory and numerical scheme", *Applied Ocean Research*, vol. 21, no. 4, pp. 167-188.